Understanding and Fighting Basement Fires

Daniel Madrzykowski
Craig Weinschenk

UL Firefighter Safety Research Institute
Columbia, MD 21045

Prepared for the International Society of Fire Service Instructors
Supported by the DHS/FEMA Assistance to Firefighters Grant Program

This report is dedicated to the memory of:
Captain Matthew LeTourneau, Philadelphia Fire Department

This publication is available free of charge from:
https://dx.doi.org/10.54206/102376/ETSA5492

Understanding and Fighting Basement Fires

Daniel Madrzykowski
Craig Weinschenk

UL Firefighter Safety Research Institute
Columbia, MD 21045

August 3, 2018

This publication is available free of charge from:
https://dx.doi.org/10.54206/102376/ETSA5492

UL Firefighter Safety Research Institute
Steve Kerber, Director

In no event shall UL be responsible to anyone for whatever use or non-use is made of the information contained in this Report and in no event shall UL, its employees, or its agents incur any obligation or liability for damages including, but not limited to, consequential damage arising out of or in connection with the use or inability to use the information contained in this Report. Information conveyed by this Report applies only to the specimens actually involved in these tests. UL has not established a factory Follow-Up Service Program to determine the conformance of subsequently produced material, nor has any provision been made to apply any registered mark of UL to such material. The issuance of this Report in no way implies Listing, Classification or Recognition by UL and does not authorize the use of UL Listing, Classification or Recognition Marks or other reference to UL on or in connection with the product or system.

Contents

List of Figures

List of Tables

List of Abbreviations

AFG	Assistance to Firefighters Grant program
BR	Bedroom
CO_2	Carbon dioxide
CO	Carbon monoxide
CPVC	Chlorinated polyvinyl chloride
DHS	U.S Department of Homeland Security
DelCo ESTC	Delaware County Emergency Services Training Center
FEMA	Federal Emergency Management Agency
HRR	Heat release rate
IDLH	Immediately dangerous to life or health
IAFC	International Association of Fire Chiefs
IAFF	International Association of Fire Fighters
IFSI	Illinois Fire Service Institute
IFSTA	International Fire Service Training Association
ISFSI	International Society of Fire Service Instructors
IR	Infrared
LODD	Line of duty death
LODI	Line of duty injury
MFRI	Maryland Fire and Rescue Institute
NFPA	National Fire Protection Association
NIOSH	National Institute for Occupational Safety and Health
NIST	National Institute of Standards and Technology
OSB	Oriented strand board
O_2	Oxygen
PE	Polyester
PP	Polypropylene
PPE	Personal protective equipment
PU	Polyurethane
RTI	Response time index
SB	Smooth bore
SFPE	Society of Fire Protection Engineers
SS	Straight stream
TPP	Thermal protection performance
UL FSRI	UL Firefighter Safety Research Institute
USFA	United States Fire Administration

Abstract

Many firefighters have been injured or killed while trying to extinguish a basement fire or a fire on a level below them. Prior research has shown basement fires present a high risk to firefighters. This risk stems from unexpected floor collapse and high heat. Prior research also indicated the tools that firefighters have traditionally used to determine the structural integrity of the floor offer little value with lightweight construction. Past experiments in small basements have indicated that the most effective method of fighting a basement fire may be from the exterior of the building.

This study went beyond earlier research by increasing the size of the basement and incorporating three different ventilation and access conditions to the basement. Those access conditions include no exterior access to the basement, limited exterior access to the basement, and exterior access to the basement. The results of the experiments show the importance of identifying a basement fire, controlling ventilation and flowing an effective hose stream into the basement from a position of advantage, as soon as possible.

These experiments highlighted the importance of identifying a basement fire during size-up and subsequently choosing the appropriate tactics that coordinate ventilation with suppression. In all experiments, the basement fire were ventilation limited. Additional ventilation without suppression was shown in to increase the hazard to any occupants trapped in the structure. Various nozzles and appliances were used to flow water into the basement. Water streams applied through the floor, through a small window remote from the seat of the fire, and through a basement level access door controlled the fire and reduced the hazard throughout the structure.

Effective water application into the basement cooled the fire gases to prevent flashover, slowed the destruction of the structure, and reduced the hazard from fire. This action made entry conditions into a basement with active burning possible for a fully protected firefighter. Effective water application also supported search operations and reduced the threat from heat and toxic gases for any trapped occupants. Occupants isolated from the fire environment by a closed door or other means were provided addition protection when compared with conditions in rooms open to the fire environment.

Acknowledgments

The authors thank the ISFSI Technical Advisory panel for sharing their firefighting experience in the development of this study, and the *Understanding and Fighting Basement Fires* course that is based in part on this report.

Table 1: ISFSI Technical Advisory Panel

Name	Title	Department	Organization
Seth Barker	Captain	Big Sky (MT) Fire Department	ISFSI
Robert Callahan	Deputy Fire Chief	District of Columbia Fire and EMS	
Brian Claybern	Captain	Independence Fire Department	ISFSI
Michael Cochrane	Captain	San Francisco Fire Department	
Frank Cook	Chief	Township of Colerain Fire and EMS	
John Culbertson	Director	Fire Service Training School, Montana State University	NAFTD
Christopher Divver	Lieutenant	Clifton (NJ) Fire Department	IAFC:CO
Brian Kazmierzak	Chief of Training	Penn Township (IN) Fire Dept.	ISFSI
Kerby Kerber	Deputy Director	DelCo (PA) Public Safety Training Center	
Stephen Kerber	Director	UL Firefighter Safety Research Institute	
Ed Kline	Chief	South Media Fire Company	
Timothy Leidig	Asst. Chief	West Chicago Fire Protection District	ISFSI
Murrey Loflin	Investigator	NIOSH	
Daniel Madrzykowski	Research Engineer	UL Firefighter Safety Research Institute	
Gary Morris	Chief	Pine-Strawberry Fire District	IAFC: SHS
Steve Pegram	Chief	Goshen Township (OH) Fire Department	President, ISFSI
George Stapleton	Administrator	Pennsylvania State Fire Academy	ISFSI
Brian Taylor	Chief	Pleasant Township Fire Department	IAFC: VCOS
Adam Thiel	Commissioner	City of Philadelphia Fire Department	

These experiments would not have been possible without the UL FSRI and the Delaware County Emergency Services Training Center (ESTC) teams. The UL FSRI team instrumented, conducted and analyzed these experiments. The authors thank: Joshua Crandall, Keith Stakes, Mike Alt, Robin Zevotek, Joseph Willi, John Regan, Steve Kerber, and Roy McLane of Thermal Fabrications.

The Delaware County (PA) ESTC provided the location and logistical support for these experiments. The Delaware County team was under the direction of Kerby Kerber. The construction and test support team included Brad Morrissey, Joe Bingham, Joe Minutolo, Vince Vitullo, Dave Nercesian (small engine repair), and Mike Gura.

Thanks are given to the dedicated team of fire instructors and firefighters that supported these experiments; including Brian (Rudy) Righter, Gary Thompson, Mark Morrissey, Matthew Poissant, Bill Norris, and Matt LeTourneau. Finally, the authors thank Chief John Norman (ret.) FDNY for his review of this document.

Section 1 Introduction

Over the years, fire fighters have died or been injured while trying to extinguish a basement fire or a fire on level lower than the front entry point of the structure. Between 1998 and 2017, NIOSH has documented 24 below-grade fires that resulted in 32 firefighter LODDs and 19 firefighter LODIs. Typically these cases involved firefighters falling through a wood floor assembly into a burning basement, or high-velocity hot gases flowing out of a basement and burning or trapping firefighters.

According to the NFPA report, "Firefighter Fatalities in the United States" in 2014 [1], six LODDs involved a basement or operating above a fire in residential occupancies. Two fatalities were trapped in a basement, two fatalities fell into a basement, and two fatalities were operating above a fire floor and were overtaken by a rapid fire event.

Many firefighters are also injured in cases involving basement fires. The fire in Prince Georges County, Md., where seven firefighters were injured, is a rare case in that it was studied and documented [2,3]. Based on newspaper reports, in the 100 days from December 28, 2015 through April 7, 2015, nine firefighters were injured due to falls through the floor of a burning home.

The Mayday Project conducted by Abbott reports that one of the top causes of a mayday is falling into basements. From more than 2,700 career department maydays reported to the project, 19% were attributed to falling into the basement [4]. Similarly, of the more than 1,900 volunteer department maydays reported to the project, 24% were due to falling into a basement [5]. All totaled, this accounts for more than 1,000 mayday incidents involving falling into basement that were voluntarily reported.

During the past 10 years, an unprecedented amount of research has been conducted to examine the firefighters work environment with the goal of improving firefighter safety and effectiveness. The majority of this research was funded by DHS/FEMA AFG. NIST and UL FSRI conducted several research studies examining the capabilities of a variety of residential flooring systems.

Section 2 Study Design

2.1 LODD and LODI Review

In addition to the 24 below-grade fires NIOSH reviewed, there have been below-grade or floor-below-fire incidents [6–26] in which changes in flow paths are thought to have had an adverse impact on firefighter and occupant safety.

Based on a review of these incidents, it is clear fires with rapidly developing or changing ventilation may lead to hot gas flows that are a significant hazard to the fire service during a response. The failure of a component of the structure, such as a door, window, or portion of a ceiling, wall or floor, can lead to the development of (or change to) a flow path. Environmental conditions such as wind can also generate hazardous thermal conditions within a flow path. Additionally, uncoordinated ventilation procedures can cause increased thermal hazards within a flow path. Table 2.1 lists the NIOSH investigation reports from the past 15 years in which it could be determined that an uncontrolled flow path played a role in the related incident. This table lists the NIOSH report number, the losses and a brief description of the flow path details.

2.2 Structural Collapse Research

UL published its research findings on the structural stability of engineered lumber in fire conditions in 2008 [27]. The experiments were conducted on a floor furnace. The research demonstrated that modern engineered wood floor assemblies failed faster than wood floor assemblies with legacy designs. The addition of 1.27 cm (0.5 in.) gypsum to the combustible floor-ceiling assembly improved thermal performance. This study also pointed out that modern tools like thermal imagers had limited use in determining the condition of the floor assembly or the fire conditions under the floor. Further, the study questioned the use of time-honored means of "sounding the floor" as a way to determine if the floor was safe to operate on.

NIST conducted experiments in two-level wood structures with a 4.88 m (16 ft) span that supported the findings of the UL study on the value of gypsum board to protect the floor assembly and the challenges for the thermal imagers. Visible contrast and surface temperature measurements provided by the thermal imagers could only be loosely correlated to thermal conditions in the lower level. The study concluded that an accurate assessment of structural integrity in nearly all experiments with a thermal imager alone would be impossible. The study also highlighted the interaction of ventilation to the fire area in order to generate the energy needed to fail the floor assemblies [28].

In 2012, UL released a study conducted with NIST that examined four types of flooring systems

Table 2.1: Flow-Path Related LODD/LODI Incidents.

NIOSH Report No.	No. of LODDs/LODIs	Flow Path Details
99-F01 [6]	3 LODDs	From apartment into hallway on 10th floor of high-rise apartment building.
99-F21 [7]	2 LODDs 2 LODIs	Basement to 1st floor.
F2000-04 [8]	3 LODDs 3 civilian deaths	1st floor to 2nd floor.
F2000-16 [9]	1 LODD 1 LODI 1 civilian death	2nd floor hallway through 2nd floor apartment.
F2000-23 [10]	1 LODD 2 LODIs	From ground level to 1st floor then to 2nd floor; flow exited through ceiling
F2000-43 [11]	1 serious LODI 2 other LODIs	1st floor to 2nd floor.
F2004-02 [12]	1 LODD	1st floor to basement.
F2005-02 [13]	1 LODD 4 LODIs	Rear to front of the building.
F2005-04 [14]	1 LODD 9 LODIs	Basement to 1st floor.
F2007-09 [15]	1 LODD 2 LODIs	3 story training burn, flow through all levels.
F2007-35 [16]	4 LODIs	1st floor to 2nd floor.
F2009-11 [17]	2 LODDs	Rear to front of the building.
F2011-13 [18]	2 LODDs	Lower level up stairs and through entry door and garage.
F2011-31 [19]	1 LODD	Fire extended from lower level apartment.
F2012-28 [20]	1 LODD 1 LODI	Attic fire extended into closed porch and then into 2nd floor.
F2013-02 [21]	1 LODD	Trapped in basement fire, SCBA degraded.
F2013-04 [22]	2 LODD 2 LODI	Flashover in assembly hall.
F2014-02 [23]	2 LODD	Fire extended from 1st to 2nd floor.
F2014-09 [24]	2 LODD 13 LODI	Wind-driven fire, unrestricted flow path.
F2014-14 [25]	1 LODD	Heavy smoke led to rapid fire growth.
F2014-25 [26]	1 LODD	Basement to 1st floor.

in a townhouse type arrangement, with a 67 m^2 (720 ft^2) floor area and a 6.1 m (20 ft) span. These experiments were conducted to examine the time to collapse for residential floor systems constructed with dimensional lumber, wood I-joists, parallel chord wood trusses and lightweight steel C-channel. The results from this study proved that any of the unprotected floor assemblies could collapse within the operational time frame of the fire department. The report again indicates

that current fire ground practices of entering on the floor above the fire and working down to the basement will not provide firefighters with the appropriate information to make a decisions to enable a safe operating environment [29].

2.3 Basement Fire Attack Research

The Fire Department of New York City, along with NIST and UL FSRI, conducted several basement fire experiments in abandoned townhouses with approximately 55.75 m^2 (600 ft^2) floor area per level and unprotected dimensional lumber floor systems. The fires were successfully attacked and controlled from exterior openings on the front and back of the structure [30].

The ISFSI, in co-operation with NIST, the South Carolina State Fire Academy and the Spartanburg Fire Department, conducted two basement experiments in acquired structures as part of the development of the AFG-funded "Translating Fire Fighting Research Results into Fire Fighter Training" Project. In both structures, the basements were partial basements with less than 55.75 m^2 (600 ft^2) of floor area. In each experiment, the fire was fought from a walk-out basement door and was controlled with an exterior attack [31].

2.4 Study Objectives

The research to date has shown that basement fires present a high hazard to firefighters due to unexpected collapse and thermal impact from fire gases flowing up the stairway. The tools and indicators firefighters have traditionally used to determine the structural integrity of the floor hold little value with lightweight construction. A limited number of experiments in townhouse-size basements or smaller have shown that the most effective method of fighting a basement fire may start on the exterior, provided access.

After the research review, the technical panel developed the following questions left unanswered by the previous studies:

1. What if the only firefighter access to the basement is the interior stairs?
2. What if there are no basement windows to the exterior?
3. Can door control be applied to basement fires?
4. What if the basement is large, in excess of 92 m^2 (1,000 ft^2)?
5. What if the access to a large basement is limited to a few windows?
6. What if the hose stream cannot hit the seat of the basement fire?

7. Are alternative fire suppression techniques such as penetrating nozzles or cellar nozzles effective in controlling a fire in a large basement, and if so, how would the attack be implemented if access to the basement were limited?

The experiments were designed to answer these questions.

Section 3 Experimental Setup

All experiments described in this report were conducted at full scale in a purpose-built residential scale structure with variable basement ventilation and access. The design of the structure, fuel load and types of experiments were planned during a workshop with the technical panel. Technical panel members were selected based on their experience related to basement fires. Three types of experiments examining increased access to the basement were conducted in the summer of 2017: 1) no exterior access to the basement, 2) limited exterior access to the basement and 3) exterior access to the basement. Access is defined to be a window, door, or other vent that would allow an average sized firefighter in full PPE to enter the basement or a victim to be removed from the basement. Windows or vents too small to allow a person to pass through the opening are considered limited access.

No exterior access is defined by a structure with no windows, doors or any other potential openings to either flow water, vent or gain entry to the basement. The only entry to the basement was via an interior stair. Here, the basement may be completely below grade. For these experiments, suppression actions could occur from the top of the stairs, or by punching a hole through the floor or a band board.

A basement that has limited exterior access may have small windows that could be used for venting and/or suppression. The basement could be below grade but have window wells or be partially above grade. Suppression in this access condition could occur through exposed windows using either the length of the stream, or with an appliance between the hose line and the nozzle.

The third type, a basement with exterior access, has large windows or doors that are at grade and would allow ventilation, suppression and/or entry. Here, suppression could occur by attacking the fire on its own level with a variety of different interior or transitional tactics.

Additionally, experiments were conducted to provide information on the impact of a residential sprinkler system with an exposed wood floor assembly, and the impact of a gypsum board ceiling protecting the wood floor assembly from a basement contents fire. The following sections describe the various types of experiments, facilities, instrumentation and fuel loads used during the tests. All experiments were conducted at the Delaware County Emergency Services Training Center (ESTC) in Sharon Hill, Pa.

3.1 Experimental Structure

A purpose-built ranch-style house with a basement was located on the grounds of the ESTC. The outer wall of the basement was composed of interlocking concrete blocks 0.6 m (2.0 ft) wide, 0.6 m (2.0 ft) high, and 1.2 m (4.0 ft) long. The interior dimensions of the basement were 13.3 m (43.6 ft) wide, 7.28 m (23.9 ft) long, and 2.74 m (9.0 ft) high. The joints and gaps between the

blocks were filled with high-temperature insulation. The walls were constructed from dimensional lumber, 3.81 cm by 8.89 cm (nominally 2 in. x 4 in. studs). The studs were lined with 1.27 cm (0.5 in.) cement board and 1.59 cm (0.625 in.) gypsum board. The ceiling had two layers of 1.59 cm (0.625 in.) gypsum board along with 1.27 cm (0.5 in.) OSB and engineered lumber I-joists. The OSB and I-joists will also be discussed in Section 3.3. Figure 3.1 provides an overview of the basement with major dimensions called out. Note that Table 3.1 defines the size of the vents (area and sill) as indicated in Figure 3.1.

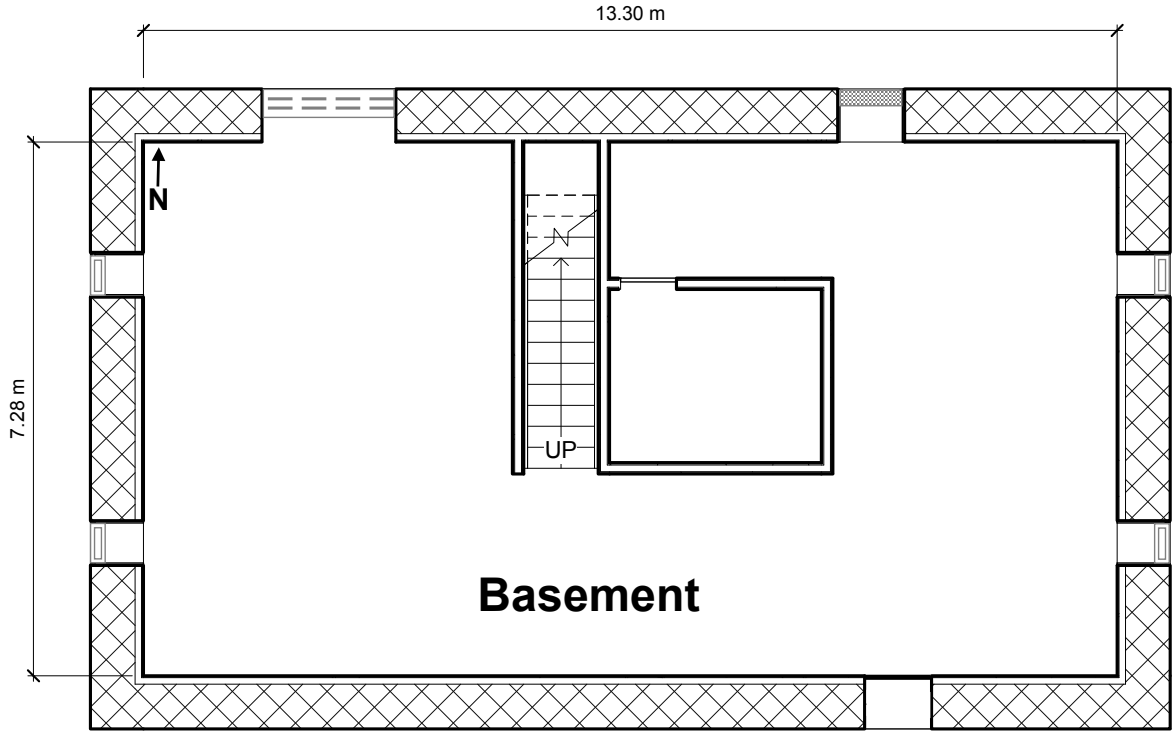

Figure 3.1: Plan view of the basement included major dimensions and locations of vents. The dimensions (area and sill height) appear in Table 3.1.

Table 3.1: Basement Vent Legend

Icon	Vent	Dimensions
	Double Doors	1.83 m W x 2.05 m H
	Large Window	1.0 m W x 0.85 m H; 1.49 m sill
	Basement Window	0.61 m W x 0.25 m H; 1.98 m sill

The exterior walls of the first floor were protected by 8 mm (0.31 in.) thick fiber cement board siding, a layer of olefin home wrap, and 1.27 cm (0.5 in.) oriented strand board (OSB). The walls were constructed from nominal dimension lumber, 3.81 cm by 8.89 cm (nominally 2 in. x 4 in. studs). The studs were lined with 1.27 cm (0.5 in.) cement board and 1.27 cm (0.5 in.) gypsum board. The interior dimensions of the first floor measured 13.77 m (45.2 ft) by 7.68 m (25.2 ft)

with a 2.44 m (8 ft) ceiling (cf. Figure 3.2). Table 3.2 defines the size of the vents (area and sill) in Figure 3.2.

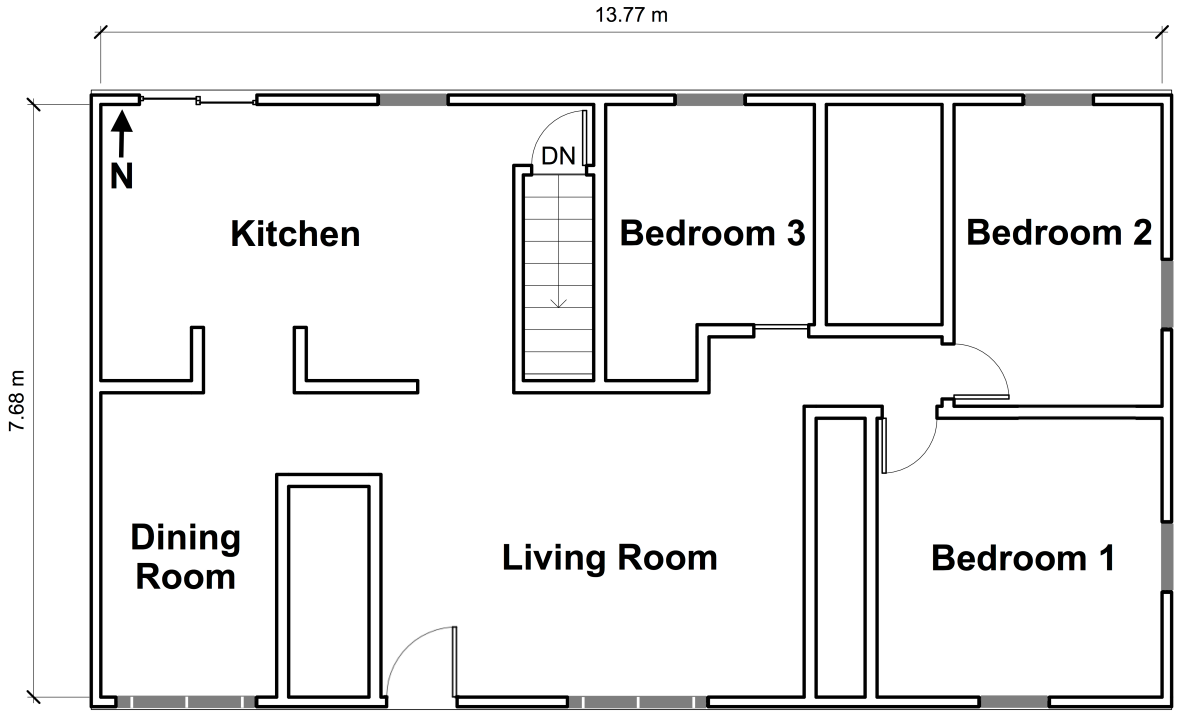

Figure 3.2: Plan view of the first floor with major dimensions and locations of vents. The dimensions (area and sill height) appear in Table 3.2.

Table 3.2: First Floor Vent Legend

Icon	Vent	Dimensions
	Slider	1.83 m W x 2.05 m H
	Single Window	0.91 m W x 1.5 m H; 0.61 m sill
	Double Window	1.82 m W x 1.5 m H; 0.61 m sill

Fully dimensioned drawings of the basement and first floor, including the location of all walls and vents, are included in Appendix A.

To characterize ventilation within the structure, a leakage test was conducted with all exterior vents closed. ASTM E 779, "Standard Test Method for Determining Air Leakage Rate by Fan Pressurization," was followed to determine the air changes per area and the equivalent leakage area [32]. The leakage in the test structure was 4 air changes per hour (ACPH) at 50 Pa (0.007 psi) with an equivalent leakage area of 0.08 m^2 (0.9 ft^2) at 10 Pa (0.0014 psi). Equivalent leakage area is defined as the area of a sharp-edged hole that would have the same leakage flow rate as the building if both were subjected to a 10 Pa pressure difference. For a single story residential structure, a tight house would have 3.5 ACPH50 (air changes per hour at 50 Pa), a moderately tight house would have 8.8 ACPH50, a typical house would have 17.5 ACPH50, and a leaky house

would have 35 ACPH50 [33]. Considering the uncertainty in typical pressure measurements (see Section 3.2.3), the test structure fell between a tight and moderately tight structure.

3.2 Instrumentation

The structure was instrumented for gas temperature, gas velocity, gas concentration, pressure and heat flux measurements. Gas temperatures were measured with both 1.3 mm (0.05 in) bare-bead, Chromel-Alumel (type K) thermocouples and 1.6 mm (0.0625 in) inconel sheathed thermocouples. Sheathed thermocouples were also used in conjunction with the bi-directional probes for gas velocity measurements. (Sheathed thermocouples allow the instrumentation to be placed in areas where suppression may occur to minimize the affect the water had on the measurement.) Gas concentrations included the measurement of oxygen, carbon dioxide and carbon monoxide. Pressure measurements were made using differential pressure sensors to effectively determine pressure rise or drop relative to ambient (outside of the structure) conditions. Schmidt-Boelter gauges were used to measure total heat flux. Table 3.3 shows the icons used in the instrumentation floor plans in Sections 3.2.1 and 3.2.2.

Table 3.3: Instrumentation Legend

Icon	Instrumentation
	Thermocouple Array
	Bi-Directional Probe & Thermocouple Array
	Pressure Tap
	Gas Concentration Tap (O_2, CO_2, CO)
	Heat Flux

3.2.1 Basement

There were four thermocouple arrays in the basement, two bare-bead arrays and two inconel sheathed arrays. Four pressure taps, two gas measurement ports and one bi-directional probe array were also installed. Each thermocouple array consisted of nine thermocouples with a top thermocouple placement of 2.54 cm (1 in.) below the ceiling. The remaining eight thermocouples were spaced in 0.31 m (1 ft) intervals below the ceiling such that the bottom thermocouple was 2.44 m (8 ft) below the ceiling. Figure 3.3 shows the location of the instrumentation within the basement. Two bare bead arrays (A and B) were 0.46 m (18 in.) off the west stairwell wall, while the two inconel shielded thermocouple arrays (C and D) were 0.15 m (6 in.) off the east wall of the instrumentation room.

The four pressure taps were located 1.22 m (4 ft) above the floor and protruded from the walls surrounding the instrument room by approximately 5 cm (2 in.). The taps were centered along their respective walls as shown by their icons in Figure 3.3. The gas concentration measurement ports were located at two elevations (0.1 m (4 in.) and 1.22 m (4 ft)) and centered along the south wall of the instrument room.

The bi-directional probe and inconel-shielded thermocouple array was installed at the third step up from the basement level and 0.325 m (1 ft) off the east wall of the stairwell. Six probes and thermocouples in the array were evenly spaced with the top location 0.28 m (11 in.) from the ceiling.

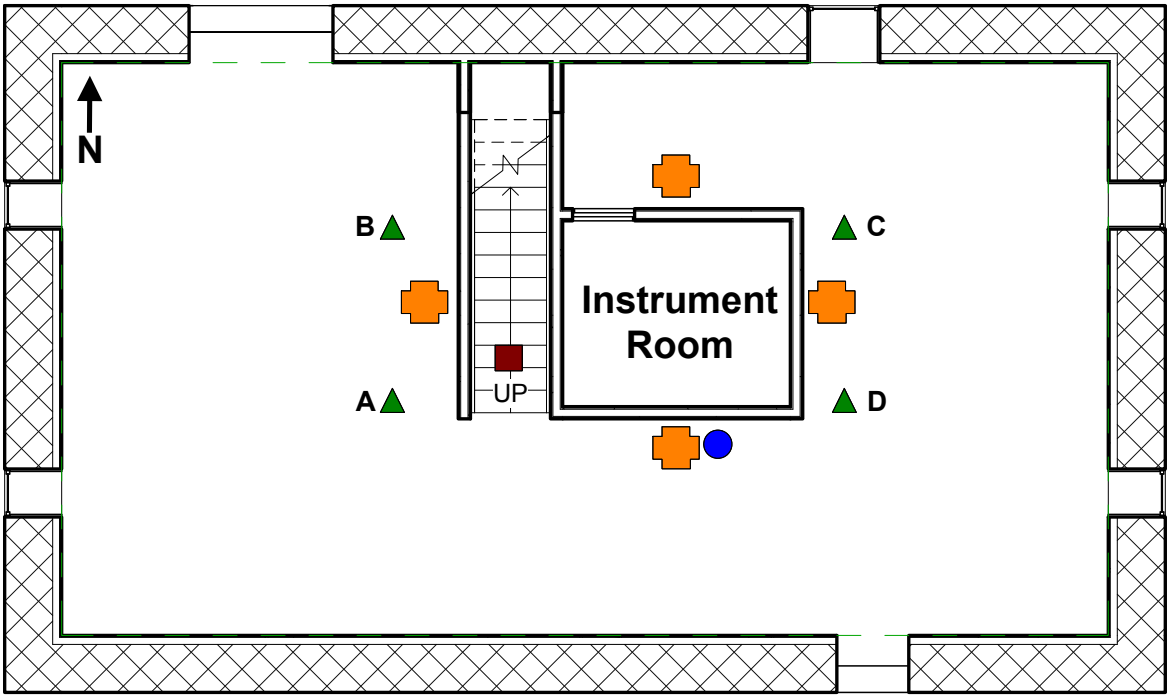

Figure 3.3: Instrumentation locations in the basement. Table 3.3 describes each instrumentation icon.

3.2.2 First Floor

Eight bare-bead thermocouple arrays were installed on the first floor. Each thermocouple array had eight thermocouples. The first was 2.54 cm (1 in.) below the ceiling, and the remaining seven thermocouples were spaced in 30.5 cm (1 ft) intervals below the ceiling (e.g. the bottom thermocouple was 213.5 cm (7 ft) below the ceiling). Each thermocouple tree was centered within its respective room, as shown in Figure 3.4. To measure pressure changes throughout the first floor, nine pressure taps were installed 1.22 m (4 ft) above the floor. In all cases, the pressure taps were centered along the walls as indicated by the pressure icons in Figure 3.4. Two gas concentration measurements ports were installed in the first floor; one centered along the east wall in bedroom 3

and one centered along the west wall of bedroom 2. In both cases, the probes were 1.22 m (4 ft) above the floor.

Two bi-directional probe and inconel-shielded thermocouple arrays were installed on the first floor. One array was installed at the top of the stairwell to the basement. Similar to the basement array, the probes were 0.325 m (1 ft) off the east wall of the stairwell. The other array was located 0.91 m (3 ft) off the south wall of the structure and 0.325 m (1 ft) off the west wall of the living room.

At the top of the stairwell, a 12.7 cm (5 in.) wide by 14.6 cm (5.75 in.) tall sample of turnout gear was installed 0.86 m (34 in.) above the floor along the north wall of the structure. The center of the sample was 0.49 m (19.25 in.) off the east wall of the stairwell. Two thermocouples were sewn into the gear to measure potential exposures, one on the outside of the outer shell fabric and one on the inside of the thermal liner of the gear. Centered behind the sample was a heat flux gauge. A second heat flux gauge was also installed 0.96 m (38 in.) above the floor but only 0.19 m (7.5 in.) off the east wall of the stairwell so that it was not protected by the gear sample. An inconel thermocouple was installed between the two heat flux gauges to measure the gas temperature local to the sample. The turnout gear had three layers, including an outer shell layer of TenCate Advance, a moisture barrier of Gore Crosstech Black, and a thermal liner of TenCate Caldura SL2i. According to information from TenCate, this three-layer composite has an NFPA 1971 TPP rating of 40 to 42.

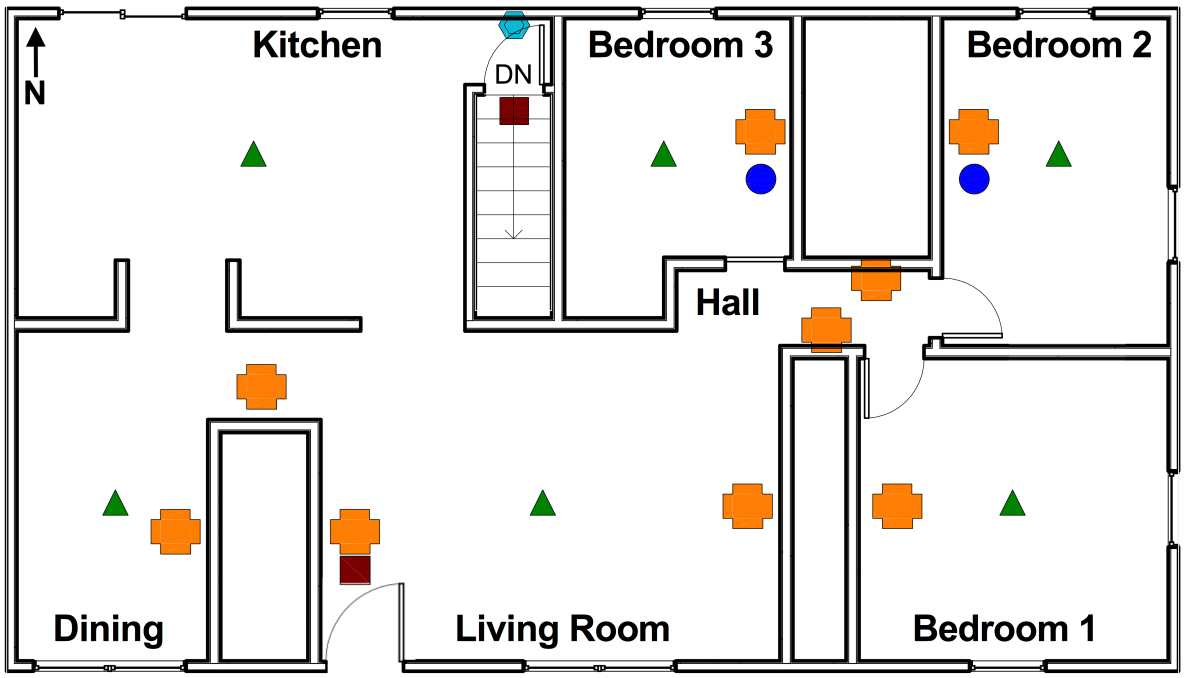

Figure 3.4: Instrumentation locations in the first floor. Table 3.3 describes each instrumentation icon.

3.2.3 Measurement Uncertainty

There were different components of uncertainty in the length, mass, temperature, heat flux, gas concentration, differential pressure, gas velocity, and water flow rate reported here. Uncertainties were grouped into two categories according to the method used to estimate them. Type A uncertainties were those evaluated by statistical methods, and Type B were those evaluated by other means [34]. Type B analysis of systematic uncertainties involved estimating the upper (+ a) and lower (- a) limits for the quantity in question such that the probability the value would be in the interval ($\pm$ a) is essentially 100 %. After estimating uncertainties by either Type A or B analysis, the uncertainties were combined in quadrature to yield the combined standard uncertainty. Then, the combined standard uncertainty was multiplied by a coverage factor of two, which resulted in an expanded uncertainty with a 95 % confidence interval (2σ). For some of these components, such as the zero and calibration elements, uncertainties were derived from referenced instrument specifications. For other components, referenced research results and past experience with the instruments provided input in the uncertainty determination.

Each length measurement was taken carefully. Length measurements, such as the room dimensions, instrumentation array locations, and fire apparatus (e.g., nozzle, sprinkler, or fan) placement, were made with a hand-held laser measurement device that had an accuracy of $\pm$ 6.0 mm (0.25 in.) over a range of 0.61 m (2.0 ft) to 15.3 m (50.0 ft) [35]. However, conditions affecting the measurement, such as levelness of the device, yielded an estimated uncertainty of $\pm$ 0.5 % for measurements in the 2.0 m (6.6 ft) to 10.0 m (32.8 ft) range. Steel measuring tapes with a resolution of $\pm$ 0.5 mm (0.02 in.) were used to locate individual sensors within an instrumentation array, and to measure and position the furniture. The steel measuring tapes were manufactured in compliance with NIST Manual 44, which specifies a tolerance of $\pm$ 1.6 mm (0.06 in.) for 9.1 m (30 ft) tapes and $\pm$ 6.4 mm (0.25 in.) for 30.5 m (100 ft) tapes [36]. Some issues, such as soft edges on the upholstered furniture, result in an estimated total expanded uncertainty of $\pm$ 1.0 %.

The load cell used to weigh the fuels prior to the experiments had a range of 0 kg (0 lb) to 200 kg (440 lb) with a resolution of a 0.05 kg (0.11 lb) and a calibration uncertainty within 1 % [37]. The expanded uncertainty is estimated to be less than $\pm$ 5 %.

The standard uncertainty in temperature of the thermocouple wire itself is $\pm$ 2.2 °C ($\pm$ 4 °F) at 277 °C (530 °F) and increases to $\pm$ 9.5 °C ($\pm$ 17.1 °F) at 871 °C (1600 °F) as determined by the wire manufacturer [38]. The variation of the temperature in the environment surrounding the thermocouple was known to be much greater than that of the wire uncertainty [39,40]. Small diameter thermocouples were used to limit the impact of radiative heating and cooling. The estimated total expanded uncertainty for temperature in these experiments is $\pm$ 15 %.

In this study, total heat flux measurements were made with water-cooled Schmidt-Boelter gauges. The manufacturer reports a $\pm$ 3 % calibration expanded uncertainty for these devices [41]. Results from an international study on total heat flux gauge calibration and response demonstrated that the uncertainty of a Schmidt-Boelter gauge is typically $\pm$ 8 % [42].

The gas measurement instruments and sampling system used in this series of experiments have

demonstrated an expanded (k = 2) relative uncertainty of ± 1 % when compared with span gas volume fractions [43]. Given the non-uniformities and movement of the fire gas environment and the limited set of sampling points in these experiments, an estimated uncertainty of ± 12 % is applied to the results [44].

Differential pressure uncertainty components were derived from pressure transducer instrument specifications and previous experience with pressure transducers. The transducers were factory calibrated and the zero and span of each were checked in the laboratory prior to the experiments, yielding an accuracy of ± 1 % [45]. The total expanded uncertainty was estimated as ± 10 %.

Bi-directional probes and single thermocouples were used to measure gas velocity. The bi-directional probes used similar pressure transducers as those used for the differential pressure measurements discussed above. Type K, 1.6 mm (0.0625 in) sheathed thermocouples were co-located with each probe. A gas velocity measurement study examining the doorway flow of pre-flashover compartment fires yielded expanded uncertainty measurements ranging from ± 0.14 to ± 0.22 for bi-directional probes of similar design [46]. The total expanded uncertainty for gas velocity in these experiments was estimated to be ± 18 %.

Water flow rate was measured with an 3.81 cm (1.5 in.) diameter electromagnetic flow meter. The meter consisted of stainless steel pipe lined with a non-conductive material. Energized coils on the outside of the non-conductive material imposed a magnetic field across the pipe. When the conductive fluid (water) flowed across the magnetic field, a voltage proportional to flow velocity was created. The manufacturer reports a ± 0.25 % calibration uncertainty for the accuracy of the measurement [47].

3.3 Fuel Load

The primary fuel load in the basement consisted of two sets of two sofas with an average mass of 48.7 kg ± 1 kg (107 lb ± 2.2 lb) and two sets of ten pallets. Each pallet was approximately 1.2 m (3.9 ft) by 1.0 m (3.3 ft) by 123 mm (4.8 in.) thick and ranged in mass from 11.2 kg (24.7 lb) to 26.4 kg (54.0 lb) with an average of 17.2 kg ± 2.9 kg (37.9 lb ± 6.4 lb). Five pallets were positioned behind each sofa to resemble a desk. Three pallets were set on end to form a U-shape and the remaining two pallets stacked on top (Figure 3.6). The sofa and pallet sets were arranged on each side of the stairwell as shown in Figure 3.5. Primary ignition occurred using an electric match on the center cushion on one of the sofas.

In addition to the sofas and pallets, the floor was lined with 22.4 m^2 (242 ft^2) of polypropylene (PP) carpet and polyurethane (PU) foam padding on each side of the stairwell (6.7 m (22 ft) by 3.35 m (11 ft)). The carpet was on average 33.1 kg ± 0.15 kg (73 lb ± 0.33 lb) and each piece of padding (two pieces of padding were used for each piece of carpet) was 9.6 kg ± 0.44 kg (21.2 lb ± 0.97 lb).

The exposed ceiling also contributed to the fuel load in the basement. The ceiling was lined with

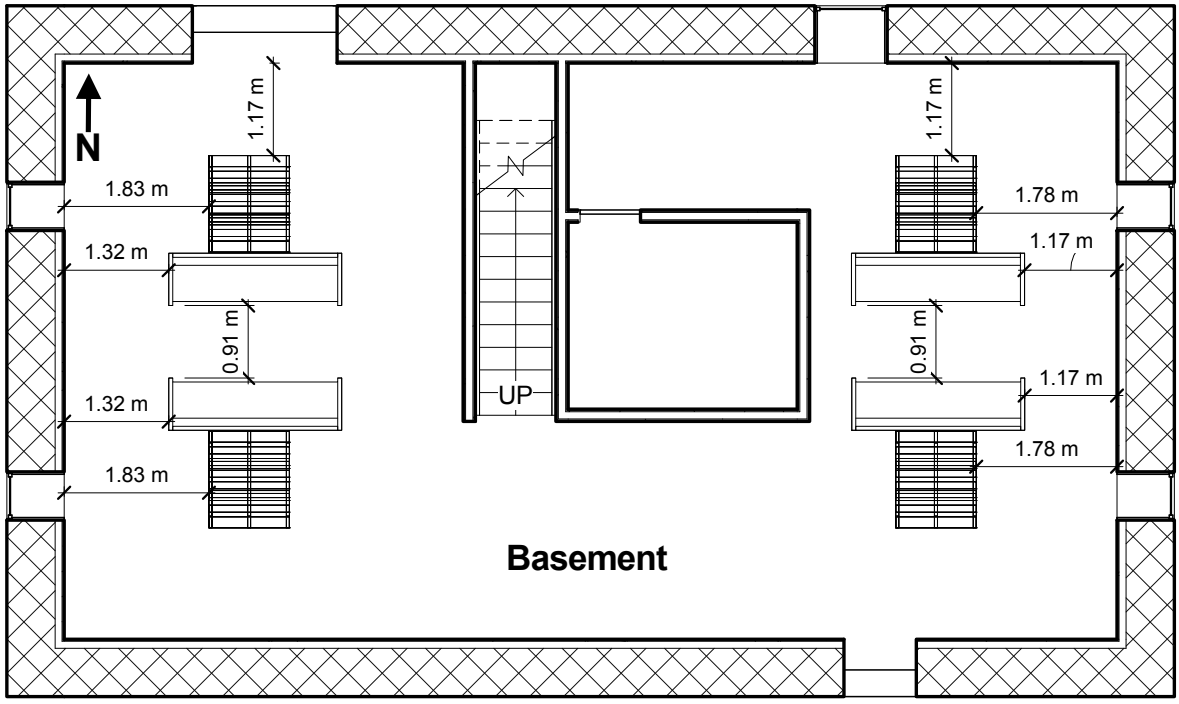

Figure 3.5: Dimensioned drawings of the fuel locations (pallets and sofas) in the basement.

1.27 cm (0.5 in.) thick OSB sheets and engineered wood i-joists. Each 1.2 m (4 ft) by 2.4 m (8 ft) OSB sheet had an average mass of 23 kg (50.6 lb). The wood I-joists were installed on 0.41 m (16 in.) centers and each 7.3 m (24 ft) long I-joist was 30.9 kg $\pm$ 1.6 kg (68.2 lb $\pm$ 3.5 lb). The wood i-joists were not load bearing. For this series of experiments, the collapse risk was removed because that had been studied previously. In these studies, the OSB and wood I-joist flooring system were in place as fuel-load and potential obstructions only.

In total, this fuel package was composed of wood, engineered wood, flexible PU foam, polyester (PE), and PP. Figure 3.6 shows the padding, carpet, sofas, pallets, OSB ceiling, and I-joists as they were installed during the experiments. All totaled, each side of the basement had a fuel load of approximately 900 kg (1,980 lb). On average, the fuel load for the basement was 27.3 kg/m^2 (5.6 lb/ft^2). This did not include the OSB panels on the floor of the basement.

Figure 3.6: Photograph of installed fuel package on the west side of the basement.

Three experiments in this series featured fuel loads different than that described above. Table 3.4 describes the differences in fuel load for the experiments with a varied configuration. Note that in Experiment 11, the addition of hay and OSB was to establish an ignition source at the ceiling level of the I-joists vs. a sofa ignition. Figure 3.7 shows the location of the hay and additional OSB, centered between the two sofas.

Table 3.4: Experiments with Fuel Variations

Experiment	Fuel Variation
7	Furniture on west side of basement only
9	Gypsum board ceiling, no exposed OSB or I-joists
11	Furniture on west side of basement only plus 8.7 kg (19.2 lb) hay and 10.7 kg (23.6 lb) OSB on ceiling above ignition sofas

Figure 3.7: Photograph of hay and OSB installed between I-joists for an experiment with a ceiling ignition.

3.3.1 Heat Release Characterization

To understand the energy release of the sofas (i.e., the primary ignition source) used in these experiments, three sofas were burned in Underwriters Laboratory's oxygen consumption calorimetry laboratory in Northbrook, Ill. The oxygen consumption calorimeter is sized to handle up to a 10 MW fire with a 9.44 m (31 ft) diameter conical hood. Bryant and Mullholland [48] estimate the uncertainty of oxygen consumption calorimeters measuring high heat release rate fires at $\pm$ 11%. They identify several sources of error within the calorimeter, with one of the primary sources being the uncertainty in the gas concentration measurements. Three identical sofas were burned, and their heat release rate (HRR) as a function of time appears in Figure 3.8.

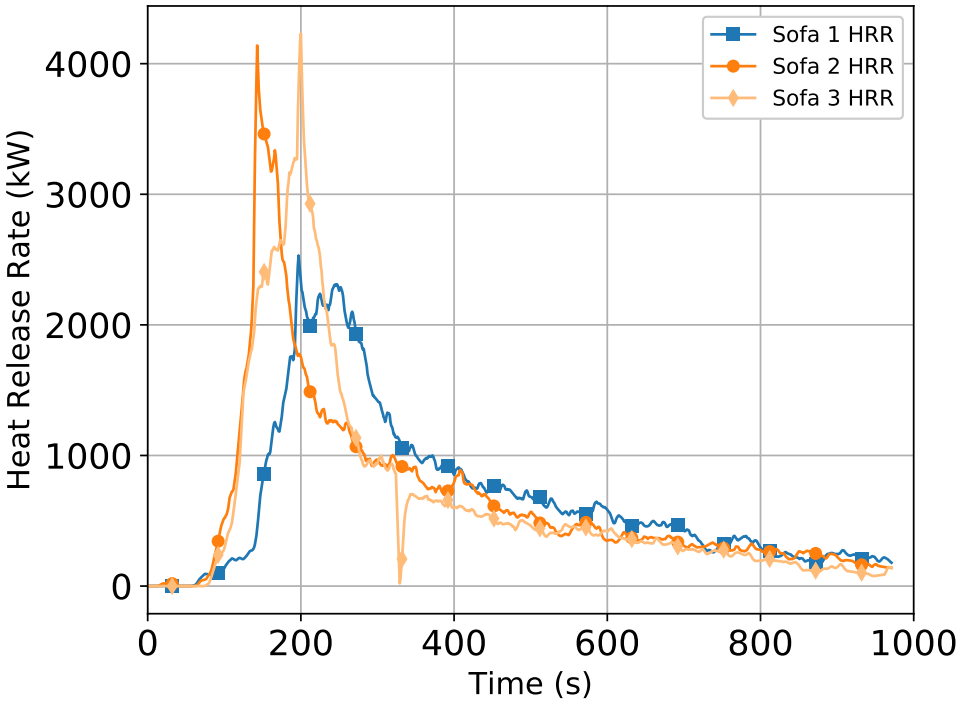

Figure 3.8: Heat release rate vs. time replicates for sofas used in experiments.

Sofa 1 had a peak HRR of 2,531 kW while the peak HRR for sofa 2 and sofa 3 were 4,140 kW and 4,230 kW, respectively. The peak HRR for sofas 2 and 3 fell within the typical uncertainty of the measurement. The peak HRR from sofa 1 was approximately 40% lower than the other two sofas, which highlights the natural variability of fuel. An integration over time for the HRR to calculate the total energy released showed more similarity (within 10%) between all three sofas. Table 3.5 shows the peak HRR and total energy release for each sofa.

Table 3.5: Sofa HRR Data

Sofa #	Peak HRR (kW)	Total Energy Released (MJ)
1	2,531	655
2	4,140	649
3	4,230	639

3.4 Firefighting Nozzles and Appliances

A variety of firefighting nozzles and appliances were used through the experiments described in Section 4. In total, six different nozzle configurations were used to provide suppression through the floor above the fire floor, through limited access windows on the fire floor, and through direct

access to the fire floor. The following sections describe the nozzles (type, pressure and flow rate) and appliances used.

3.4.1 Smooth Bore

A 15/16 in. diameter smooth bore nozzle was used during these experiments. The nozzle was capable of flowing 180 gpm with 50 psig water pressure at the nozzle. This nozzle was used when there was no or limited exterior access to the basement. Hence, the nozzle was flowed down through a hole in the floor assembly or through a small basement window. In the case of the small windows a fire department-fabricated basement window pipe was used. Figure 3.9 shows the smooth bore nozzle used in these experiments.

Figure 3.9: Example of smooth bore nozzle used in experiments.

3.4.2 Combination

A combination or adjustable spray pattern nozzle was used in all three types of basement access experiments. The nozzle was set to flow 150 gpm with a pressure at the nozzle of 75 psig. For cases in which there was no exterior access to the basement, suppression occurred through the floor or at the top of the stairs with the nozzle set to a fog stream. For the cases in which there was limited access (through basement windows) or direct access to the basement, the nozzle was set to straight stream. The combination nozzle used in these experiments is shown in Figure 3.10.

3.4.3 Cellar

The cellar nozzle was connected to a pipe with a 90 $^{\circ}$ bend and an extension with a bail to allow it to connect to fire hose and remain controllable while the nozzle end was through the floor. The cellar

Figure 3.10: Example of combination nozzle used in experiments.

nozzle used (see Figure 3.11) was set to flow 140 gpm at 100 psig. This nozzle was used when there was no exterior access to the basement and suppression occurred through a hole punched through the floor.

Figure 3.11: Example of cellar nozzle used in experiments.

3.4.4 Bresnan Distributor

The Bresnan distributor nozzle was used in a similar fashion as the cellar nozzle; it was connected to an extension pipe as shown in Figure 3.12. The Bresnan distributor flowed 160 gpm at 100 psig. This nozzle was used when there was no exterior access to the basement. The Bresnan distributor was used in experiments in which suppression took place through the floor.

Figure 3.12: Example of Bresnan distributor nozzle used in experiments.

3.4.5 Piercing

Two types of piercing nozzles were used. One nozzle flowed 125 gpm at 100 psig (Figure 3.13 (top)) and the other flowed 150 gpm at 100 psig (Figure 3.13 (bottom)). The 125 gpm piercing nozzle had a spray pattern that discharged small water droplets from a small ring of holes around the tube. The water spray extended approximately 3 m (10 ft) away from the nozzle on all sides (Figure 3.14). The larger piercing nozzle was flowed at 150 gpm for these experiments to provide comparisons to several of the other nozzles with similar water flow rates. This nozzle had a series of holes in a conical shaped tip that discharged water streams that tended to flow around and down from the nozzle more so than straight out horizontally from the nozzle (Figure 3.14). This resulted in the spray having a smaller area of interaction with fire gases and other fuels near the basement ceiling than the 125 gpm piercing nozzle. This nozzle has the capability with a higher nozzle pressure to flow 300 gpm or more.

The piercing nozzles were used in the experiments where there was limited or no exterior access to the basement. This resulted is suppression applications through the floor or through the large basement window.

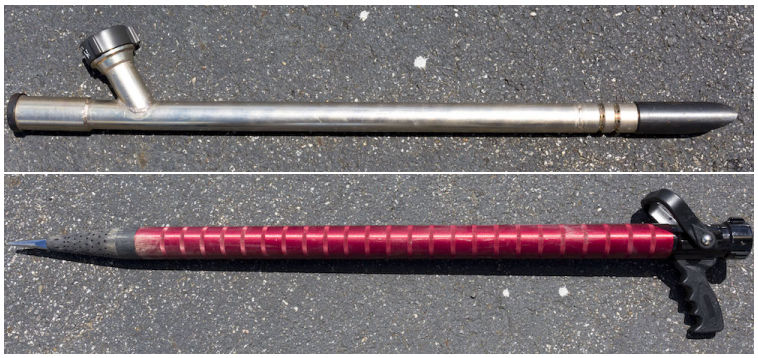

Figure 3.13: Examples of piercing nozzles: 125 gpm (top) and 150 gpm (bottom) used during experiments.

Figure 3.14: Examples of piercing nozzles: 125 gpm (left) and 150 gpm (right) spray patterns.

Section 4 Experiments

The configuration of ventilation openings was established prior to ignition. The main parameters were the status of the door (open or closed) at the top of the basement stairs and the front door. Additional pre-test ventilation setups included the status of the small windows on the east and west side of the basement, as well as the inclusion of 0.15 m (6 in.) diameter pipes in the basement to provide ventilation directly to the basement. Table 4.1 describes the different pre-ignition ventilation configurations.

Table 4.1: Ventilation Conditions

Configuration	Ventilation
Baseline	All exterior vents closed & stairwell door closed
Top of Stairs	Stairwell door open
Above Grade	Front door open & stairwell door open
Basement Windows (Location) *	Small basement window(s) open
Basement Leakage (#)	Addition of localized basement leakage pipes

* there were four basement windows, 2 each on the east and west side of the structure
# refers the number of leakage pipes open prior to ignition

The total area of the basement leakage when all four pipes were opened was approximately 735 cm^2 (114 $in.^2$) (Section 3.1). The pipes were installed in the wall at an access point between the concrete blocks on the south (side A) side of the basement (see Figure 3.1). Figure 4.1 shows the leakage pipes as they were installed for relevant experiments.

The experiments in this series can be categorized into three different groups based on access to the basement (Section 3): no exterior vents or access to the basement (see Table 4.2), exterior vents but no exterior access to the basement (see Table 4.4), and exterior vents with direct exterior access to the basement (see Table 4.6).

For the experiments in which suppression occurred through a hole punched through the floor connecting the first floor to the basement, that hole was located approximately 0.61 m (24 in.) from the doorway and 0.41 m (16 in.) off the wall immediately to the left of the front door. This location was selected to be close to the front door to minimize potential hazards to the firefighters who operated the nozzle. Note that this location did put an intentional bias toward the western half of the basement with respect to water flow.

Figure 4.1: Leakage pipes (0.15 m (6 in.) diameter) installed in the side A wall of the basement.

4.1 No Exterior Access to the Basement

Seven experiments had no windows, doors, or any other potential openings to either flow water, vent or gain entry to the basement. The basement was considered to be below grade, and the only access was entry via an interior stair. To isolate the basement, the four basement windows and large window shown in Figure 3.1 were covered over by 1.27 cm (0.5 in.) cement board. The double doors were closed, and any discernible gaps were sealed. Table 4.2 provides the status of ventilation prior to ignition and the suppression approach for the test, when applicable.

Table 4.2: No Exterior Access to Basement

Exp #	Pre-Ignition Ventilation	Suppression Details
1	Baseline	No suppression used
2	Top of stairs	No suppression used
3	Above grade	No suppression used
4	Above grade & basement leakage (x1)	Suppression through floor
10	Above grade & basement leakage (x4)	Sprinkler
11	Above grade & basement leakage (x4)	Suppression through floor
12	Above grade & basement leakage (x4)	Nozzle top of stairs

Experiments 1, 2, and 3 all featured the same fuel configuration, and an electric match was used to ignite the northeast sofa in the basement (see Figure 3.5). The difference between the experiments shown in Table 4.2 was the increase in pre-ignition ventilation between the tests. In Experiment 1,

all of the exterior doors and windows were closed prior to ignition, and the front door and stairwell door were opened 780 s and 970 s post ignition, respectively. The basement doors on the north side (side C) were opened 1,140 s post ignition. Experiment 2 differed because the stairwell door was open prior to ignition, and the front door and north side basement doors were opened 720 s and 915 s after ignition, approximately 250 s earlier than Experiment 1. Finally, Experiment 3 started with both the front door and stairwell door open and no additional ventilation was made during the duration of the experiment. For all three experiments, peak temperatures on the fire side of the basement reached approximately 600 °C (1,112 °F). However, no firefighter suppression was needed. Because there was no ventilation (airflow) on the same level as the fire, the fire in all three cases eventually self-extinguished. (Time history plots of temperature, pressure, velocity and gas concentration are included in Appendix B.1, B.2, and B.3 for Experiments 1, 2, and 3 respectively.) It is worth noting that the web of the wood I-joists had small areas of burn-through after only a few minutes of exposure to flames during these initial experiments.

For Experiment 4, ventilation was added to the basement in the form of 0.15 m (6 in.) diameter pipes shown in Figure 4.1. Prior to ignition of the northeast sofa in the basement, only one of the pipes was open, as noted in Table 4.2. At 270 s post ignition, the second pipe was opened. Pipes 3 and 4 were opened at 300 s and 330 s, respectively. The addition of ventilation directly to the basement provided sufficient oxygen to prevent the fire from self-extinguishing. To suppress the fire, five different nozzle and stream combinations were used through a hole punched through floor just inside the front door. The straight stream, when flowed into the basement from above, passed through the heated gases and impacted the floor. Table 4.3 shows the timing and duration of the suppression actions.

Table 4.3: Experiment 4 Suppression Actions

Nozzle & Stream	Start Time (s)	End Time(s)	Duration (s)
Straight Stream	1,084	1,105	21
150 gpm Piercing Nozzle	1,176	1,214	38
125 gpm Piercing Nozzle	1,364	1,453	89
Cellar Nozzle	1,648	1,742	94
Bresnan Distributor Nozzle	2,129	2,230	101
Basement Entry Side A Straight Stream	2,439	2,479	40
	2,507	2,542	35

(Appendix B.4 includes the time history plots of temperature, pressure, velocity, and heat flux for Experiment 4.)

Experiments 10, 11, and 12 all featured the same pre-ignition ventilation as Experiment 4, except that for these three experiments, all four basement leakage pipes (see Figure 4.1) were open prior to ignition. A residential sprinkler system was installed in the basement for Experiment 10.

Pendent-style residential sprinklers were installed below the unfinished basement ceiling in accordance with NFPA 13D [49]. NFPA 13D provides the following for basements with ceilings: “In basements where ceiling are not required for the protection of piping or where metallic pipe is in-

stalled, residential sprinklers shall be permitted to be positioned in a manner that anticipates future installation of a finished ceiling [49]." In Experiment 10, the sprinklers were positioned vertically to allow for the potential installation of 12.7 mm (0.5 in.) thick gypsum board.

The sprinklers were listed as residential sprinklers, meaning they had a fast-response thermal element. The sprinklers had a response time index (RTI) of 50 $(\text{m-s})^{\frac{1}{2}}$ or less with a temperature rating of 68 °C (155 °F). The k factor of the sprinklers was 4.9. The listing included a coverage area of 3.66 m (12 ft) square up to 4.88 m (16 ft) square with a water flow rate of 49.2 Lpm (13 gpm) at 48.2 kPa (7 psig).

The sprinkler system was self contained. It had a 1,136 L (300 gal) water supply connected to an electric pump rated for 75.7 Lpm (20 gpm) at 172.4 kPa (25 psig). The piping feeding the system was 3.81 cm (1.5 in.) diameter CPVC. Further details of the sprinkler arrangement appear in Figure 4.2.

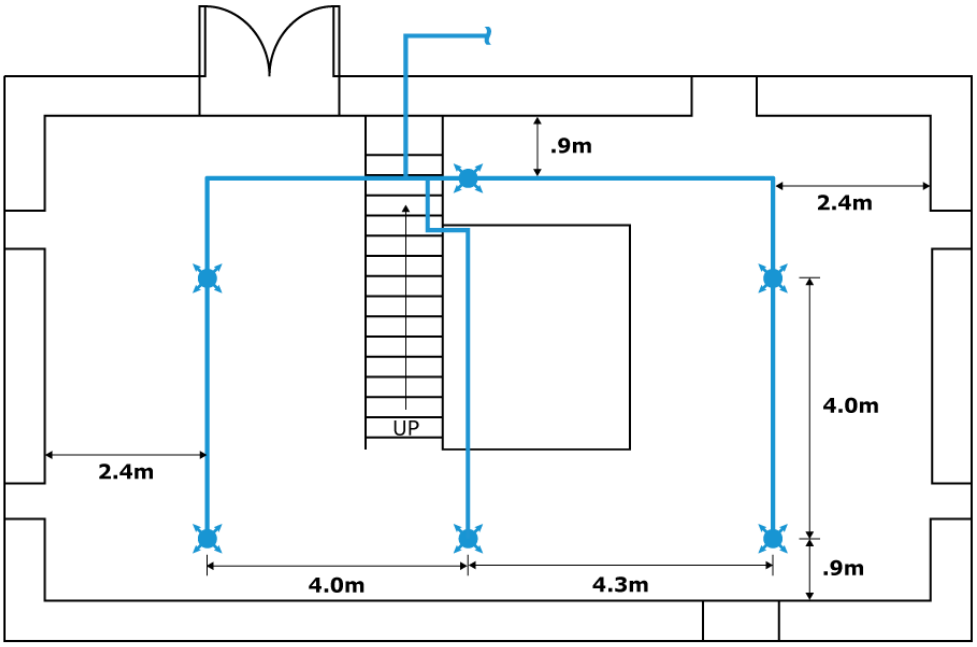

Figure 4.2: Floor plan indicating the location of the sprinkler heads and piping network installed for the experiment.

Ignition occurred on the southeast sofa. The sprinkler system activated 128 s after ignition, with the first sprinkler head activation occurring at the head closest to the sofa. In total, three heads activated: both heads on the ignition side of the basement, as well as the sprinkler head near the bottom of the stairwell. (Appendix B.10 includes the time history plots of temperature, pressure, gas concentration, and heat flux for Experiments 10.)

Similar to Experiment 4, Experiment 11 suppression occurred through a hole punched through floor with a 125 gpm piercing nozzle. In contrast to Experiment 4, the ignition point for this exper-

iment was on the west side of the basement at an elevated position, between the I-joists (Table 3.4 and Figure 3.7). Initial suppression through the floor occurred 877 s after ignition, but the full flow rate was not established until 940 s. The nozzle was shutdown 1,114 s after ignition. (Appendix B.11 includes the time history plots of temperature, pressure, gas concentration, velocity and heat flux for Experiments 11.)

To simulate an interior attack at the top of the stairwell, a nozzle was installed at the stairwell threshold in Experiment 12. Figure 4.3 shows the configuration prior to the test. Note that the bale was rigged to be opened from an exterior position. The nozzle was shut off by closing a gated wye valve that was also outside the structure.

Figure 4.3: Photographs of the nozzle at the top of the stairwell from the side (left) and looking down the stairs (right) in Experiment 12.

The combination nozzle was set to a narrow fog pattern, and suppression started 511 s after ignition and flowed for approximately 30 s. (The data for this experiment, including time history plots of temperature, pressure, gas concentration, velocity, and heat flux are included in Appendix B.12.)

4.2 Limited Exterior Access to the Basement

Three experiments were conducted using windows that did not provide direct access to the basement but could be used for venting and suppression. In these experiments, the four small windows (Figure 3.1) were not protected. The large window was still protected by 1.27 cm (0.5 in.) cement board, the double doors were closed, and any discernible gaps were sealed. Additionally, the interior stairwell door and front door were open at the time of ignition. Table 4.6 shows the three experiments increased in pre-ignition basement ventilation from one window to two windows to four windows and the respective suppression actions taken, when applicable. In these experiments, the basement leakage pipes were not used.

Table 4.4: Limited Exterior Access to Basement

Exp #	Pre-Ignition Ventilation	Suppression Details
5	Above grade & basement window (NE)	No suppression used
6	Above grade & basement window (NE & SE)	Suppression through small windows
7	Above grade & basement window (All 4) First floor slider & basement leakage*	Suppression through floor

* The side A cement board where pipes were installed was raised in lieu of the pipes such that the leakage area was approximately 1,271 cm ^{2} (197 in.^{2}).

In Experiment 5, the northeast basement window, in addition to the stairwell door and front door, was open prior to ignition. Ignition occurred on the north sofa on the east side of the basement. Similar to Experiments 1, 2, and 3, thermocouples on the ignition side reached approximately 600 °C (1112 °F), but no firefighter suppression was needed. Although there was ventilation to the basement via the window, due to its small size of 0.61 m (2 ft) x 0.25 m (10 in.) H and high sill 1.98 m (6.5 ft) above the floor, the ventilation was inefficient and the fire eventually self-extinguished. (The data for this experiment, including time history plots of temperature, pressure, gas concentration, velocity, and heat flux are included in Appendix B.5.)

For Experiment 6, both basement windows on the east of the basement were completely broken out (i.e., the pane was removed) prior to ignition on the north sofa on the east side of the basement. The windows on the west side of the basement were both broken after ignition with the southwest window broken 180 s after ignition and the northwest window broken 213 s after ignition. The basement temperatures peaked at approximately 600 °C (1,112 °F), but the fire was in decay until the sliding glass door on the first floor was opened 1,500 s after ignition to provide additional exhaust ventilation; then the fire started to grow again. For the experiment, four main suppression actions, outlined in Table 4.5, were taken. In each case, water was flowed for approximately 30 s, the fire was allowed to regrow and the next suppression action was performed.

(Appendix B.6 includes the time history plots of temperature, pressure, gas concentration, velocity, and heat flux for Experiment 6.)

Experiment 7 combined the basement window ventilation (all four small windows) and first floor

Table 4.5: Experiment 6 Suppression Actions

Nozzle & Stream	Start Time (s)	End Time(s)	Duration (s)
Straight Stream southwest (AB) window	1,800	1,831	30
Solid Stream Pipe southwest (AB) window	3,120	3,152	32
Straight Steam northeast (CD) window	3,480	3,510	30

slider open with the direct ground-level ventilation of the pipes. However, instead of using pipes, in Experiment 7 the side A cement board where pipes were installed in other experiments was raised in lieu of the pipes such that the leakage area was approximately 1,271 cm ^{2} (197 in.^{2}). This was in addition to the stairwell door and front door being open prior to ignition. Recall from Table 3.4, in Experiment 7 there were only pallets and sofas on the west side of the basement. The ignition sofa was the northwest sofa. Similar to Experiments 4 and 11, suppression was through the floor. The difference in Experiment 7 was that a combination nozzle was used and the fire was ignited on the west side of the basement, closer to the hole through the floor. A straight stream was applied 274 s after ignition and flowed for 32 s. The combination nozzle was switched to a fog stream and applied 375 s after ignition for 32 s. (Appendix B.7 includes the time history plots of temperature, pressure, velocity, and heat flux for Experiment 7.)

4.3 Exterior Access to the Basement

Two experiments were conducted in which the basement had a large window or door above grade that would allow ventilation, suppression, and entry. In these experiments, the four small windows were covered over by 1.27 cm (0.5 in.) cement board, but the protection was removed from the large window. In one experiment (Experiment 8), the double doors were replaced by a sliding glass door, while in the other experiment (Experiment 9), the double doors were closed, limiting access to just the large window. Table 4.6 shows the pre-ignition ventilation and suppression details.

Table 4.6: Access to Basement

Exp #	Pre-Ignition Ventilation	Suppression Details
8	Top of stairs & basement leakage (x2)	Suppression through basement slider
9	Above grade & basement leakage (x4)	Suppression through large window

Experiment 8 represented the impact of uncoordinated ventilation as well as suppression from a hand line on the same level as the fire. In this experiment, the double doors on the north side of the basement were replaced with a sliding glass door to create a walkout basement. Prior to ignition, the interior stairwell door was open and there were two 0.15 m (6 in.) diameter pipes to provide local ventilation. In this experiment, the leakage to the basement was designed to replicate a dryer vent with the exhaust passing through one of the small basement windows. Figure 4.4 shows the installation of the vents from inside and outside the basement.

Figure 4.4: Photographs of installed dryer vent from the inside of the basement (left) and outside the structure (right).

Ignition occurred on the northeast sofa in the basement. At 181 s after ignition, the front door was opened, followed by the basement slider being opened approximately 40 s later. The remaining portion of the basement slider was vented 549 s after ignition, and suppression with a straight stream hand line was not initiated until 621 s after ignition. (Appendix B.8 includes the time history plots of temperature, pressure, velocity, gas concentration, and heat flux for Experiment 8.)

For Experiment 9, the stairwell door and front door were open prior to ignition, and the four basement leakage pipes were installed and open. The fuel load was modified for this experiment (Table 3.4) as the OSB and engineered wood I-joists were not installed to examine potential impact of the ceiling being constructed from exposed fuel. Instead, the ceiling was finished with 1.59 cm (0.625 in.) gypsum board. The large window on the north side of the basement was used as the primary access to the basement. At 598 s after ignition, a piercing nozzle was used to make the initial attack through the window. Water flowed for 50 s before the piercing nozzle was shut down. The fire was allowed to regrow before an indirect straight stream attack was made 755 s after ignition for 27 s. Final suppression occurred 877 s after ignition for 15 s with a direct straight stream attack through the window. (The data for Experiment 9, including time history plots of temperature, pressure, gas concentration, velocity, and heat flux are included in Appendix B.9.)

Section 5 Results

Results from the experiments are grouped and presented in an order similar to Section 4: no exterior access to the basement, limited exterior access to the basement, and exterior access to the basement.

5.1 No Exterior Access to the Basement

5.1.1 Experiment 1

All exterior vents were closed prior to ignition in addition to the door at the top of interior stairwell. The fire was ignited on the north east sofa in the basement. Figure 5.1 shows the time history of the temperature profile at the thermocouple array closest to the area of ignition (see thermocouple array location C in Figure 3.3).

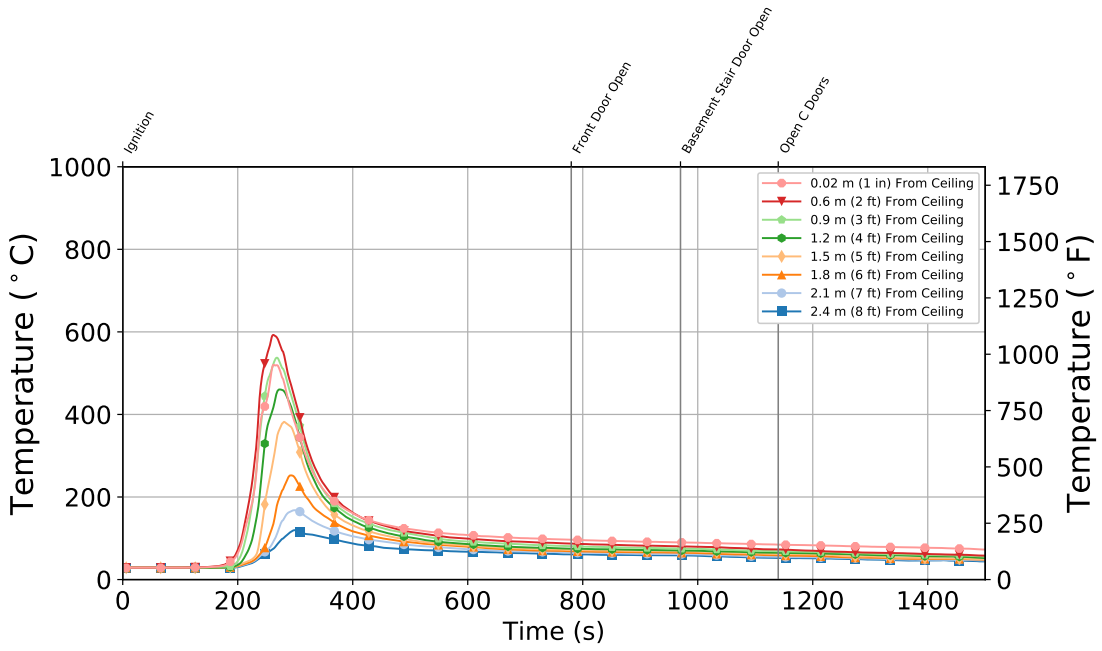

Figure 5.1: Experiment 1 - Thermocouple temperature time history from the Quadrant C thermocouple array in the basement.

The temperature curve followed the typical stages of fire growth: ignition, growth, fully developed, and decay. Because there were no suppression actions taken in Experiment 1, fire dynamics dictate that the decay occurred either because of a lack of fuel or a lack of oxygen. Figure 5.2 shows the fuel packages on the non-ignition and ignition side of the basement after Experiment 1 concluded.

Figure 5.2: Photographs of the post-fire fuel packages on the non-ignition side (left) and ignition side (right).

Examination of the gas concentration time history in Figure 5.3 in conjunction with the post-fire images, indicated that a lack of ventilation to the basement led to the fire being self-extinguished.

As the oxygen level decreased, the combustion efficiency was reduced. This resulted in an increase in carbon dioxide (CO_2) and carbon monoxide (CO) generation. Once the oxygen levels dropped below 15 %, flaming combustion was limited if not suppressed. In this experiment, flaming combustion ceased. (Note: the CO_2 measurement at the 1.2 m (4 ft) above the floor was not recorded due to an equipment problem.) To further illustrate the impact of ventilation, consider Figure 5.4. This thermocouple array was on ignition side, but notice that the peak temperatures were slightly higher than at the array closer to the ignition sofa in Figure 5.1. The reason for this was that there was more fresh air available for combustion at this location (from the non-ignition side of the basement and from flow down the stairs).

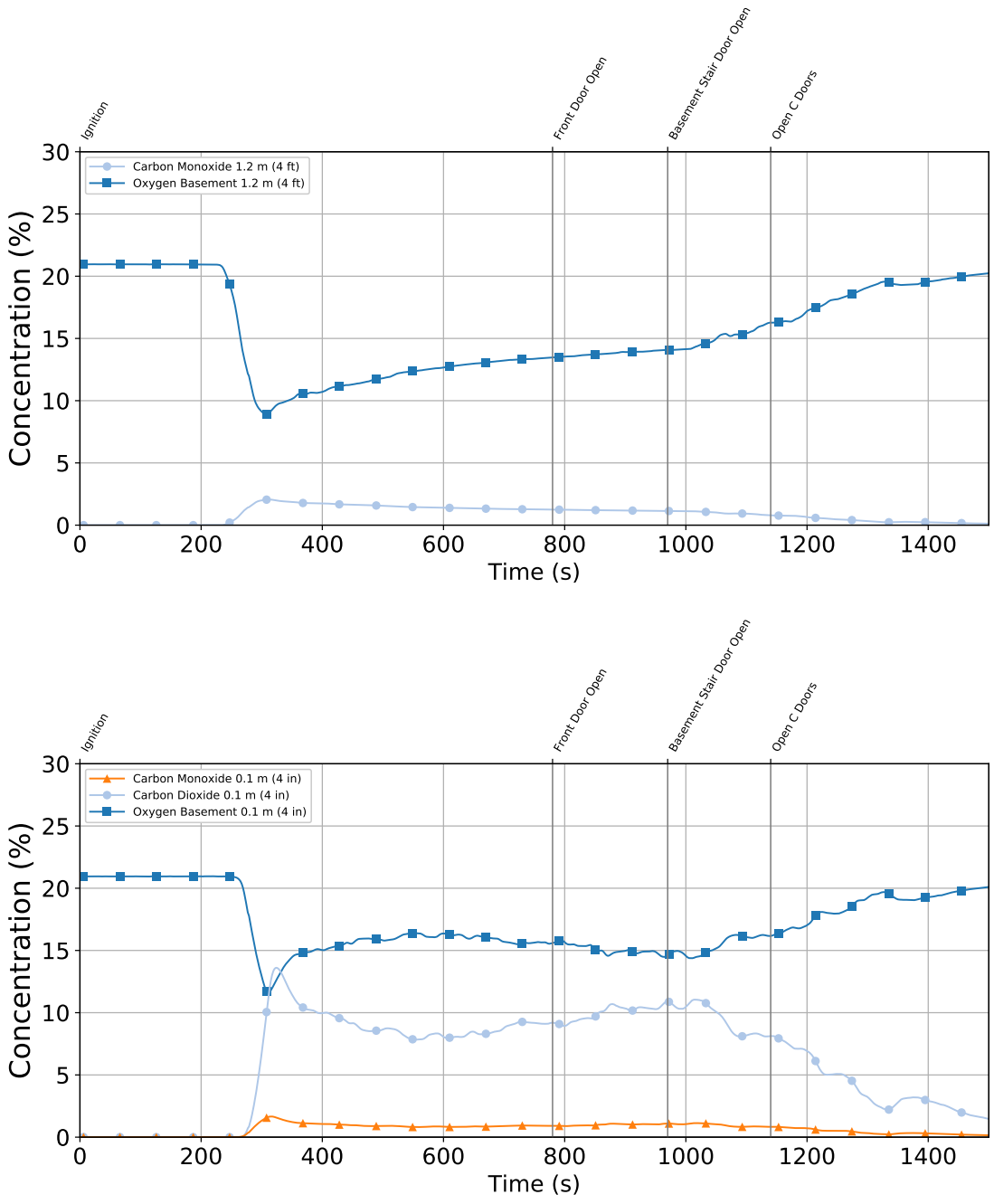

Figure 5.3: Experiment 1 - Gas concentration time history from the 1.2 m (4 ft) (top) and 0.1 m (4 in.) (bottom) elevations in the basement.

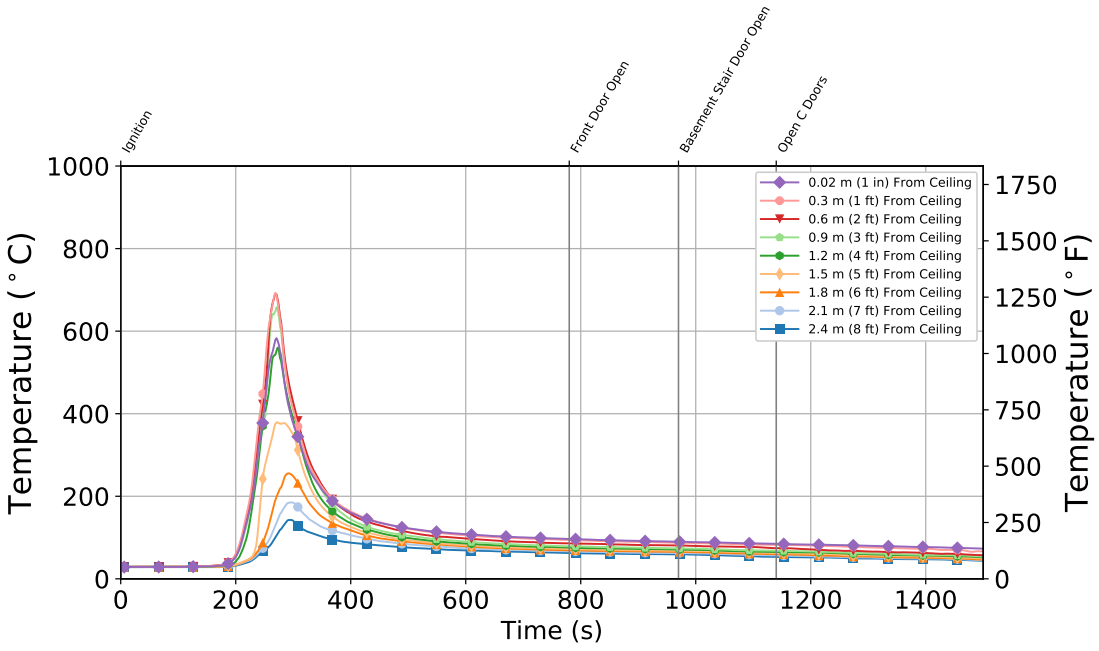

Figure 5.4: Experiment 1 - Thermocouple temperature time history from the Quadrant D thermocouple array in the basement.

To better understand the impact of the basement fire within the structure, consider pressure measurements made 1.2 m (4 ft) above the floor. Figure 5.5 shows the time history of basement pressure.

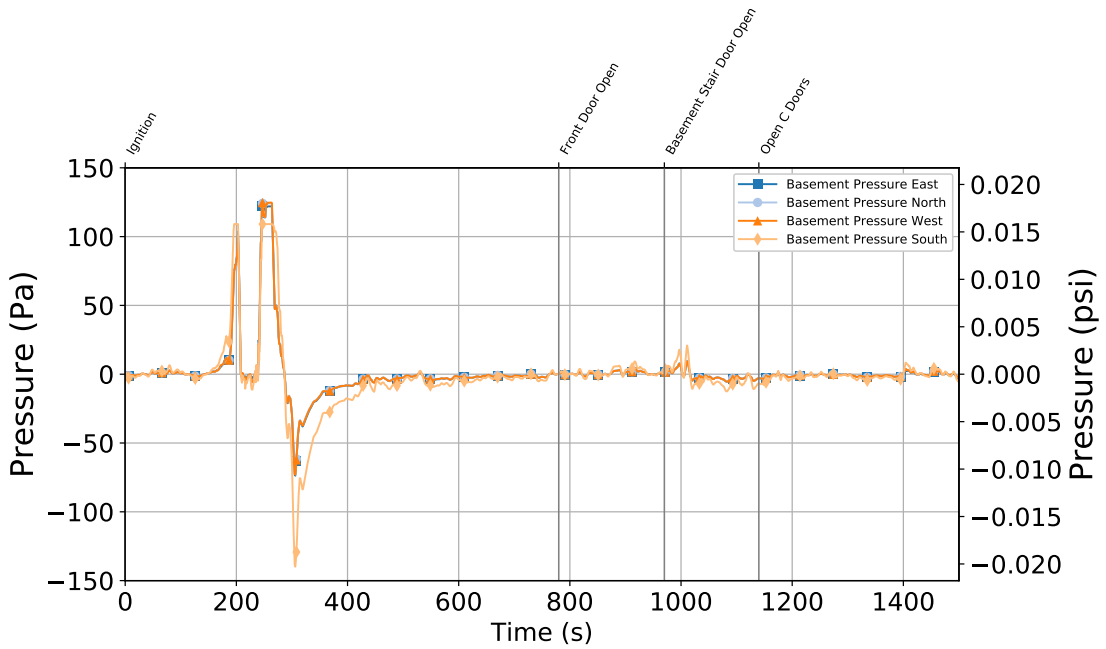

Figure 5.5: Experiment 1 - Basement pressure time history at 6 locations 1.2 m (4 ft) above the floor.

Notice the pressure pulses. Initially, the fire grew and the pressure built. As the oxygen was depleted, a hot gas layer developed, the volume of flaming fire decreased, and the pressure dropped. Then, air was drawn from other portions of the basement and around gaps at the stairwell door. Flaming combustion increased again but below the hot gas layer. Pressure increased again and exceeded the limits of the instrumentation (125 Pa or 0.018 psi). Once the oxygen dropped below the level to sustain flaming combustion, the heat release rate decreased. This resulted in a decrease in the temperature of the gases in the basement. The decrease in gas temperature caused the gas to contract, which resulted in a negative pressure in the basement. This means the pressure outside the basement was higher and air flowed into the basement through leaks and cracks until the pressure equalized.

Finally, an examination of the pressure throughout the first floor (Figure 5.6) as well as the gas concentration in the open bedroom on the first floor (Figure 5.7) showed the impact of the closed door.

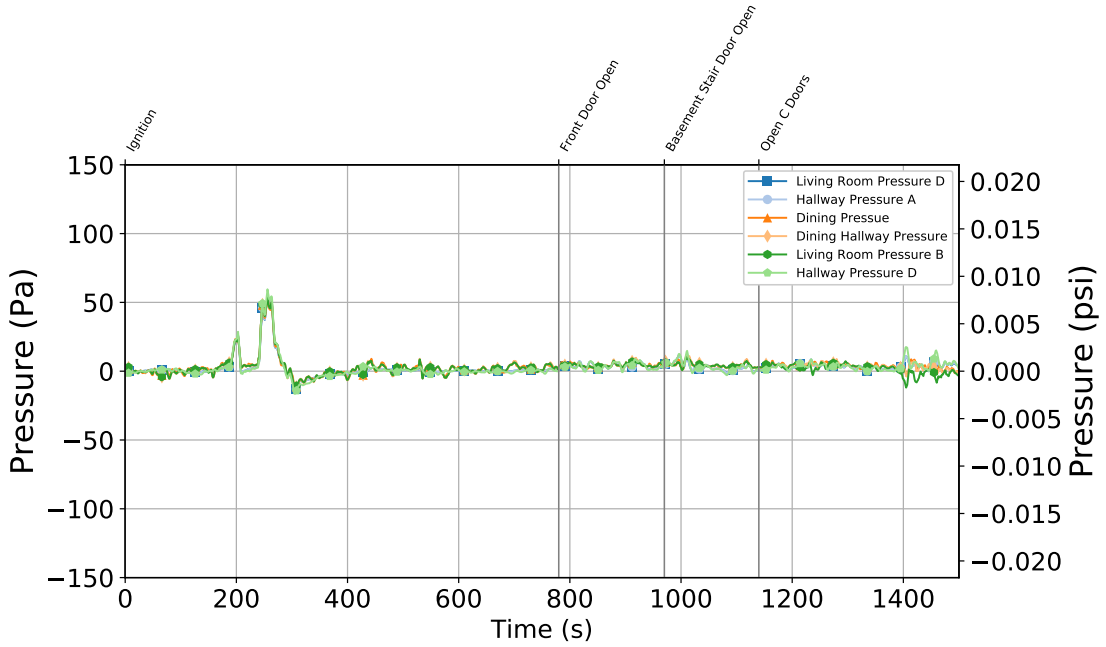

Figure 5.6: Experiment 1 - First floor pressure time history at 6 locations 1.2 m (4 ft) above the floor.

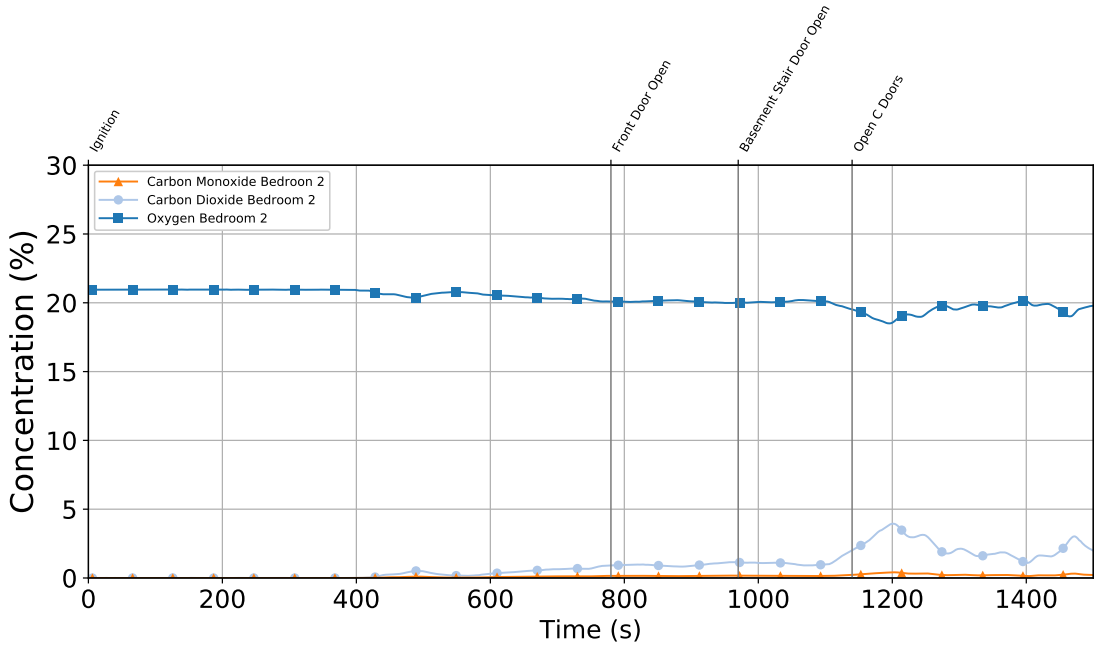

Figure 5.7: Experiment 1 - Gas concentration time history from the 1.2 m (4 ft) in the first floor open bedroom.

Pressure throughout the first floor showed similar behavior as the basement, but the closed stairwell door limited the flow of gases to the first floor, and therefore the magnitude of the pressure fluctua-

tions were smaller. Additionally, the lowest the oxygen concentration measured was approximately 20 %.

An overview of the conditions within the structure when the fire was at its peak (approximately 270 s after ignition) and 400 s after ignition appear in Figure 5.8. The red arrow indicates the flow of hot gases.

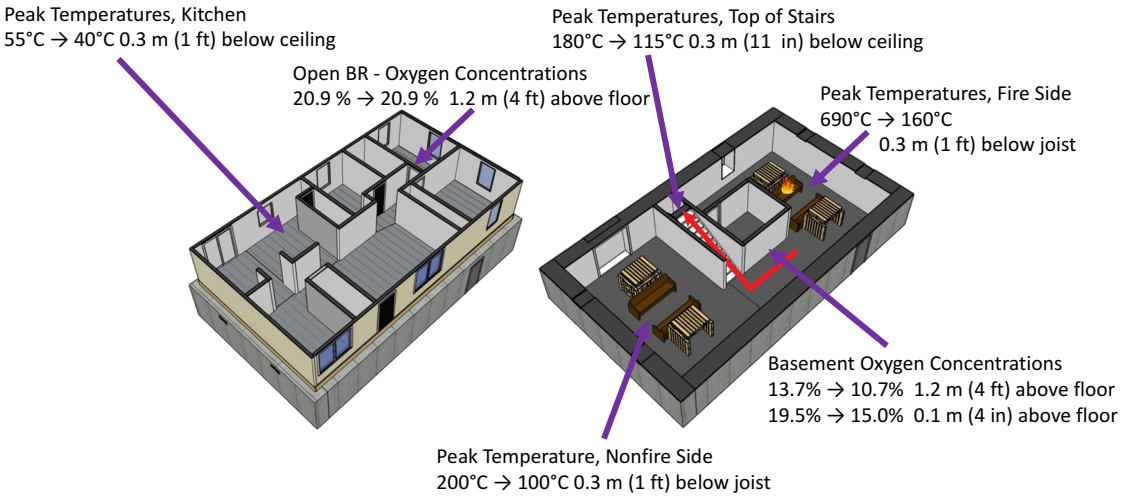

Figure 5.8: Experiment 1 - Isometric images of basement and first floor with selected measurements at peak conditions, 270 s after ignition, and at 400 s after ignition. The red arrow indicates the flow of hot gases.

5.1.2 Experiment 2

All exterior windows, doors, and vents were closed at the time of ignition. The interior door at the top of the stairwell was open prior to ignition. The ignition sofa was the northeast sofa in the basement, the same as Experiment 1. Figure 5.9 shows the time history of the temperature profile at the thermocouple array closest to the area of ignition (thermocouple array location C in Figure 3.3).

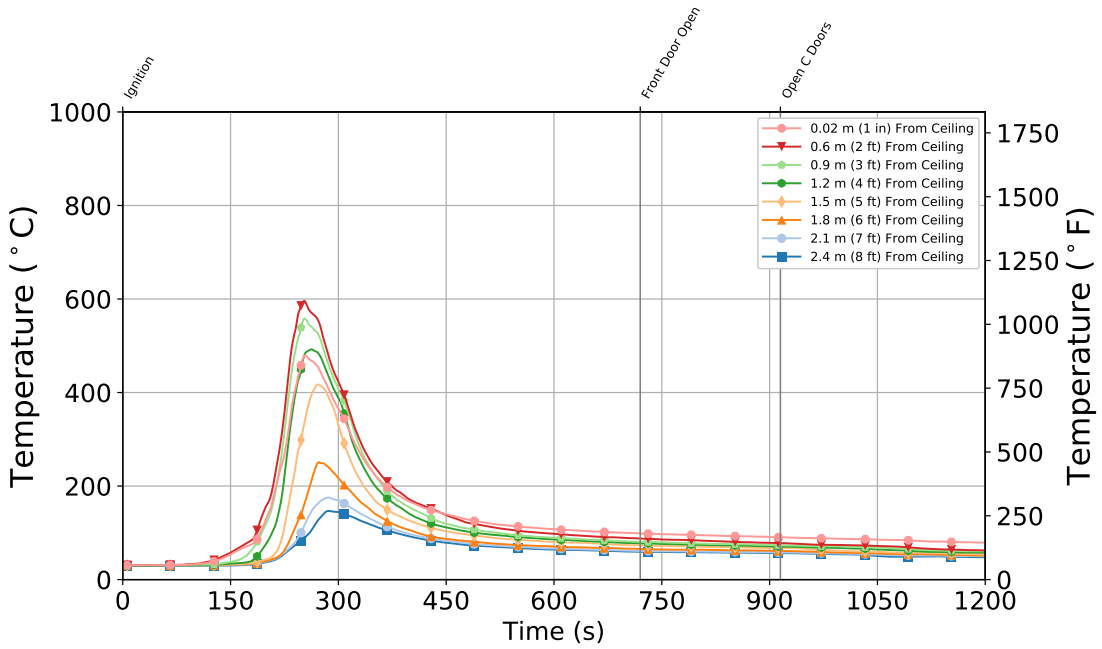

Figure 5.9: Experiment 2 - Thermocouple temperature time history from the Quadrant C thermocouple array in the basement.

The open stairwell door did not produce a significant change in the fire behavior in the basement compared to Experiment 1. The temperature curve followed the typical fire growth curve, including similar peak temperatures. The absence of firefighter suppression in Experiment 2 was related to the lack ventilation on the basement level. The low oxygen concentrations shown in Figure 5.10 coupled with excess fuel in the basement indicated the fire self-extinguished due to becoming too fuel rich.

One place where the impact of the open stairwell door is evident is with an examination of pressure in the basement and throughout the first floor (see Figure 5.11).

Notice the pressure pulses compared to Experiment 1. The open stairwell door did not have a noticeable impact on basement pressure, but without a closed door restricting flow to the first floor, the same behavior was evident throughout the first floor. For the pressure to increase on the first floor, combustion products from fire in the basement would had to fill the first floor. Gas concentrations in the open bedroom show the increased hazard on the first floor as a result of the open door. Figure 5.12 shows the oxygen concentration dropped below 15 % and that CO_2 and CO peaked at 9 % and 1 %, respectively — an increased hazard compared to Experiment 1.

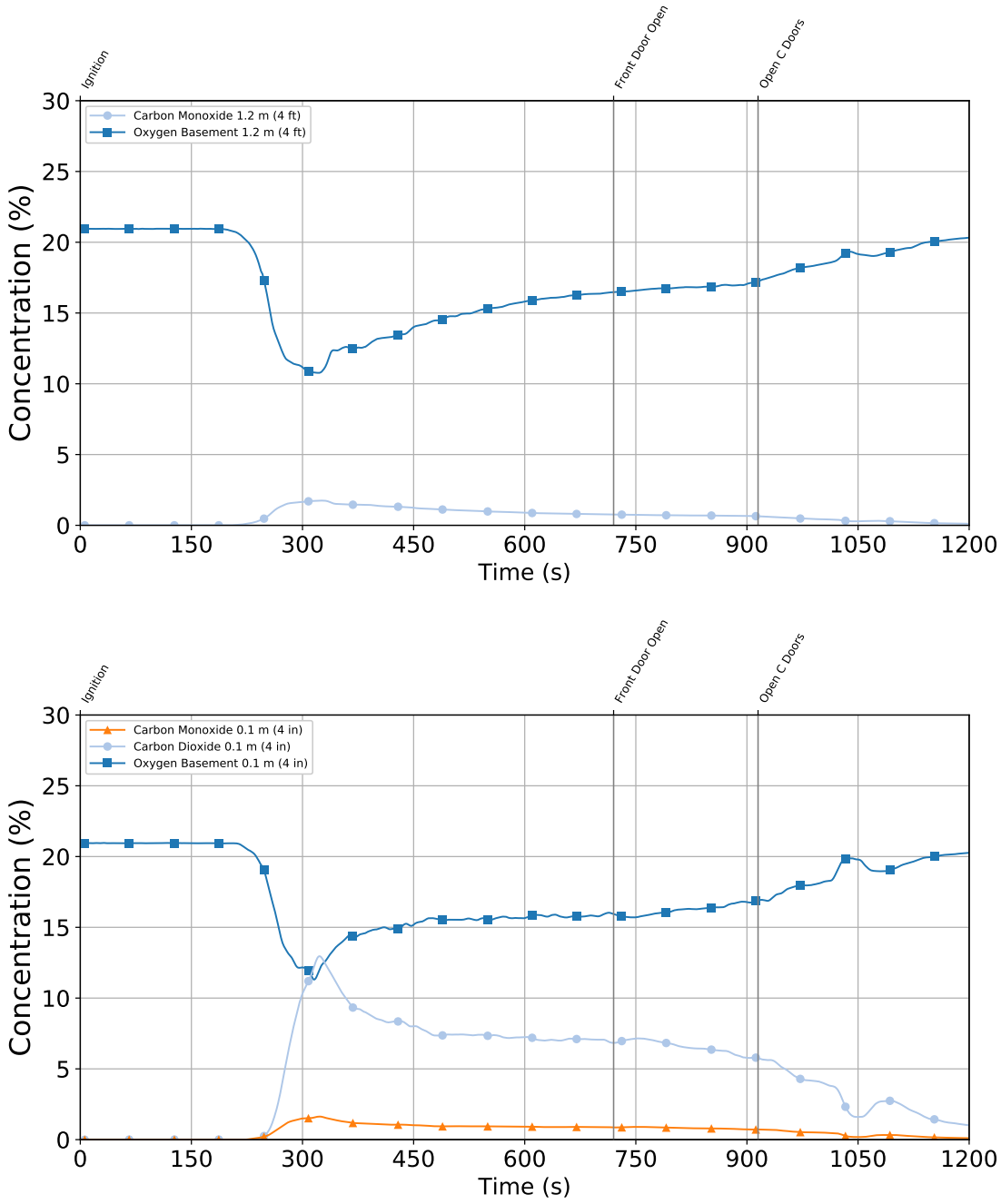

Figure 5.10: Experiment 2 - Gas concentration time history from the 1.2 m (4 ft) (top) and 0.1 m (4 in.) (bottom) elevations in the basement.

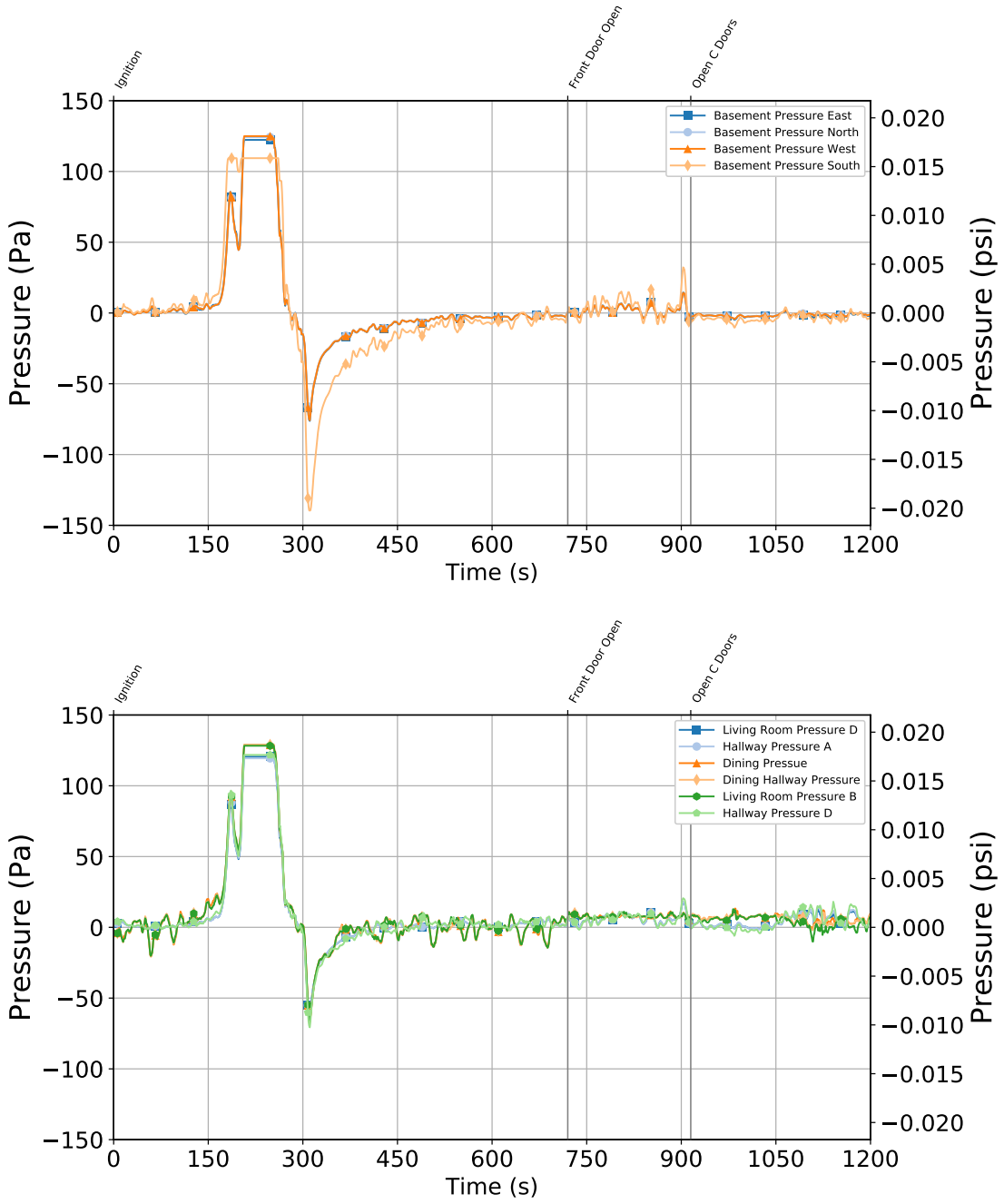

Figure 5.11: Experiment 2 - Pressure time history 1.2 m (4 ft) above the floor in the basement (top) and throughout the first floor (bottom).

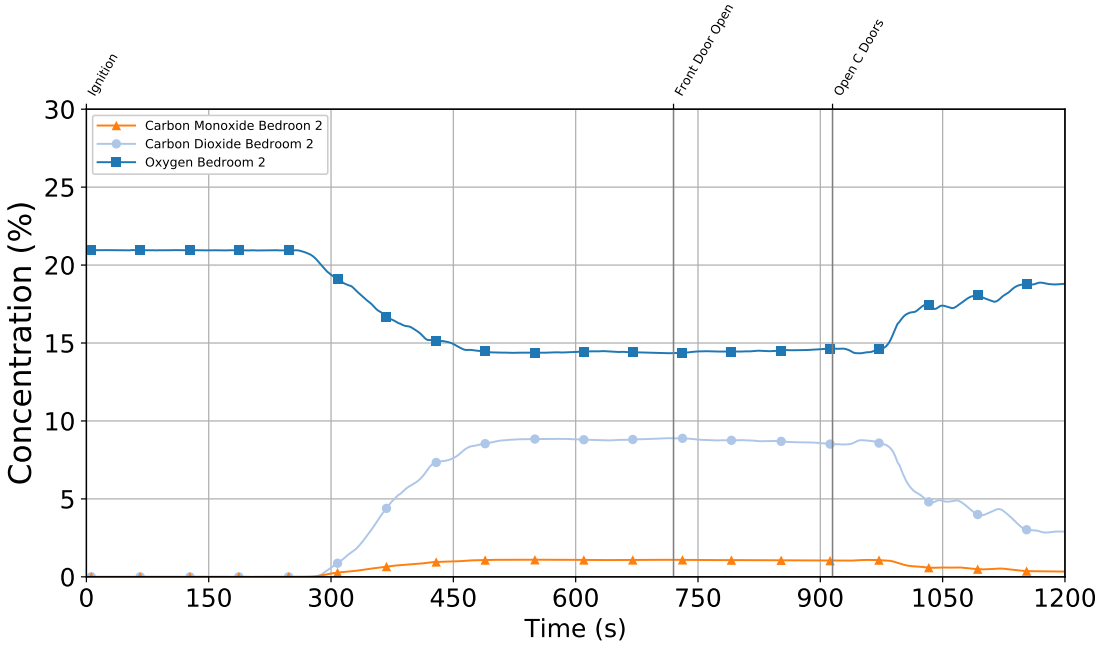

Figure 5.12: Experiment 2 - Gas concentration time history from the 1.2 m (4 ft) in the first floor open bedroom

An overview of the conditions within the structure when the fire was at its peak conditions (approximately 250 s after ignition) and 600 s after ignition appear in Figure 5.13. The red arrows indicate the flow of hot gases, and the green arrows indicate the flow of fresh air.

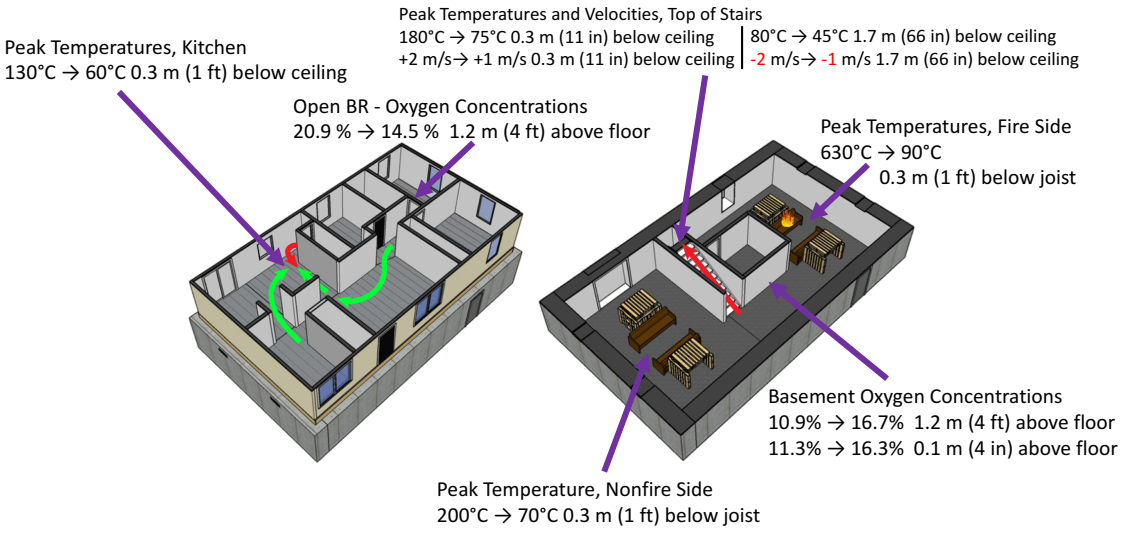

Figure 5.13: Experiment 2 - Isometric images of basement and first floor with selected measurements at peak conditions, 250 s after ignition, and 600 s after ignition. The red arrows indicate the flow of hot gases, and the green arrows indicate the flow of fresh air.

5.1.3 Experiment 3

All exterior windows and vents were closed prior to ignition. The interior stairwell door and the front door on the first floor were open prior to ignition. The ignition conditions were the same as Experiment 1 and 2. Examination of the temperature profile at the thermocouple array closest to the area of ignition, Figure 5.14, shows a similar temperature profile and peak values compared to Experiments 1 and 2.

The temperature curve followed the same fire-growth curve with similar peak temperatures as Experiments 1 and 2. The addition of the open front door for the duration of the experiment did not produce a noticeable impact on the basement temperature. The open exterior vent (front door) prevented significant pressure build-up within the structure. Figure 5.15 shows the change in pressure in the basement and on the first floor.

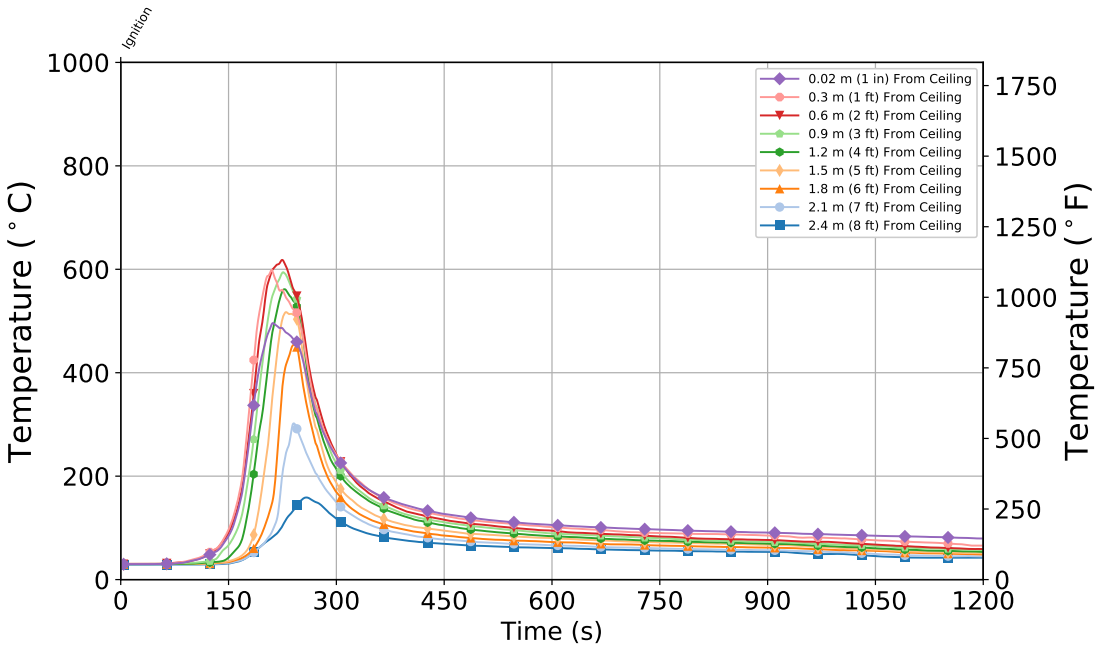

Figure 5.14: Experiment 3 - Thermocouple temperature time history from the Quadrant C thermocouple array in the basement.

The first floor showed no discernible pressure increases, and the maximum basement pressure increase was approximately 14 Pa (0.002 psi). There was still a negative pressure generated in the basement (Figure 5.15) as the gases cooled and contracted. However, because the structure was no longer closed, the magnitude was lower compared to Experiments 1 and 2.

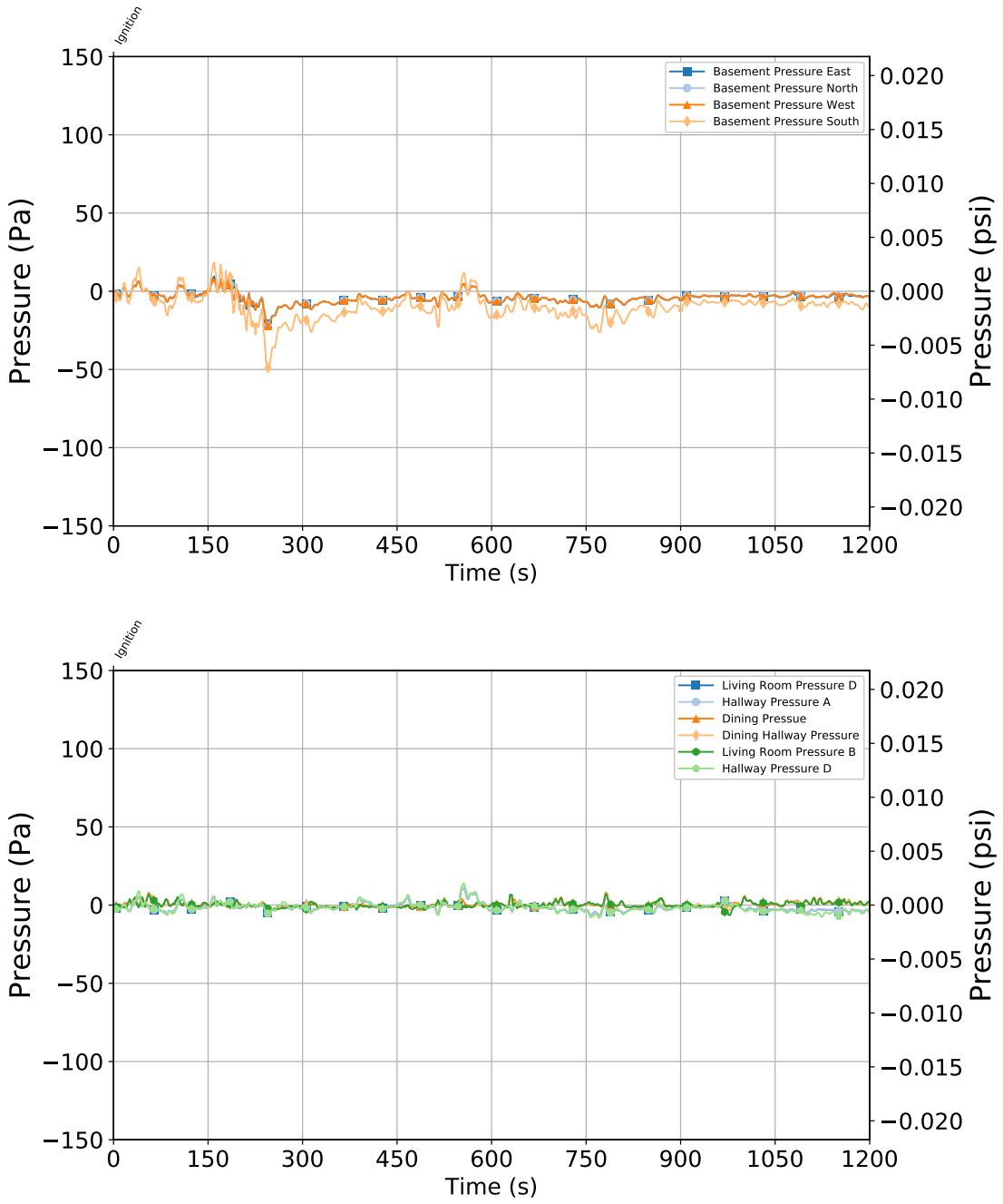

Figure 5.15: Experiment 3 - Pressure time history 1.2 m (4 ft) above the floor in the basement (top) and throughout the first floor (bottom).

Although the open front door provided an outlet for combustion gases to exit the structure as evident from the lack of pressure build-up, the exhaust flow path did not short circuit flow throughout the first floor. In other words, combustion products still filled open volumes as shown by the similar gas concentrations in the open bedroom (Figure 5.16) compared to Experiment 2 with the closed front door.

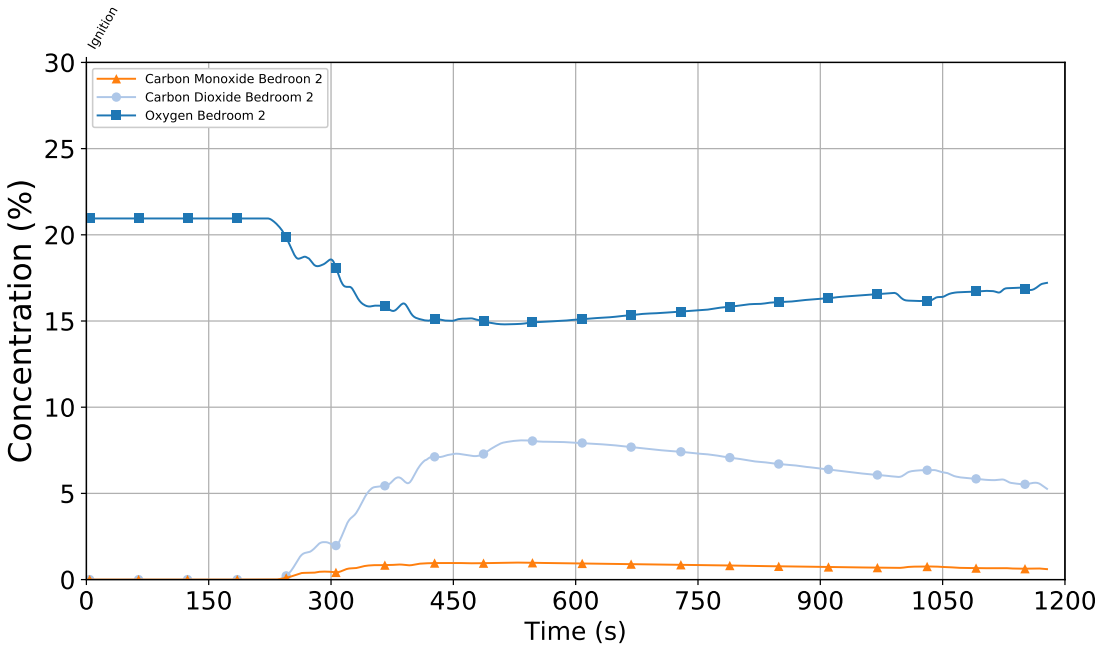

Figure 5.16: Experiment 3 - Gas concentration time history from the 1.2 m (4 ft) in the first floor open bedroom

An overview of the conditions within the structure when the fire was at its peak to conditions approximately 225 s after ignition and 600 s after ignition appear in Figure 5.17. The red arrows indicate the flow of hot gases, and the green arrows indicate the flow of fresh air.

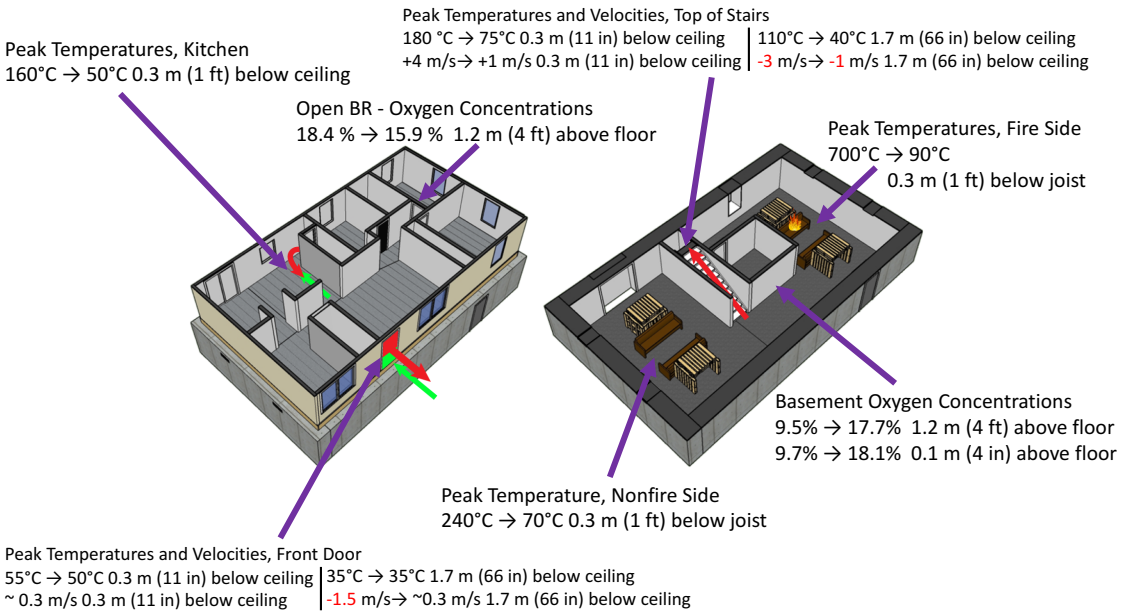

Figure 5.17: Experiment 3 - Isometric images of basement and first floor with selected measurements at peak conditions, 225 s after ignition and 600 s after ignition. The red arrows indicate the flow of hot gases and the green arrows indicate the flow of fresh air.

5.1.4 Experiment 4

All exterior windows were closed, but vent pipes were introduced into the basement along the south-side wall. One 0.15 m (6 in.) diameter pipe was open prior to ignition, and three additional pipes were opened at approximately 270 s, 300 s, and 330 s after ignition. The door at the top of the stairs and the front door were open for the duration of the experiment. The fire was ignited on the northeast sofa in the basement. Figure 5.18 shows the time history of the temperature profile at the thermocouple array closest to the area of ignition.

Experiments 1 through 3 had no opening or vent to the basement other than the door at the top of the stairs. Other than protecting the upstairs when closed, the door at the top of the stairs (essentially a vertical vent) did little to change the course of the fire in the basement. However, the small opening near the floor of the basement (low in the combustion compartment) provided enough oxygen to sustain a fire in the basement.

The temperature curve followed a similar fire-growth curve of ignition, growth, fully developed, and decay, but when the vent pipes in the basement were uncapped, sufficient oxygen was provided to allow the fire to regrow and reach a steady state before a series of suppression actions were performed (approximately 500 s after ignition). The suppression in this experiment occurred from a whole punched through the floor just inside the open front door. After each suppression action, the fire was allowed to regrow before the next operation was performed. (Recall the suppression actions and respective durations from Table 4.3.)

To further see the impact of the basement ventilation, consider pressure measurements made 1.2 m

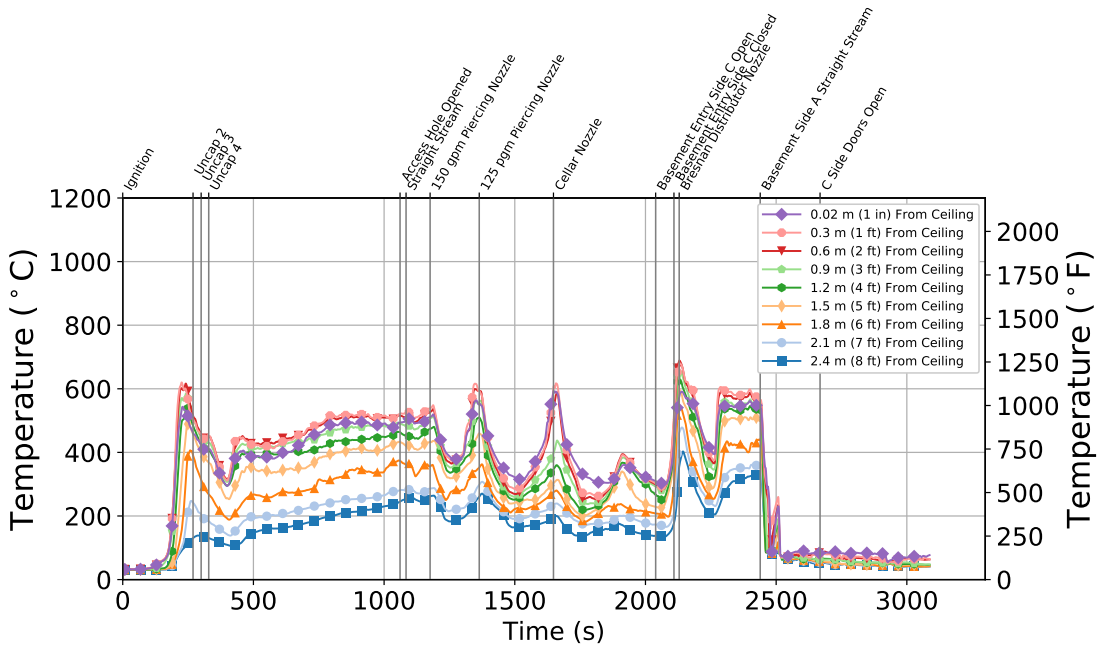

Figure 5.18: Experiment 4 - Thermocouple temperature time history from the Quadrant C thermocouple array in the basement.

(4 ft) above the floor. Figure 5.19 shows the time history of the basement pressure. For both Figure 5.19 and Figure 5.20, the time axis was adjusted to the start of the suppression actions.

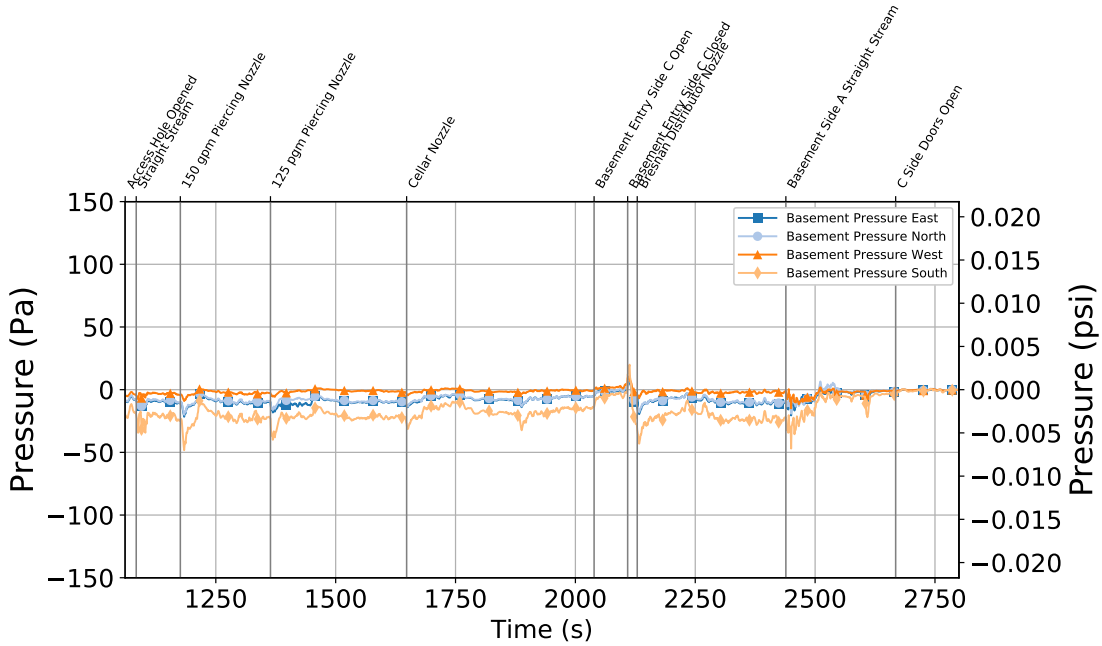

Figure 5.19: Experiment 4 - Basement pressure time history at four locations 1.2 m (4 ft) above the floor. The time axis begins when the suppression hole to basement was opened.

Note that the basement was under negative pressure. The potential exhaust vent size was the basement doorway at the top of the stairs. That opening measured about 1.67 m^2 (18 ft^2). From the velocities at the top of the stair (Figure 5.20), about two-thirds of the doorway was used as an exhaust vent, or about 1.1 m^2 (12 ft^2). The remaining 0.55 m^2 (6 ft^2) of the doorway was used as an intake. The total area of the basement floor intake vent pipes was 0.07 m^2 (0.8 ft^2). Therefore, the exhaust was outflowing the intake vents given the 2 to 1 exhaust vent area advantage with convection aiding the exhaust flow up the stairs. The result was negative pressure in the basement.

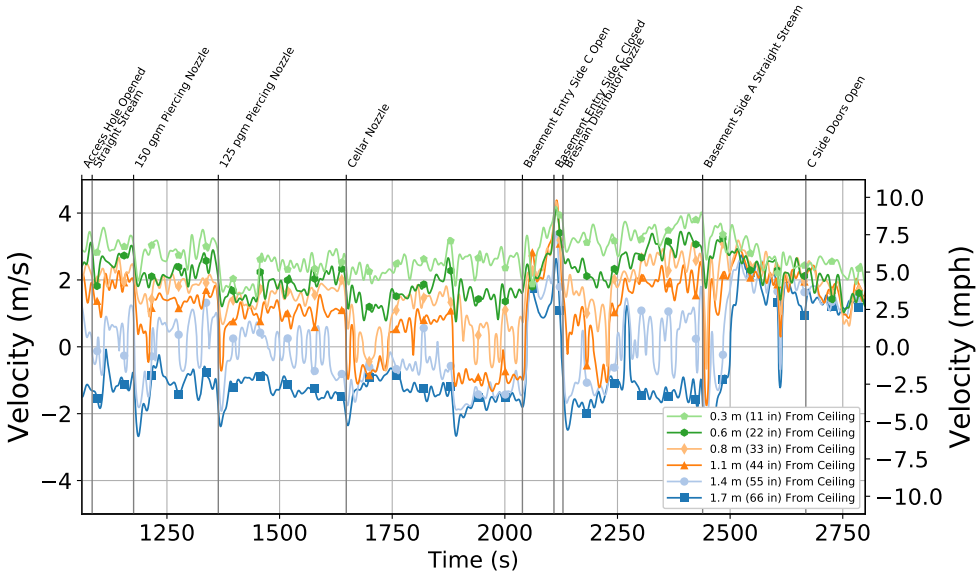

Figure 5.20: Experiment 4 - Velocity measurements at the top of the interior stairwell. The time axis begins when the suppression hole to basement was opened.

When the Side-C basement doors were opened between 2,039 s and 2,109 s, all the velocities at the top of the stairs were positive indicating a uni-directional flow. This was because the open basement doors (at the same level as the fire) acted as a large intake vent.

Figures 5.21 – 5.25 show the impact throughout the structure from the suppression actions taken through the floor. The red arrows indicate the flow of hot gases and the green arrows indicate the flow of fresh air. The blue icon represents the suppression location. Note that as shown in Figure 5.18 and Figure 5.25, the act of opening and subsequently closing the basement side c doors shortly before using the Bresnan distributor nozzle was likely a contributing factor in the sharp changes in temperature.

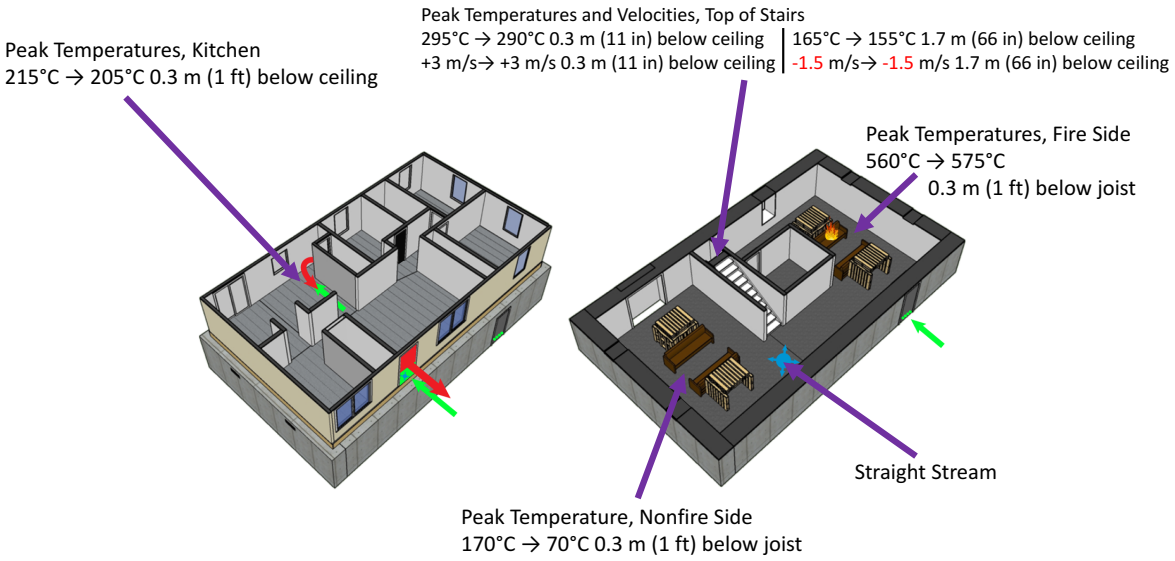

Figure 5.21: Experiment 4 - Isometric images of basement and first floor with selected measurements at time of straight stream suppression. The first set of numbers was 1,084 s after ignition (just prior to the start of hose stream), and the second was at 1,105 s post ignition, after the stream was shut down. The straight stream flowed for approximately 20 s. The red arrows indicate the flow of hot gases, the green arrows indicate the flow of fresh air, and the blue icon indicates the location of suppression.

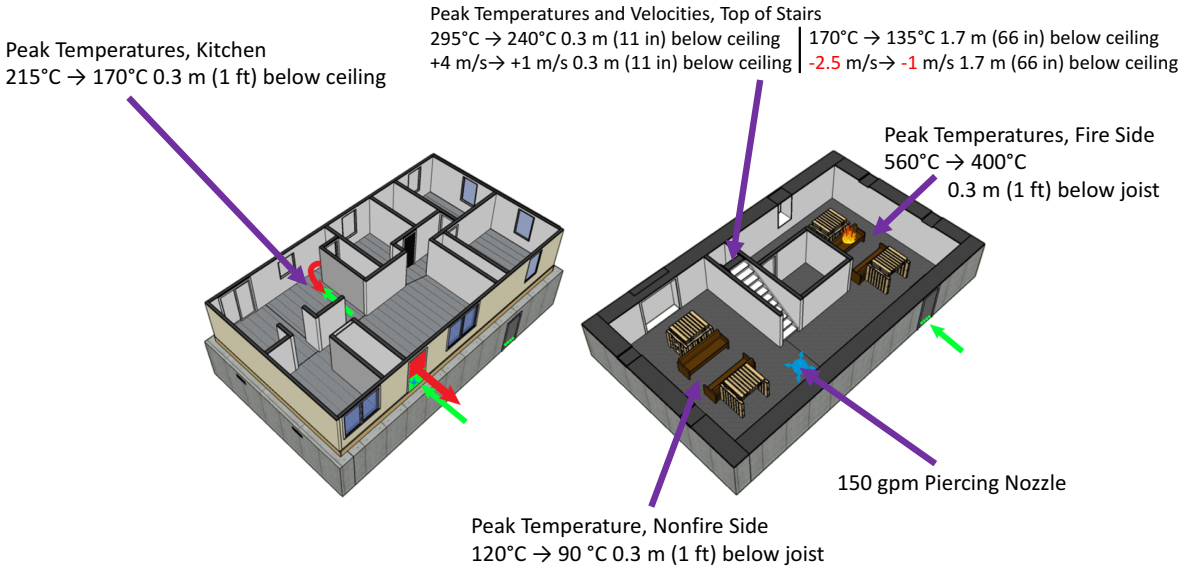

Figure 5.22: Experiment 4 - Isometric images of basement and first floor with selected measurements at time of water application from a 150 gpm piercing nozzle. The first set of numbers was 1,176 s after ignition (just prior to the start of water flow), and the second was 1,230 s post ignition, after the water was shut down. The 150 gpm piercing nozzle flowed for approximately 40 s. The red arrows indicate the flow of hot gases, the green arrows indicate the flow of fresh air, and the blue icon indicates the location of suppression.

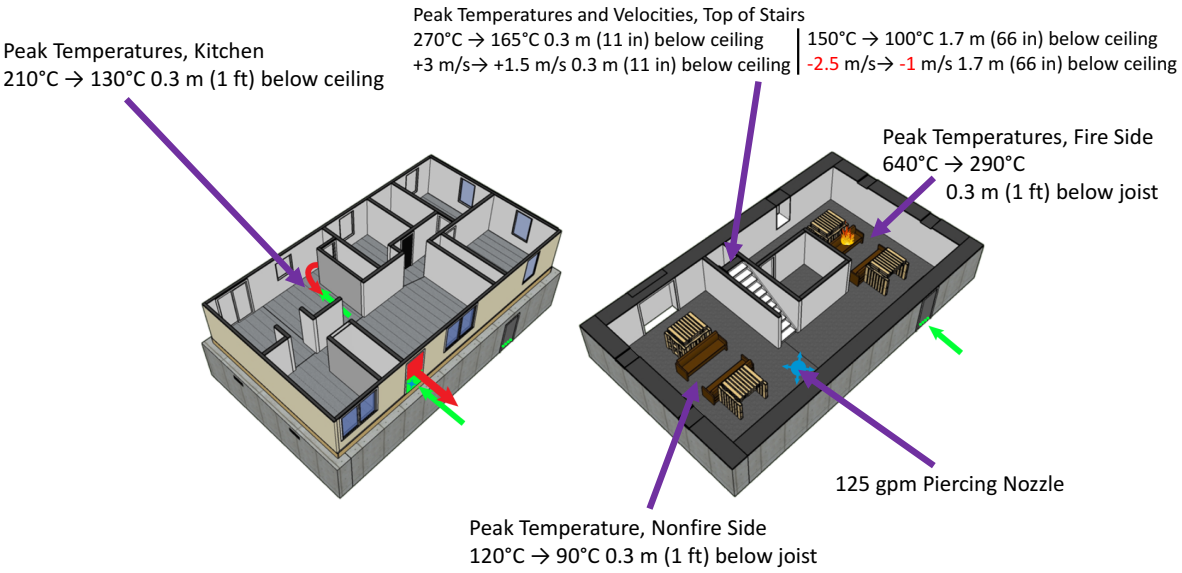

Figure 5.23: Experiment 4 - Isometric images of basement and first floor with selected measurements at time of water application from a 125 gpm piercing nozzle. The first set of numbers was 1,364 s after ignition (just prior to the start of water flow), and the second was 1,500 s post ignition, after the water was shut down. The 125 gpm piercing nozzle flowed for approximately 90 s. The red arrows indicate the flow of hot gases, the green arrows indicate the flow of fresh air and the blue icon indicates the location of suppression.

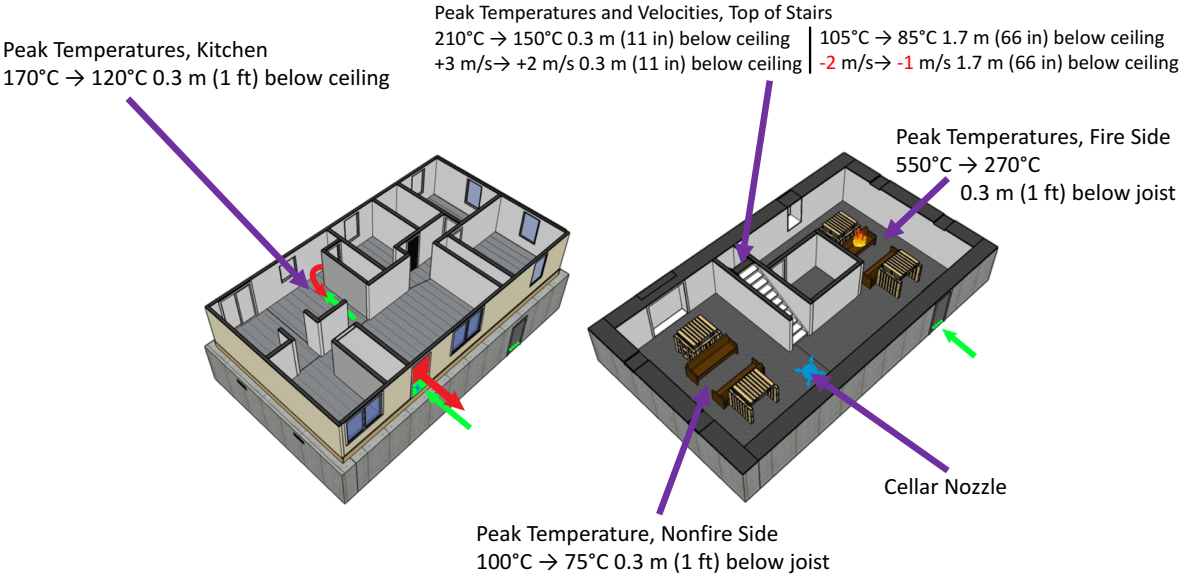

Figure 5.24: Experiment 4 - Isometric images of basement and first floor with selected measurements at time of water application from a cellar nozzle. The first set of numbers was 1,648 s after ignition (just prior to the start of water flow), and the second was 1,764 s post ignition, after the water was shut down. The cellar nozzle flowed for approximately 95 s. The red arrows indicate the flow of hot gases, the green arrows indicate the flow of fresh air, and the blue icon indicates the location of suppression.

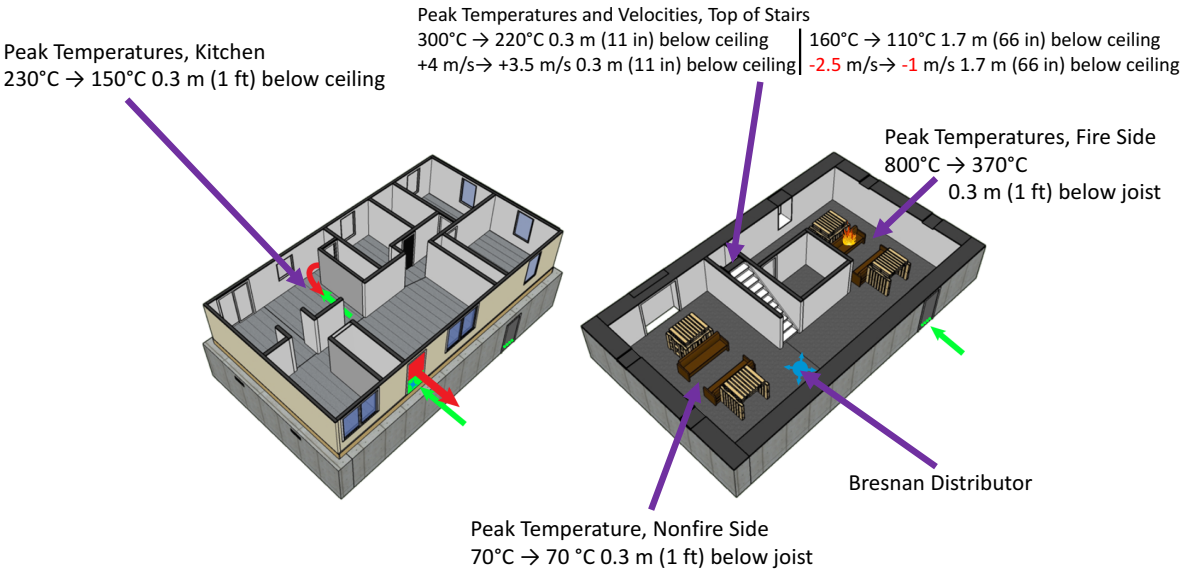

Figure 5.25: Experiment 4 - Isometric images of basement and first floor with selected measurements at time of water application from a Bresnan distributor nozzle. The first set of numbers was 2,129 s after ignition (just prior to the start of water flow), and at the second was 2,275 s post ignition, after water was shut down. The Bresnan distributor nozzle flowed for approximately 100 s. The red arrows indicate the flow of hot gases, the green arrows indicate the flow of fresh air, and the blue icon indicates the location of suppression.

5.1.5 Experiment 10

All exterior windows and the front door were closed, but all four basement ventilation pipes along the south-side wall were open prior to ignition. The interior door at the top of the stairwell was open prior to ignition. The ignition sofa was the southeast sofa in the basement. A six-head, self-contained (pump and water supply tank) NFPA 13D compliant sprinkler system was installed in the basement (see Figure 4.2). The first sprinkler activated 128 s after ignition. In total, three sprinklers activated. Figure 5.26 shows the time history of the temperature profile at the thermocouple array closest to the area of ignition.

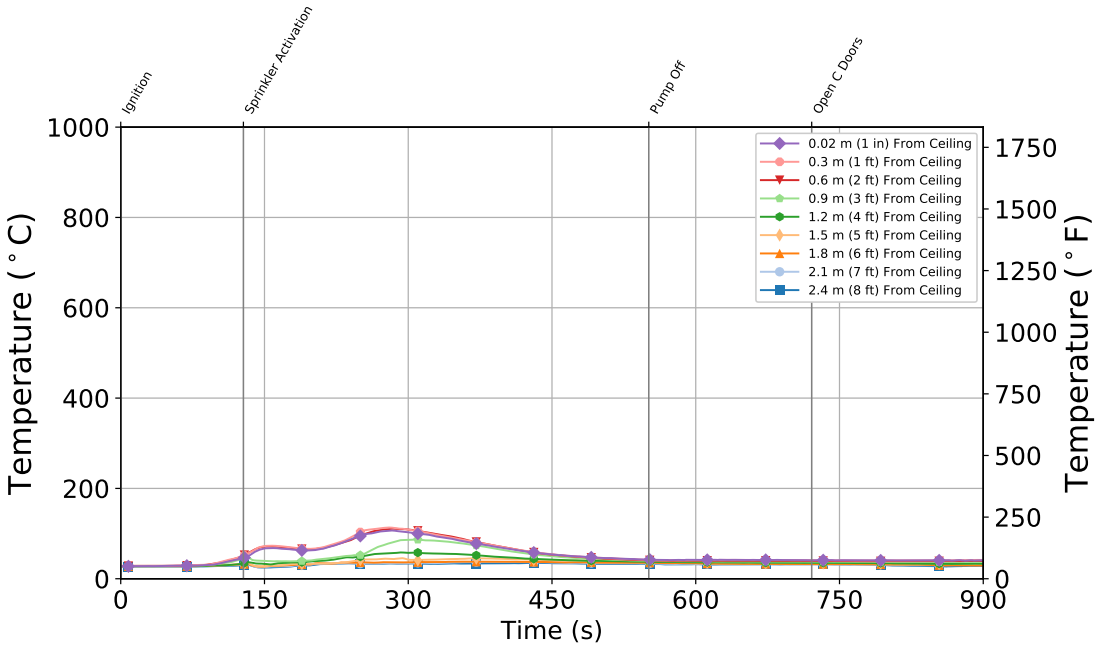

Figure 5.26: Experiment 10 - Thermocouple temperature time history from the Quadrant C thermocouple array in the basement.

The temperature profile reflects a typical fire-growth curve of ignition, growth, fully developed, and decay except that the sprinkler activation prevented temperatures in the basement from exceeding 120 °C (248 °F) compared to the 600 °C (1,112 °F) seen in the experiments with similar pre-ignition ventilation (Experiments 1, 2, and 3). Note that while there was a temperature rise after sprinkler activation, no additional suppression was needed after the sprinkler pump was turned off. The difference was also evident with respect to gas concentration. Figure 5.27 shows the gas concentration for the basement 1.2 m (4 ft) and 0.1 m (4 in.) above the floor.

Compared to the experiments in which a lack of oxygen was the primary reason for the fire being suppressed (Experiments 1, 2, and 3), the oxygen concentrations in the sprinkler experiment never dropped below 18.5%, whereas oxygen concentrations were as low as 10% in fires with similar access and ventilation. Figure 5.28 shows the fire never spread from the ignition sofa, and that there was sufficient fuel remaining for the fire to continue to burn. The presence and activation of the sprinkler system limited the hazard (high temperature and toxic gases) throughout the structure.

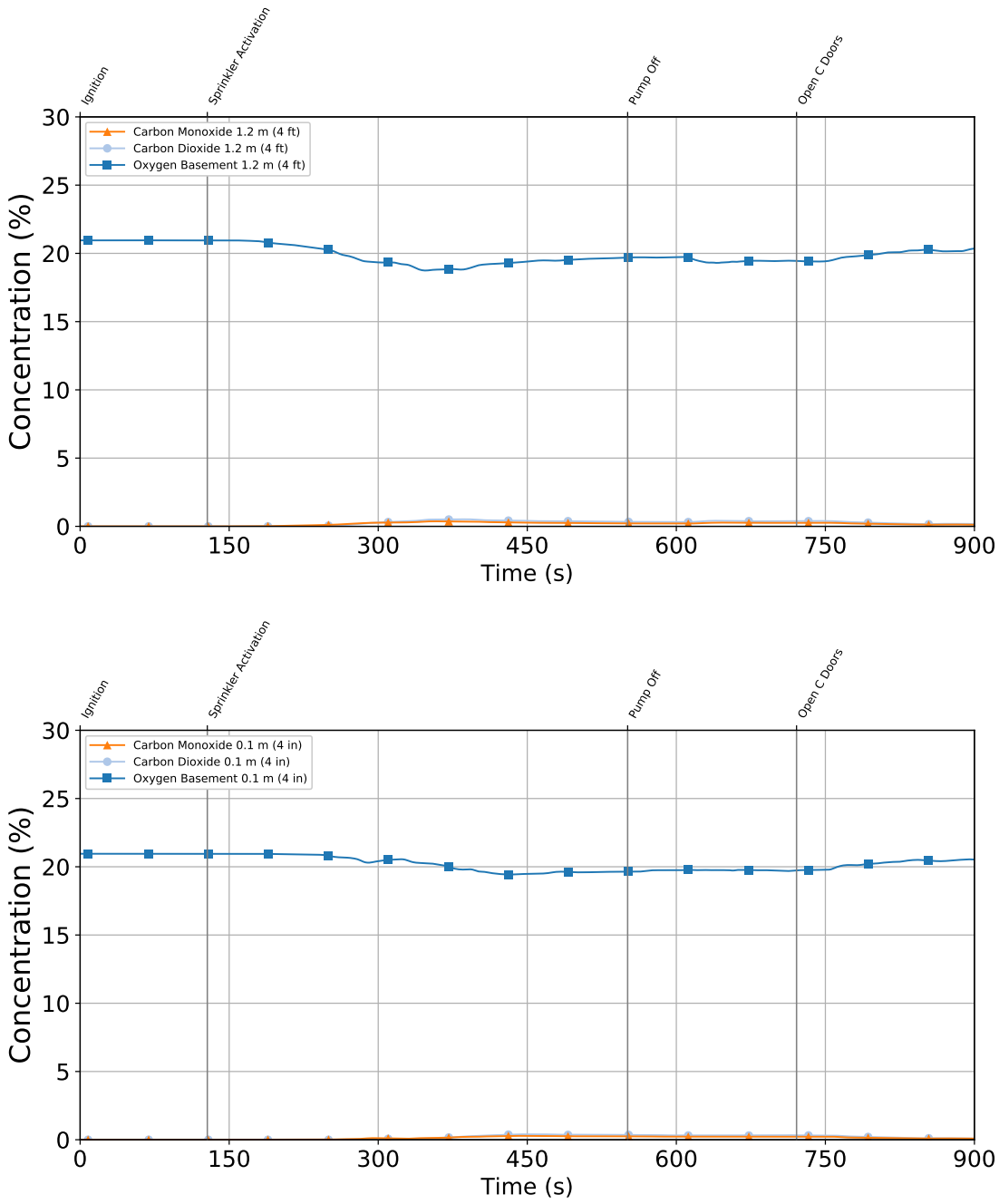

Figure 5.27: Experiment 10 - Gas concentration time history from the 1.2 m (4 ft) (top) and 0.1 m (4 in.) (bottom) elevations in the basement.

Figure 5.28: Photograph of the post-fire fuel packages on the ignition side.

An overview of the conditions within the structure when the fire was at its peak conditions (approximately 275 s after ignition) and 500 s after ignition when the sprinkler pump was shut off appear in Figure 5.17. The red arrows indicate the flow of hot gases, the green arrows indicate the flow of fresh air, and the blue icons show the locations of the activated sprinklers.

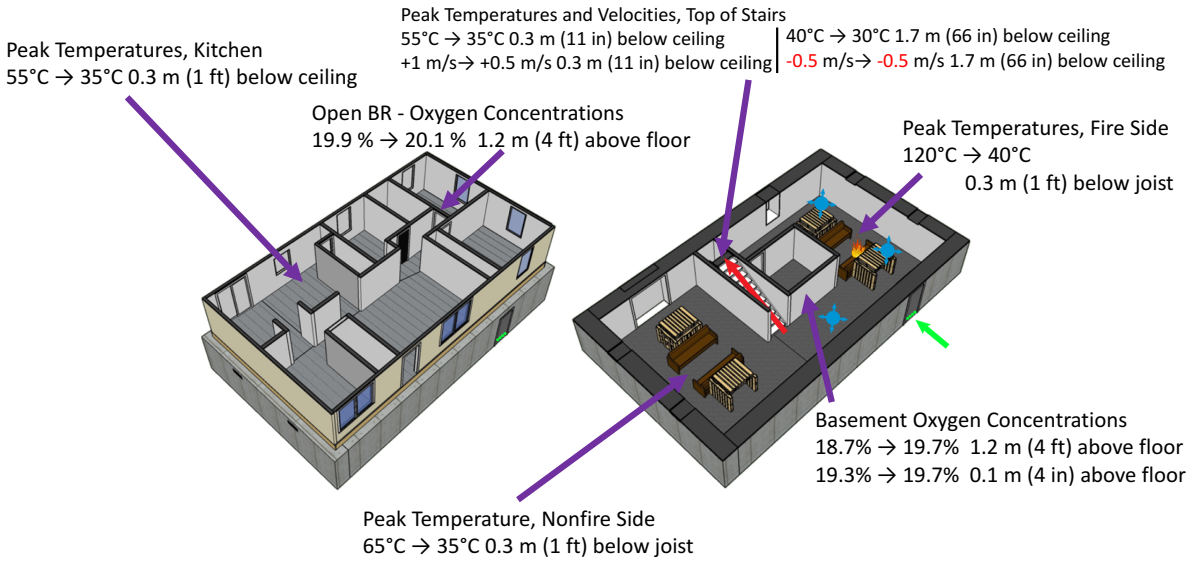

Figure 5.29: Experiment 10 - Isometric images of basement and first floor with selected measurements at peak conditions 275 s after ignition and 500 s after ignition when the sprinkler pump was turned off. The red arrows indicate the flow of hot gases, the green arrows indicate the flow of fresh air, and the blue icons represent the sprinklers that activated.

5.1.6 Experiment 11

The front door and interior stairwell door were open at the time of ignition. Additionally, the four basement vent pipes, each 0.15 m (6 in.) in diameter, were open prior to ignition. Ignition occurred in a modified fuel arrangement on the west side of the basement in the ceiling. (Recall from Figure 3.7, a pre-experiment image of the fuel arrangement.) Figure 5.30 shows the time history of the temperature profile at the thermocouple array closest to the area of ignition.

The temperature curve from Quadrant B in Figure 5.30 followed a similar fire-growth curve of ignition, growth, fully developed, and decay. The initial ramp up and decay followed by a second ramp of fire development is all fire dynamics; no changes were made in vent conditions. This appears in measurements of the gas concentrations in the basement at the 1.2 m (4 ft) level.

The initial drop in oxygen concentration relates to the rise in temperature from the first fire growth. As the oxygen decreased to a low of 5 %, the fire entered a decay phase. As the fire decayed, combustion products exited the structure through the open interior stairwell and open front door. Oxygen was replaced through the open vent pipes in the basement. Once oxygen recovered to above 15 % approximately 575-600 s after ignition, the fire was able to regrow. Figure 5.32 shows

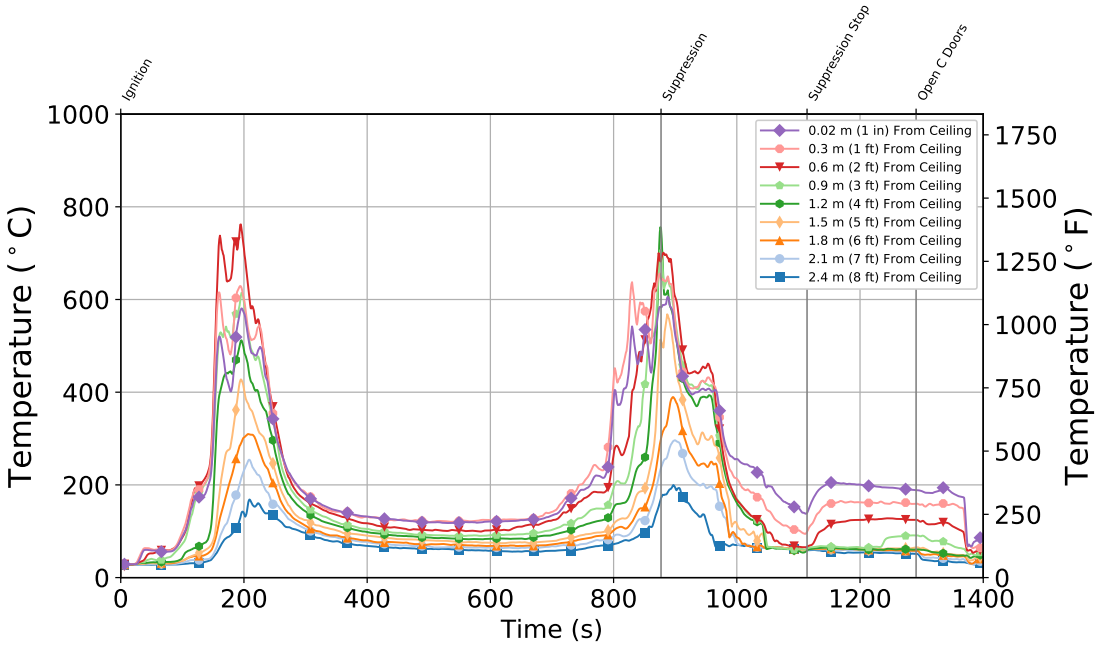

Figure 5.30: Experiment 11 - Thermocouple temperature time history from the Quadrant B thermocouple array in the basement.

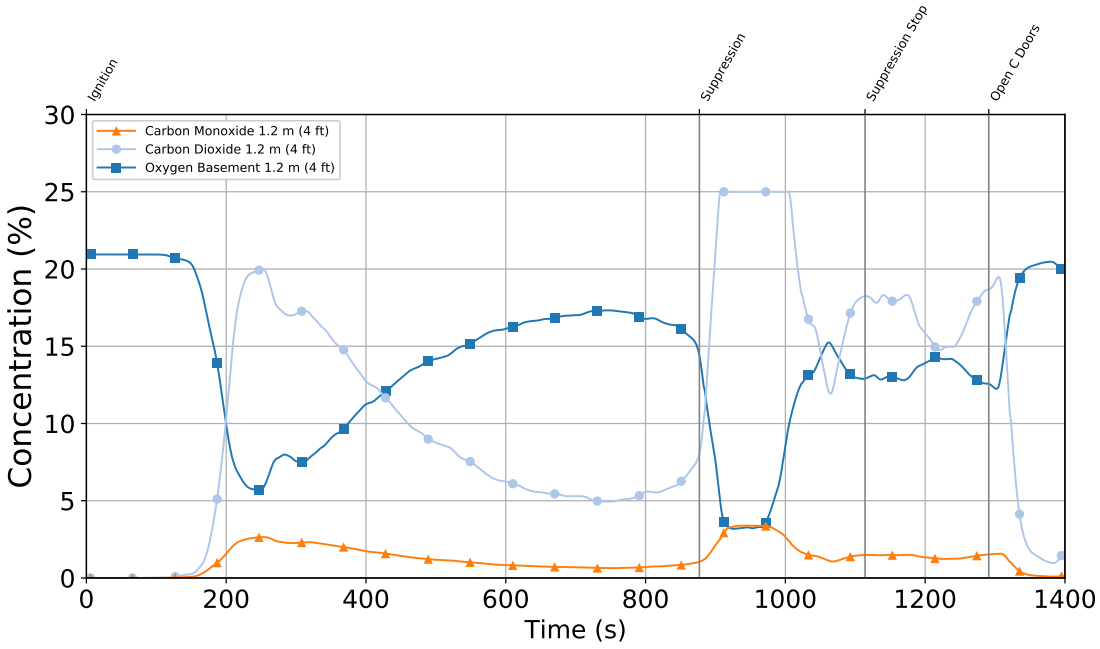

Figure 5.31: Experiment 11 - Gas concentration time history from the 1.2 m (4 ft) elevation in the basement.

the post-experiment fuel on the fire side. Despite the fire starting between the joists, both sofas on the west side of the basement were partially consumed. Suppression was initiated with a 125 gpm

piercing nozzle through the floor. Full flow rate occurred 940 s after ignition and the nozzle was shutdown 1,114 s after ignition.

Figure 5.32: Photograph of the post-fire fuel packages on the ignition side.

Figure 5.33 shows the impact throughout the structure from the suppression actions taken through the floor. The red arrows indicate the flow of hot gases, the green arrows indicate the flow of fresh air, and the blue icon represents the suppression location. While the suppression action is similar to those in Experiment 4, in Experiment 11, the fire was ignited on the west side of the basement, the same side as suppression.

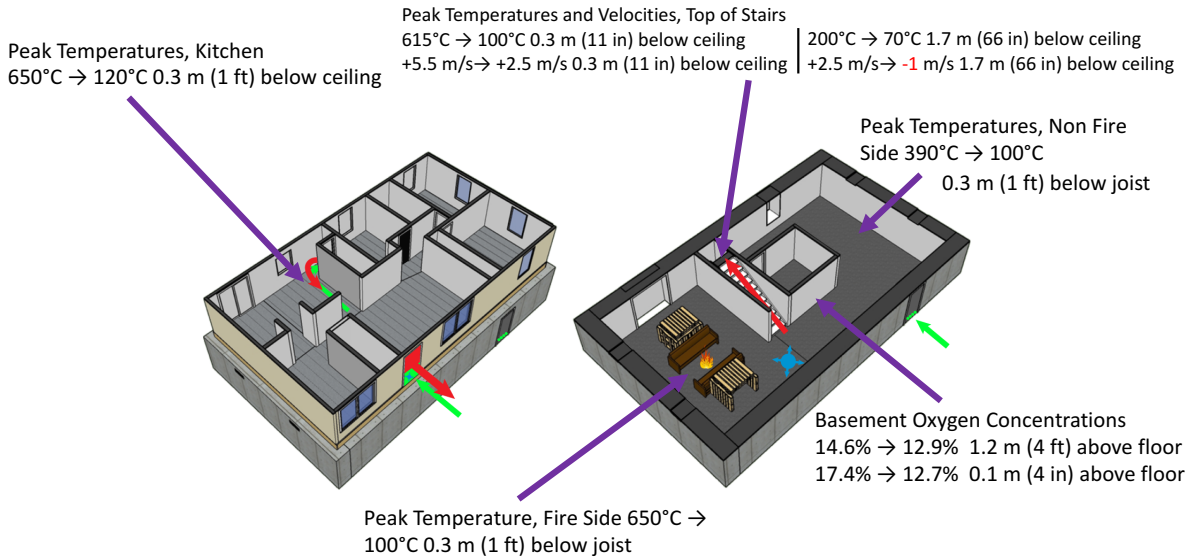

Figure 5.33: Experiment 11 - Isometric images of basement and first floor with selected measurements at peak conditions approximately 875 s after ignition, and at 1,117 s after suppression actions concluded. The red arrows indicate the flow of hot gases, the green arrows indicate the flow of fresh air, and the blue icon represents the location of suppression.

5.1.7 Experiment 12

The front door and interior stairwell door were open at the time of ignition. In addition, the four basement vent pipes, each 0.15 m (6 in.) in diameter, were open prior to ignition. The fire was ignited on the east side of the basement, and suppression was conducted from a fog nozzle with remote operation from the top of the stairwell (see Figure 4.3). Figure 5.34 shows the time history of the temperature profile at the thermocouple array closest to the area of ignition.

The temperature curve from Quadrant C in Figure 5.34 followed a similar fire curve to that of Experiment 11. The initial ramp up and decay followed by a second increase in fire growth were due to fire dynamics; no changes were made in vent conditions. This can be seen in the measurements of the gas concentrations in the basement at the 1.2 m (4 ft) level.

The initial drop in oxygen concentration relates to the rise in temperature from the first fire growth. When the oxygen concentration decreased to 5 %, the fire entered a decay phase. As the fire decayed, combustion products exited the structure through the open interior stairwell and the open front door. At the same time oxygen entered the basement through the open vent pipes. Once oxygen recovered to above 15 % approximately 500 s after ignition, the fire was able to regrow.

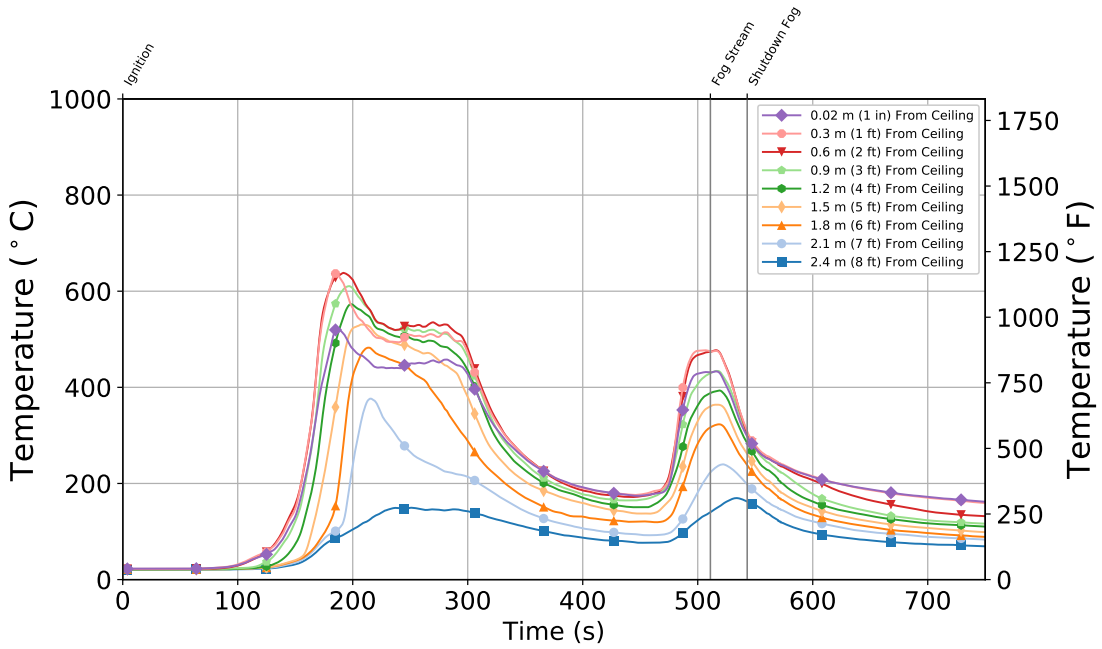

Figure 5.34: Experiment 12 - Thermocouple temperature time history from the Quadrant C thermocouple array in the basement.

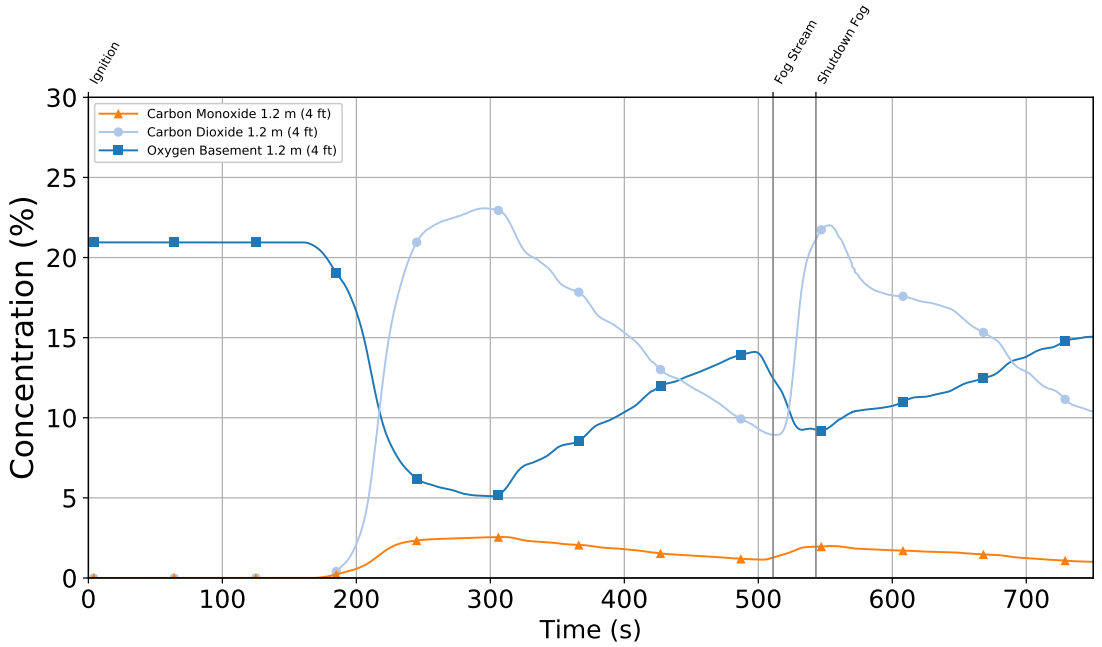

Figure 5.35: Experiment 12 - Gas concentration time history from the 1.2 m (4 ft) elevation in the basement.

The impact of the fog stream appears in the data from the velocity probes at the top of the stairs (Figure 5.36) and the velocity probe in each vent pipe (Figure 5.37).

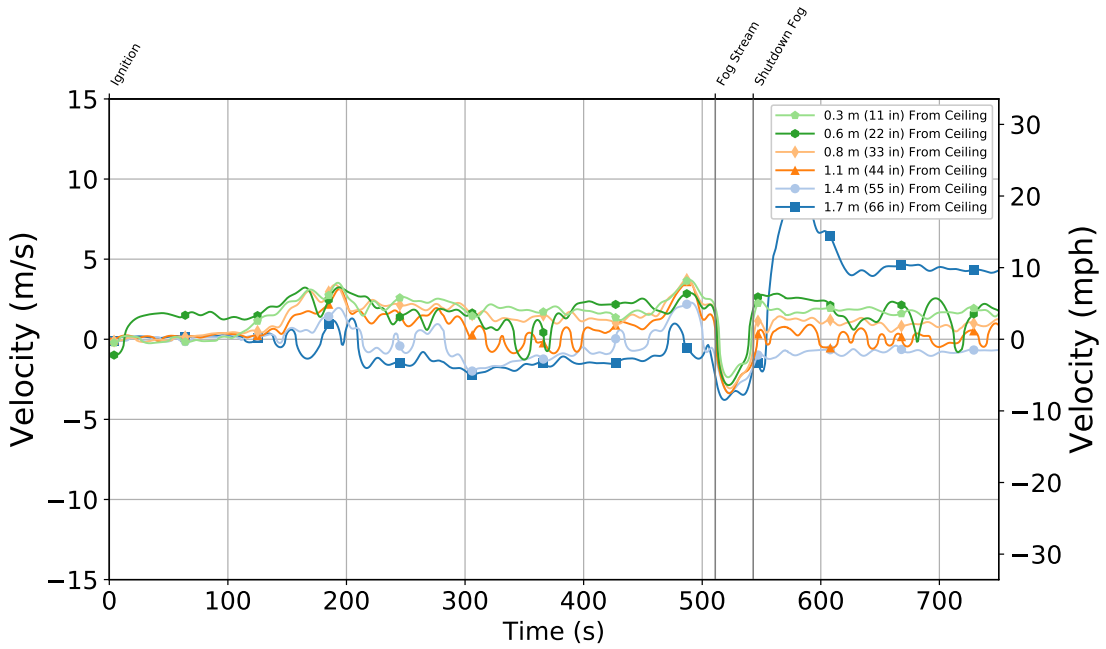

Figure 5.36: Experiment 12 - Velocity measurements at the top of the interior stairwell.

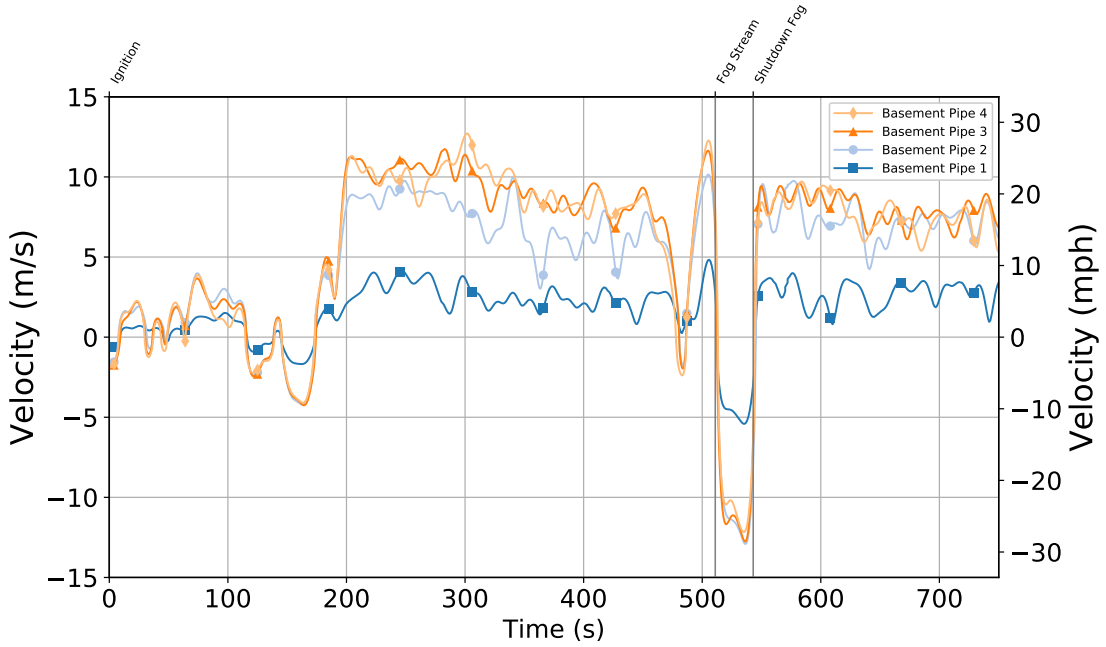

Figure 5.37: Experiment 12 - Velocity measurements in each of the basement leakage pipes.

Prior to fog stream application, the velocity at the top of stairs was mostly exhaust flow (flowing from the basement to the first floor). At its peak, the bottom probe indicated air flow down the stairs at approximately 2 m/s (4.4 mph). When the fog stream was turned on, the doorway transitioned from mostly exhaust to completely intake (supply air to the basement). Velocities ranged from

2.5 m/s (5.6 mph) to 3.5 m/s (7.8 mph). The fog stream limited combustion products from flowing up the stairs. A similar switch in flow direction was observed in the basement vent pipes. Prior to the fog stream, the vent pipes acted as a supply to the basement (approximately 8 m/s (18 mph)) and became an exhaust flow (11.5 m/s (25 mph)) while the fog stream was flowing.

Figure 5.38 shows the impact throughout the structure from the fog stream at the top of the stairwell. The red arrow indicates the flow of hot gases, the green arrows indicate the flow of fresh air, and the blue arrow represents the suppression location.

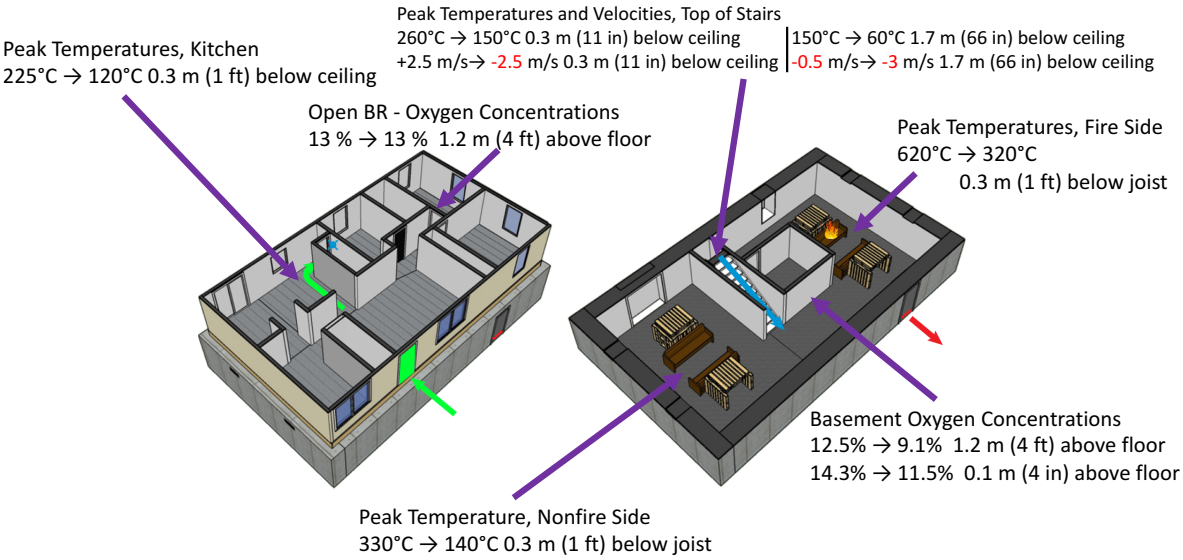

Figure 5.38: Experiment 12 - Isometric view images of basement and first floor with selected measurements at peak conditions, 510 s after ignition, and 545 s after ignition when suppression actions concluded. The red arrow indicates the flow of hot gases, the green arrows indicate the flow of fresh air, and the blue arrow represents the location of fog stream at the top of the stairwell.

5.2 Limited Exterior Access to the Basement

5.2.1 Experiment 5

The fire behavior in Experiment 5 was similar to that of Experiments 1, 2, and 3. The northeast basement window was open prior to ignition, but the remaining three basement windows were closed prior to ignition. Additionally, the door at the top of interior stairwell and the front door were open. The fire was ignited on the northeast sofa in the basement. Figure 5.39 shows the time history of the temperature profile at the thermocouple array closest to the area of ignition.

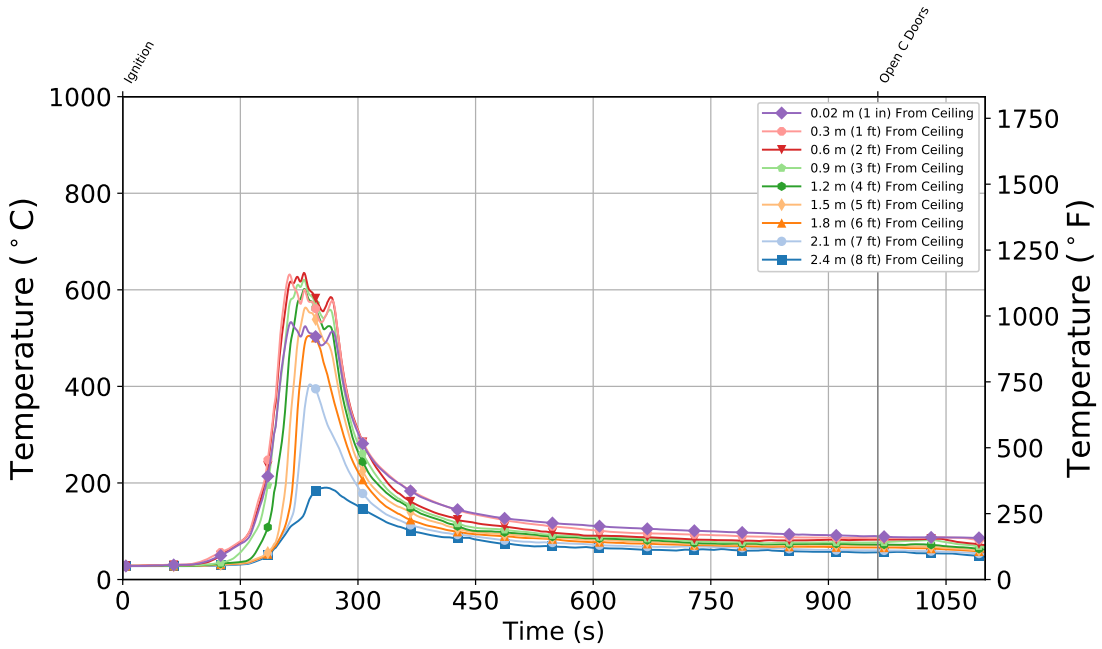

Figure 5.39: Experiment 5 - Thermocouple temperature time history from the Quadrant C thermocouple array in the basement.

Much like Experiments 1, 2, and 3, the temperature curve followed the typical fire growth curve: ignition, growth, fully developed, and decay. No suppression actions were taken in Experiment 5, the fire behavior was the result of a vent located high on a basement wall, which did not provide sufficient oxygen to the basement. Recall from Table 3.1 that the sill of the basement window was 1.98 m (6.5 ft).

Examination of the gas concentration time history in Figure 5.40 showed that a lack of efficient ventilation to the basement led to the fire being self-extinguished due to a lack of oxygen.

As the oxygen level decreased, the combustion efficiency was reduced. This resulted in an increase in CO_2 and CO. Once the oxygen levels dropped below 15 %, flaming combustion was limited if not suppressed. In this experiment, flaming combustion ceased. An overview of the conditions within the structure when the fire was at its peak to conditions approximately 225 s after ignition

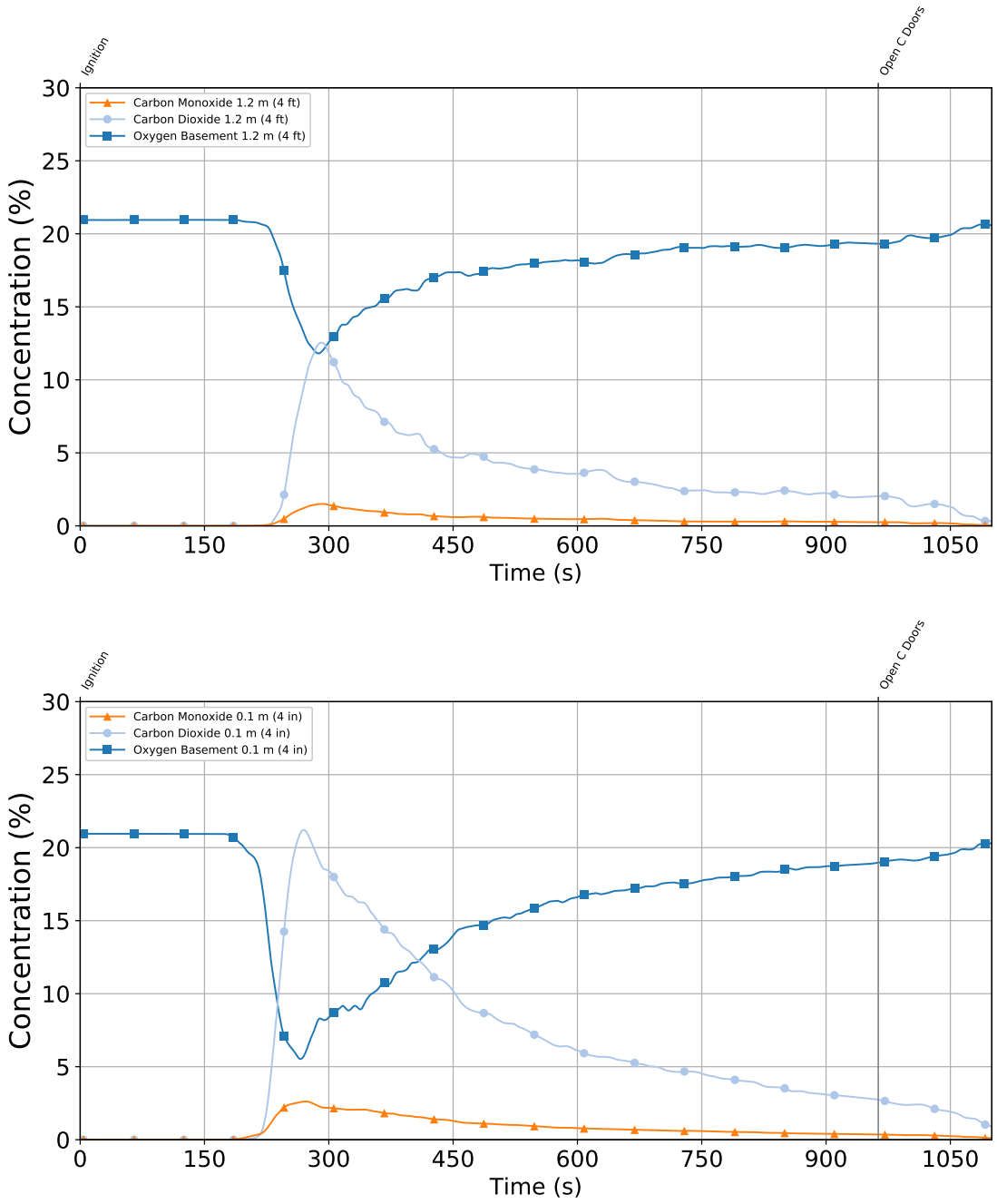

Figure 5.40: Experiment 5 - Gas concentration time history from the 1.2 m (4 ft) (top) and 0.1 m (4 in.) (bottom) elevations in the basement.

and 600 s after ignition appear in Figure 5.41. The red arrows indicate the flow of hot gases, and the green arrows indicate the flow of fresh air.

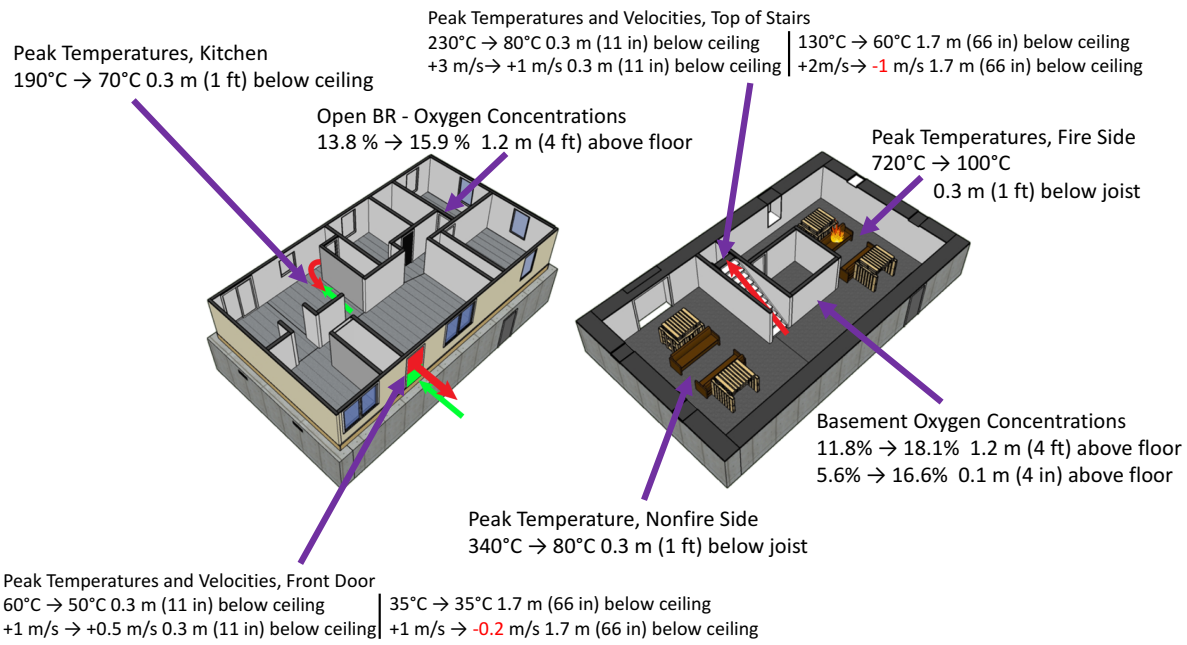

Figure 5.41: Experiment 5 - Isometric images of basement and first floor with selected measurements at peak conditions, 225 s after ignition and 600 s after ignition. The red arrows indicate the flow of hot gases, and the green arrows indicate the flow of fresh air.

5.2.2 Experiment 6

In Experiment 6, the front door, interior stairwell door, and side D basement windows were open prior to ignition. The remaining windows and vents were closed prior to ignition. Ignition occurred on the northeast sofa in the basement. Figure 5.42 shows the time history of the temperature profile at the thermocouple array closest to the area of ignition. The two basement windows on side B were broken 180 s (AB window) and 213 s (BC window) after ignition.

The temperature curve from Quadrant B in Figure 5.42 followed a typical fire growth curve of ignition, growth, fully developed, and decay. In this experiment, pressure from the wind limited exhaust gases from exiting front door. The limited exhaust flow resulted in reduced burning in the basement, so the first floor sliding glass door was opened at 1,500 s after ignition to relieve pressure upstairs. This led to an increased flow through the basement, and enabled the fire to grow.

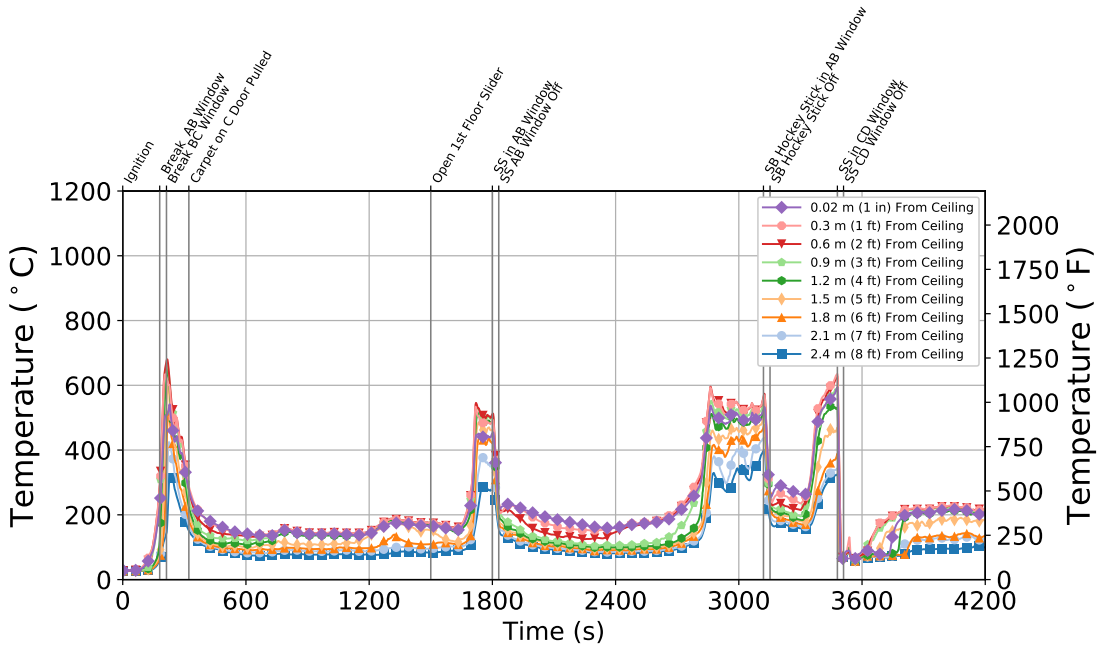

Figure 5.42: Experiment 6 - Thermocouple temperature time history from the Quadrant C thermocouple array in the basement.

An overview of the conditions within the structure prior to the slider being opened (1,480 s after ignition) and after the upstairs sliding glass door was opened (1,723 s post ignition) is shown in Figure 5.43. The red arrows indicate the flow of hot gases, and the green arrows indicate the flow of fresh air.

Notice the increased temperatures and velocities at the top of the stairs in Figure 5.43. Also notice the negative impact on the oxygen level in the open bedroom due to increased burning in the basement. Suppression occurred by flowing water through the basement windows, both the AB window and CD window. Both a straight stream and a solid stream from a smooth bore nozzle were utilized. The first two attacks were through the side window closest to the AB corner. From this location, the stream was not able to hit seat of the fire, but was able to cool fire gases and fuel in its path. Figures 5.44 and 5.45 show an overview of the impact of these two suppression actions. The straight stream was applied 1,800 s after ignition and the solid stream was applied 3,120 s after ignition (after the fire regrew following initial attack). Notice the significant temperature decreases throughout the structure as well as the oxygen recovery.

The third suppression action was a straight stream through the basement window on the CD corner of the structure; that is the fire side of the basement. Figure 5.46 shows the impact of the straight stream suppression through the fire-side window, 3,480 s after ignition. The fire side attack improved conditions throughout the structure as evident by the temperature and oxygen measurements shown in Figure 5.46.

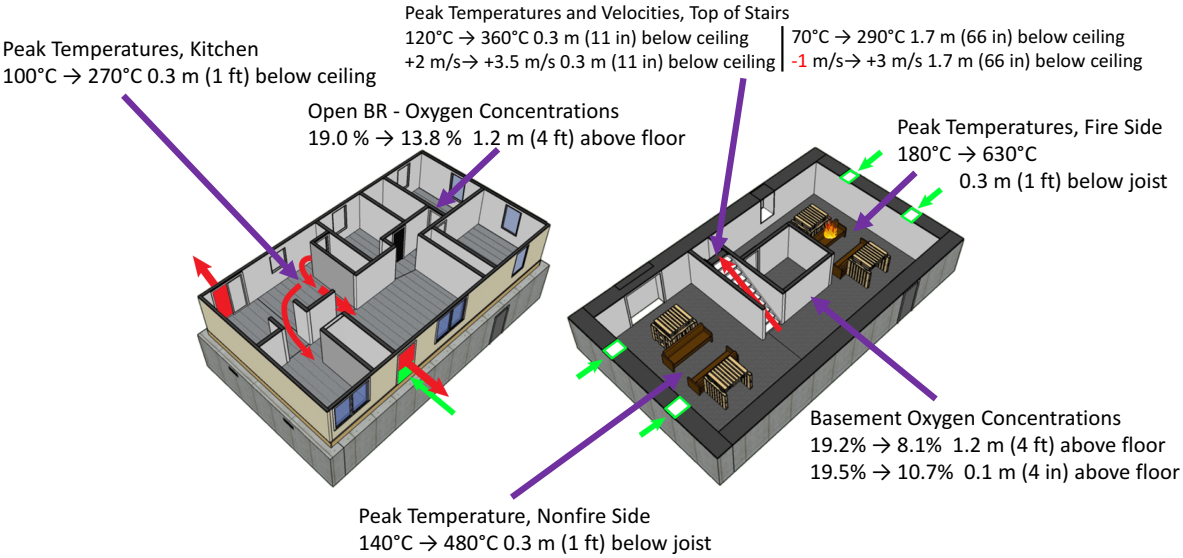

Figure 5.43: Experiment 6 - Isometric images of basement and first floor with selected measurements prior to the slider being opened (1,480 s after ignition) and after the slider was opened (1,723 s post ignition). The red arrows indicate the flow of hot gases, and the green arrows indicate the flow of fresh air.

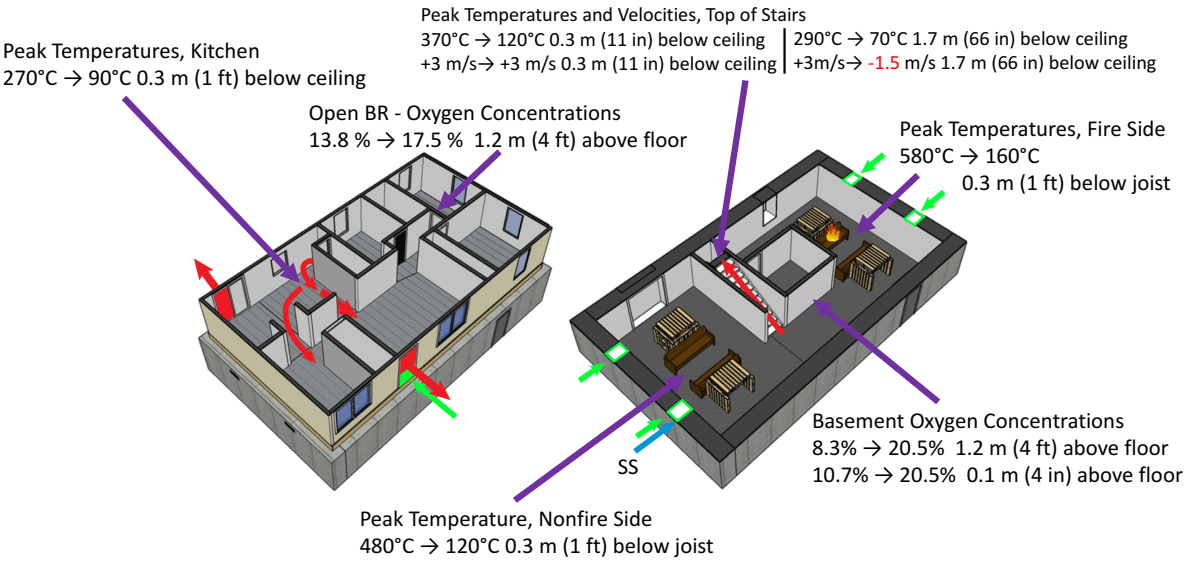

Figure 5.44: Experiment 6 - Isometric images of basement and first floor with selected measurements prior to the straight stream being applied through the AB window (1,800 s after ignition) and after suppression (2,300 s post ignition) stopped. The red arrows indicate the flow of hot gases, the green arrows indicate the flow of fresh air, and the blue arrow indicates the location of the suppression.

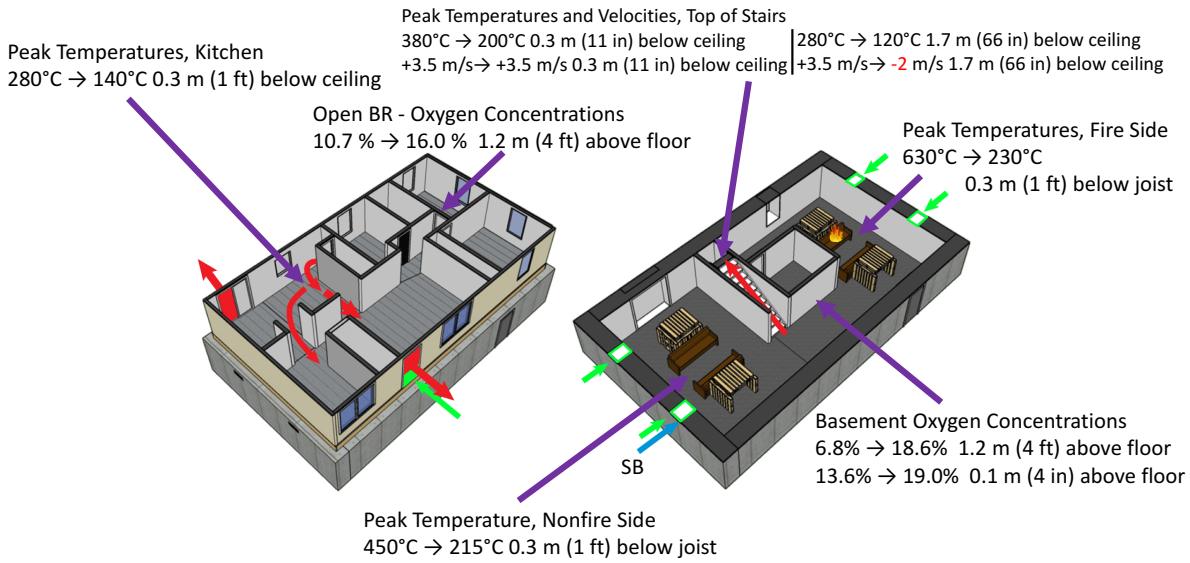

Figure 5.45: Experiment 6 - Isometric images of basement and first floor with selected measurements prior to the solid stream from a smooth-bore nozzle being applied through the AB window (3,120 s after ignition) and after suppression (3,300 s post ignition) stopped. The red arrows indicate the flow of hot gases, the green arrows indicate the flow of fresh air, and the blue arrow indicates the location of the suppression.

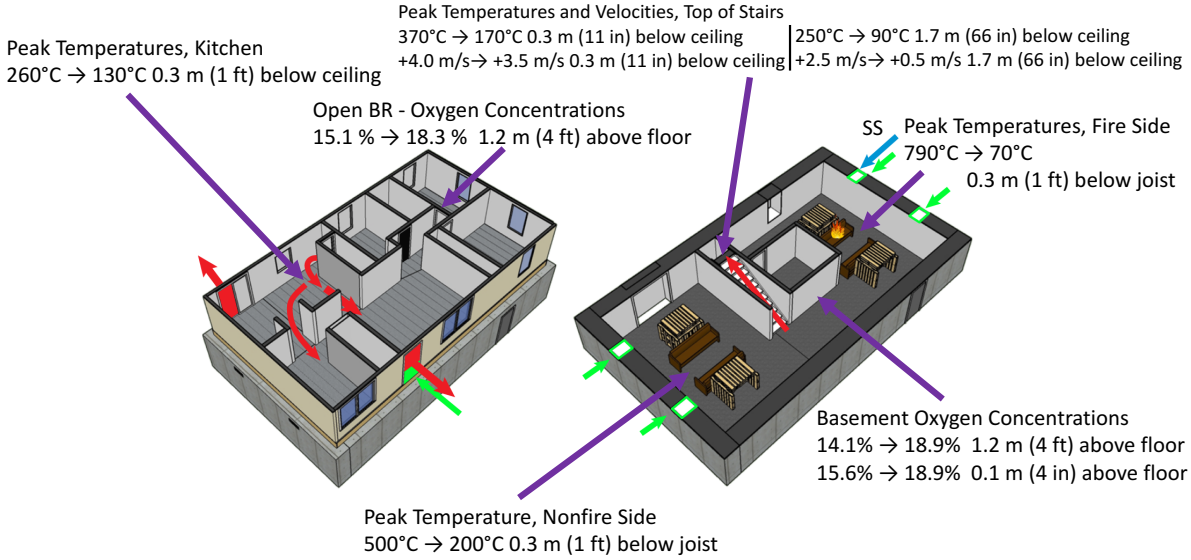

Figure 5.46: Experiment 6 - Isometric images of basement and first floor with selected measurements prior to the straight stream being applied through the CD window (3,480 s after ignition) and after suppression (3,515 s post ignition) stopped. The red arrows indicate the flow of hot gases, the green arrows indicate the flow of fresh air, and the blue arrow indicates the location of the suppression.

To further illustrate the impact of the suppression actions and the impact of a closed door, Figure 5.47 shows the gas concentrations at 1.2 m (4 ft) above the floor for the open and closed bedrooms.

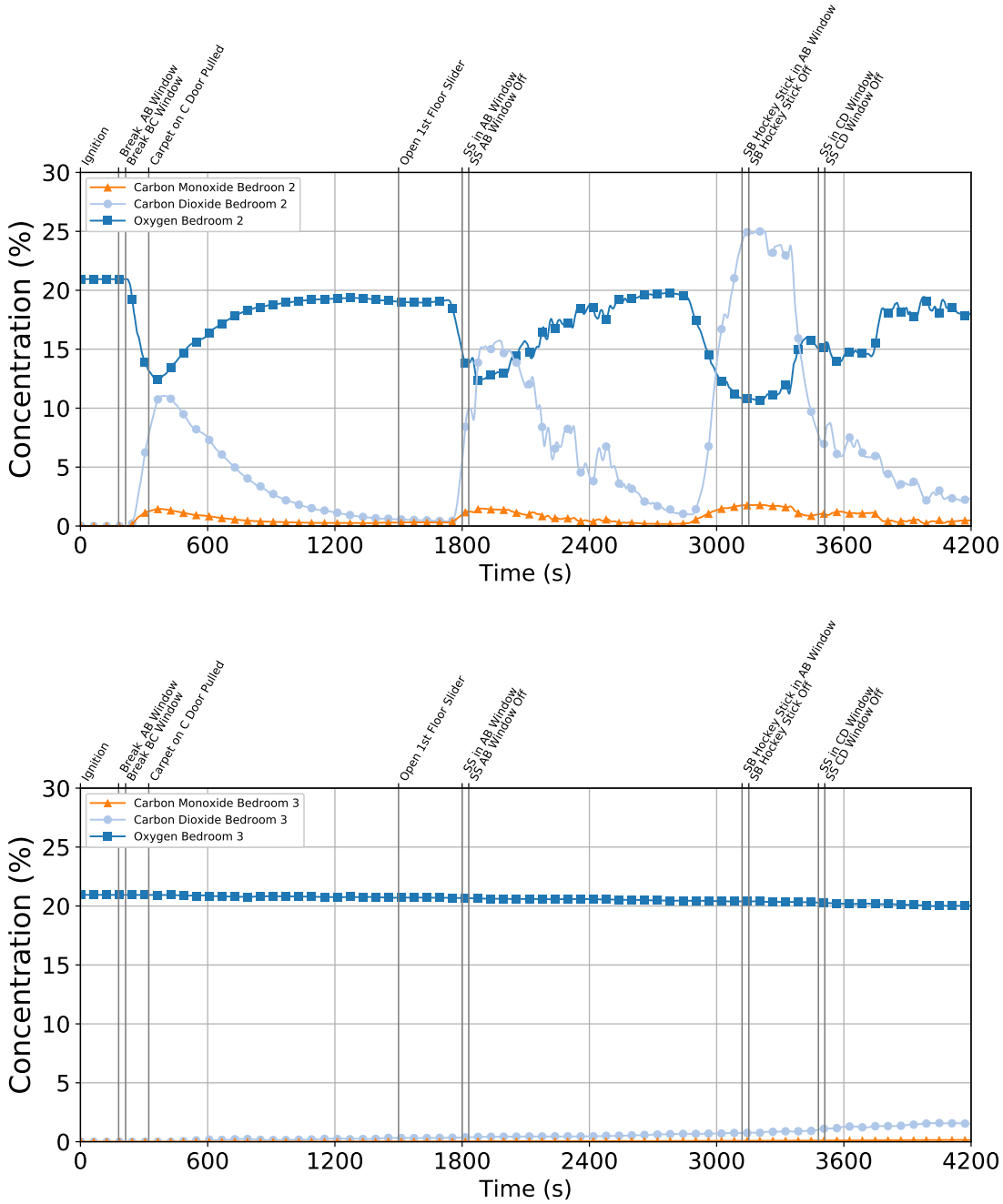

Figure 5.47: Experiment 6 - Gas concentration time history from the open bedroom (top) and the closed bedroom (bottom), both 1.2 m (4 ft) above the floor on the first floor of the structure.

In the open bedroom after each attack ,the oxygen concentration increased and toxic gases decreased. After more than an hour, the closed bedroom had very little drop in oxygen or increase

of carbon dioxide and carbon monoxide levels. It is important to mention, that this is strictly a comparison of the impact of the door alone. No other leaks or vents into the bedrooms were considered.

5.2.3 Experiment 7

In Experiment 7, the front door, interior stairwell door, kitchen sliding glass door and all four basement windows were open prior to ignition. Instead of using vent pipes, the A side cement board blocking the side A basement doorway was modified to provide a single rectangular opening at floor level. The remaining windows and vents were closed prior to ignition. Ignition occurred on the northwest sofa in the basement. Figure 5.48 shows the time history of the temperature profile from Quadrant B, the thermocouple array closest to the area of ignition.

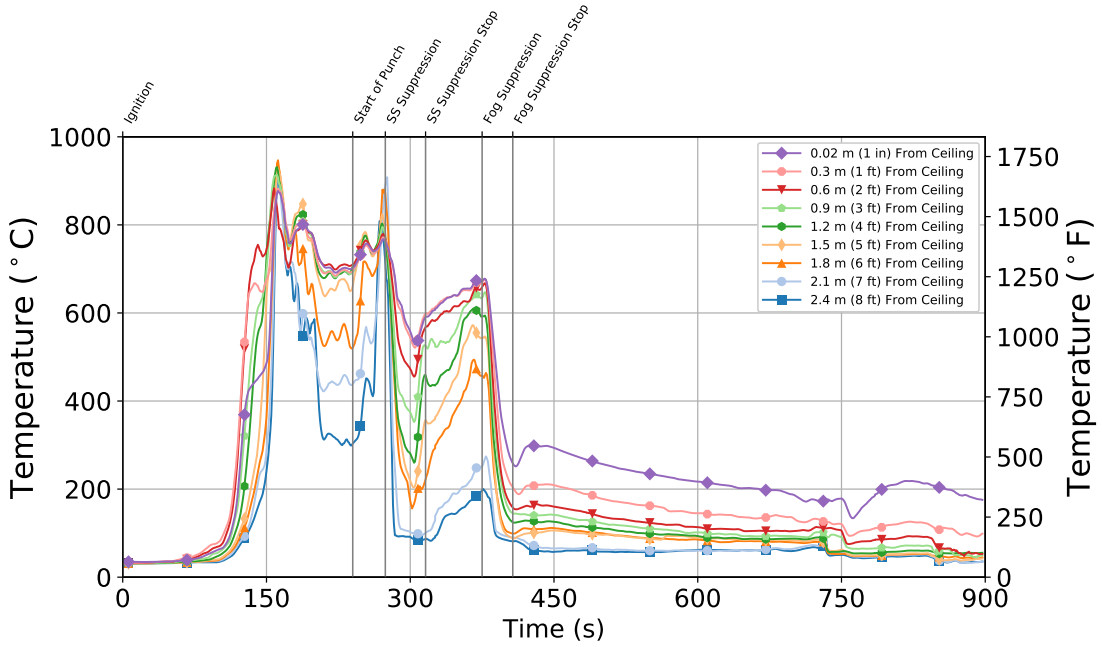

Figure 5.48: Experiment 7 - Thermocouple temperature time history from the Quadrant B thermocouple array in the basement.

The temperature curve in Figure 5.48 showed ignition, growth, fully developed, and a slight decay. The basement ventilation of the open windows and leakage through the side A floor vent provided sufficient oxygen for combustion, which prevented the sharp decrease in temperature shown in other experiments. Suppression actions in Experiment 7 occurred by using both a straight stream and fog stream through a hole punched through the floor. In this case, the location of the suppression hole was above the fire side. The straight stream application occurred 275 s after ignition, and the fog stream application occurred 375 s after ignition. Figure 5.49 provides an overview of the impact of the straight stream applied through the floor. The red arrows indicate the flow of hot gases, the green arrows indicate the flow of fresh air, and the blue icon indicates the location of

suppression.

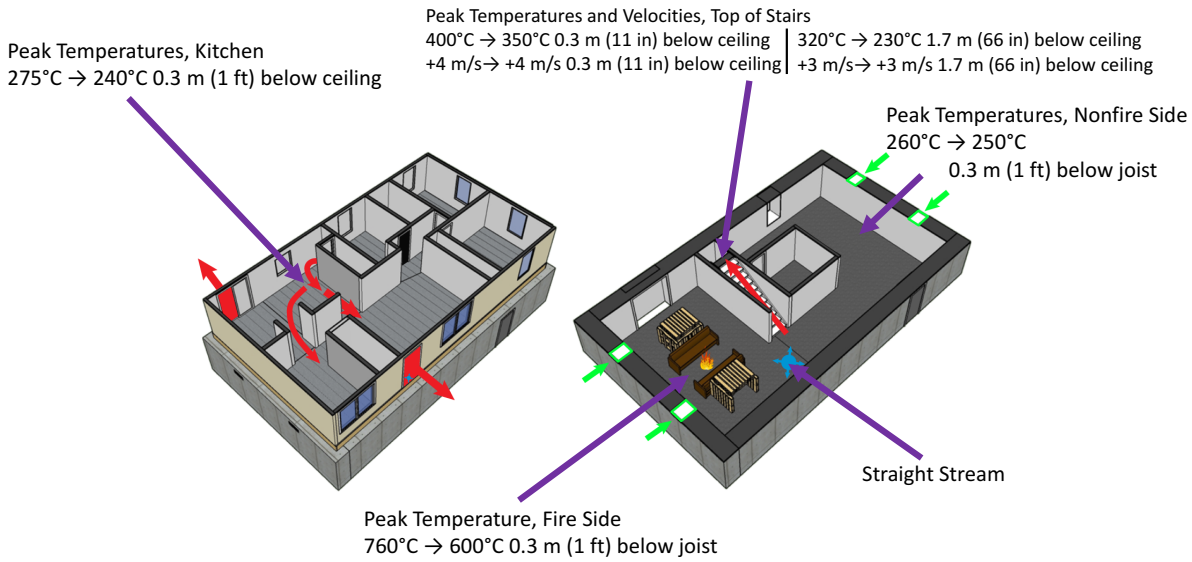

Figure 5.49: Experiment 7 - Isometric images of basement and first floor with selected measurements prior to the straight stream being applied through the floor (275 s after ignition) and after suppression (315 s post ignition) stopped. The red arrows indicate the flow of hot gases, the green arrows indicate the flow of fresh air, and the blue arrow indicates the location of the suppression.

There was improvement in temperature throughout the structure following the use of the straight stream, but the fog stream application through the floor had a more significant impact in decreasing temperatures. The impact appears in Figure 5.48 and the overview image, Figure 5.50. The wide angle of the fog stream led to more coverage of the basement fuel compared to the narrow area of coverage of the straight stream, and thus, provided a more significant impact.

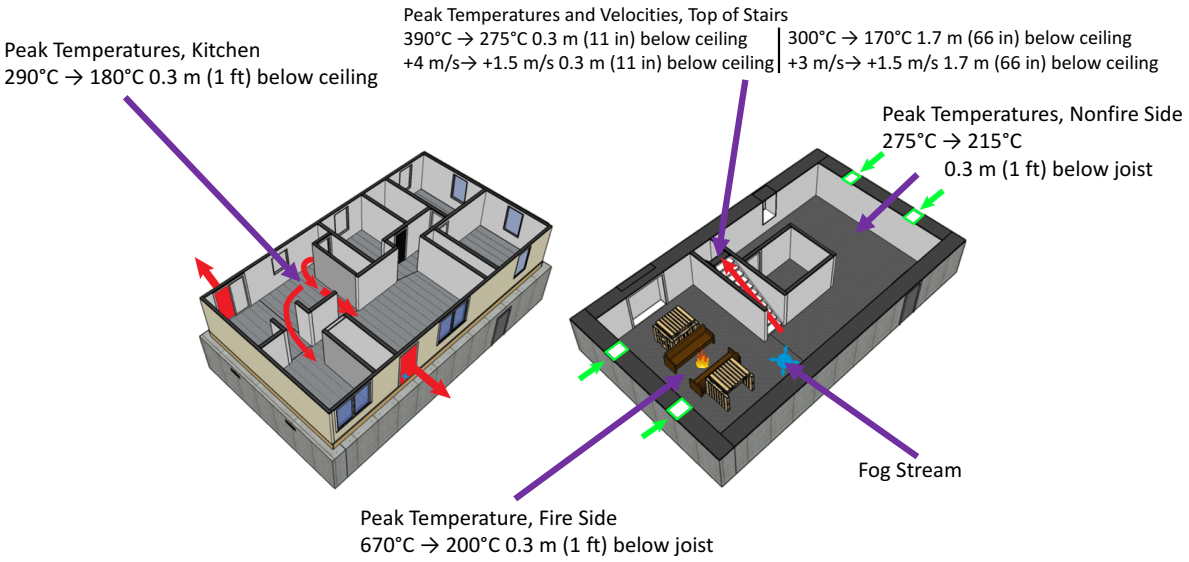

Figure 5.50: Experiment 7 - Isometric images of basement and first floor with selected measurements prior to the solid stream from a fog stream nozzle being applied through the floor (375 s after ignition) and after suppression (415 s post ignition) stopped. The red arrows indicate the flow of hot gases and the green arrows indicate the flow of fresh air. The blue icon indicates the location of the suppression.

5.3 Exterior Access to the Basement

5.3.1 Experiment 8

The interior stairwell door and two pipe vents installed to reflect a dryer vent and a hot water heater vent were open prior to ignition. The front door was opened approximately 180 s after ignition, and the side C basement sliding glass door installed specifically for this experiment was opened 210 s after ignition. The slider was fully vented (the fixed pane was broken out by a firefghter) 550 s after ignition. Suppression did not occur until 620 s after ignition. The 440 s delay between initial ventilation actions and the start of suppression actions was to simulate an uncoordinated attack. The fire was ignited on the northeast sofa in the basement. Figure 5.51 shows the time history of the temperature profile at the thermocouple array closest to the area of ignition.

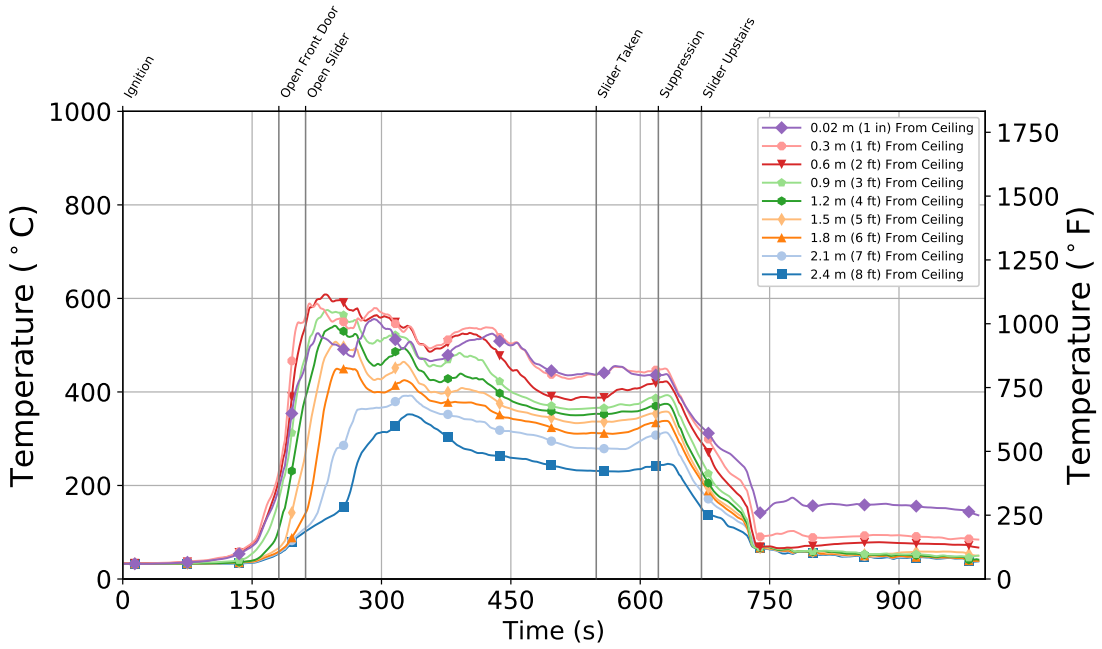

Figure 5.51: Experiment 8 - Thermocouple temperature time history from the Quadrant C thermocouple array in the basement.

The Quadrant C temperature curve in Figure 5.51 showed ignition, growth, and fully developed fire stages. However, at this location the temperature do not indicate that flashover occurred. The basement ventilation of the two vent pipes and open sliding glass door were sufficient to sustain the basement fire. On the non-ignition side of the basement, the impact of opening the sliding glass door was more evident. Figure 5.52 shows the temperature profile from the thermocouple array at Quadrant A. Notice the rapid temperature rise in the 20 s after the sliding glass door was vented. The increased ventilation of the ventilation-limited fire in the basement, resulted in a transition through flashover in this portion of the basement where the fire was provided with sufficient oxygen to maintain combustion.

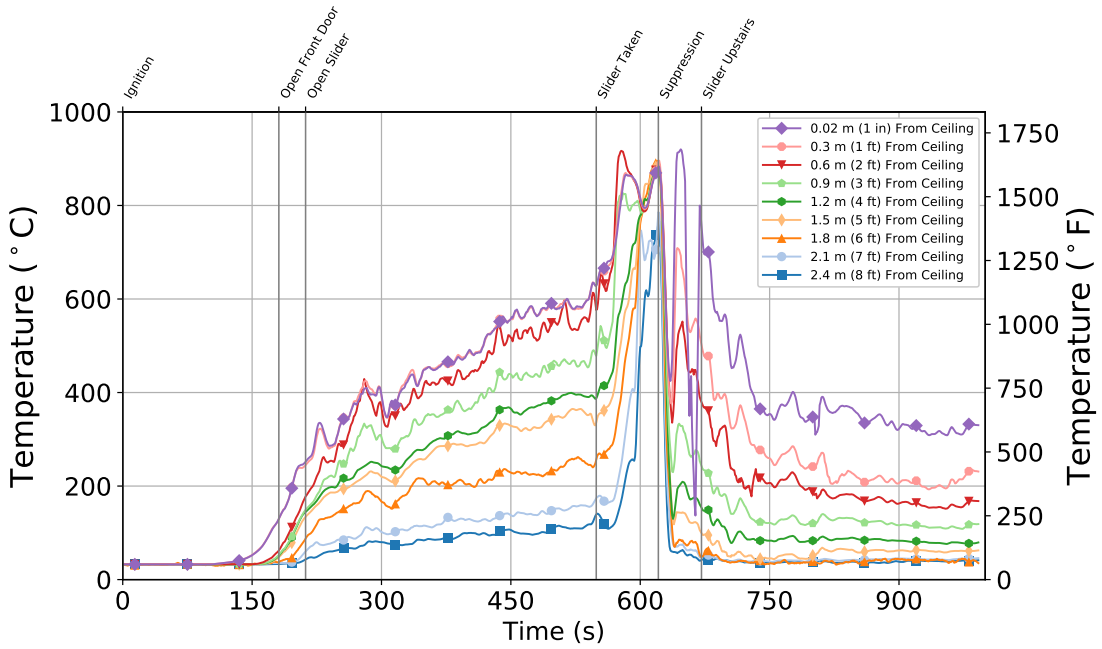

Figure 5.52: Experiment 8 - Thermocouple temperature time history from the Quadrant A thermocouple array in the basement.

An overview of the conditions within the structure before and after the sliding glass door was vented (approximately 525 s after ignition and 570 s after ignition respectively) in Figure 5.53. The red arrows indicate the flow of hot gases, and the green arrow indicates the flow of fresh air.

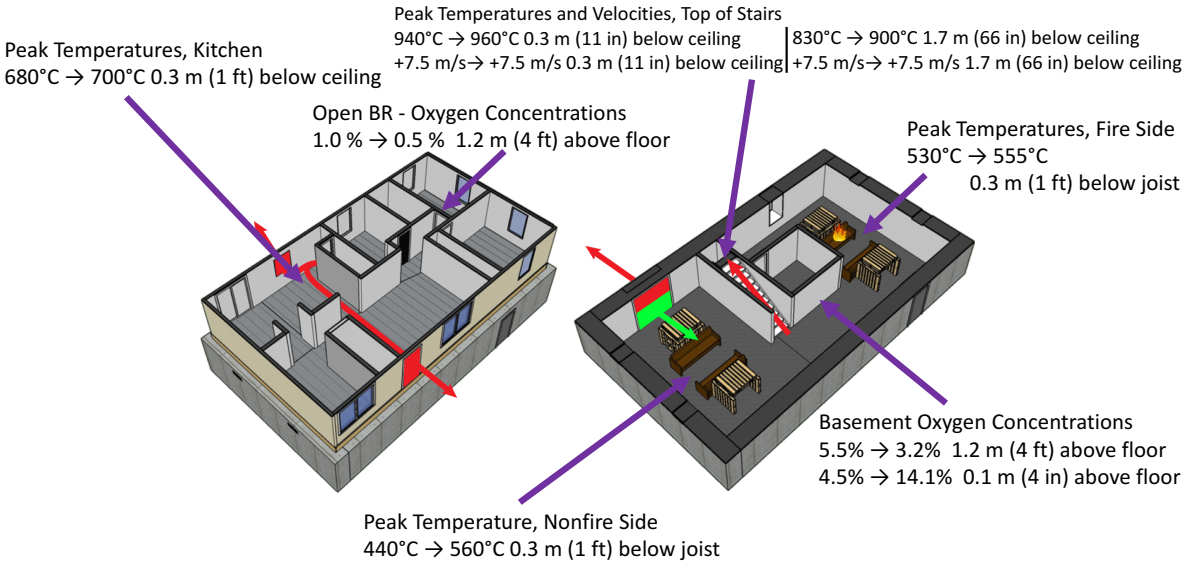

Figure 5.53: Experiment 8 - Isometric images of basement and first floor with selected measurements before the sliding glass door was vented 525 s after ignition, and at 570 s after ignition. The red arrows indicate the flow of hot gases, and the green arrow indicated the flow of fresh air.

Examination of the temperature and velocity results from the top of the stairs showed that firefighters would not have been able to make it down that stair due to high heat and gas velocity. Figure 5.54 shows temperatures throughout the stairwell exceeded 900 °C (1,650 °F) with velocities between 5–10 m/s (11–20 mph). These conditions resulted in both high convective and high radiative heating rates that would quickly overcome the protective capabilities of structural firefighter protective gear.

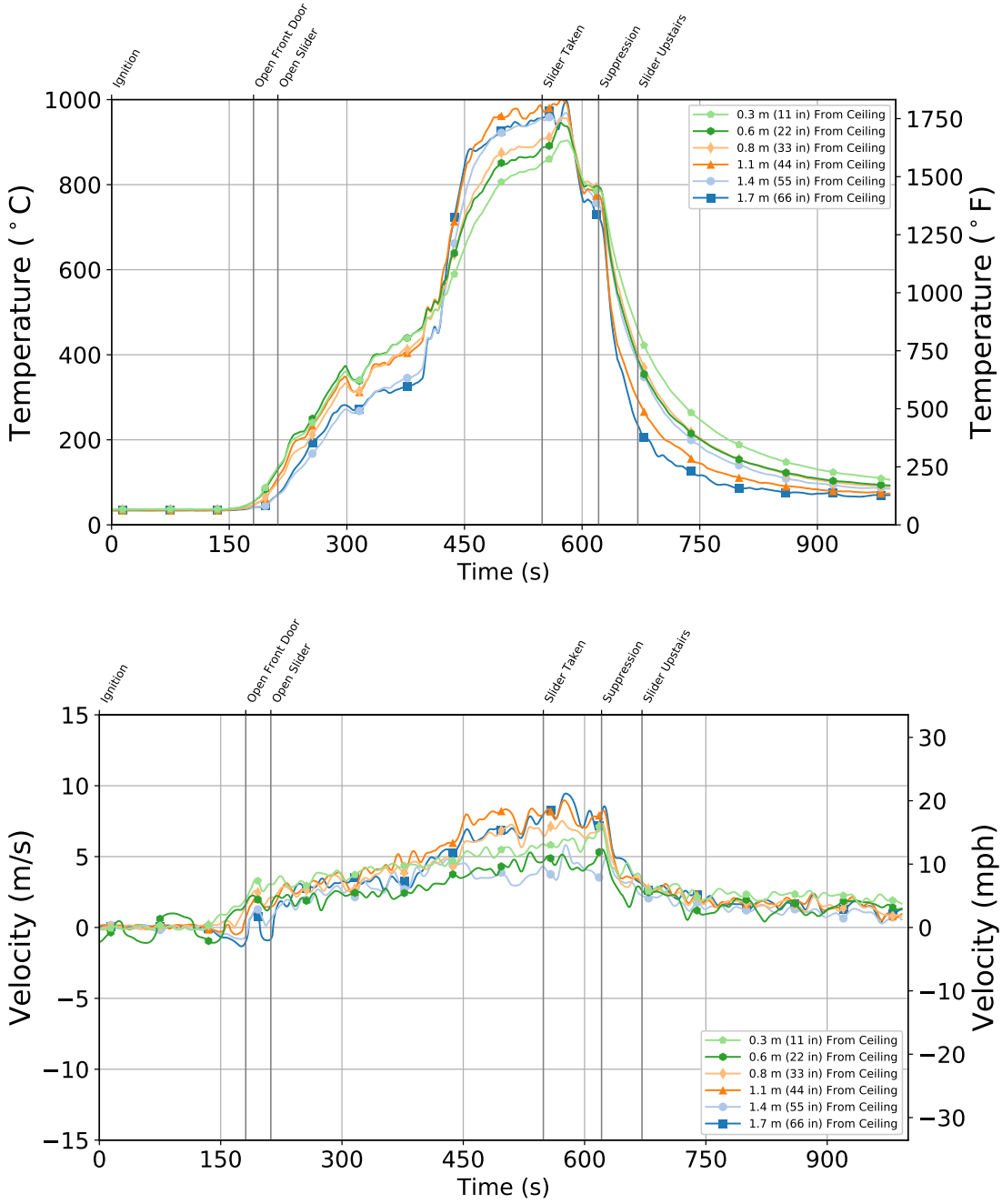

Figure 5.54: Experiment 8 - Thermocouple temperature time history at the top of the stairwell (top) and velocity time history at the top of the stairs (bottom.

Suppression was initiated when a straight stream flowed through the basement sliding glass door opening approximately 620 s after ignition. Figure 5.55 shows the overview of the impact of suppression actions 105 s after they were initiated. Notice the temperatures, gas concentrations and velocities up the stairs all improved.

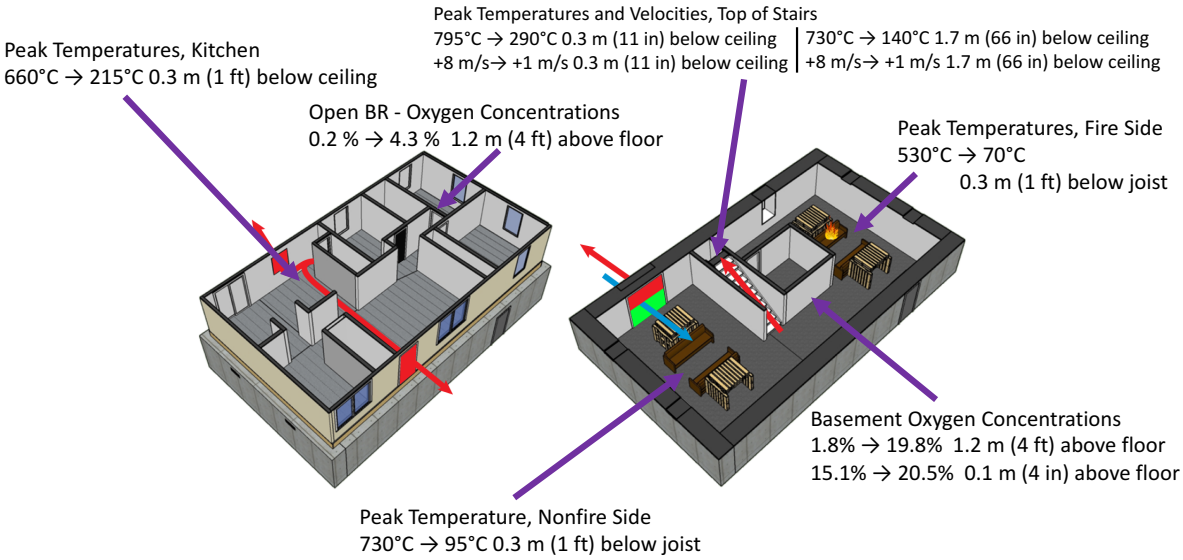

Figure 5.55: Experiment 8 - Isometric images of basement and first floor with selected measurements before suppression began, approximately 620 s after ignition, and at 725 s after primary knockdown. The red arrows indicate the flow of hot gases, the green rectangle indicates the flow of fresh air, and the blue arrow shows the direction of water application.

To further show the impact of a closed door, Figure 5.56 shows the gas concentrations at 1.2 m (4 ft) above the floor of the open and closed bedrooms.

In the open bedroom, the room was almost completely devoid of oxygen and had CO_2 levels that hit the upper limit of the measurement device capabilities at 25 %. CO levels also hit a maximum of 3.3 % (33000 ppm). In the closed bedroom, there was very little decrease in oxygen concentration (20.2 % O_2) and relatively small increases of carbon dioxide (1.1 %) and carbon monoxide levels (0.2 %).

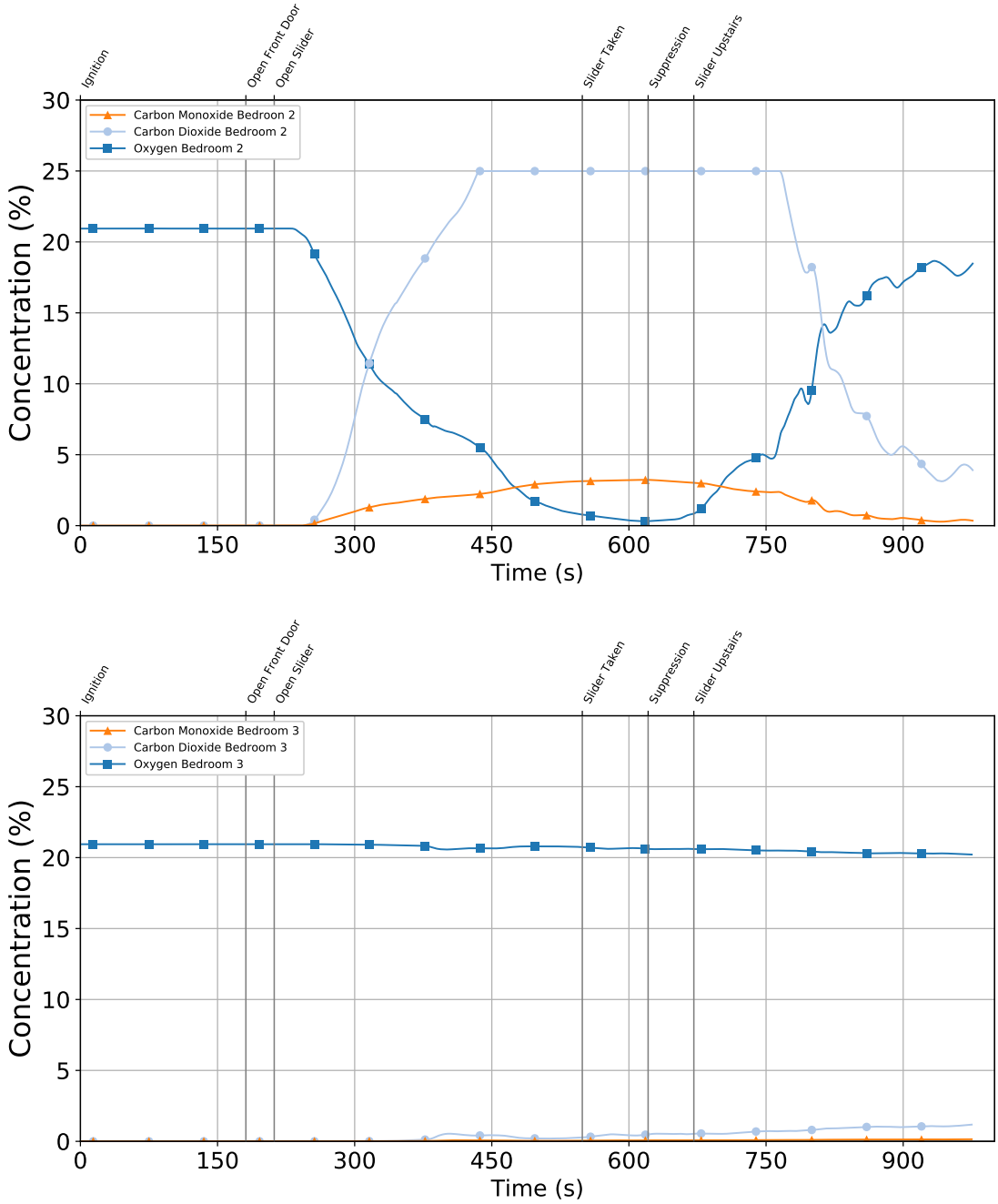

Figure 5.56: Experiment 8 - Gas concentration time history from the open bedroom (top) and the closed bedroom (bottom), both at 1.2 m (4 ft) above the floor on the first floor of the structure.

5.3.2 Experiment 9

The front door and interior stairwell door were open prior to ignition for Experiment 9. Additionally, the four basement vent pipes were open prior to ignition. All other windows and vents were closed. In this experiment, the exposed OSB and wood I-joists (fuel) were replaced with a gypsum

board exposure. Gypsum board covering of the exposed wood floor assembly would remove some of the fuel load and mitigate the structural collapse hazard for a limited amount of time. Figure 5.57 shows the time history of the temperature profile at the thermocouple array closest to the area of ignition, which occurred on the northeast sofa.

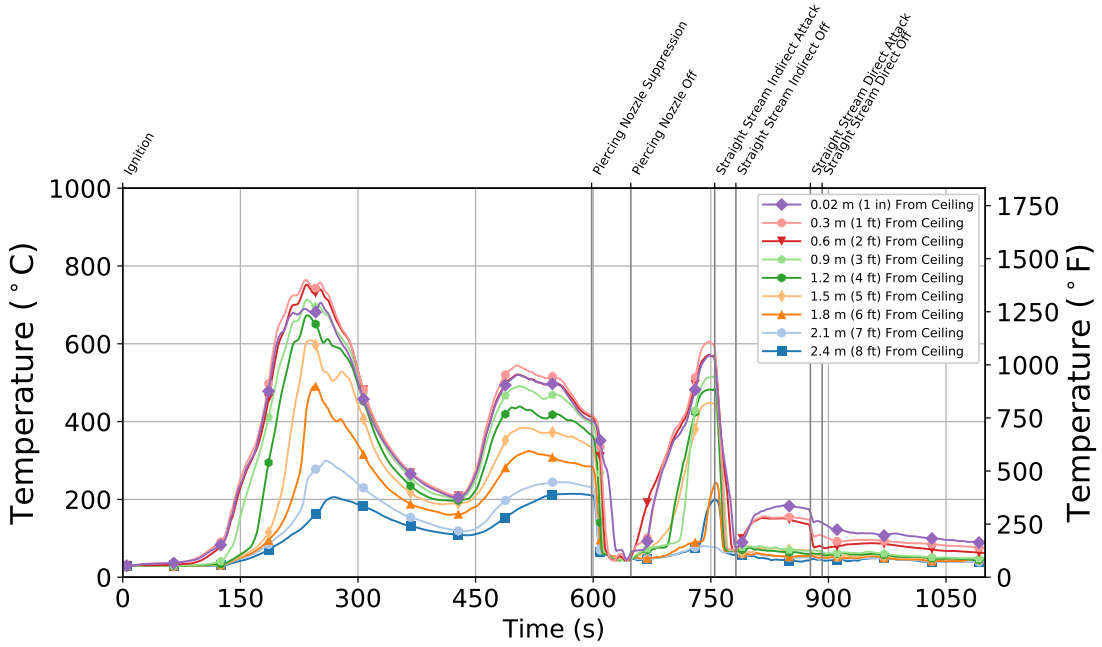

Figure 5.57: Experiment 9 - Thermocouple temperature time history from the Quadrant C thermocouple array in the basement.

The temperature curve from Quadrant C in Figure 5.57 followed a fire-growth curve of ignition, growth, fully developed, and decay. The initial ramp up and decay followed by a second period of fire growth is from fire dynamics; no changes were made in vent conditions and no suppression actions were taken during these times. This is evident in the gas concentration measurements in the basement at the 1.2 m (4 ft) level (Figure 5.58).

The initial decrease in oxygen concentration relates to the rise in temperature from the first fire growth. As the oxygen reached a low of 8 %, the fire entered a decay phase. As the fire decayed, combustion products exited the structure through the open interior stairwell and the open front door. Oxygen was replaced through the open vent pipes in the basement. The fire then regrew until the first suppression was made by a piercing nozzle through the large basement window on side C. Despite the lack of fuel from the wood floor assembly (on the ceiling), the contents fire alone generated a ventilation limited fire condition and therefore presented a high hazard.

An overview of the fire conditions within the structure before and after suppression with the 150 gpm piercing nozzle suppression approximately 600 s after ignition and 650 s after ignition, respectively is shown in Figure 5.59. The red arrows indicate the flow of hot gases, the green arrows indicate the flow of fresh air. The blue arrow represents the location of the suppression.

The piercing nozzle lowered temperatures and improved gas concentrations throughout the base-

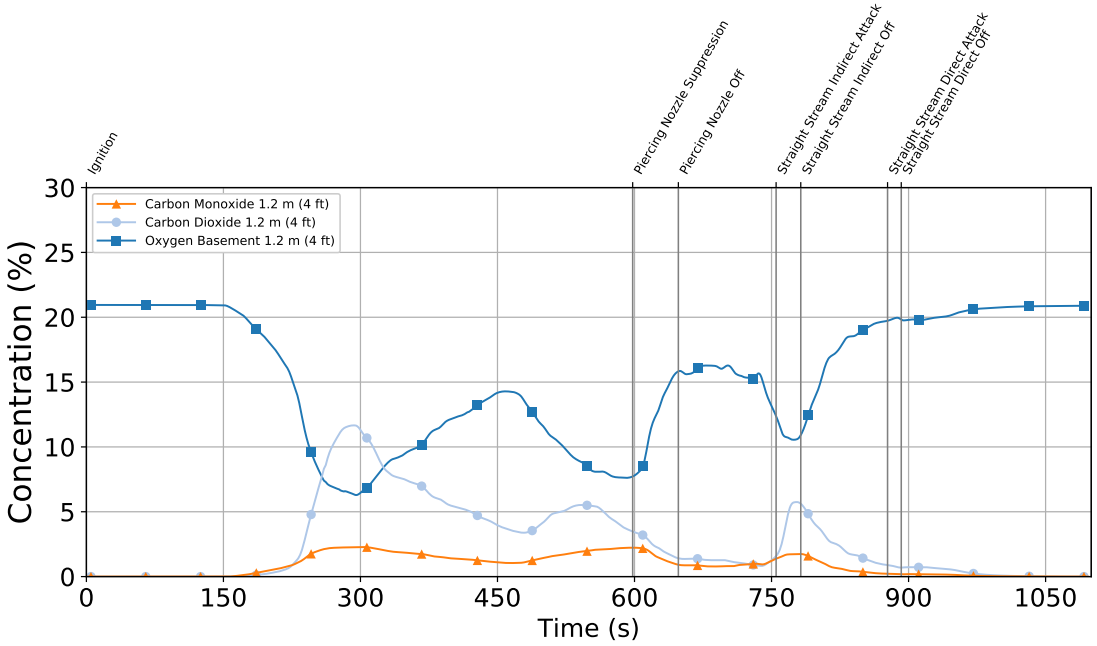

Figure 5.58: Experiment 9 - Gas concentration time history from the 1.2 m (4 ft) elevation in the basement.

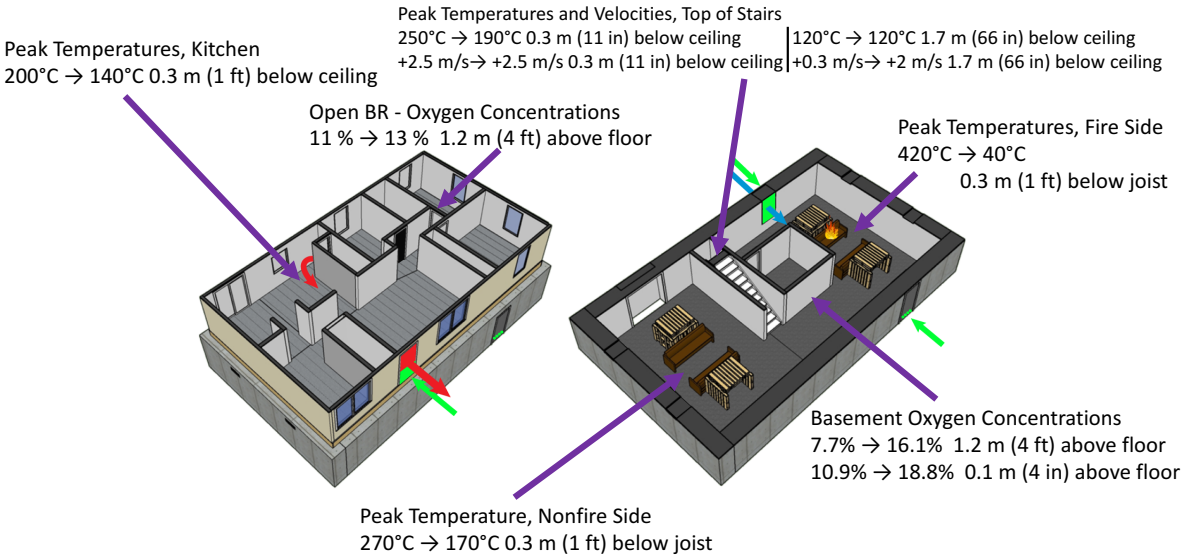

Figure 5.59: Experiment 9 - Isometric images of basement and first floor with selected measurements before and after the 150 gpm piercing nozzle at approximately 600 s after ignition and 650 s after ignition, respectively. The red arrows indicate the flow of hot gases, the green arrows indicate the flow of fresh air, and the blue arrow indicates the location of the suppression.

ment and first floor following water application. After the piercing nozzle was used, the large basement window was cleared to become an open vent. The additional ventilation led to fast regrowth as shown in Figure 5.57. Upon regrowth, a straight stream was applied through the vent

opening 755 s after ignition. The straight stream had better penetration into the room compared to the piercing nozzle. The impact of the straight stream appears in Figure 5.60.

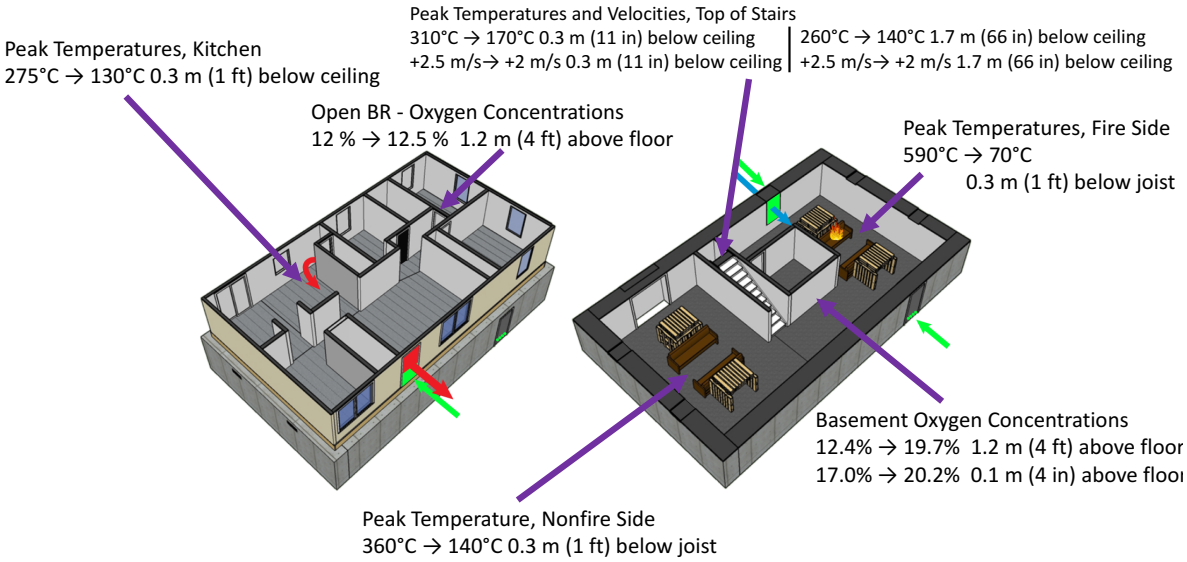

Figure 5.60: Experiment 9 - Isometric images of basement and first floor with selected measurements before and after the straight stream suppression approximately 755 s after ignition and 782 s after ignition, respectively. The red arrows indicate the flow of hot gases, the green arrows indicate the flow of fresh air, and the blue arrow indicates the location of the suppression.

Section 6 Tactical Considerations

Over the years, below-grade fires have provided the fire service with many LODDs and LODIs to learn from. Combining the real world experience with science yields an understanding of how basement fires grow, how they react to different ventilation conditions, and how firefighters can control them in an effective manner. This section highlights some of the key takeaways from this study.

There is no single way to fight a fire. The tactical considerations presented here are supported by both research measurements and firefighting experience. They are titled as considerations because before they can be implemented on the fire ground, each firefighting group — be it a crew, a station, a battalion, department, or mutual aid departments — needs to determine how and when they will embrace the tactics. This report provides the support for why a firefighting group may want to use these tactical considerations.

6.1 Size-Up Is Critical

A size-up of the critical factors is a must on every fire ground. In terms of below-grade fires, key elements of a size-up would include building geometry, fire location and extension, construction type, basement ventilation, basement access, training, and available resources.

Size-up information should include the geometry or layout of structure. The Pang fire, which resulted in the loss of four Seattle firefighters in 1995, was a wake-up call about the hazards of operating above a basement fire. The Pang warehouse had one story above grade on the street where the fire crews entered. The initial crews did not realize that the fire was in the basement of the warehouse. The warehouse basement was partially below grade and accessible at grade from another side of the building. The four firefighters that died fell through the floor into the basement fire.

In response to the Pang fire, some departments required their company officers to conduct a size-up to determine if a building has access at different levels, determine if the fire is below grade, and assess the extent of the fire prior to developing an incident action plan and committing firefighters to interior operations.

Unfortunately, many departments continue to attack below-grade fires by having their initial companies enter through the front door, regardless of the building arrangement, the location of the fire, or the extent of the fire. Between 1998 and 2017, NIOSH documented 24 below grade fires that resulted in 32 firefighter LODDs and 19 LODIs. Typically, these cases involved the firefighters falling through a wood floor assembly into a burning basement or firefighters being overwhelmed by high velocity hot gases flowing from the basement on to an upper level.

This report references previous research conducted on both the structural collapse hazards of basement fires and the threat of rapid fire growth from a change in ventilation a basement fires. This study further demonstrates the need for a thorough size up and use of tactics designed for a below-grade fire. Knowing the floor level that the fire is on prior to committing resources can make for a more effective and efficient attack.

The series of images in Figures 6.1 – 6.3 show both a standard camera image (what a person might see) and an equivalent image from a thermal imaging camera. In Figure 6.1, the pair of images are of the closed front door on the first floor of the structure. In both the standard and thermal imaging views, there was 'nothing showing.' The bright areas on the bottom of the door are due to sunlight.

Figure 6.1: Comparison images 'nothing showing' of a closed door with a standard camera (left) and an IR camera (right).

Figure 6.2 shows same doorway as Figure 6.1, this time just after the doorway was opened. In both images, the hazard behind the door becomes clear. The structure is filled with smoke, with the hottest temperatures toward the ceiling as indicated in the thermal imaging view. In a basement fire with little to no ventilation at the basement level, the thermal conditions at the door may not appear to exhibit a high hazard, but the structure of the floor still could be compromised. The hole made by a firefighter falling through the floor may be enough of a change in ventilation to enable a flashover of the basement or localized burning in the area of the downed firefighter.

Figure 6.2: Comparison images of a open door with a standard camera (left) and an IR camera (right).

In the standard image of the two windows in Figure 6.3, it would be difficult to distinguish the differences in the potential hazard from sight alone. The thermal image view shows a hot versus a cool room. One of the rooms was open to the fire environment while the other room was isolated or protected from the fire environment by a closed door.

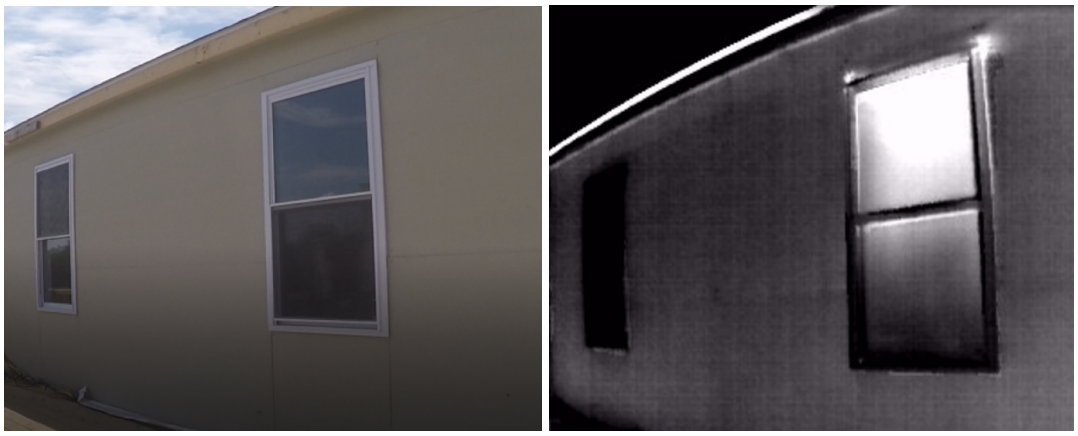

Figure 6.3: Comparison images of the first floor of side C of the structure with a standard camera (left) and an IR camera (right).

Once the front door has been opened the presence and height of a neutral plane in the front doorway may provide valuable information regarding the location of the fire. If the below grade fire has an air intake below grade the front door will exhibit a neutral plane that is low to the floor or no neutral plane with smoke down to the floor. If the below grade intake is sufficient to sustain combustion, the temperature and velocity of the smoke exiting the front door will be higher than the exhaust flow from a below grade fire without any air supply. Consider the front door velocity data for three experiments with varying basement ventilation. Experiment 3, Figure 6.4, had no basement access or leakage and only the top two probes measured exhaust flow. This indicated that the neutral plane was between 0.6 m (22 in.) and 0.8 m (33 in.) below the top of the doorway.

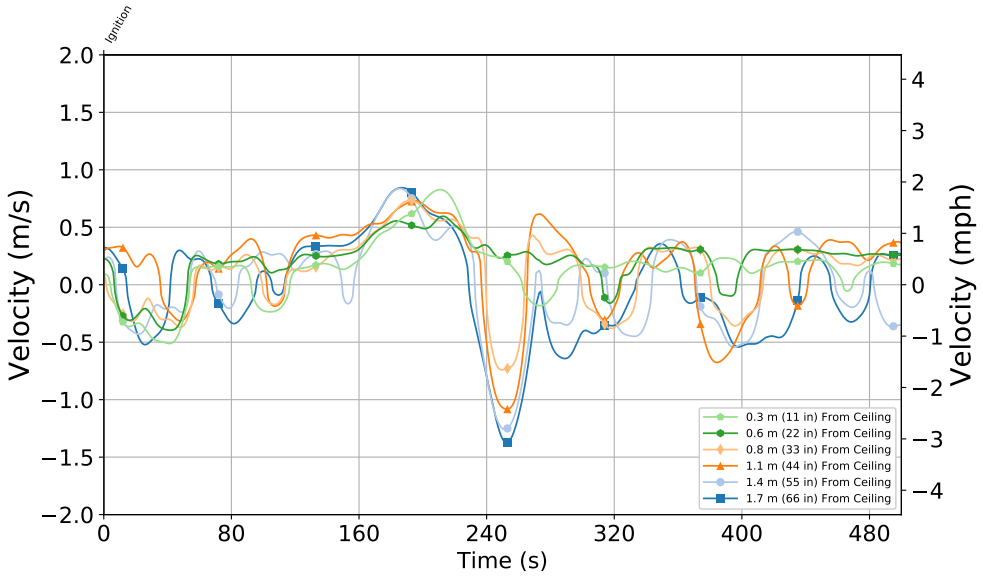

Figure 6.4: Experiment 3 - Front door velocity time history. Positive values indicate gases leaving the structure and negative values indicate air entering the structure.

In Experiment 4, leakage was added to the basement in terms of four, 0.15 m (6 in.) diameter

pipes. Figure 6.5 shows that the addition of ventilation to the basement lowered the neutral plane. The top three probes measured exhaust flow, which indicated that the neutral plane was between 0.8 m (33 in.) and 1.1 m (44 in.) from the top of the doorway. The third experiment, Experiment 8, had direct access to the basement through a sliding glass door. Upon the slider being opened, all six probes at the front door indicated exhaust flow. Therefore, a neutral plane did not exist on the first floor or it was lower than the probe that was 1.7 m (66 in.) below the top of the doorway. Note the increase in magnitude for case with the most significant basement ventilation.

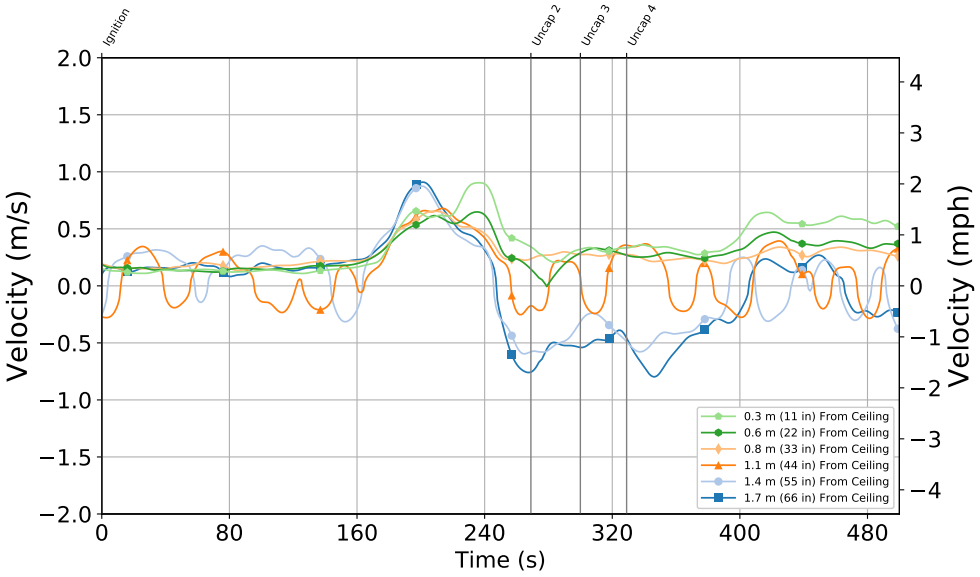

Figure 6.5: Experiment 4 - Front door velocity time history. Positive values indicate gases leaving the structure and negative values indicate air entering the structure.

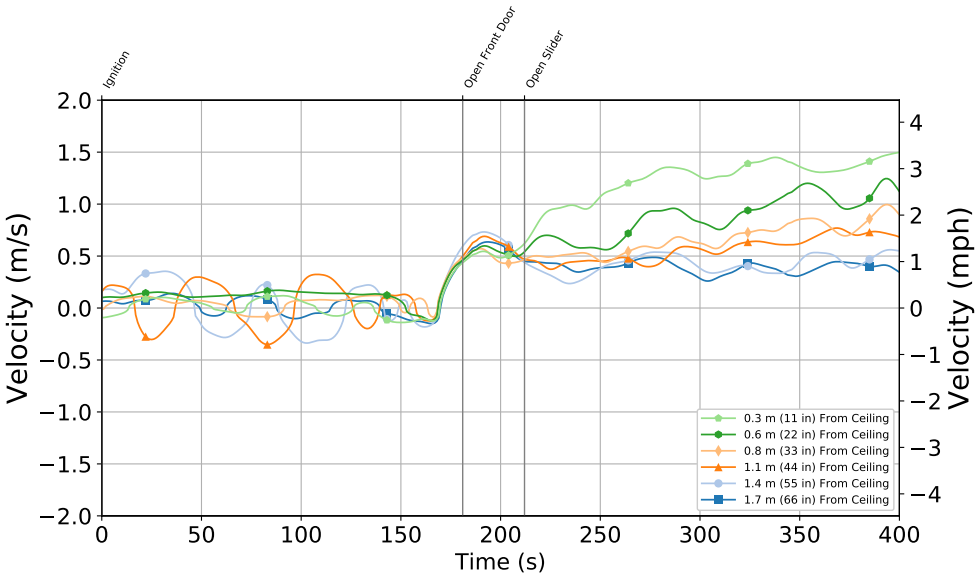

Figure 6.6: Experiment 5 - Front door velocity time history. Positive values indicate gases leaving the structure and negative values indicate air entering the structure.

The scenario of a basement fire with the potential for basement ventilation can set-up a false indicator on the location of the fire. With the front door serving as the only opening between the fire in the basement and the exterior of the structure, bi-directional flow through the front door may be misleading as to the location of the fire. Normally the presence of a clear neutral plane would indicate the fire is on the same level as the doorway. Not the case here. Figure 6.7 shows three IR images of the front for the three experiments (Experiments 3, 4, and 8) discussed above. Based on the experiment data, the red plus signs indicate hot gases leaving the structure (exhaust) while the green minus signs indicate ambient air entering the structure (intake).

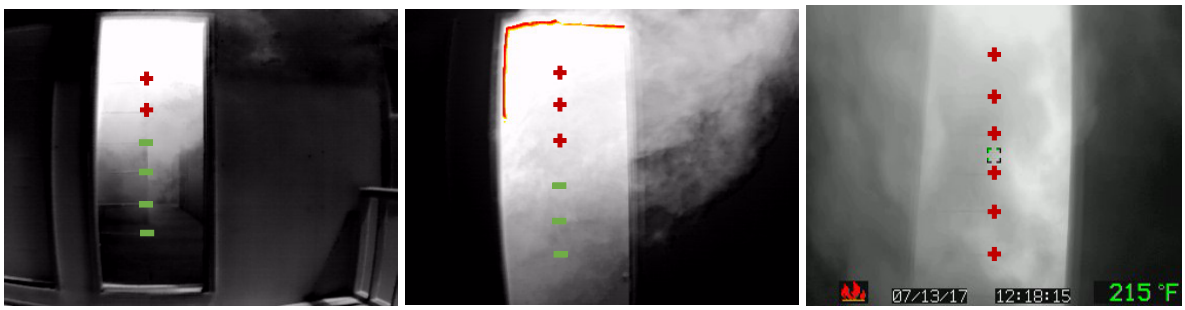

Figure 6.7: Comparison IR camera images of neutral planes from Experiment 3(left), Experiment 4(center), and Experiment 8 (right). The red plus signs indicate hot gases leaving the structure while the green minus signs indicate ambient air entering the structure.

If firefighters enter the structure, above the fire floor, any addition of below grade ventilation could result in a rapid increase the HRR of the fire in the basement. The increased HRR in the basement will increase the temperatures and velocity of the hot gas flows up the stairs and out the front door. This could place the entry firefighters in the exhaust portion of the flow path, a high hazard area of

operation.

The use of thermal imagers on the fire ground is a study by itself, but the images are presented to show that an increased knowledge of the fire ground could impact the decision making on scene. Utilizing firefighter skill, training, and tools to assess the scene through a size-up can improve the effectiveness and efficiency of the fire attack.

6.2 Below-Grade Fires are Likely to be Ventilation-Limited

Previous work in acquired structures by UL and NIST in Chicago, Ill. [29] and Governors Island, N.Y. [30] had shown that basement fires are likely to be ventilation limited. For these experiments, the structure was purpose built. Based on standard leakage calculation methods and without additional leakage to the basement, the experimental structure used for the project was considered tight to moderately tight (recall Section 3.1). For all basement fire experiments in this study, regardless of leakage or ventilation conditions, the fires were ventilation-limited. In Experiment 5, in which the interior basement door was open, a basement side window near ignition was open and the front door was open at time of ignition. Figures 6.8 and 6.9 show the decrease in temperature on the fire side of the basement in conjunction with the decrease in oxygen concentration below 15 %.

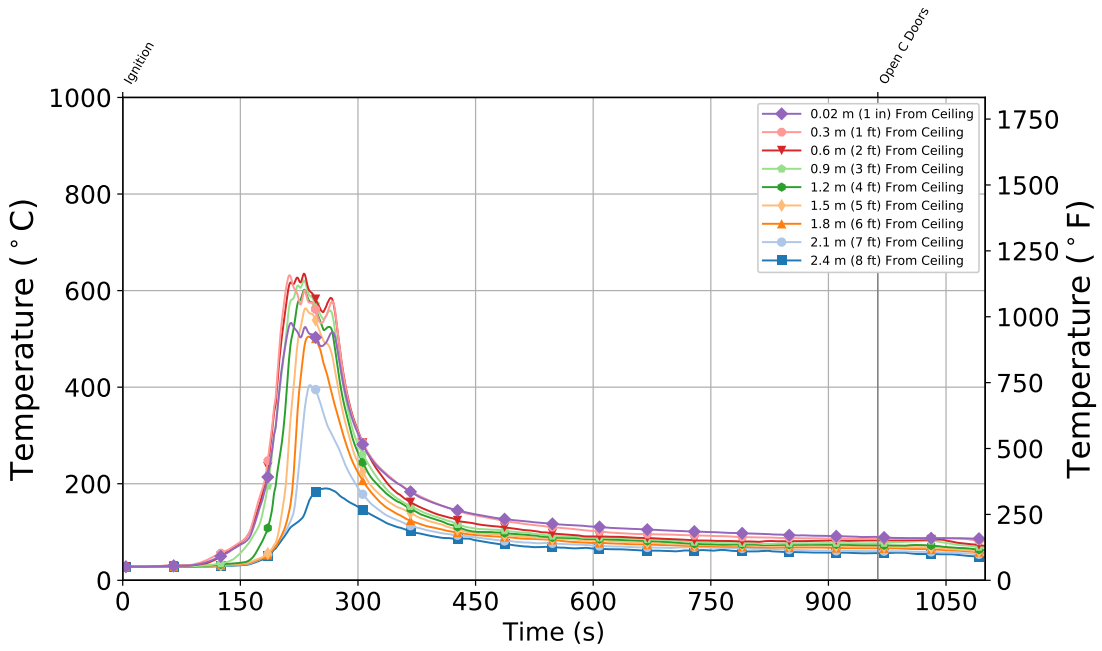

Figure 6.8: Experiment 5 - Thermocouple temperature profile from Quadrant C, fire side.

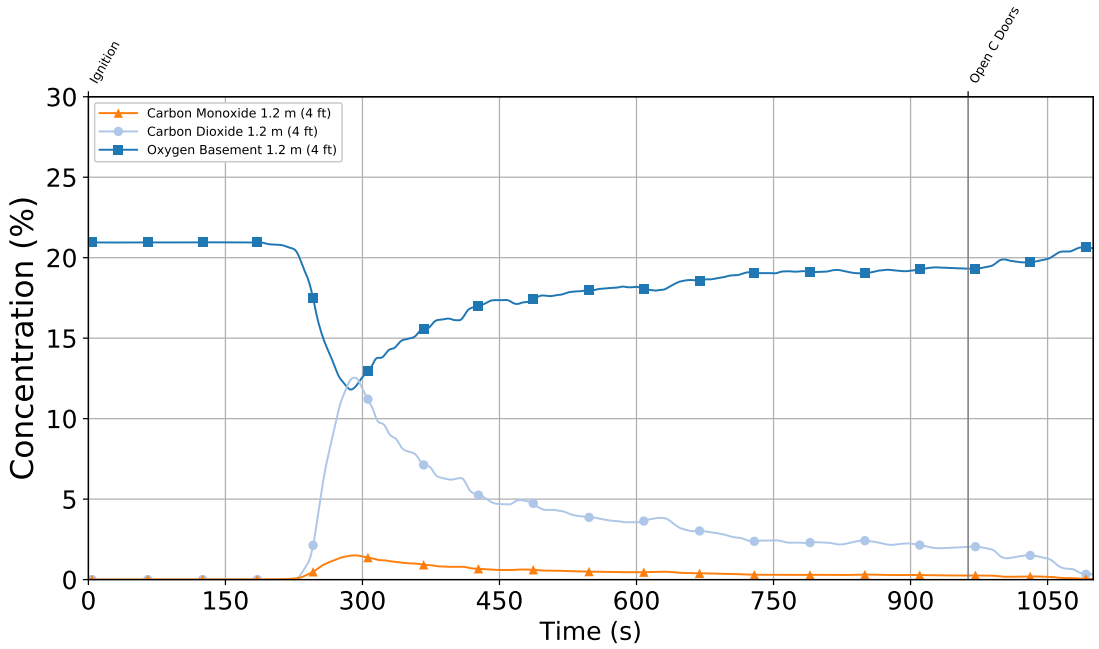

Figure 6.9: Experiment 5 - Gas concentration in the basement 1.2 m (4 ft) above the floor.

Consider the experiment with the most significant basement leakage, Experiment 8. During this experiment, the basement sliding glass door was completely vented (1.83 m (6 ft) wide) in addition to two 0.15 m (6 in) vent pipes in the basement and open doors at the top of the stairs, and the front of the structure providing a path for a portion of the fire exhaust flow upstairs. In Figure 6.10, the gas concentration at 1.2 m shows some recovery to approximately 15 % at 450 s after ignition but quickly drops below 5 % after half of the sliding glass door was opened.

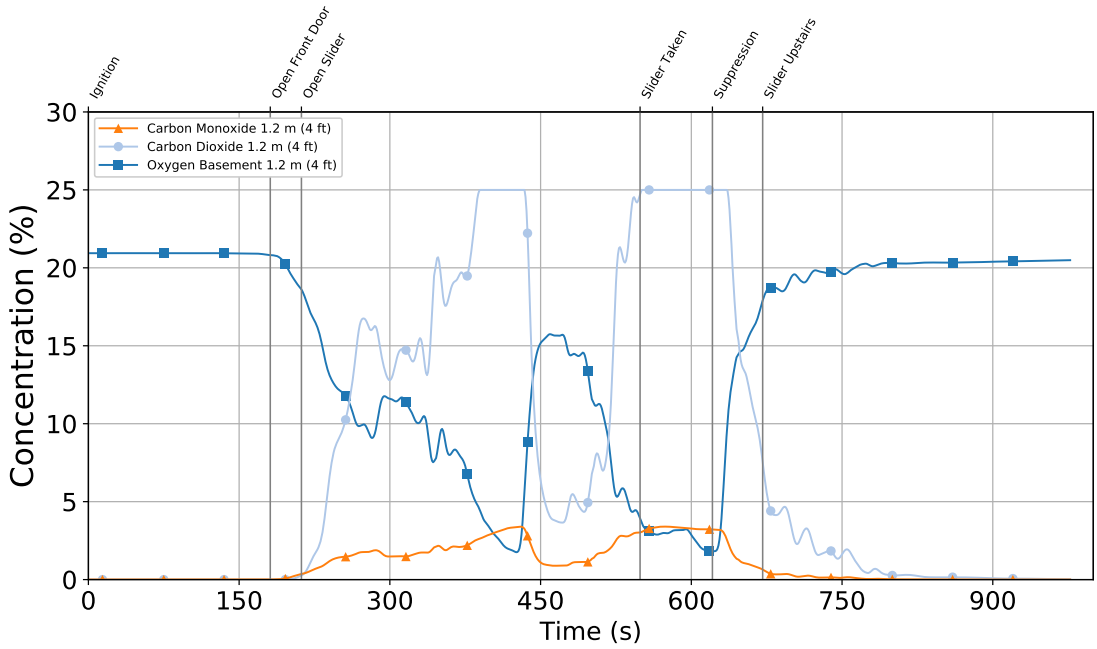

Figure 6.10: Experiment 8 - Gas concentration in the basement 1.2 m (4 ft) above the floor.

The photograph in Figure 6.11 shows flames extending outside of the basement from the sliding glass door opening and through the failed window at the top of the stairs prior to suppression at approximately 600 s after ignition. Flaming combustion is occurring outside of the structure because that is the only location where there is sufficient oxygen to support burning. This is a clear indication that the oxygen concentration within the structure cannot support the combustion of the heat and fuel that is being generated in the structure. Even though there is fire coming out of multiple openings the fire is still ventilation limited. Additional openings anywhere in the structure would continue to increase the size of the fire.

Figure 6.11: Photograph of flaming combustion extending outside of the structure indicating the presence of a ventilation-limited structure fire during Experiment 8.

6.3 Coordinating Ventilation with Water Application is Required to Limit the Growth of a Ventilation-Limited Fire

Coordination is the combined effort to cool the fire/fuel gases and ventilate to reduce the hazard. Remember, the simple act of opening a door or taking a window is an act of ventilation. It is important to conduct those acts with purpose and in coordination with suppression actions. A few examples of prior research has shown the positive impact of a coordinated attack in ventilated fire, including: the Governors Island experiments in New York [30], UL's vertical ventilation experiments [50], and UL FSRI's fire attack experiments [51].

In eight of the 12 experiments conducted, suppression actions were performed. In the four cases without suppression, the fires were self-extinguished due to a lack of oxygen in the basement. Of the eight suppression experiments, two of those experiments were uncoordinated: Experiment 6 and Experiment 8.

In Experiment 6, the upstairs sliding glass door was opened 1,480 s after ignition to provide additional ventilation because wind was limiting the exhaust through the front door. Figure 6.12 shows an overview of the structure prior to the sliding glass door being opened and after the sliding glass door was opened (1,723 s post ignition). Notice the increase in temperatures and velocities as well as the decrease in oxygen concentration throughout the structure. The red arrows indicate the flow

of hot gases, and the green arrows indicate the flow of fresh air.

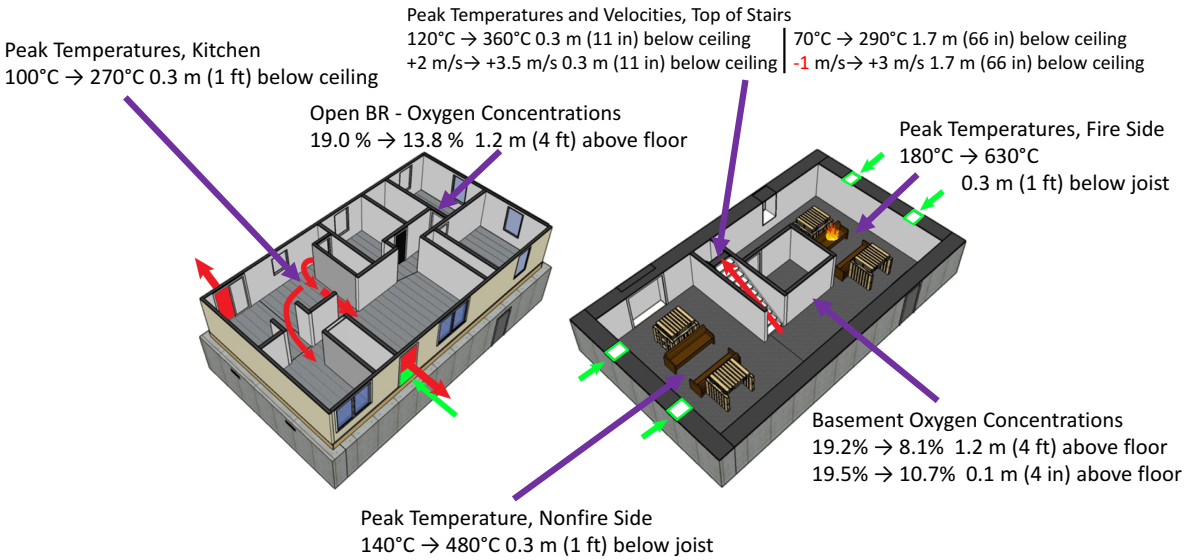

Figure 6.12: Experiment 6 - Isometric images of basement and first floor with selected measurements prior to the sliding glass door being opened (1,480 s after ignition) and after the sliding glass door was opened (1,723 s post ignition). The red arrows indicate the flow of hot gases, and the green arrows indicate the flow of fresh air.

The second example of an uncoordinated attack was Experiment 8. In this case, the basement slider was opened 220 s after ignition and completely vented 550 s after ignition. An overview of the conditions within the structure before and after the basement sliding glass door was vented at approximately 525 s after ignition and 570 s after ignition respectively, are shown in Figure 6.13. Note the increase of the hazard within the structure and that the ventilation led to the fire conditions shown in Figure 6.11. The red arrows indicate the flow of hot gases, and the green arrows indicate the flow of fresh air.

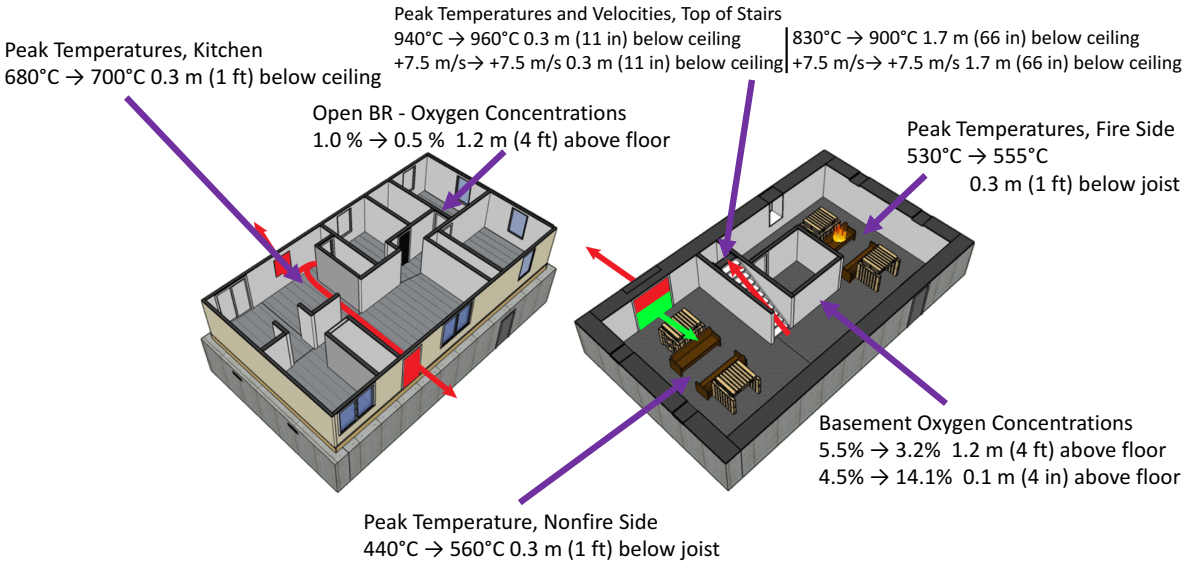

Figure 6.13: Experiment 8 - Isometric images of basement and first floor with selected measurements before the sliding glass door was taken, 525 s after ignition, and at 570 s after ignition. The red arrows indicate the flow of hot gases and the green arrows indicate the flow of fresh air.

6.4 Water Application into the Below-Grade Space is Key to Smoke Cooling

There are several ways in which smoke cooling can occur when there is no or limited access to directly apply water into the fire compartment. In these experiments, smoke cooling occurred by either flowing water through a hole punched through the floor, flowing water through a remote, limited access basement window, or flowing water down the stairs using a remotely operated nozzle. Figure 6.14 shows the flow pattern of a straight stream, 150 gpm piercing nozzle, and a fog stream flowing through a hole in the floor.

Figure 6.14: Photograph of straight stream (top left), the 150 gpm piercing nozzle (top right), and fog stream (bottom) flowing through a hole punched through the floor.

From the flows in Figure 6.14, the difference in coverage area between the straight stream compared to the fog stream and piercing nozzle is evident. Although the streams used were, by experimental design, not able to directly put water on the seat of the fire, the wider patterns tended to be more effective in cooling the fire gases/smoke and wetting fuels in the area. Table 6.1 shows the impact of cooling basement fire side temperatures in the cases in which the suppression action was conducted in a part of the basement without direct access.

Table 6.1: Impact of Remote Suppression Tactic on Smoke Cooling on Fire Side of Basement

Exp #	Suppression Action	Fire Side Basement Temperature (°C)	
		Before Suppression	After Suppression
4[+]	Straight Stream Through Floor	560	575
	150 gpm Piercing Through Floor	560	400
	125 gpm Piercing Through Floor	640	290
	Cellar Nozzle Through Floor	550	270
	Bresnan Distributor Through Floor	800	370
6	Straight Stream Opposite Window	580	160
	Smooth Bore Opposite Window	630	230
12	Fog Stream Top of Stairs	620	320

[+] Suppression through floor was opposite basement fire side (Figure 6.15).

Gas temperatures at 610 °C are typically considered a threshold for flashover. Prior to suppression actions, the basement conditions were at or near flashover conditions, provided there was sufficient oxygen present. After every smoke cooling suppression action in Table 6.1, except straight stream through the floor, there was a significant reduction in fire-side temperature, reducing the hazard throughout the basement. Although the straight stream suppression through the floor showed a slight increase in temperature the change was within the experimental uncertainty of the measurement. In other words, there was negligible change in the temperature from the straight stream. Figure 6.15 shows the location of the suppression hole in the basement relative to the fire in Experiment 4. Recall from Section 4 the that hole was located approximately 0.61 m (24 in.) from the doorway and 0.41 m (16 in.) off the wall immediately to the left of the front door.

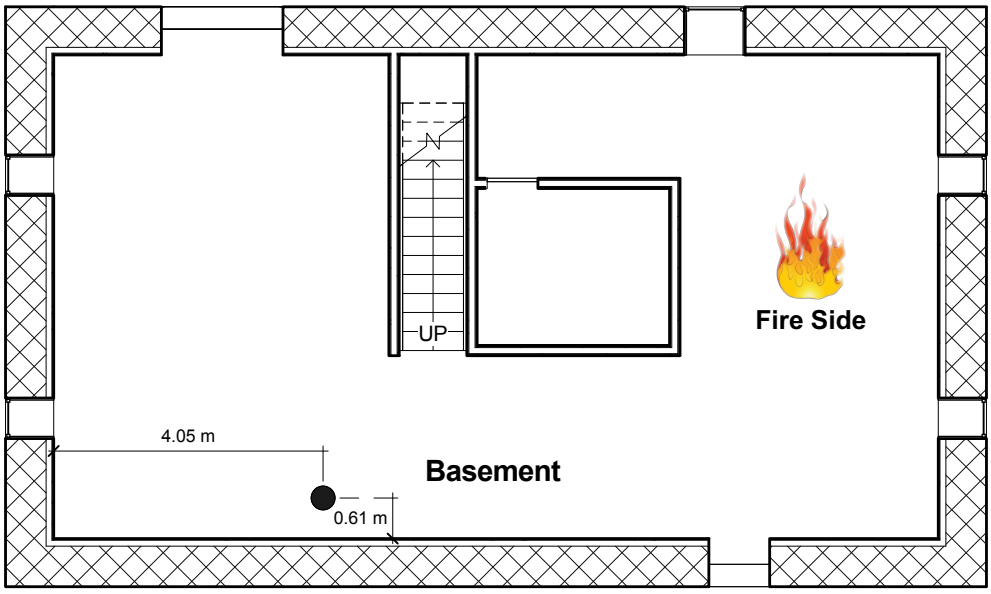

Figure 6.15: Dimensioned schematic indicating the location of the hole for through-floor suppression and location of the fire.

6.5 Effective Water Application into the Below-Grade Space Reduces the Hazard Throughout the Structure

To quantify the impact of effective water application in the basement on reducing the hazard throughout the structure, the change in temperature at the fire-side thermocouple 0.3 m (1 ft) below the basement ceiling as well as the thermocouple 0.28 m (11 in.) below the ceiling at the top of stairwell were examined. The temperature changes for experiments in which there was fire suppression appear in Table 6.2. Note that several experiments had multiple suppression actions.

Table 6.2: Impact of Suppression Action at Ignition and Top of Stairwell

Exp #	Suppression Action	Change in Temperature (°C)	
		Fire Side	Top of Stairwell
4[+]	Straight Stream Through Floor	+15	-5
	150 gpm Piercing Through Floor	-160	-55
	125 gpm Piercing Through Floor	-350	-95
	Cellar Nozzle Through Floor	-280	-60
	Bresnan Distributor Through Floor	-430	-80
6	Straight Stream Opposite Window	-420	-250
	Smooth Bore Opposite Window	-400	-180
	Straight Stream Fire Window	-720	-200
7[*]	Straight Stream Through Floor	-160	-50
	Fog Stream Through Floor	-470	-115
8	Basement Slider Interior	-635	-685
9	150 gpm Piercing in Window	-380	-60
	Straight Stream in Window	-520	-140
11[*]	125 gpm Piercing Through Floor	-550	-515
12	Fog Stream Top of Stairs	-300	-115

[+] Suppression through floor was opposite basement fire side.
[*] Suppression through floor was above basement fire side.

The results show that all suppression actions, except straight stream through the floor from Experiment 4, had a significant impact in lowering temperatures in the basement as well as the temperatures of the gases at the top of interior stairwell. In Experiment 4, the hole through the floor was on the non fire side (as noted by the [+] in Table 6.2). Due to the tight pattern of a straight stream and given that the stream was pointed directly at the floor, it had a negligible impact on the temperatures remote from the application area. The temperature on the fire side was 560 °C prior to the straight stream application. Given the uncertainty of a thermocouple measurement of ±15 % (see Section 3.2.3), it cannot be conclusively determined if the change in temperature was a result of suppression. The thermocouple 0.3 m (1 ft) below the basement ceiling on the non fire side (area of application) dropped by 100 °C, indicating that there was a reduction in hazard where there was water. Effective water application into a below grade fire will slow the destruction of the

structure and improve the conditions for accessing the basement from the interior stair. Water on the fire side is most effective and the more surfaces of burning objects that get water, the better. The more hot smoke that gets water, the better.

A Note Of Caution: Although it may be easy to make assessments about the relative effectiveness of the suppression actions in Table 6.2 based on the absolute change in the temperature, the hazard in the structure was not uniform for each suppression action. In other words, the temperature at the start of suppression was not constant. Several factors influenced the fire behavior, with the most dominate element being the state of ventilation at the time of suppression.

6.6 Options Exist to Make a Coordinated and Effective Attack

There are options to make a coordinated and effective attack in a basement fire with limited access. This can occur from the top down by punching or cutting a hole through the floor with available common firefighter tools to feed a line in, or by using a piercing nozzle. A second option to get water through the side of the building by punching or cutting through a band board, concrete block, through small basement windows, or vents (in the case of a crawl space fire). Figure 6.16 shows a straight stream flowing directly through a side window as well as a straight stream angled off the ceiling to create a broken stream to change the water distribution within the structure.

Figure 6.16: Photograph of straight stream through a window (left) and the broken stream produced by angling the stream off the ceiling (right).

6.7 When Possible, It Is Best to Fight the Fire on its Own Level

If the plan of attack for a basement fire is to enter the structure and attack the fire by advancing down an interior stairwell, firefighters would be exposed to the thermal conditions at the top of stairwell. For Experiments 3-12, heat flux gauges and instrumented turnout gear samples were installed along the wall opposite the stairwell (see Figure 3.4) 0.86 m (34 in.) above the floor.

Table 6.3 shows the exterior temperature of the gear as well as the heat flux exposure prior to each suppression action in the series of experiments.

Table 6.3: Thermal Exposure Conditions at the Top of the Stairs

Exp #	Suppression Action	Turnout Gear Temperature	Exposure Heat Flux
3	N/A	122 °C	10 kW/m^2
4$^+$	Straight Stream Through Floor	218 °C	15 kW/m^2
	150 gpm Piercing Through Floor	220 °C	16 kW/m^2
	125 gpm Piercing Through Floor	202 °C	16 kW/m^2
	Cellar Nozzle Through Floor	160 °C	10 kW/m^2
	Bresnan Distributor Through Floor	220 °C	15 kW/m^2
5	N/A	158 °C	10 kW/m^2
6	Straight Stream Opposite Window	280 °C	20 kW/m^2
	Smooth Bore Opposite Window	273 °C	21 kW/m^2
	Straight Stream Fire Window	250 °C	14 kW/m^2
7*	Straight Stream Through Floor	540 °C	53 kW/m^2
	Fog Stream Through Floor	290 °C	24 kW/m^2
8	Basement Slider Interior	898 °C	86 kW/m^2
9	150 gpm Piercing in Window	208 °C	10 kW/m^2
	Straight Stream Basement Window	286 °C	13 kW/m^2
10	Residential Sprinkler	50 °C	2 kW/m^2
11*	125 gpm Piercing Through Floor	630 °C	45 kW/m^2
12	Fog Stream Top of Stairs	200 °C	16 kW/m^2

$^+$ Suppression through floor was opposite basement fire side.
* Suppression through floor was above basement fire side.

From work describing the firefighter operational environment, a typical exposure is on the order of 2-3 kW/m^2 [52]. In all experiments except the one with a functional sprinkler system, the heat flux exposure at the top of the stairwell was approximately 10 kW/m^2 or higher. Additionally, SCBA face pieces start to soften at heat flux exposures of 15+ kW/m^2 [53]. From NFPA 1971, turnout gear is tested to 260 °C (500 °F) for 5 minutes [54]. In many of the experiments, exterior gear temperatures were near or above this value. Table 6.4 shows the exterior temperature of the gear as well as the heat flux exposure after each suppression action was performed from the series of experiments.

Table 6.4: Thermal Exposure Conditions at the Top of the Stairs Following Each Suppression

Exp #	Suppression Action	Turnout Gear Temperature	Exposure Heat Flux
3	N/A		
4[+]	Straight Stream Through Floor	209 °C	13 kW/m^2
	150 gpm Piercing Through Floor	166 °C	7 kW/m^2
	125 gpm Piercing Through Floor	125 °C	4 kW/m^2
	Cellar Nozzle Through Floor	115 °C	4 kW/m^2
	Bresnan Distributor Through Floor	166 °C	7 kW/m^2
5	N/A		
6	Straight Stream Opposite Window	82 °C	3 kW/m^2
	Smooth Bore Opposite Window	140 °C	6 kW/m^2
	Straight Stream Fire Window	120 °C	6 kW/m^2
7[*]	Straight Stream Through Floor	248 °C	15 kW/m^2
	Fog Stream Through Floor	170 °C	9 kW/m^2
8	Basement Slider Interior	184 °C	8 kW/m^2
9	150 gpm Piercing in Window	136 °C	4 kW/m^2
	Straight Stream Basement Window	140 °C	4 kW/m^2
10	Residential Sprinkler	40 °C	0 kW/m^2
11[*]	125 gpm Piercing Through Floor	81 °C	1 kW/m^2
12	Fog Stream Top of Stairs	96 °C	1 kW/m^2

[+] Suppression through floor was opposite basement fire side.
[*] Suppression through floor was above basement fire side.

Following suppression actions, in all cases exterior gear temperature dropped below 260 °C (500 °F). Heat flux exposure dropped below 10 kW/m^2 in all but the two cases involving the straight stream suppression through the floor. Even in those cases, the potential exposure hazard at the top of the stairwell was lowered significantly.

6.8 Occupants Behind Closed Doors Have the Best Chance for Survival

To compare the impact of a closed bedroom door vs. an open bedroom door, all the experiments had a closed bedroom and open bedroom instrumented with thermocouples and gas concentration (O_2, CO, and CO_2) measurement ports. The gas concentrations and thermocouple temperatures were measured 1.2 m (4 ft) above the floor. For each experiment in Table 6.5, the values (gas concentrations and temperature) for the closed and open door were determined at the time from ignition when the oxygen in the open bedroom reached its first minimum value. Carbon monoxide values at the time post-ignition oxygen reached its first minimum value are also presented (Ta-

ble 6.7). For experiments in which gas concentrations were unavailable, the time was selected based on the first maximum temperature value at 1.2 m (4 ft) in the open bedroom. Table 6.5 shows the comparison of oxygen and temperature for a closed and open bedroom on the first floor, and Table 6.7 shows the comparison of carbon monoxide and temperature.

Table 6.5: Impact of Open and Closed Door On Temperature and Oxygen

Exp #	Time (s)	Closed Door		Open Door	
		Temperature (°C)	Oxygen (%)	Temperature (°C)	Oxygen (%)
1	1200	37	20.9	42	18.4
2	600	33	20.9	53	14.3
3	533	33	20.9	48	14.7
4	1200	37	N/A	92	N/A
5	480	30	20.8	50	13.8
6	360	30	20.8	64	12.4
7	220	36	N/A	82	N/A
8	620	38	20.6	150	0.3
9	430	29	20.7	56	12.5
10	540	28	20.8	32	19.9
11	910	31	20.9	110	N/A
12	410	21	20.9	54	11.1

In all 12 experiments, the oxygen concentration in the bedroom behind the closed door remained above 20 % and the temperature remained at or below 38 °C (100 °F). The open at-grade basement door with the front door as an exhaust vent flow path (Experiment 8) provided the best ventilation scenario for the fire. As a result, it also provided the worst-case exposure conditions throughout the structure both in the basement and upstairs. From Table 6.5, despite the oxygen dropping close to 0 % and temperatures at 150 °C (302 °F) in the open bedroom, the oxygen concentration in the closed bedroom only dropped to 20.6 %. Table 6.6 shows the physiological effects of decreasing oxygen percentage in the environment [55].

Table 6.6: Impact of Oxygen Deprivation [55]

Oxygen (%) Range	Effects
19.5	Minimum acceptable O_2 level
15-19	Decreased ability to work strenuously Impaired coordination, early symptoms
12-14	Respiration increases, judgment impacted
10-12	Respiration increases, lips blue
8-10	Mental failure, fainting, nausea, unconsciousness, vomiting
6-8	8 minute exposure is fatal; 6 minute exposure is 50% fatal; 4-5 minute exposure - possible recovery
4-6	Coma in 40 seconds, death

The carbon monoxide concentrations also show the positive impact of a closed door. Table 6.7 shows the carbon monoxide and temperature values presented at the time when the oxygen concentration reached its first minimum value in the open bedroom.

Table 6.7: Impact of Open and Closed Door On Temperature and Carbon Monoxide

Exp #	Time (s)	Closed Door		Open Door	
		Temperature (°C)	CO (%, [ppm])	Temperature (°C)	CO (%, [ppm])
1	1200	37	0.1 [1000]	42	0.5 [5000]
2	600	33	0.1 [1000]	53	1.1 [11000]
3	533	33	0.1 [1000]	48	1.1 [11000]
4	1200	37	N/A	92	N/A
5	480	30	0.1 [1000]	50	1.1 [11000]
6	360	30	0	64	1.5 [15000]
7	220	36	N/A	82	N/A
8	620	38	0.2 [2000]	150	3.3 [33000]
9	430	29	0.1 [1000]	56	1.3 [13000]
10	540	28	0.1 [1000]	32	0.2 [2000]
11	910	31	0	110	1.9 [19000]
12	410	21	0	54	1.7 [17000]

For the worst-case exposure, Experiment 8, the open bedroom CO concentration was 3.3 % (33,000 ppm) compared to 0.2% (2,000 ppm) in the closed bedroom. In all other experiments, the peak CO concentration in the closed bedroom was only 0.1 % (1,000 ppm) compared to a range between 0.5 % (5,000 ppm) and 1.9 % (19,000 ppm) in the open bedroom. Table 6.8 shows the physiological impact of increasing levels of CO exposure [55, 56].

Table 6.8: Impact of Carbon Monoxide Inhalation [55, 56]

CO (%, [ppm])	Time	Effect
0.005 [50]	8 hr	Permissible exposure level
0.02 [200]	3 hr	Slight headache, discomfort
0.06 [600]	1 hr	Headache, discomfort
0.1-0.2 [1000-2000]	30 min	Slight heart palpitation
	1.5 hr	Tendency to stagger
	2 hr	Confusion, nausea, headache
0.2-0.25 [2000-2500]	30 min	Unconsciousness
0.32 [3200]	5-20 min	Headache, dizziness and nausea
	30 min	Death
0.64 [6400]	1-2 min	Headache, dizziness and nausea
	10-15 min	Death
1.28 [12,800]	1-3 min	Death

6.9 Residential Sprinklers Effectively Limit the Hazard

The impact of the residential sprinkler system on the hazard in the structure was determined using the minimum oxygen concentration in the basement at 1.2 m (4 ft), and the peak temperature on the fire side of the basement also at the 1.2 m (4 ft) elevation. These two measurements address the thermal hazard and gas inhalation hazard. Table 6.9 shows the peak temperature and minimum oxygen percentage for each of the experiments. The residential sprinkler system experiment, Experiment 10, is highlighted.

Table 6.9: Impact of Residential Sprinkler System

Exp #	Peak Fire Side Temperature @ 1.2 m (4 ft)	Minimum Basement O_2 @ 1.2 m (4 ft)
1	380 °C	8.8 %
2	415 °C	10.7 %
3	545 °C	9.4 %
4	530 °C	N/A %
5	575 °C	11.9 %
6	795 °C	9.2 %
7	940 °C	N/A
8	850 °C	1.8 %
9	640 °C	6.2 %
10	40 °C	18.8 %
11	425 °C	5.7 %
12	550 °C	5.1 %

The experiment with the functional sprinkler system had a peak fire side temperature of 40 °C (104 °F) compared to the other experiments which had peak temperatures at 1.2 m (4 ft) in excess of 350 °C (660 °F). Similarly, the oxygen concentration never dropped below 18.8 % in the sprinkler experiment compared to a range of 11.9 % to 1.8 % for the non sprinklered experiments. Recall the hazards of low oxygen from Table 6.6.

In addition to maintaining tenable conditions for civilians in the structure, who are not intimate with the fire, the sprinkler system limits the fire's ability to compromise the structural integrity of the flooring system.

Section 7 Research Needs

This study has added to the understanding of the fire dynamics of basement fires for a range of different ventilation and access conditions. In addition, several options for effectively fighting basement fires were demonstrated and documented, and the information was developed into a training program. Based on the gap assessment developed by the technical panel at the beginning of the study there are two areas which could benefit from additional study: use of thermal imagers for size-up and tactical progression and assessment of fire damage to the structure prior to entry.

Size-up is a fundamental component of every firefighting operation. One critical factor of size-up is finding where the fire is located. This study and previous studies showed that basement fires can provide misleading and/or limited visual cues to the first arriving officer [28, 29].

In this study, thermal imagers were used as part of a size-up process, and they provided valuable information that could not be seen with the naked eye. This was shown in the tactical considerations for size-up (see Section 6.1), such as quickly identifying rooms exposed to the fire environment versus rooms isolated from the fire environment. Thermal imagers also help visualize the movement of heated soot particles to assess the direction and magnitude of the smoke flow in structures with little to no visibility.

We also know thermal imagers have limitations, especially with regard to trying to determine the extent of fire in a basement or the structural stability of the floor just prior to entering the structure. The materials typically used in residential wall and wood floor assemblies are good insulators (i.e. poor conductors of heat). As a result, a thermal imager will not provide a reliable indication of the thermal conditions on the other side of a wall, floor, or ceiling. For example, UL FSRI and NIST have documented cases in which post-flashover conditions ($>$ 600 °C (1,112 °F)) existed below a wood floor assembly, while the energy flow through the floor "seen" by a thermal imager yielded an "apparent temperature" reading of 38 °C to 93 °C (100 °F to 200 °F) [28, 29]. Because of the insulating qualities of materials used in building construction, a firefighter with limited understanding of how a thermal imager operates may believe that based on the thermal imager information the floor is safe to walk on. In this case, the thermal imager cannot provide an assessment of the structural integrity of the floor. Therefore it is essential that the firefighter using a thermal imager understands that the floor structure could be compromised.

Thermal imagers are great examples of devices that provide capabilities to firefighters that were unknown just a few decades ago. Thermal imagers are also great examples of devices that require specific training to use safely and effectively on the fire ground. The development of that training to improve the use of thermal imagers for size-up should be the focus of a future study.

Section 8 Summary

Many firefighter LODIs and LODDs have occurred while operating at a basement fire or a fire on a level below them. In response to these losses, the ISFSI partnered with UL FSRI to examine tactics that could increase the effectiveness and safety of fighting basement fires. A technical panel was assembled to examine previous LODIs and LODDs and previous basement fire research results to develop the research questions for this study. This study was supported by a DHS/FEMA Assistance to Firefighters Grant.

Prior research has shown the high risks presented by basement fires are unexpected floor collapse and rapid onset of high heat. Prior research also indicated the methods that firefighters have traditionally used to determine the structural integrity of the floor are of little value with lightweight construction. Past experiments in townhouse basements have indicated that the most effective method of fighting a basement fire may be through the use of a transitional attack, beginning from the exterior of the building prior to moving in for search and extinguishment.

This study went beyond earlier research by increasing the size of the basement and incorporating three different ventilation and access conditions to the basement: no exterior access to the basement, limited exterior access to the basement, and exterior access to the basement. A variety of fire nozzles and appliances were used to examine means of effectively flowing water into the basement through the floor above, through small side windows, and through basement level doorways. Each of these suppression methods provided a means of fighting the fire at its own level, without having to operate over the fire on an unrated wood floor assembly as well as remaining out of the exhaust portion of the basement fire flow in the basement stairway.

The basement fires were all ventilation limited. These experiments highlighted the importance of identifying a basement fire during size-up and choosing the appropriate tactics that coordinate ventilation with suppression. Any additional ventilation without suppression was shown to increase the size of the fire and increase the hazard to any occupants trapped in the structure.

Effective water application into the basement cooled the fire gases to prevent flashover, slowed the destruction of the structure, and reduced the hazard from fire throughout the structure. Reducing the hazard from the basement fire made entry conditions into a basement with active burning possible for a fully protected firefighter. This action would also support search operations and reduce the threat from heat and toxic gases for any trapped occupants. Occupants isolated from the fire environment by a closed door or other means were provided addition protection when compared with conditions in rooms open to the fire environment.

Although the installation of a protective gypsum board ceiling over the wood floor assembly would effectively delay the onset of structural collapse, it did not reduce the fire hazard generated by the burning contents in the basement. The results of the residential sprinkler system experiment demonstrated the capability of the system to eliminate the structural collapse threat and maintain tenable conditions throughout the structure.

References

[1] Firefighter Fatalities in the United States in 2014. Technical report, U.S. Department of Homeland Security, Federal Emergency Management Agency, U.S. Fire Administration, National Fire Data Center and The National Fallen Firefighters Foundation, Emmitsburg, Maryland, August 2015.

[2] C.G. Weinschenk, K.J. Overholt, and D. Madrzykowski. Simulation of a Wind Driven Residential Basement Fire - Riverdale Heights, MD. NIST Technical Note 1870, National Institute of Standards and Technology, Gaithersburg, Maryland, 2015.

[3] S.K. Hoglander and S. Conver-White. House Fire with Significant Firefighter Injuries – Riverdale Heights, MD. Safety Investigation Team Report, Prince George's County Fire/Emergency Medical Services Department, Lanham, Maryland, 2013.

[4] D Abbott. Project MAYDAY, Career, 2015-2017.5, 30 Months. http://projectmayday.net/public/res/pdf/2017_Mayday_Project_Career.pdf, 2017.

[5] Donald Abbott. Project MAYDAY, 2015-2017, Volunteers. http://projectmayday.net/public/res/pdf/2017_Mayday_Project_Volunteers.pdf, 2017.

[6] T.A. Pettit, F. Washenitz, and K. Cortez. Three Fire Fighters Die in a 10-Story High-Rise Apartment Building – New York. NIOST 99-F01, NIOSH Fire Fighter Fatality Investigation and Prevention Program, 1999.

[7] F. Washenitz, R. Braddee, T.A. Pettit, and E. Schmidt. Two Fire Fighters Die and Two Are Injured in Townhouse Fire – District of Columbia. NIOSH 99-F21, NIOSH Fire Fighter Fatality Investigation and Prevention Program, 1999.

[8] T.P Mezzanotte, E. Schmidt, T.A. Pettit, and D. Castillo. Structure Fire Claims the Lives of Three Career Fire Fighters and Three Children – Iowa. NIOSH F2000-04, NIOSH Fire Fighter Fatality Investigation and Prevention Program, 2001.

[9] M. McFall and E. Schmidt. Arson Fire Claims the Life of One Volunteer Fire Fighter and One Civilian and Severely Injures Another Volunteer Fire Fighter – Michigan. NIOSH F2000-16, NIOSH Fire Fighter Fatality Investigation and Prevention Program, 2001.

[10] M. McFall, R. Braddee, and T. Mezzanotte. Career Fire Fighter Dies and Three Are Injured In a Residential Garage Fire – Utah. NIOSH F2000-23, NIOSH Fire Fighter Fatality Investigation and Prevention Program, 2000.

[11] M. McFall. A Volunteer Assistant Chief Was Seriously Injured and Two Volunteer Fire Fighters Were Injured While Fighting a Townhouse Fire – Delaware. NIOSH F2000-43, NIOSH Fire Fighter Fatality Investigation and Prevention Program, 2001.

[12] S. Berardinelli, B. Oerter, J. Tarley, and T. Merinar. Career Battalion Chief and Career Master Fire Fighter Die and Twenty – Nine Career Fire Fighters are Injured during a Five Alarm Church Fire – Pennsylvania. NIOSH F2004-02, NIOSH Fire Fighter Fatality Investigation and Prevention Program, 2006.

[13] R.E. Koedam, T. Merinar, and M. Bowyer. One Probationary Career Firefighter Dies and Four Career Firefighters are Injured at a Two-Alarm Residential Structure Fire – Texas. NIOSH F2005-02, NIOSH Fire Fighter Fatality Investigation and Prevention Program, 2007.

[14] M. McFall, V. Lutz, and S. Berardinelli. Career Fire Fighter Dies While Exiting Residential Basement Fire – New York. NIOSH F2005-04, NIOSH Fire Fighter Fatality Investigation and Prevention Program, 2006.

[15] J. Tarley, S. Berardinelli, and T. Merinar. Career Probationary Fire Fighter Dies While Participating in a Live – Fire Training Evolution at an Acquired Structure – Maryland. NIOSH F2007-09, NIOSH Fire Fighter Fatality Investigation and Prevention Program, 2008.

[16] R. Braddee, M. Bowyer, and S. Berardinelli. Four Career Fire Fighters Injured While Providing Interior Exposure Protection at a Row House Fire – District of Columbia. NIOSH F2007-35, NIOSH Fire Fighter Fatality Investigation and Prevention Program, 2008.

[17] T. Merinar, J. Tarley, and S.T. Miles. Career Probationary Fire Fighter and Captain Die as a Result of Rapid Fire Progression in a Wind-Driven Residential Structure Fire – Texas. NIOSH F2009-11, NIOSH Fire Fighter Fatality Investigation and Prevention Program, 2010.

[18] M. Bowyer and M. Loflin. A Career Lieutenant and Fire Fighter/Paramedic Die in a Hillside Residential House Fire – California. NIOSH F2011-13, NIOSH Fire Fighter Fatality Investigation and Prevention Program, 2012.

[19] M. Loflin, T. Hales, and S.T. Miles. Career Fire Fighter Dies during Fire-Fighting Operations at a Multi-family Residential Structure Fire – Massachusetts. NIOSH F2011-31, NIOSH Fire Fighter Fatality Investigation and Prevention Program, 2013.

[20] M.E. Bowyer, S.C. Wertman, and M. Loflin. Career Captain Sustains Injuries at a 2-1/2 Story Apartment Fire then Dies at Hospital – Illinois. NIOSH F2012-28, NIOSH Fire Fighter Fatality Investigation and Prevention Program, 2013.

[21] J. Tarley, S.T.. Miles, and M. Bowyer. Volunteer Captain Dies After Floor Collapse Traps Him in Basement – New York. NIOSH F2013-02, NIOSH Fire Fighter Fatality Investigation and Prevention Program, 2014.

[22] S. Wertman and T. Merinar. Two Career Lieutenants Killed and Two Career Fire Fighters Injured Following a Flashover at an Assembly Hall Fire–Texas. NIOSH F2013-04, NIOSH Fire Fighter Fatality Investigation and Prevention Program, 2014.

[23] M. Bowyer, M. Loflin, and S. Wertman. Two Career Fire Fighters Die in a Rapid Fire Progression While Searching for Tenants – Ohio. NIOSH F2014-02, NIOSH Fire Fighter Fatality Investigation and Prevention Program, 2015.

[24] M. Loflin, M. Bowyer, S.T. Miles, and S. Wertman. Lieutenant and Fire Fighter Die and 13 Fire Fighters are injured in a Wind-driven Fire in a Brownstone – Massachusetts. NIOSH F2014-09, NIOSH Fire Fighter Fatality Investigation and Prevention Program, 2016.

[25] T. Merinar and M. Loflin. Career Fire Lieutenant Dies in Cluttered Apartment Fire on 19th Floor of High-rise Residential Building – New York. NIOSH F2014-14, NIOSH Fire Fighter Fatality Investigation and Prevention Program, 2016.

[26] M. Bowyer, S. Miles, and P. Moore. Career Female Fire Fighter Dies After Becoming Lost and Running Out of Air in a Residential Structure Fire – Pennsylvania. NIOSH F2014-25, NIOSH Fire Fighter Fatality Investigation and Prevention Program, 2017.

[27] Mark Izydorek, Patrick Zeeveld, Matthew Samuals, and James Smyser. Structural stability of engineered lumber in fire conditions. Report, Underwriters Laboratories, Northbrook, Illinois, September 2008.

[28] D. Madrzykowski and J. Kent. Examination of the Thermal Conditions of a Wood Floor Assembly Above a Compartment Fire. NIST TN 1709, National Institute of Standards and Technology, July 2011.

[29] S. Kerber, B. Backstrom, J. Dalton, and D. Madrzykowski. Full-Scale Floor System Field and Laboratory Fire Experiments. Report, Underwriters Laboratories, Northbrook, Illinois, January 2012.

[30] UL Firefighter Safety Research Institute. Scientific Research for the Development of More Effective Tactics - Governors Island. Online Training, April 2014.

[31] International Society of Fire Service Instructors. Principles of Modern Fire Attack: SLICE-RS. Online Training, August 2014.

[32] ASTM International. *Standard E 779: Standard Test Method for Determining Air Leakage Rate by Fan Pressurization*, 2010.

[33] A.K. Persilly. Airtightness of Commercial and Institutional Buildings: Blowing Holes in the Myth of Tight Buildings. In *Thermal Envelopes VII Conference*, pages 829–837, Clearwater, FL, 1998.

[34] B.N. Taylor and C.E. Kuyatt. Guidelines for Evaluating and Expressing the Uncertainty of NIST Measurement Results. NIST Technical Note 1297, National Institute of Standards and Technology, Gaithersburg, Maryland, 1994.

[35] Stanley Hand Tools, New Britain, Connecticut. *User Manual TLM 100*, 2013.

[36] T. Butcher, S. Cook, L. Crown, and R. Harshman. NIST Handbook 44: Specifications, Tolerances, and Other Technical Requirements for Weighing and Measuring Devices. Technical report, National Institute of Standards and Technology, Gaithersburg, Maryland, 2012.

[37] Ohaus Corporation, Pine Brook, New Jersey. *Manual for SD Series Bench Scale*, 2000.

[38] Omega Engineering Inc., Stamford, Connecticut. *The Temperature Handbook*, 2004.

[39] L.G. Blevins. Behavior of bare and aspirated thermocouples in compartment fires. In *National Heat Transfer Conference, 33rd Proceedings*, pages 15–17, 1999.

[40] W.M. Pitts, E. Braun, R. Peacock, H. Mitler, E. Johnson, P. Reneke, and L.G. Blevins. Temperature uncertainties for bare-bead and aspirated thermocouple measurements in fire environments. *ASTM Special Technical Publication*, 1427:3–15, 2003.

[41] Medtherm Corporation, Huntsville, Alabama. *64 Series Heat Flux Transducers*, 2003.

[42] W.M. Pitts, A.V. Murthy, J.L. de Ris, J. Filtz, K. Nygård, D. Smith, and I. Wetterlund. Round robin study of total heat flux gauge calibration at fire laboratories. *Fire Safety Journal*, 41(6):459–475, 2006.

[43] M. Bundy, A. Hamins, E.L. Johnsson, S.C. Kim, G.H. Ko, and D.B. Lenhart. Measurements of Heat and Combustion Products in Reduced-Scale Ventilated-Limited Compartment Fires. NIST Technical Note 1483, National Institute of Standards and Technology, Gaithersburg, Maryland, 2007.

[44] A. Lock, M. Bundy, E.L. Johnsson, A. Hamins, G.H. Ko, C. Hwang, P. Fuss, and R. Harris. Experimental study of the effects of fuel type, fuel distribution, and vent size on full-scale underventilated compartment fires in an ISO 9705 room. NIST Technical Note 1603, National Institute of Standards and Technology, Gaithersburg, Maryland, 2008.

[45] Setra Systems, Boxborough, Massachusetts. *Setra Model 264 Very Low Pressure Transducer Data Sheet Rev E.*, 2002.

[46] R.A. Bryant. A comparison of gas velocity measurements in a full-scale enclosure fire. *Fire Safety Journal*, 44:793–800, 2009.

[47] Badger Meter, Milwaukee, Wisconsin. *M-Series M2000 Electromagnetic Flow Meter*, MAG-DS-01047-EN-06 edition, 2015.

[48] R.A. Bryant and G. Mullholland. A guide to characterizing heat release rate measurement uncertainty for full-scale fire tests. *Fire and Materials*, 32:121–139, 2008.

[49] National Fire Protection Association, Quincy, Massachusetts. *NFPA 13D, Standard for the Installation of Sprinkler Systems in One- and Two-Family Dwellings and Manufactured Homes*, 2016.

[50] Stephen Kerber. Study of the effectiveness of fire service vertical ventilation and suppression tactics in single family homes. Report, Underwriters Laboratories, Northbrook, Illinois, June 2013.

[51] R Zevotek, K Stakes, and J Willi. Impact of Fire Attack Utilizing Interior and Exterior Streams on Firefighter Safety and Occupant Survival: Full Scale Experiments. Technical report, Underwriters Laboratories Firefighter Safety Research Institute, Columbia, Maryland, 2017.

[52] D. Madrzykowski. Fire Fighter Equipment Operational Environment (FFEOE): Evaluation of Thermal Conditions. Technical report, The Fire Protection Research Foundation, Quincy, Massachusetts, 2017.

[53] A. Putorti, A. Mensch, N. Bryner, and G. Braga. Thermal Performance of Self-Contained Breathing Apparatus Facepiece Lenses Exposed to Radiant Heat Flux. Technical Report TN 1785, National Institute of Standards and Technology, Gaithersburg, Maryland, 2013.

[54] National Fire Protection Association, Quincy, Massachusetts. *NFPA 1971, Standard on Protective Ensembles for Structural Fire Fighting and Proximity Fire Fighting*, 2013.

[55] Occupational Safety & Health Administration et al. Application of the Permit-Required Confined Spaces (PRCS), 29 CFR 1910.146. *Washington, DC: OSHA*, 2002.

[56] T. Greiner. Carbon Monoxide Concentrations: Table (AEN-172). https://www.abe.iastate.edu/extension-and-outreach/carbon-monoxide-concentrations-table-aen-172/, 1997. Accessed 2018-01-25.

Appendix A Dimensioned Floor Plans

A.1 Basement Dimensions

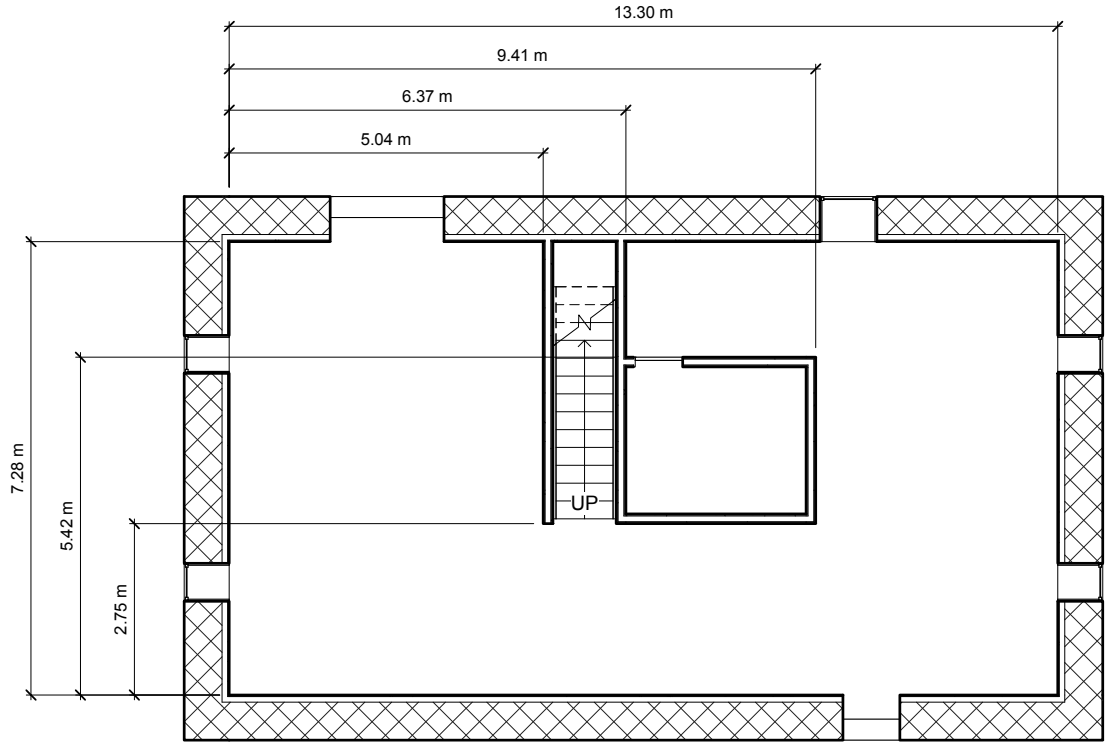

Figure A.1: Fully Dimensioned Floor Plan of the Basement

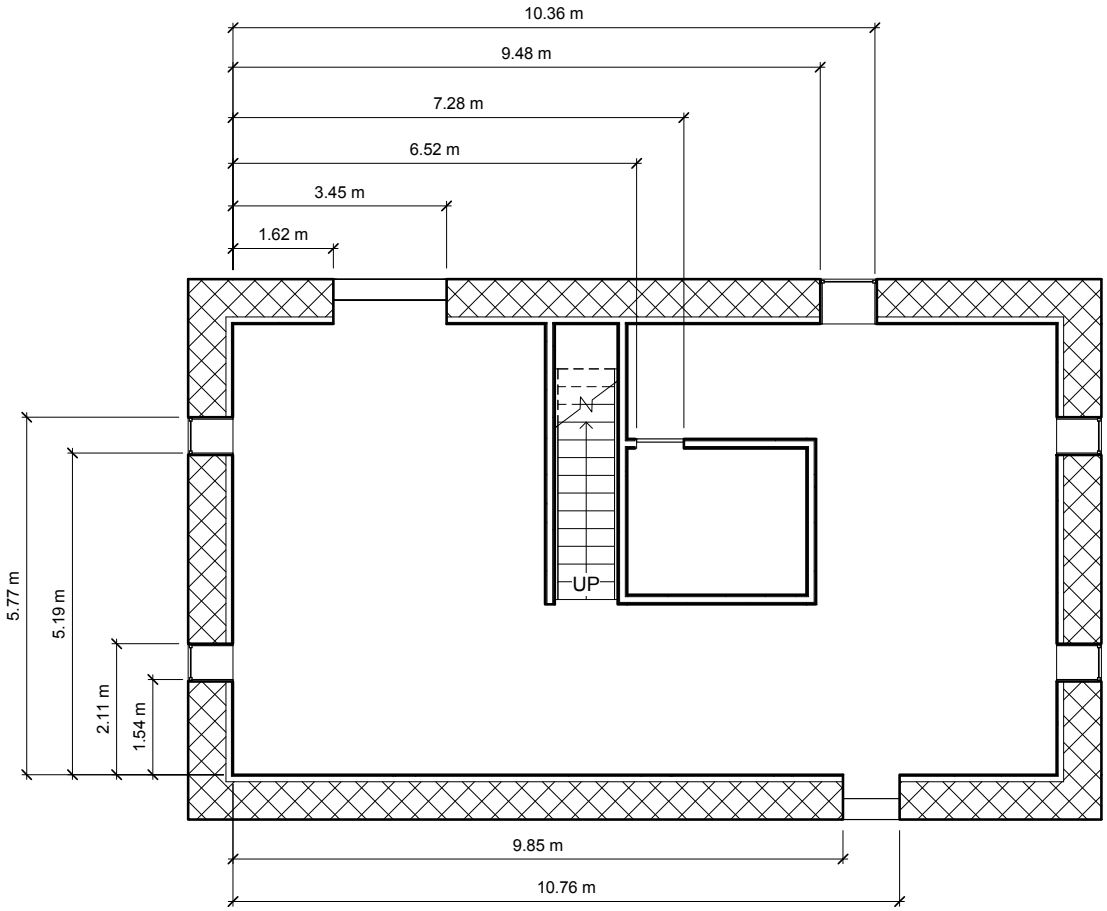

Figure A.2: Fully Dimensioned Floor Plan of the Basement Vent Locations

A.2 First Floor Dimensions

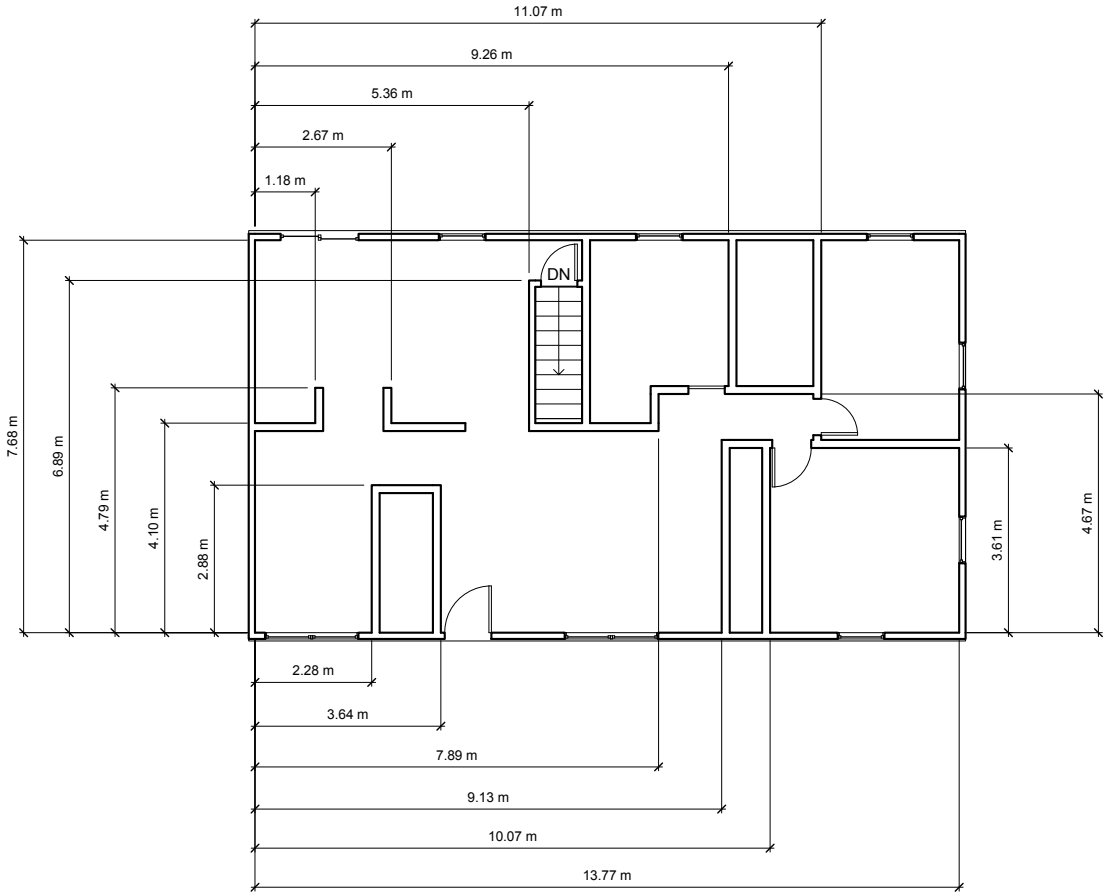

Figure A.3: Fully Dimensioned Floor Plan of the First Floor

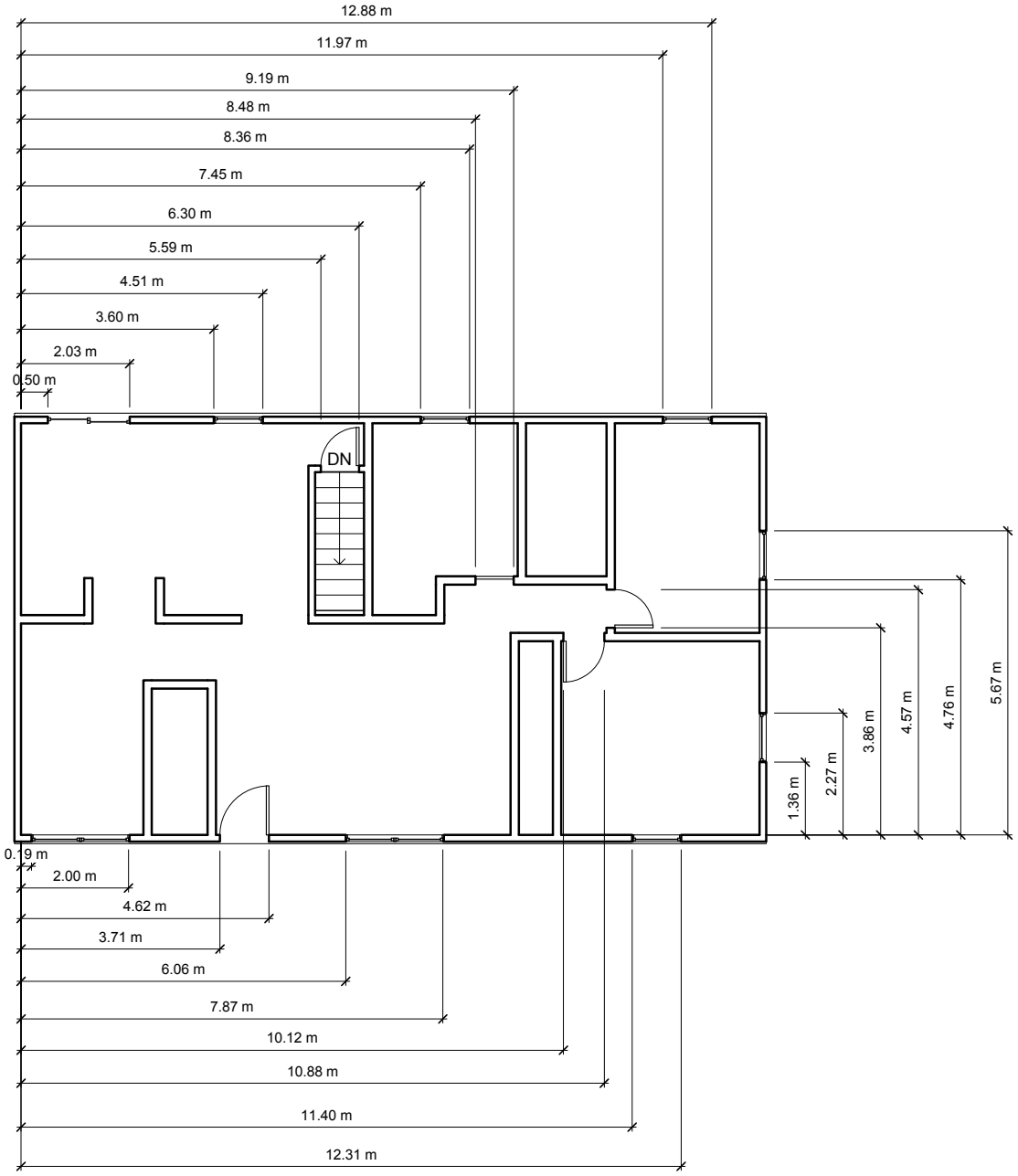

Figure A.4: Fully Dimensioned Floor Plan of the First Floor Vent Locations

Appendix B Experimental Data

B.1 Experiment 1

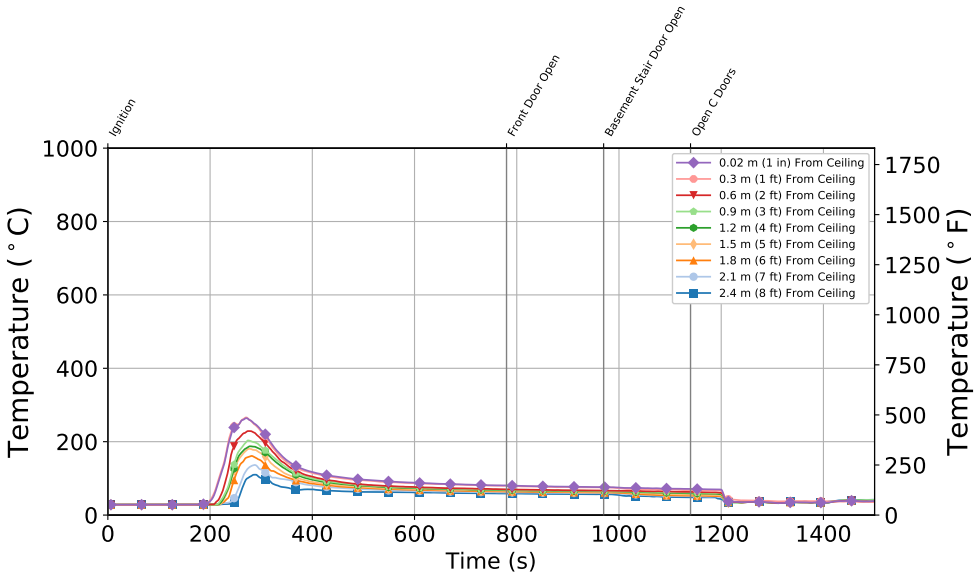

Figure B.1: Experiment 1 - Thermocouple temperature time histories from the Quadrant A thermocouple array in the basement.

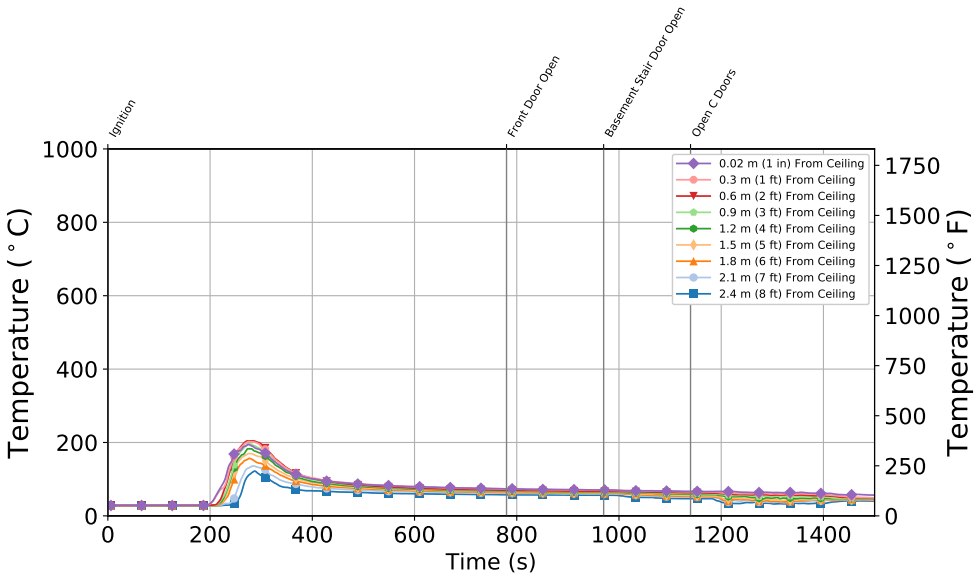

Figure B.2: Experiment 1 - Thermocouple temperature time histories from the Quadrant B thermocouple array in the basement.

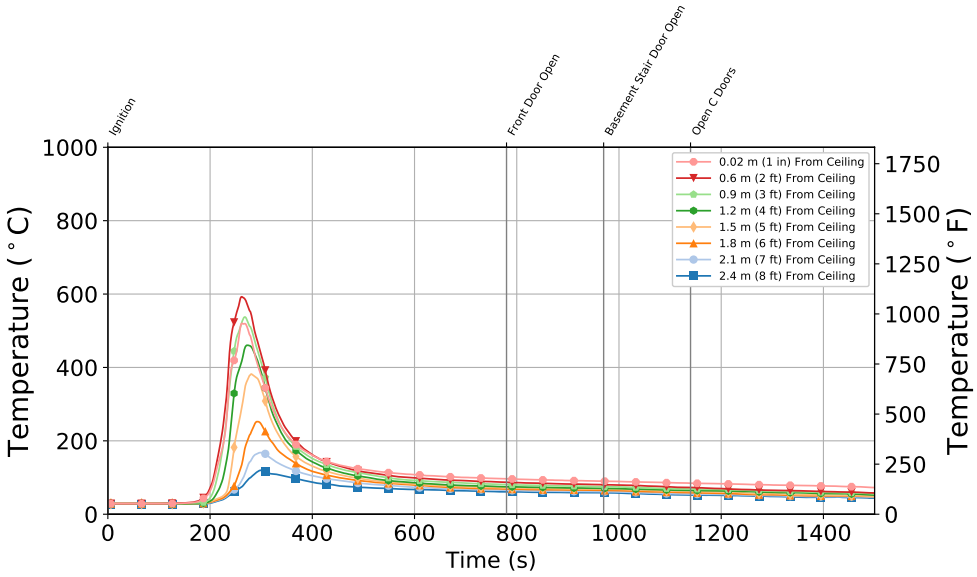

Figure B.3: Experiment 1 - Thermocouple temperature time histories from the Quadrant C thermocouple array in the basement.

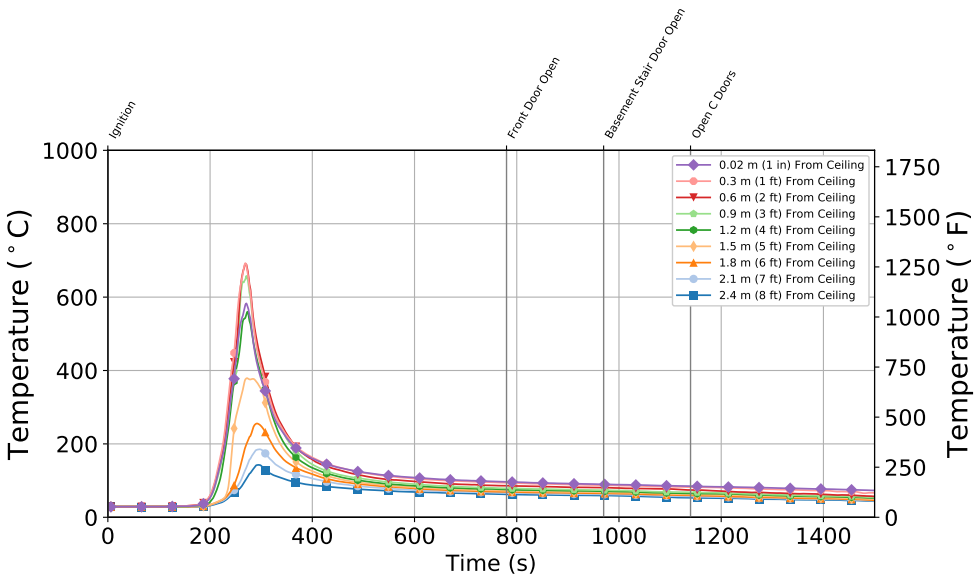

Figure B.4: Experiment 1 - Thermocouple temperature time histories from the Quadrant D thermocouple array in the basement.

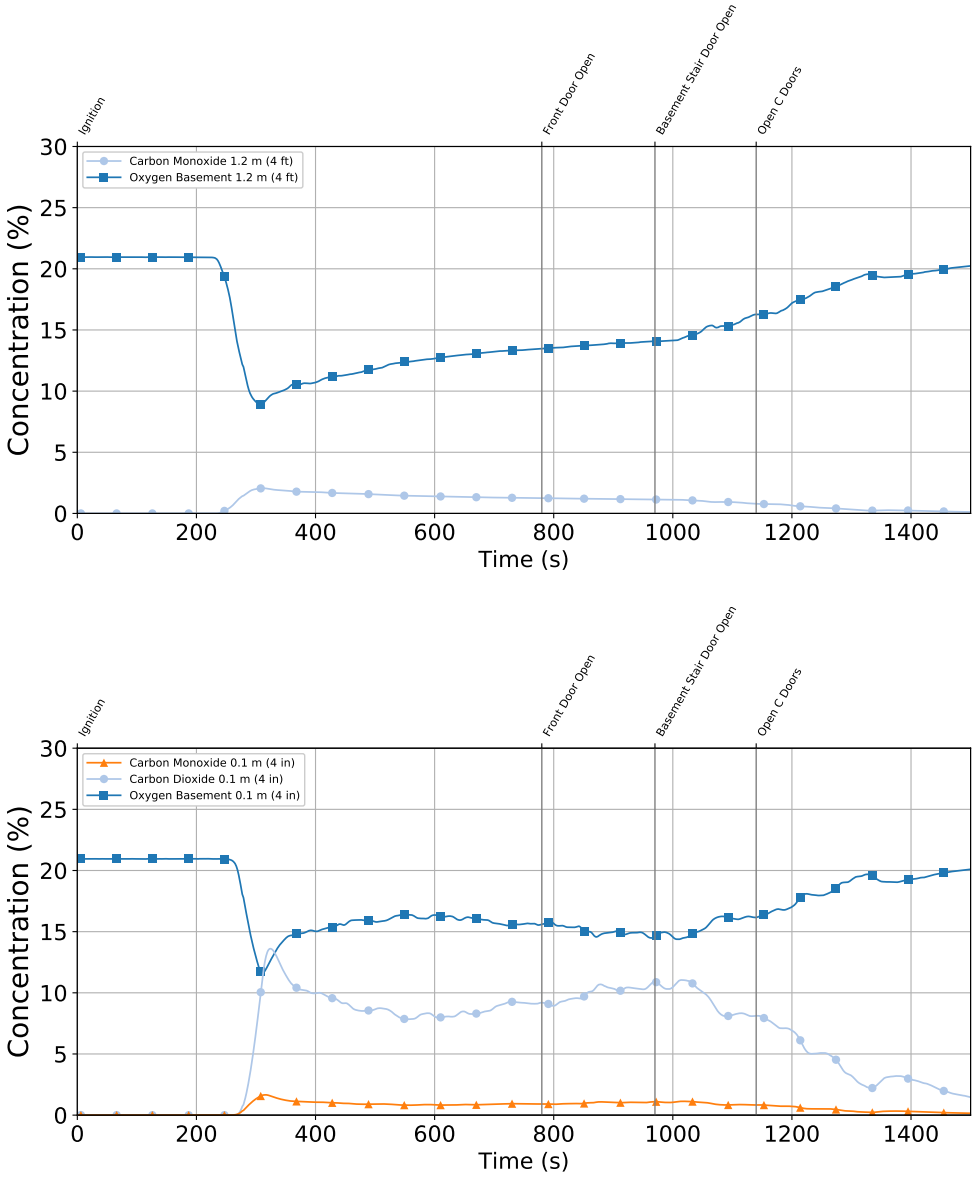

Figure B.5: Experiment 1 - Gas concentration time histories from the 1.2 m (4 ft) (top) and 0.1 m (4 in.) (bottom) elevations in the basement.

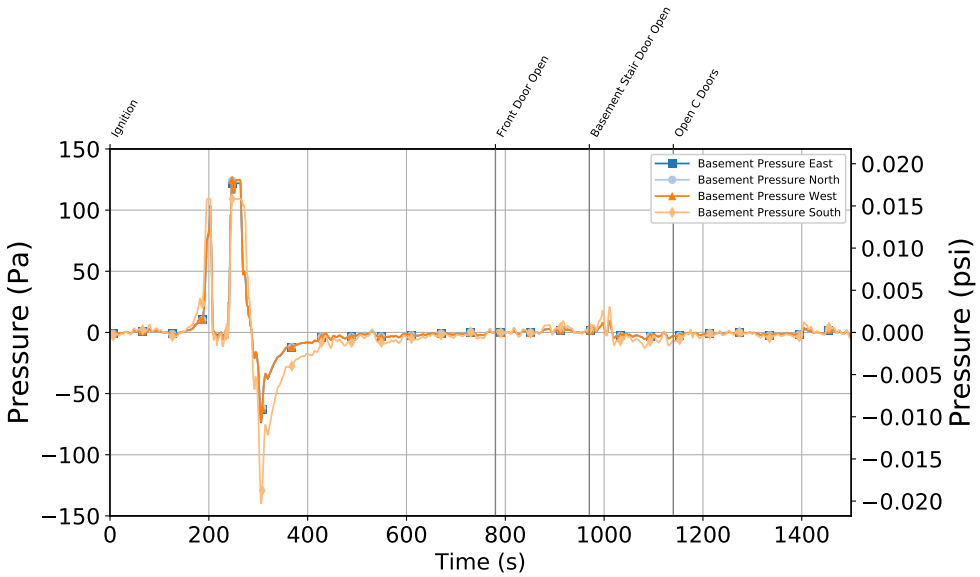

Figure B.6: Experiment 1 - Basement Pressure at 6 locations 1.2 m (4 ft) Above the Floor

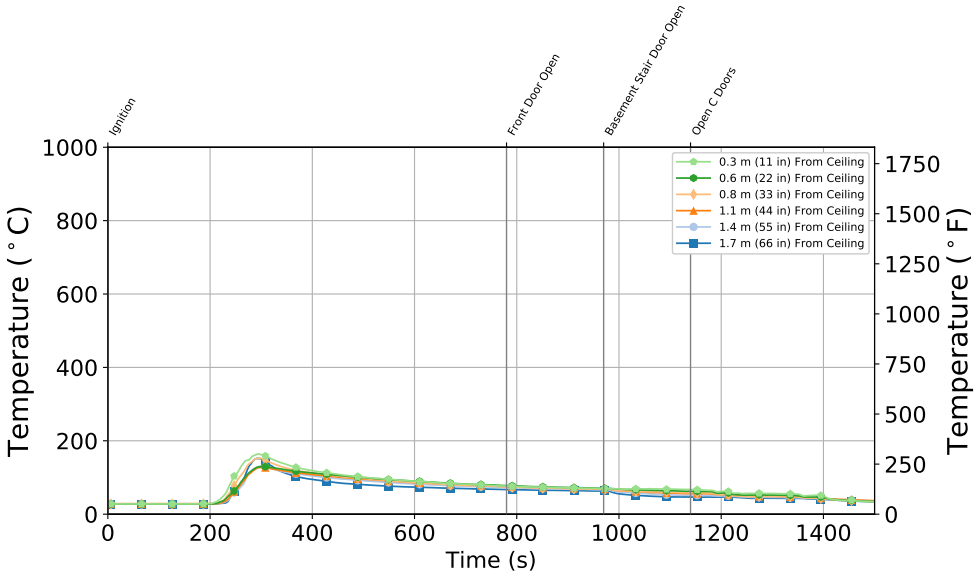

Figure B.7: Experiment 1 - Stair Thermocouple Temperature at Basement Level

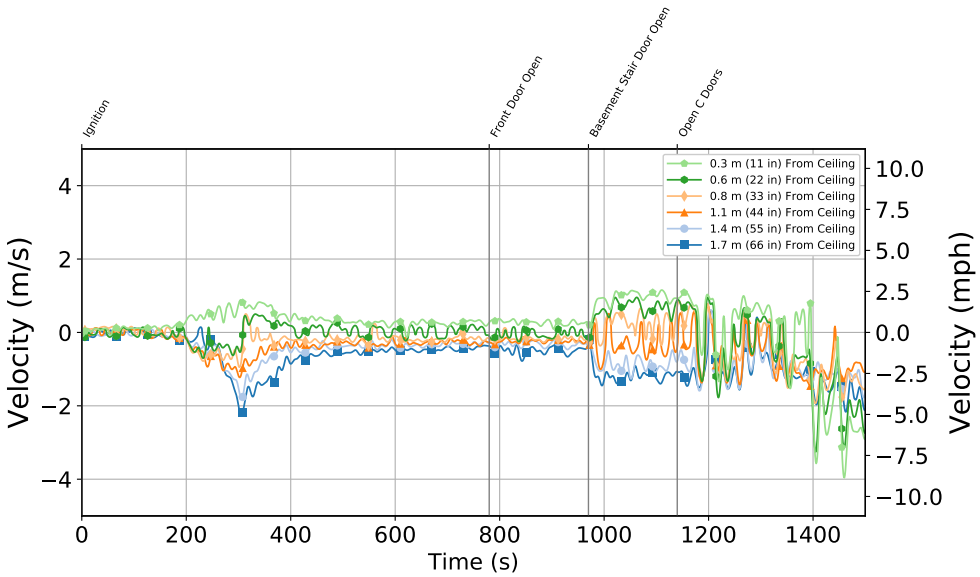

Figure B.8: Experiment 1 - Stair Velocity at Basement Level

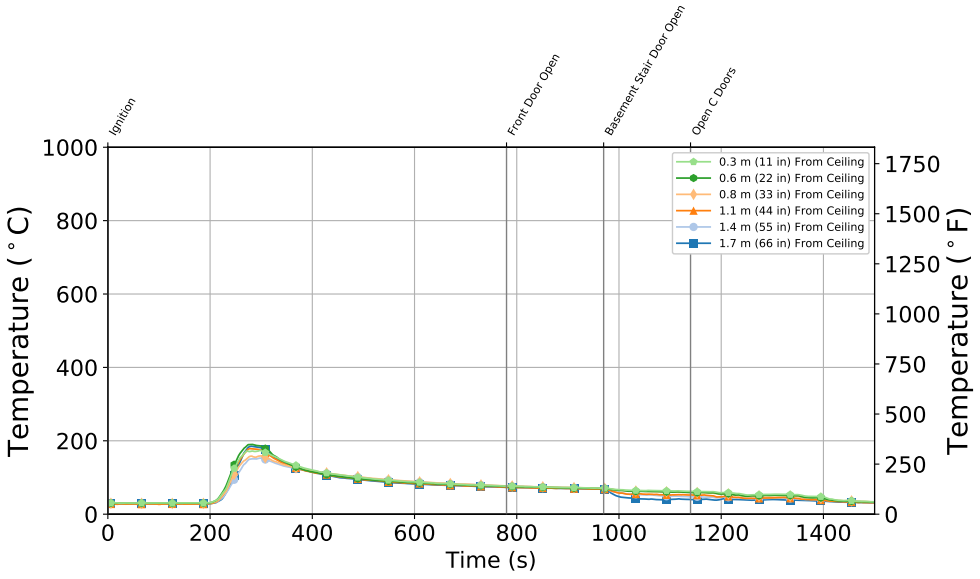

Figure B.9: Experiment 1 - Stair Thermocouple Temperature at First Floor

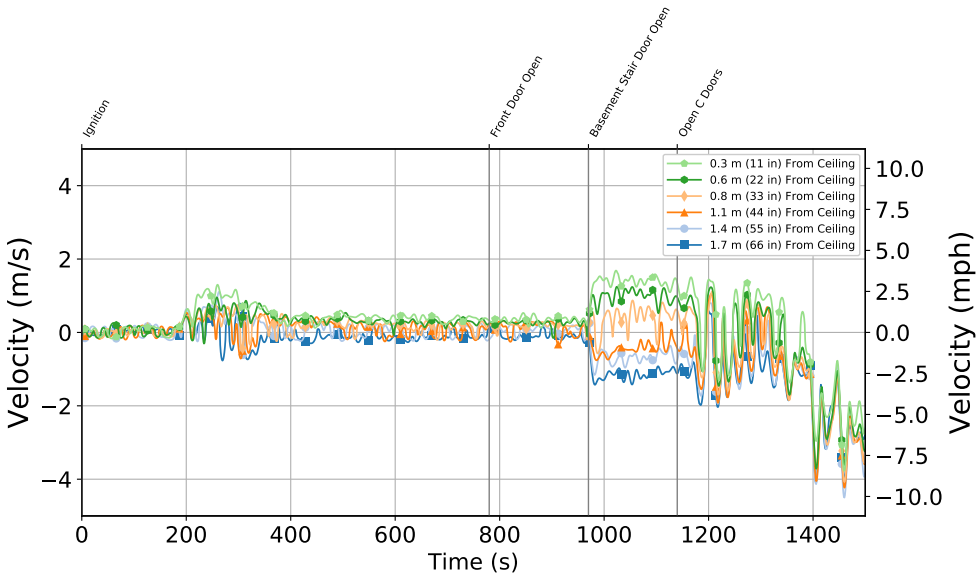

Figure B.10: Stair Velocity at First Floor

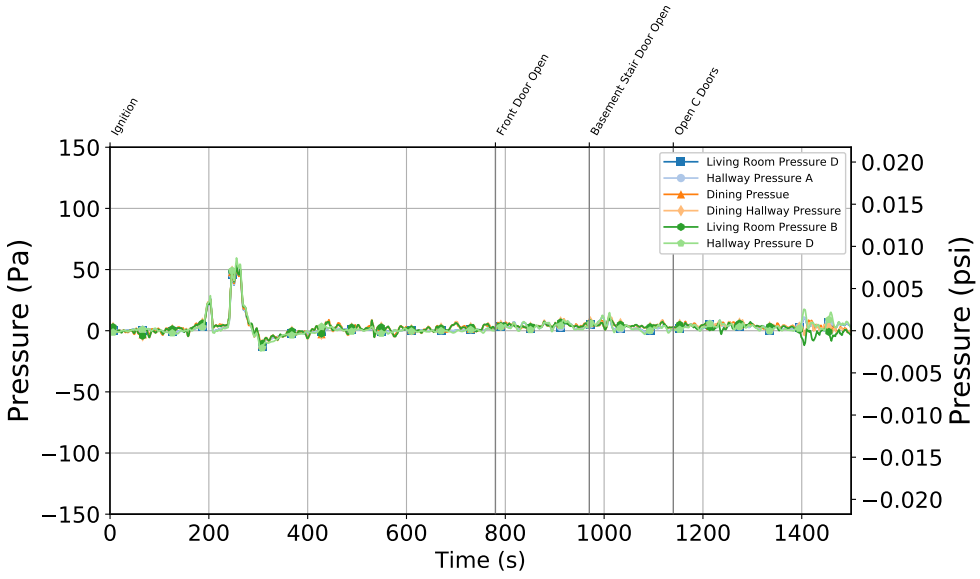

Figure B.11: Experiment 1 - First Floor Pressure at 6 locations 1.2 m (4 ft) Above the Floor

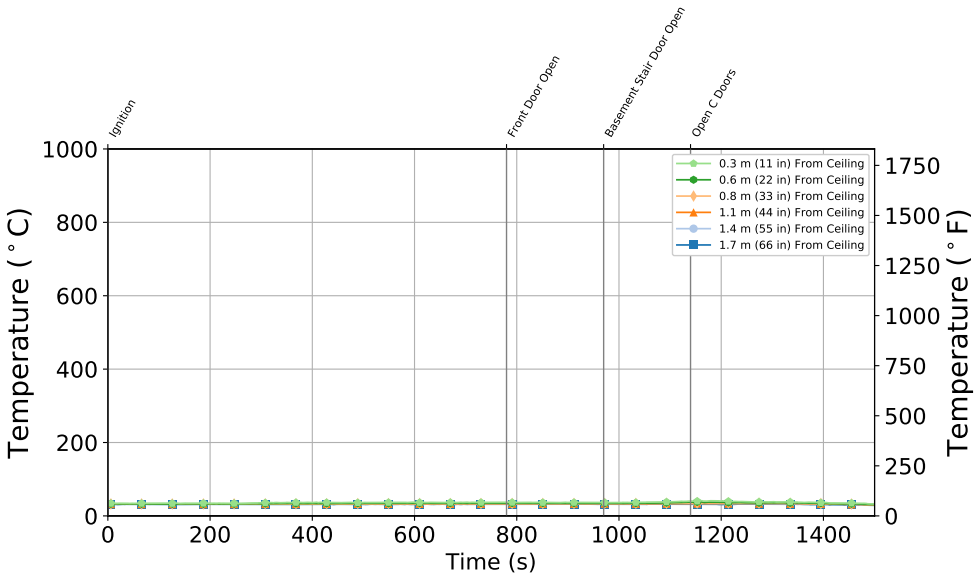

Figure B.12: Experiment 1 - Front Door Thermocouple Temperature at First Floor

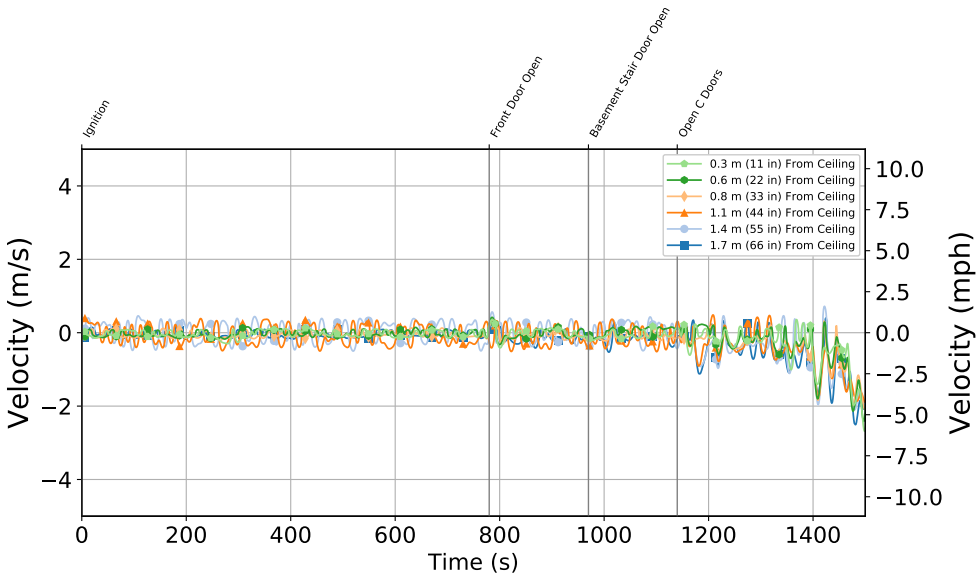

Figure B.13: Experiment 1 - Front Door Velocity at First Floor

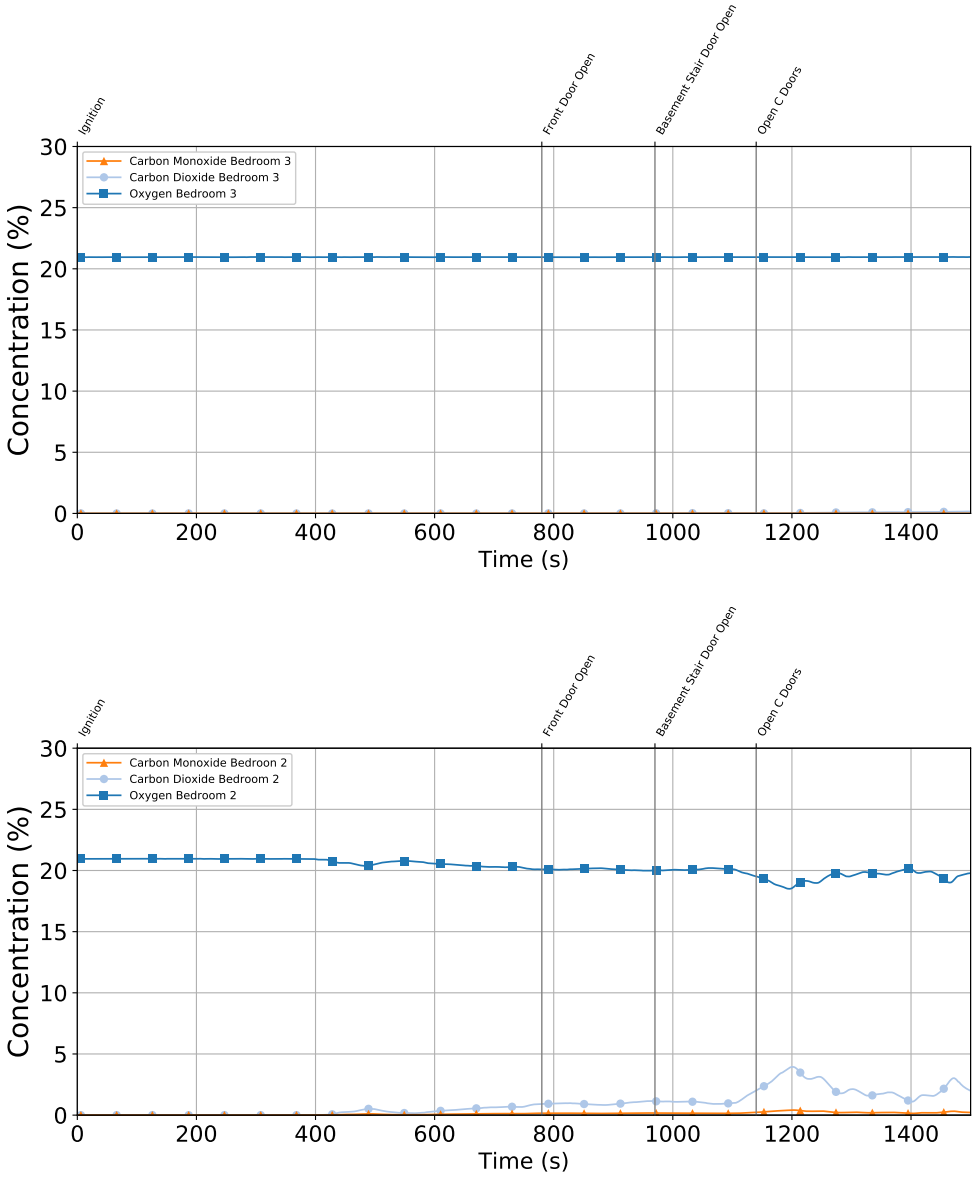

Figure B.14: Experiment 1 - Gas concentration time histories from the closed bedroom at 1.2 m (4 ft) (top) and from the open bedroom at 1.2 m (4 ft) (bottom).

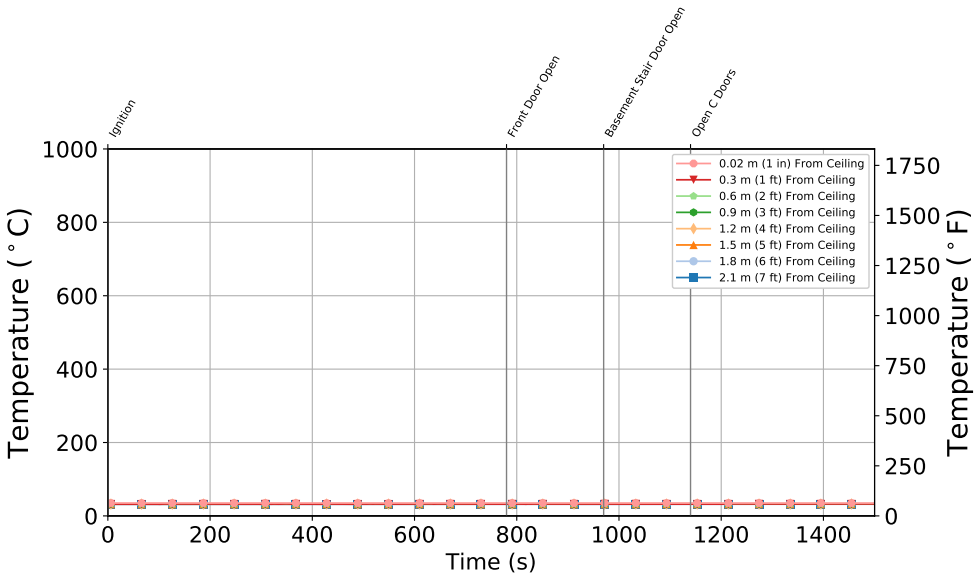

Figure B.15: Experiment 1 - Bedroom 3 (Closed) Bedroom

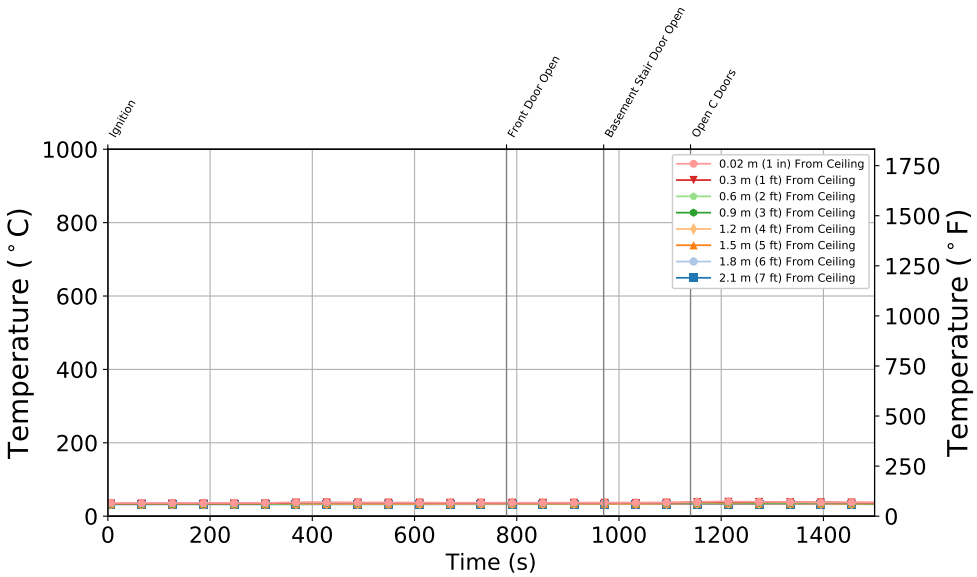

Figure B.16: Experiment 1 - Bedroom 2 (Open) Bedroom

B.2 Experiment 2

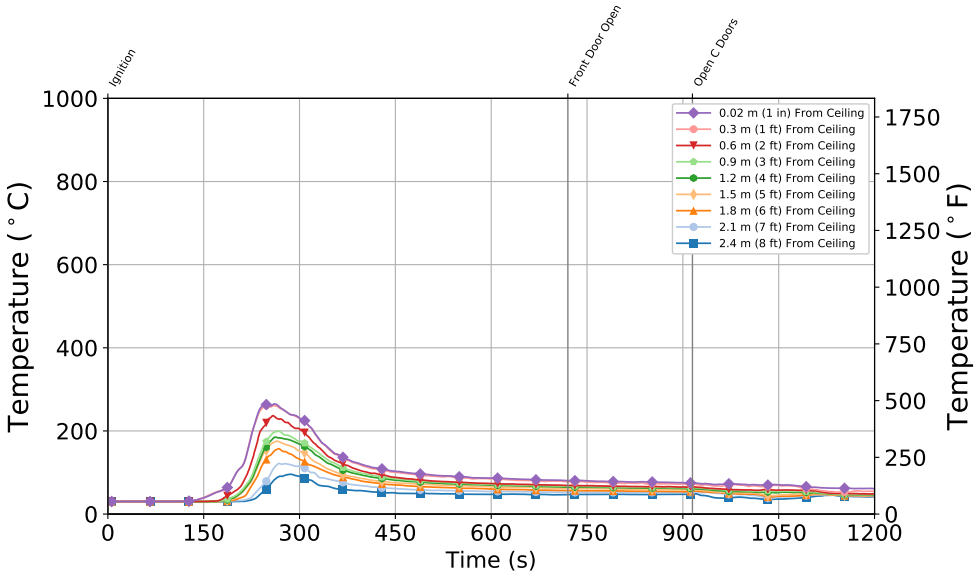

Figure B.17: Experiment 2 - Thermocouple temperature time histories from the Quadrant A thermocouple array in the basement.

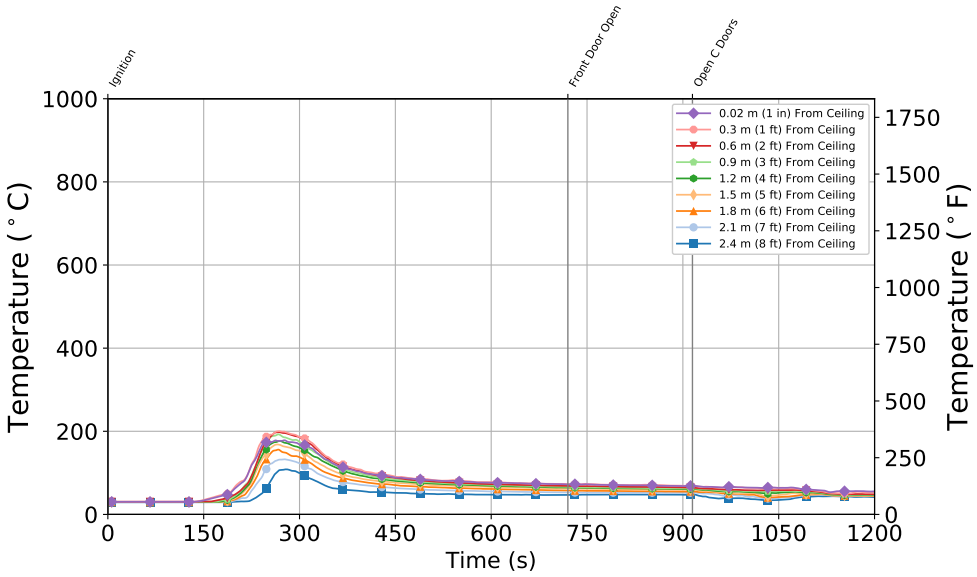

Figure B.18: Experiment 2 - Thermocouple temperature time histories from the Quadrant B thermocouple array in the basement.

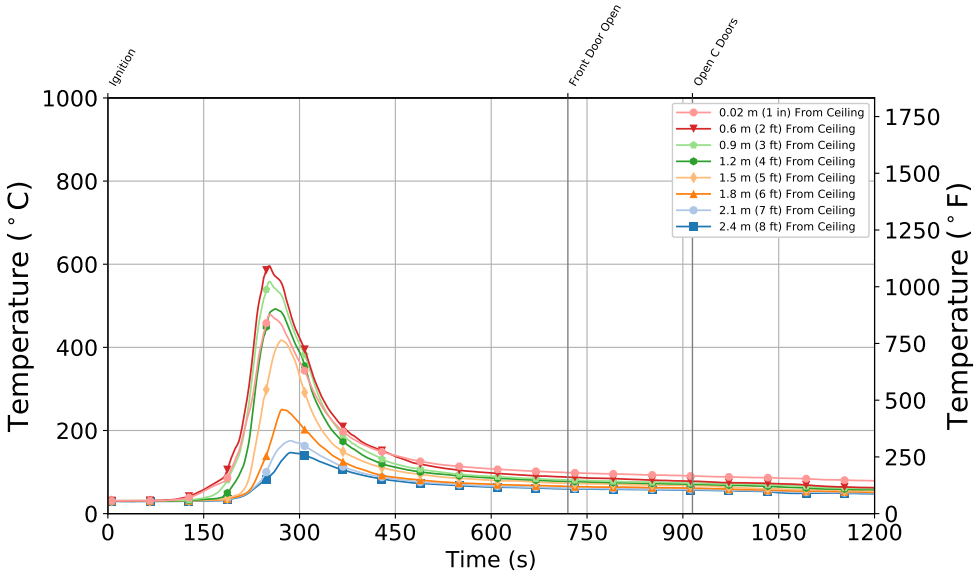

Figure B.19: Experiment 2 - Thermocouple temperature time histories from the Quadrant C thermocouple array in the basement.

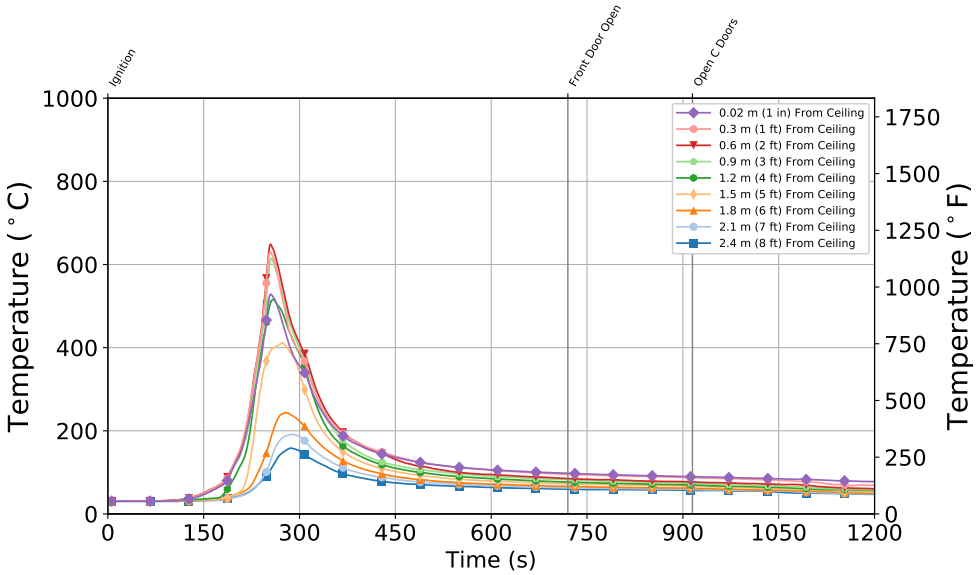

Figure B.20: Experiment 2 - Thermocouple temperature time histories from the Quadrant D thermocouple array in the basement.

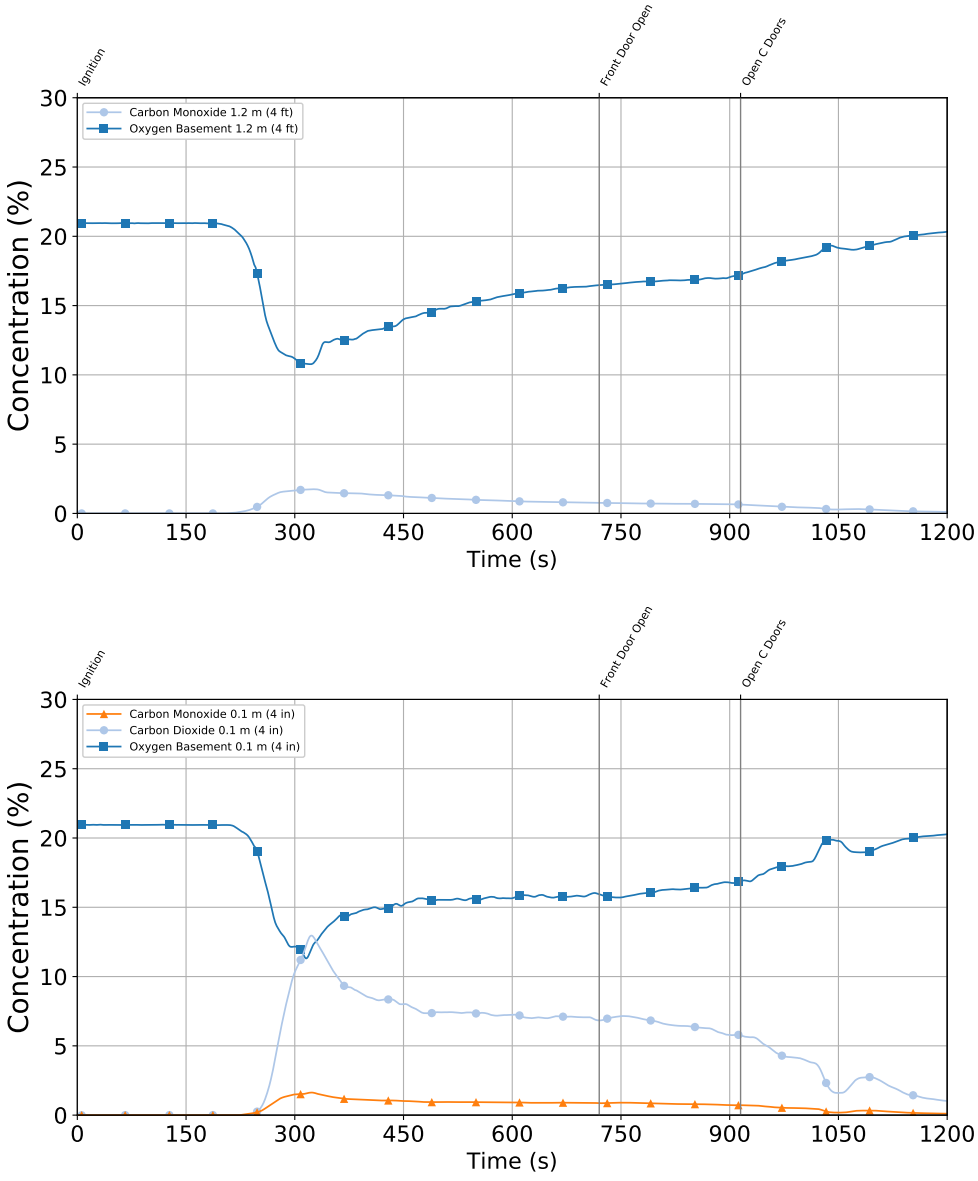

Figure B.21: Experiment 2 - Gas concentration time histories from the 1.2 m (4 ft) (top) and 0.1 m (4 in.) (bottom) elevations in the basement.

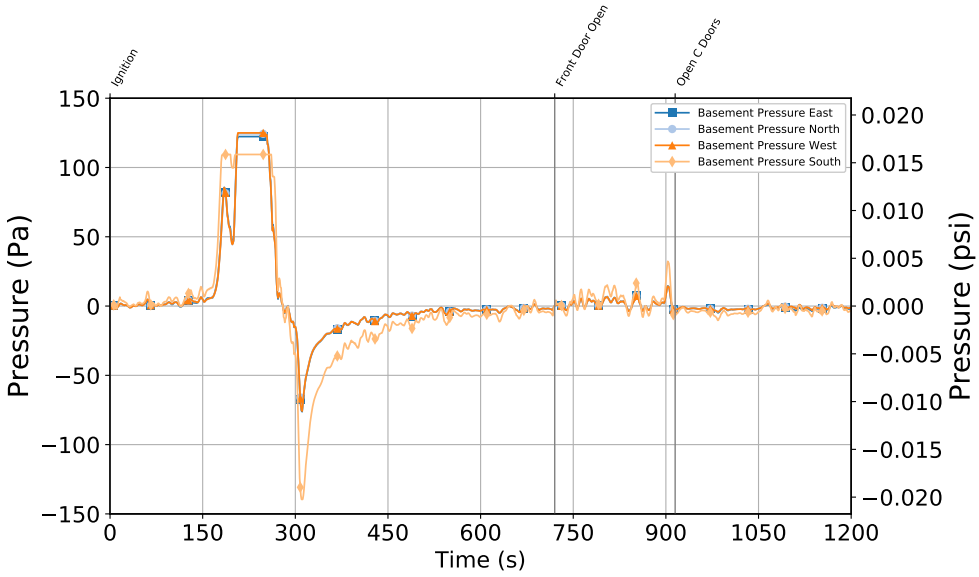

Figure B.22: Experiment 2 - Basement Pressure at 6 locations 1.2 m (4 ft) Above the Floor

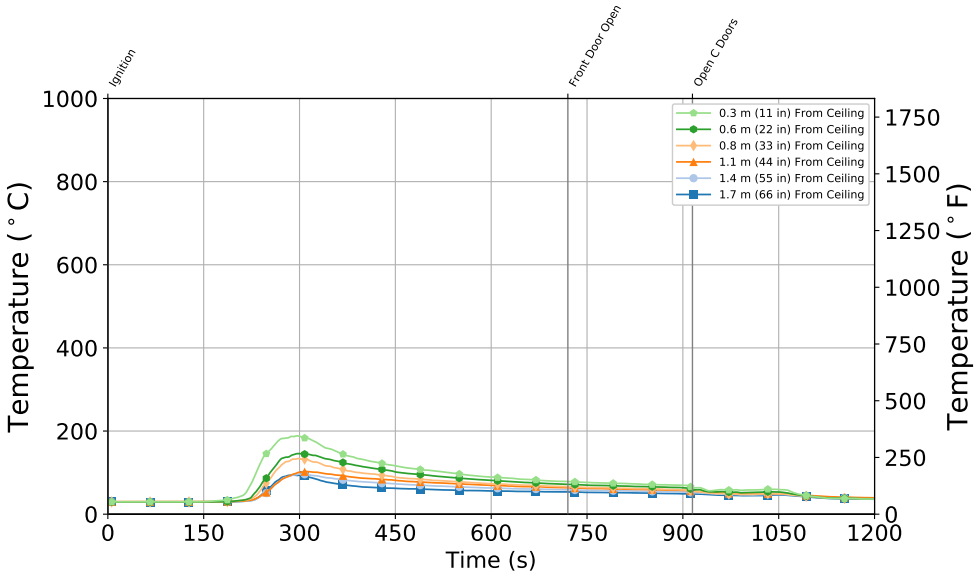

Figure B.23: Experiment 2 - Stair Thermocouple Temperature at Basement Level

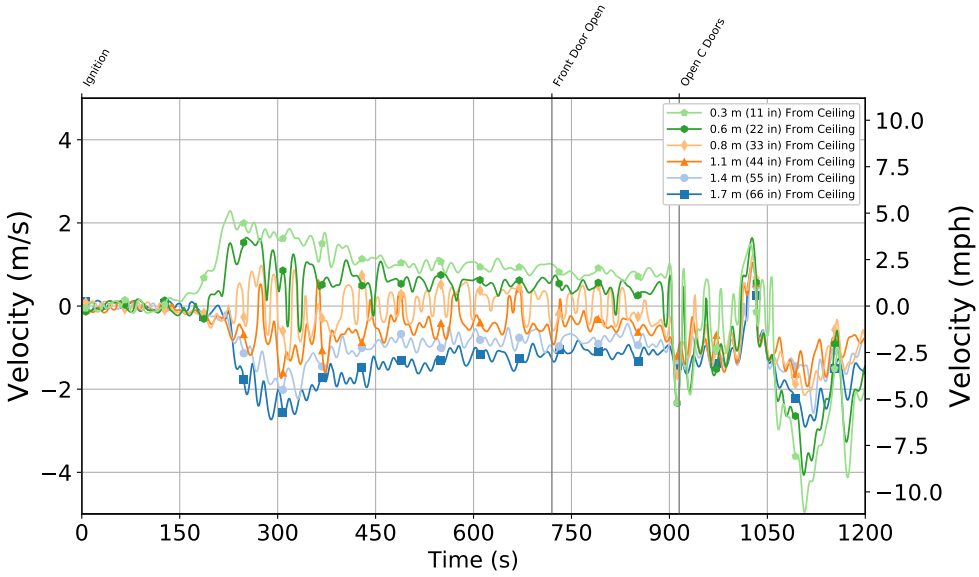

Figure B.24: Experiment 2 - Stair Velocity at Basement Level

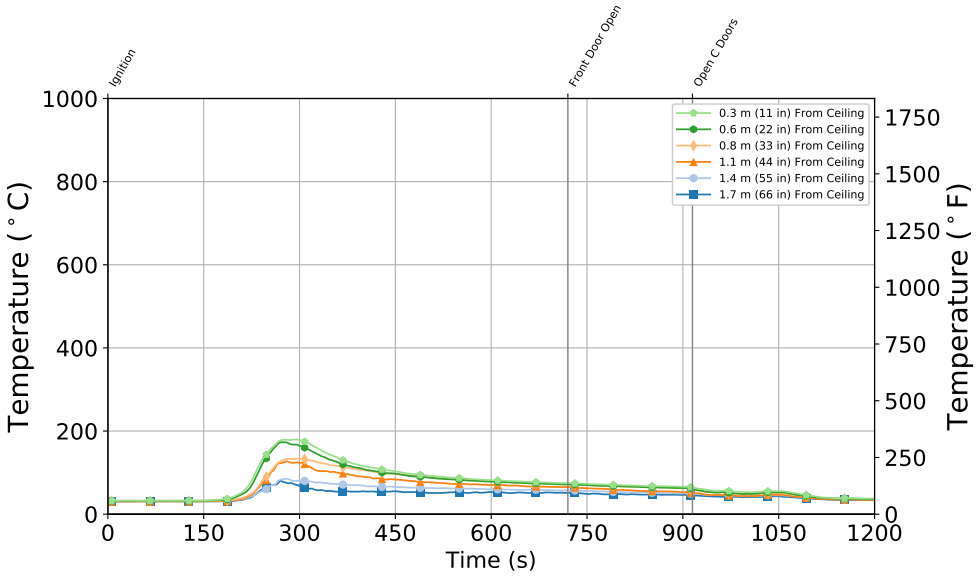

Figure B.25: Experiment 2 - Stair Thermocouple Temperature at First Floor

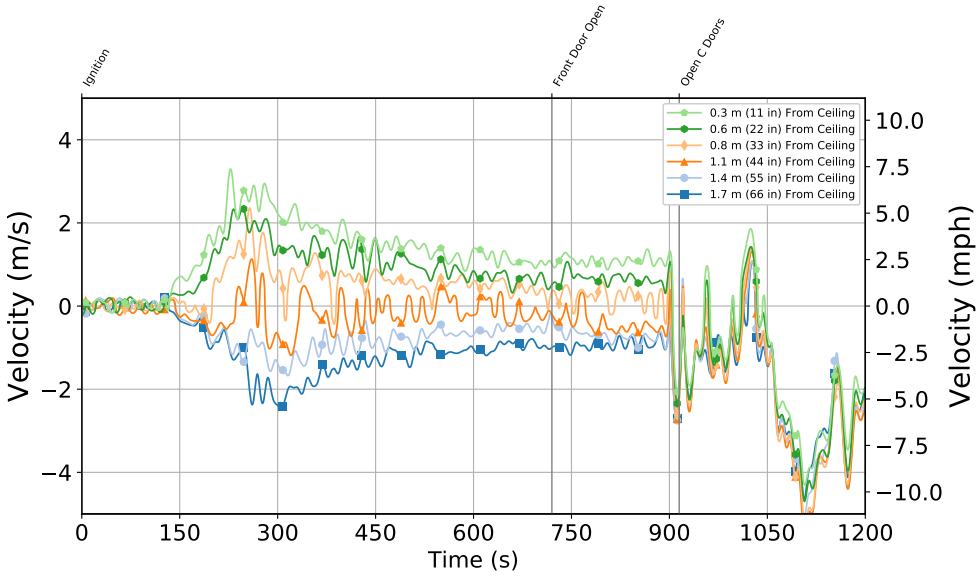

Figure B.26: Stair Velocity at First Floor

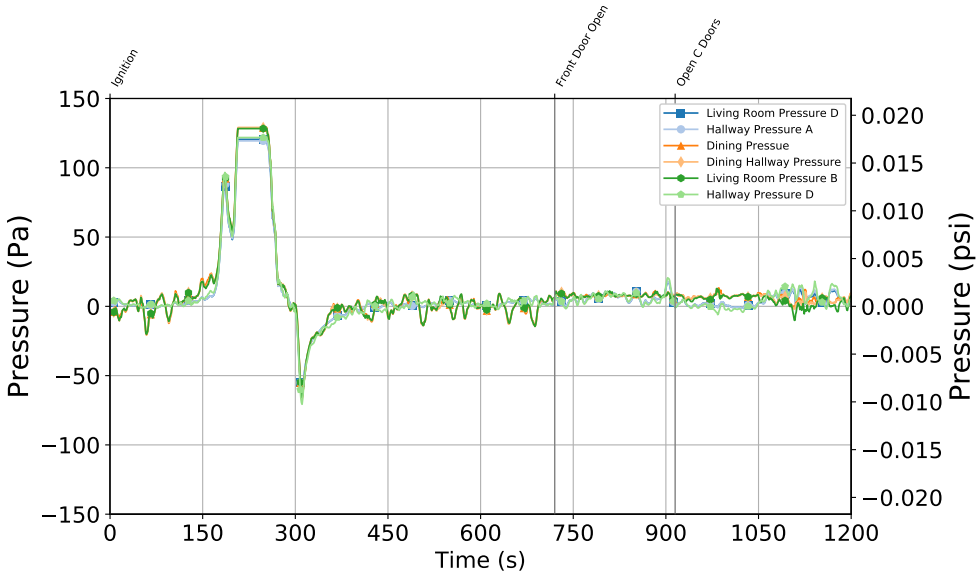

Figure B.27: Experiment 2 - First Floor Pressure at 6 locations 1.2 m (4 ft) Above the Floor

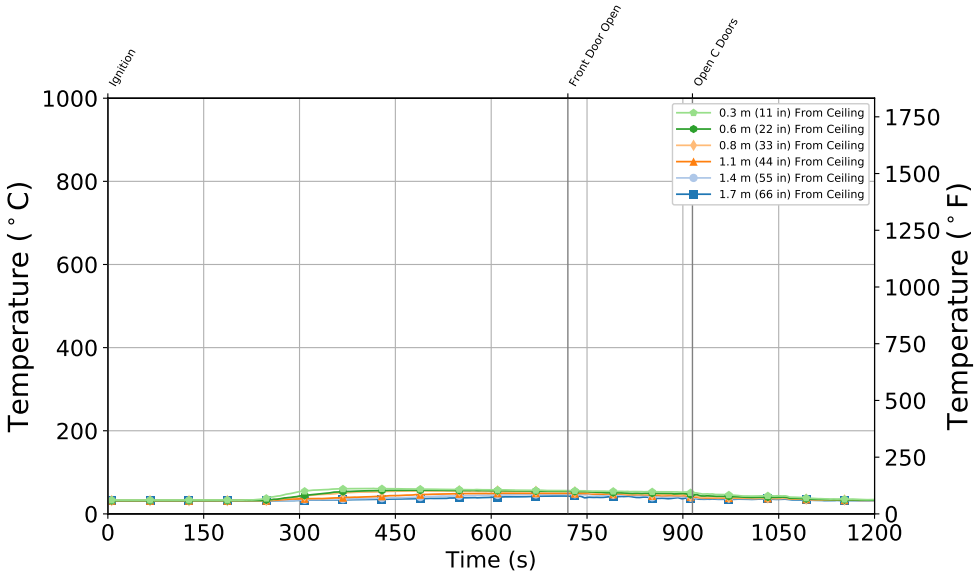

Figure B.28: Experiment 2 - Front Door Thermocouple Temperature at First Floor

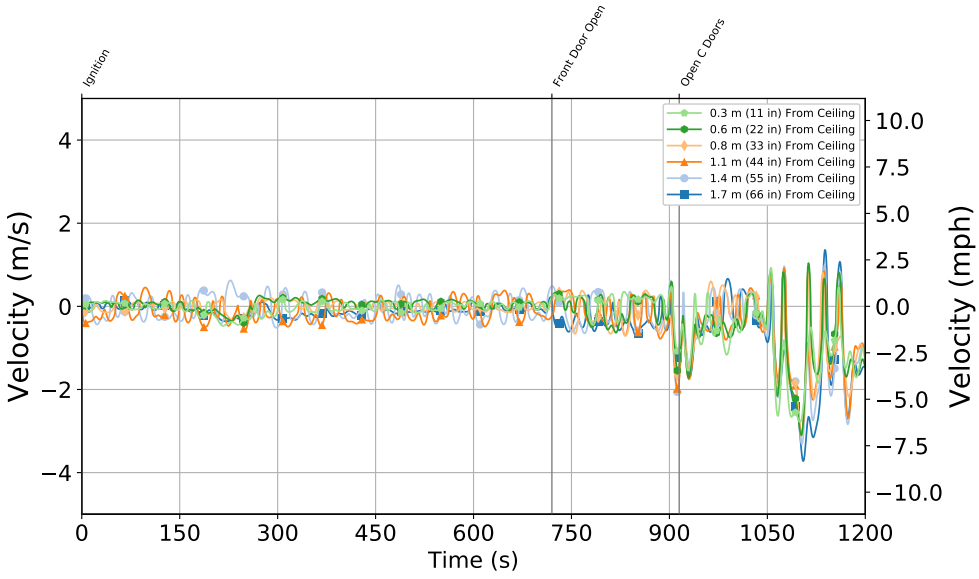

Figure B.29: Experiment 2 - Front Door Velocity at First Floor

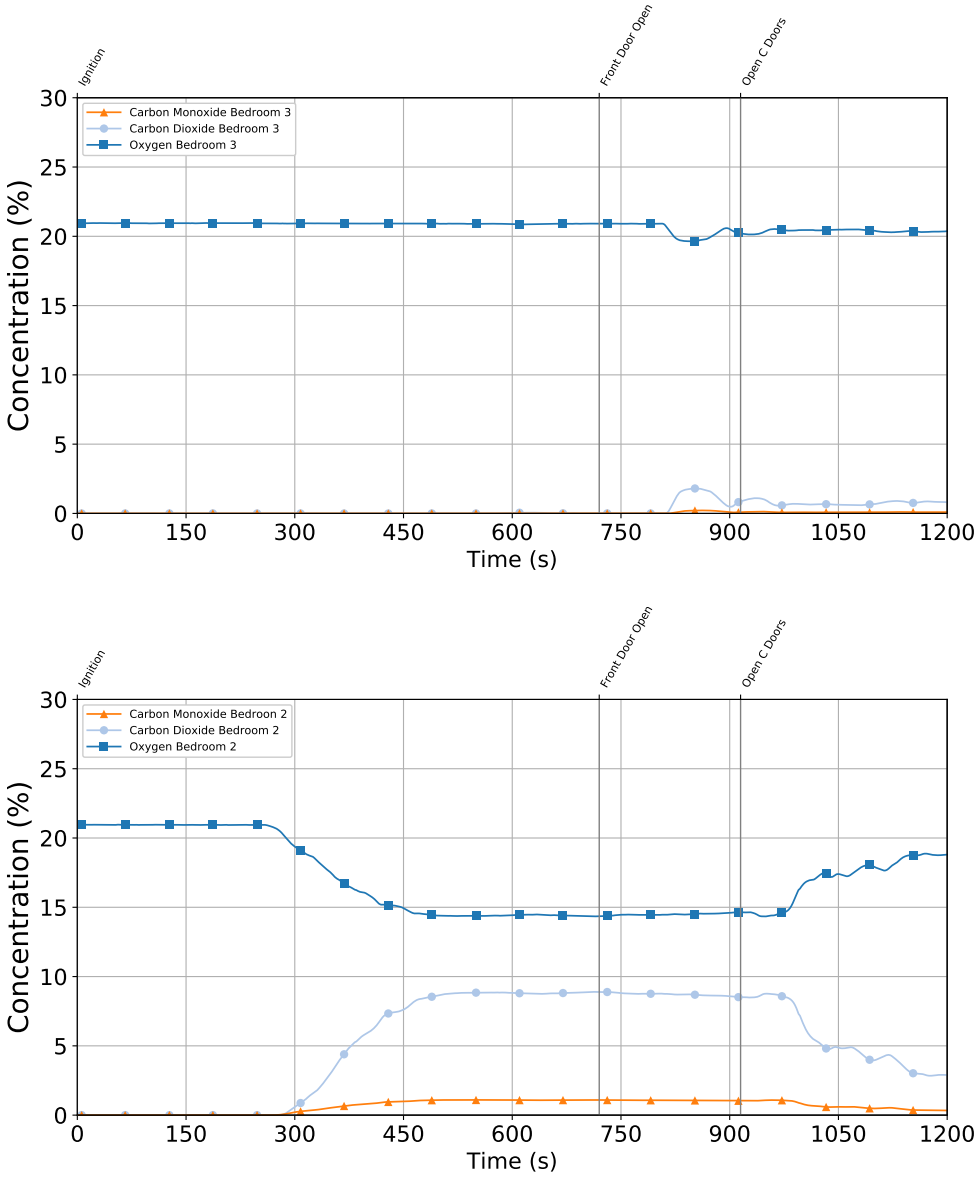

Figure B.30: Experiment 2 - Gas concentration time histories from the closed bedroom at 1.2 m (4 ft) (top) and from the open bedroom at 1.2 m (4 ft) (bottom).

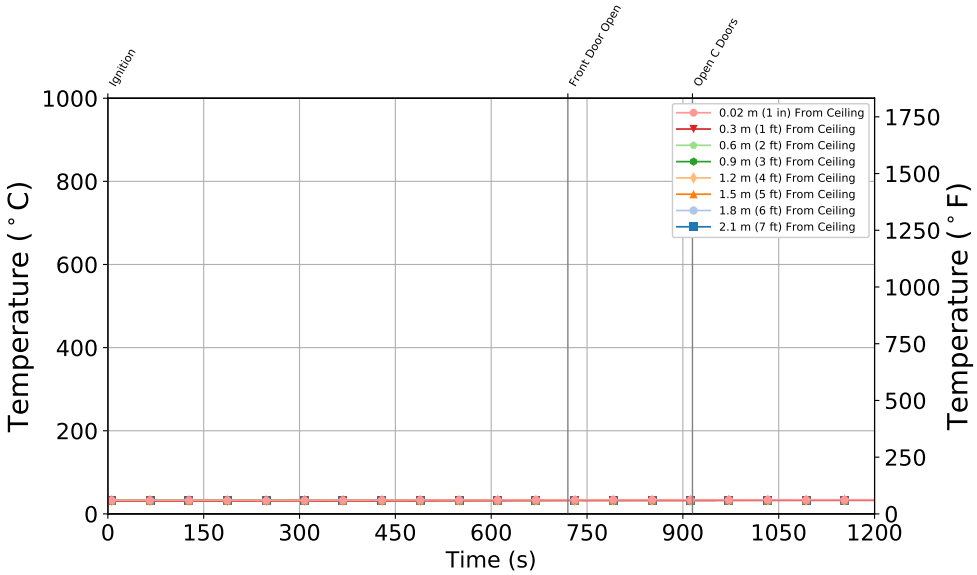

Figure B.31: Experiment 2 - Bedroom 3 (Closed) Bedroom

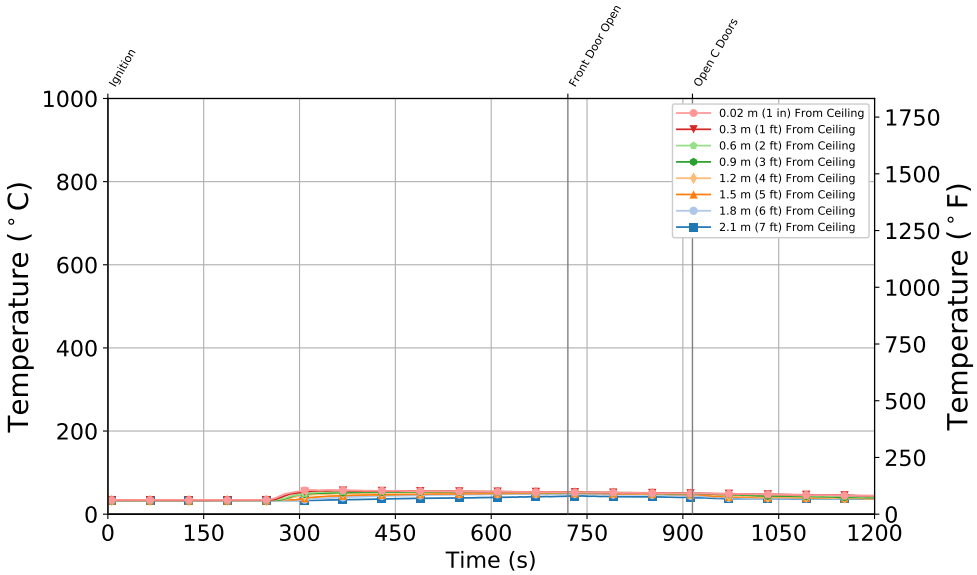

Figure B.32: Experiment 2 - Bedroom 2 (Open) Bedroom

B.3 Experiment 3

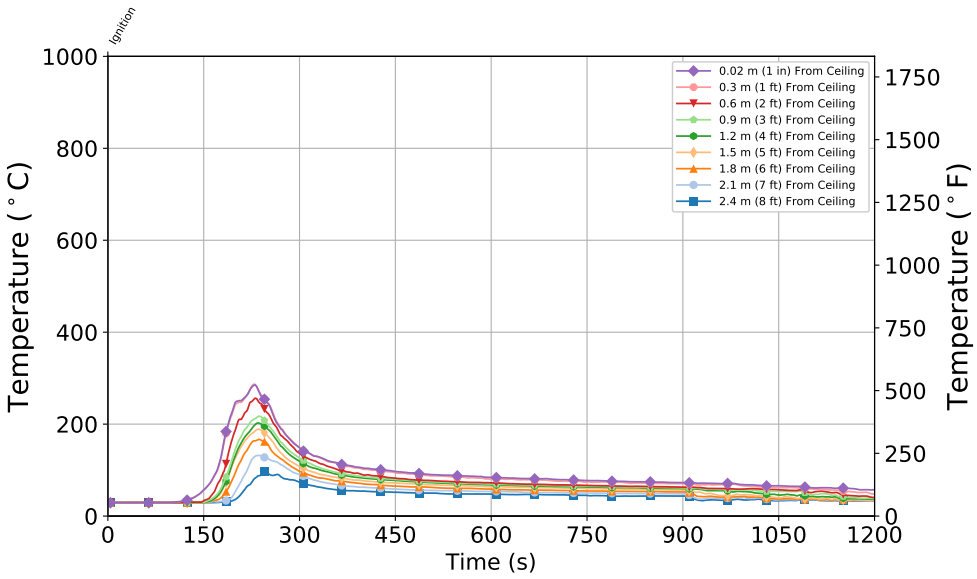

Figure B.33: Experiment 3 - Thermocouple temperature time histories from the Quadrant A thermocouple array in the basement.

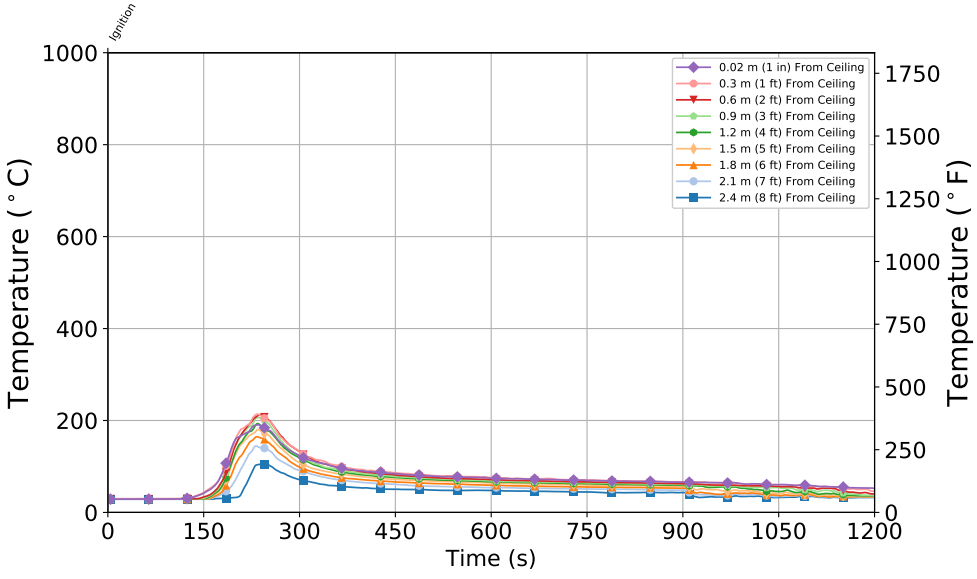

Figure B.34: Experiment 3 - Thermocouple temperature time histories from the Quadrant B thermocouple array in the basement.

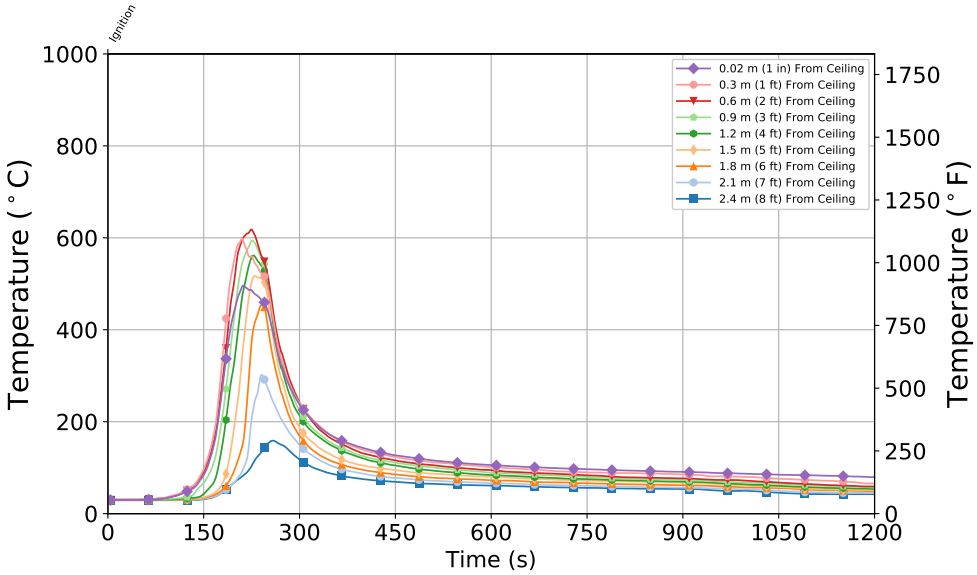

Figure B.35: Experiment 3 - Thermocouple temperature time histories from the Quadrant C thermocouple array in the basement.

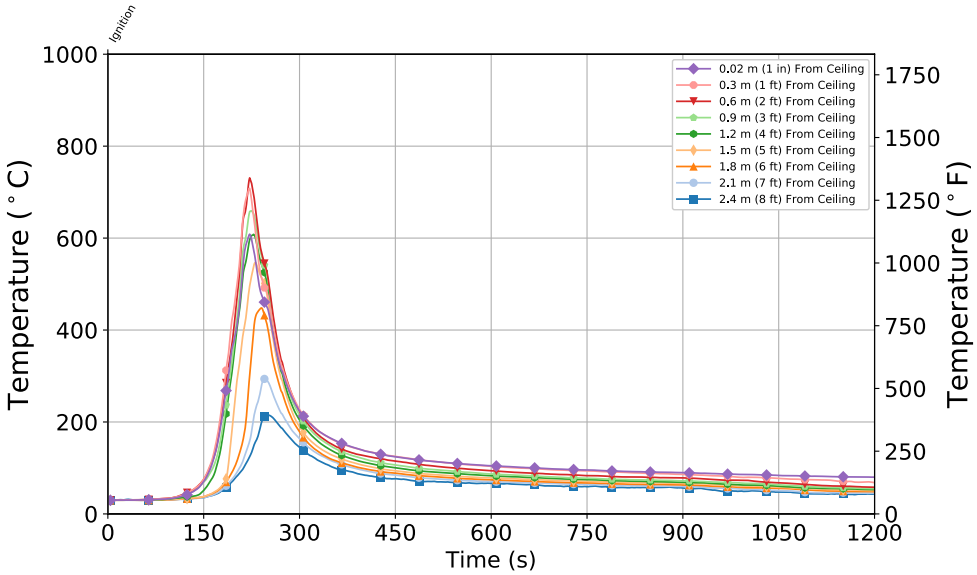

Figure B.36: Experiment 3 - Thermocouple temperature time histories from the Quadrant D thermocouple array in the basement.

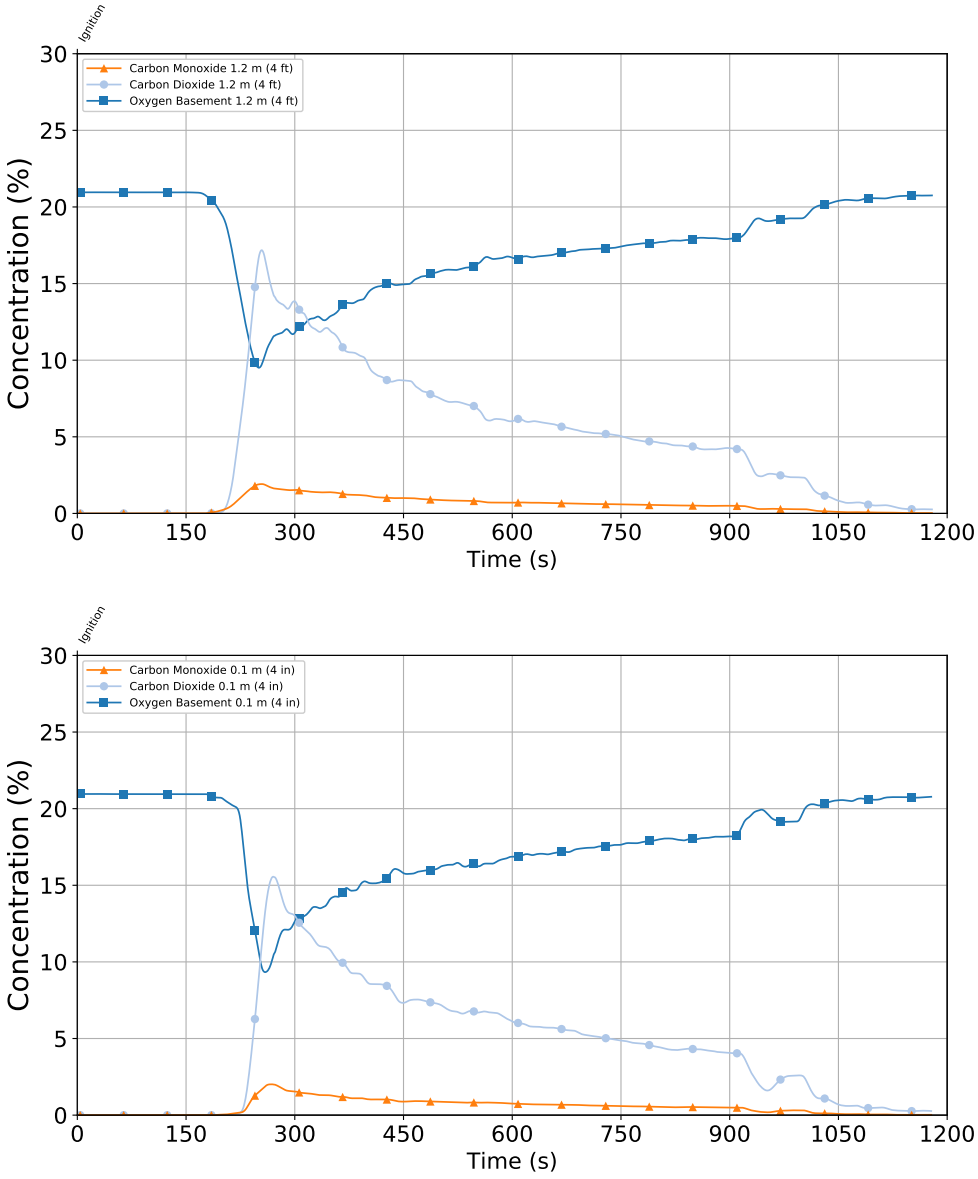

Figure B.37: Experiment 3 - Gas concentration time histories from the 1.2 m (4 ft) (top) and 0.1 m (4 in.) (bottom) elevations in the basement.

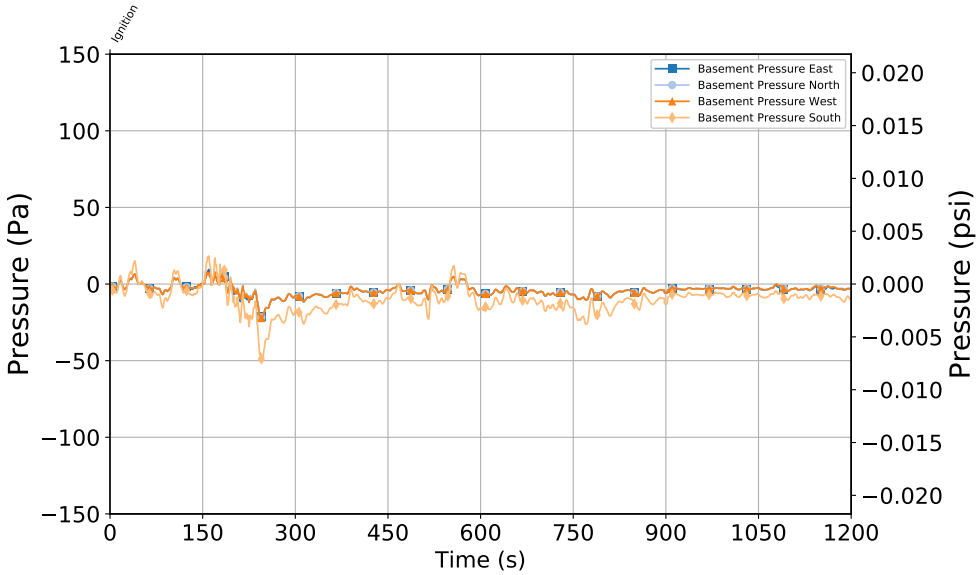

Figure B.38: Experiment 3 - Basement Pressure at 6 locations 1.2 m (4 ft) Above the Floor

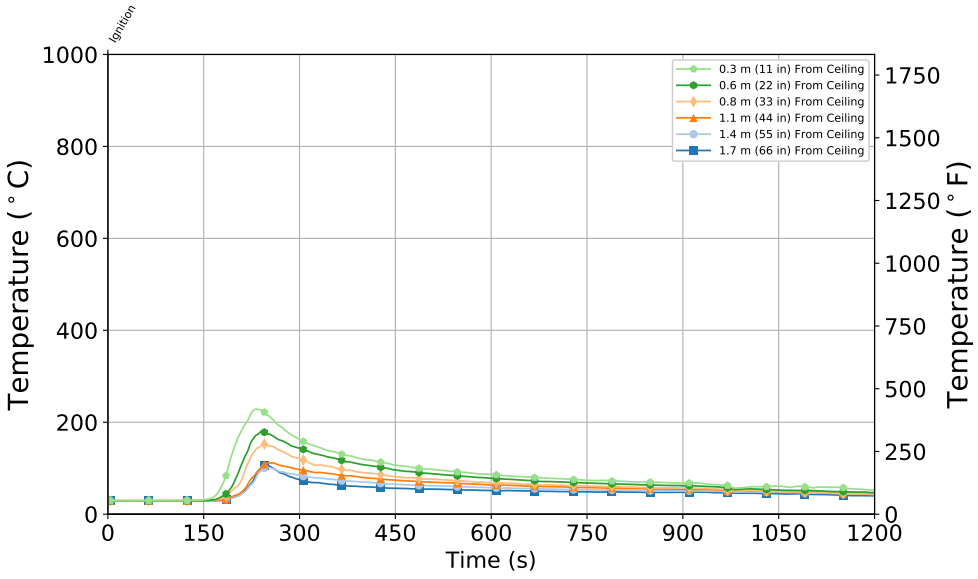

Figure B.39: Experiment 3 - Stair Thermocouple Temperature at Basement Level

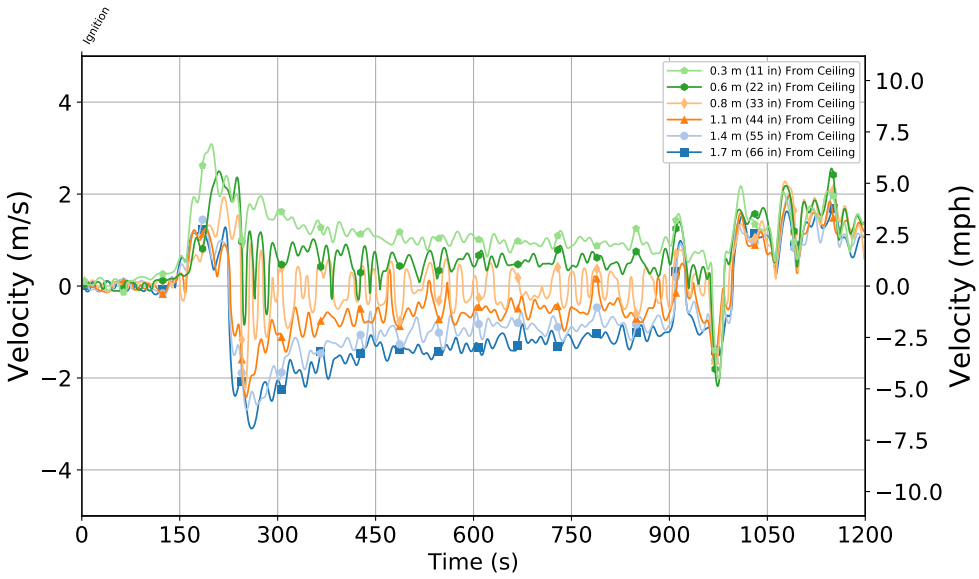

Figure B.40: Experiment 3 - Stair Velocity at Basement Level

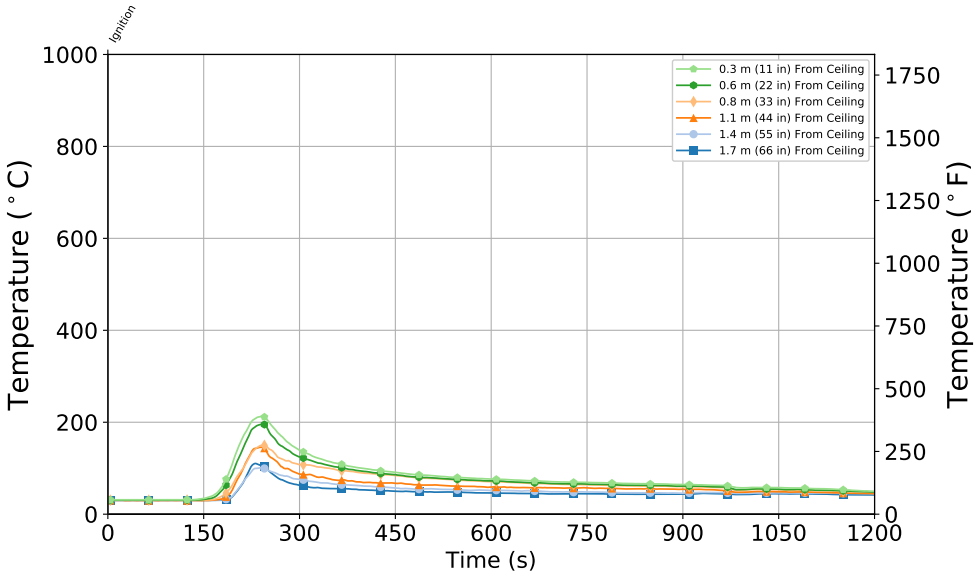

Figure B.41: Experiment 3 - Stair Thermocouple Temperature at First Floor

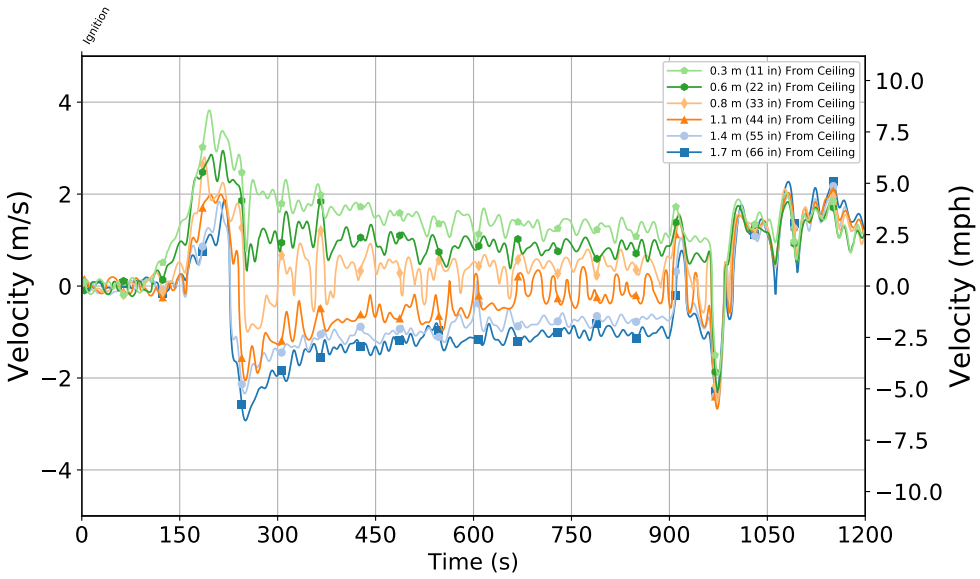

Figure B.42: Stair Velocity at First Floor

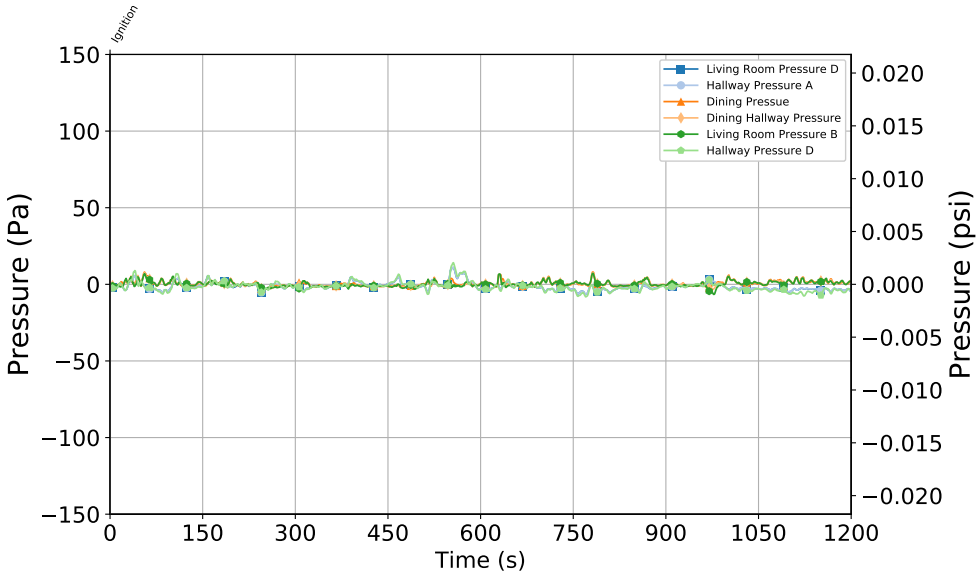

Figure B.43: Experiment 3 - First Floor Pressure at 6 locations 1.2 m (4 ft) Above the Floor

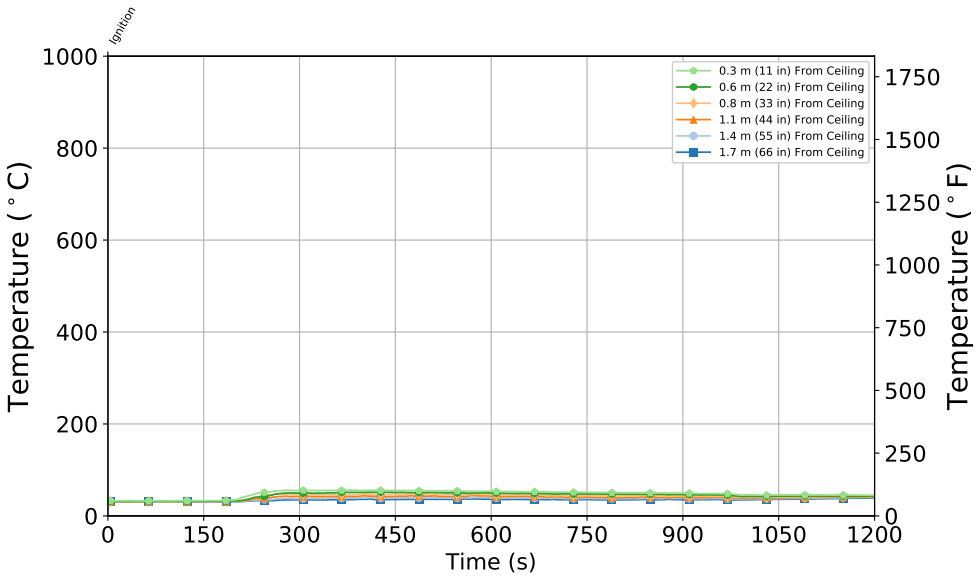

Figure B.44: Experiment 3 - Front Door Thermocouple Temperature at First Floor

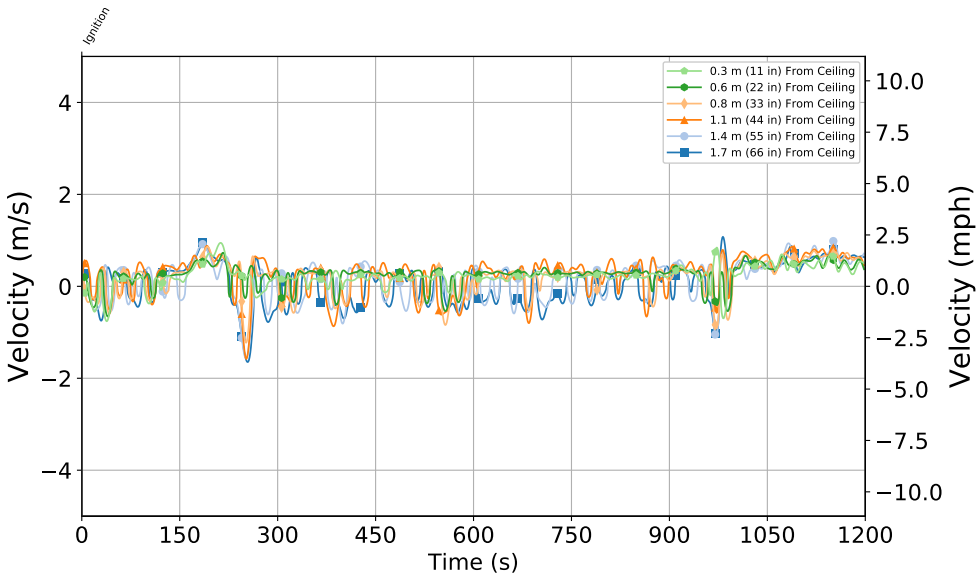

Figure B.45: Experiment 3 - Front Door Velocity at First Floor

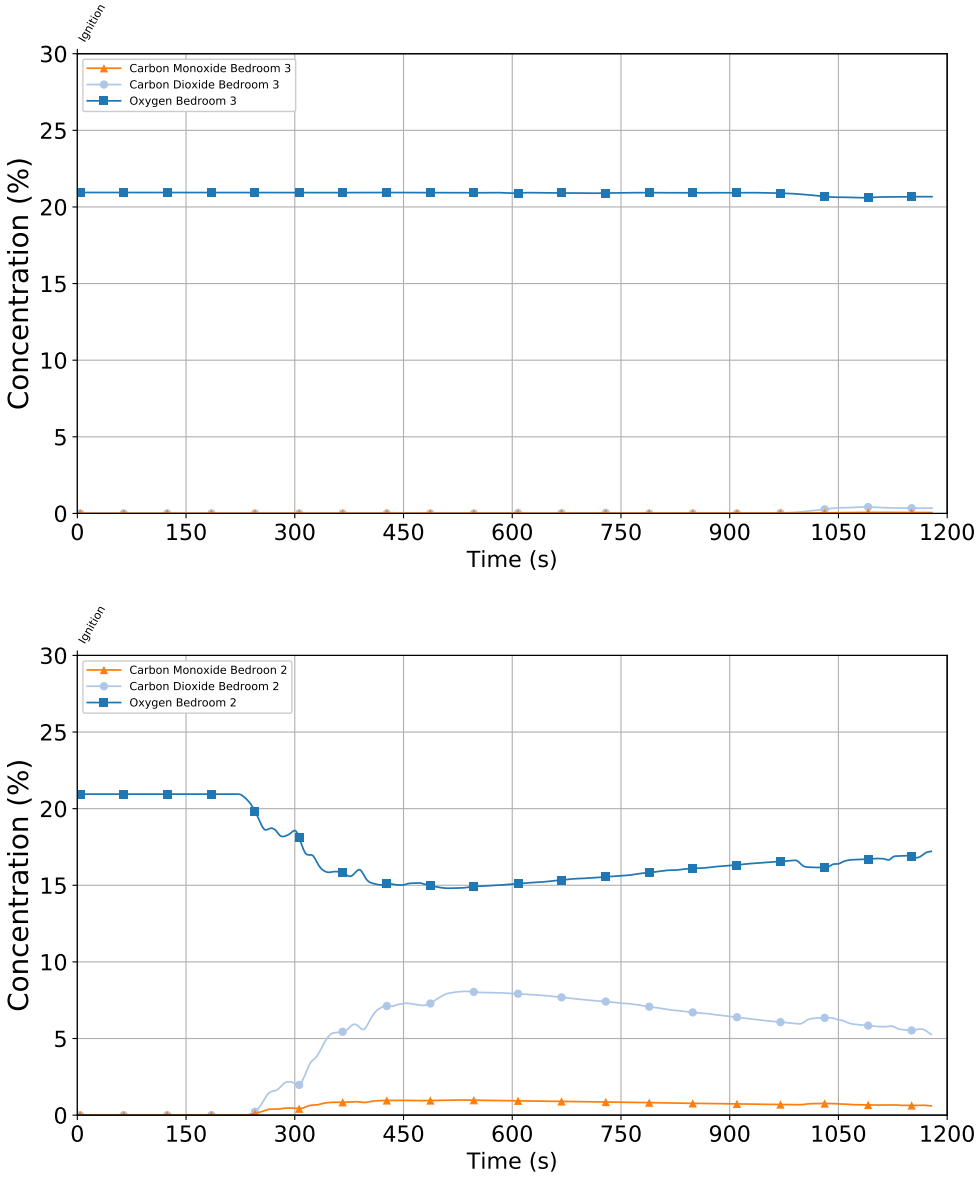

Figure B.46: Experiment 3 - Gas concentration time histories from the closed bedroom at 1.2 m (4 ft) (top) and from the open bedroom at 1.2 m (4 ft) (bottom).

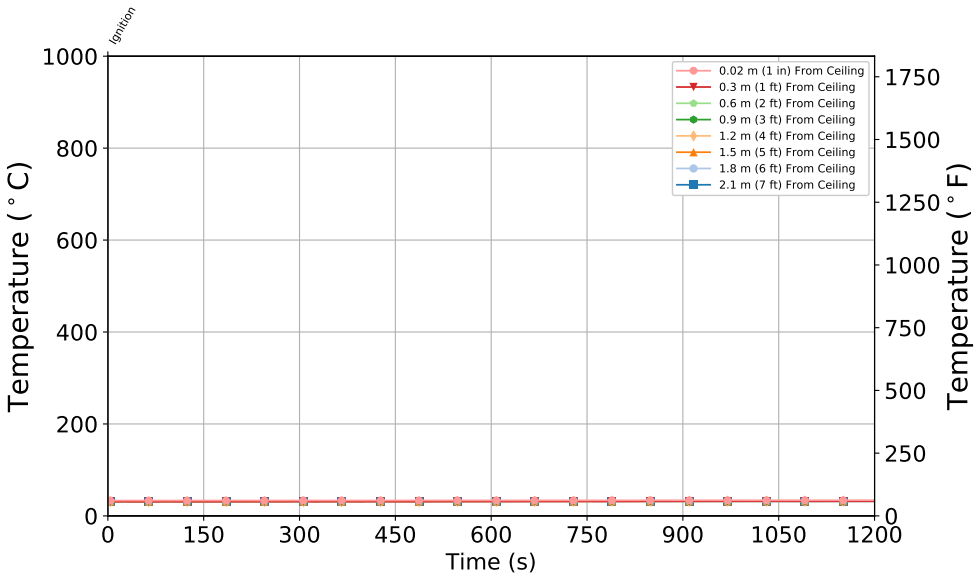

Figure B.47: Experiment 3 - Bedroom 3 (Closed) Bedroom

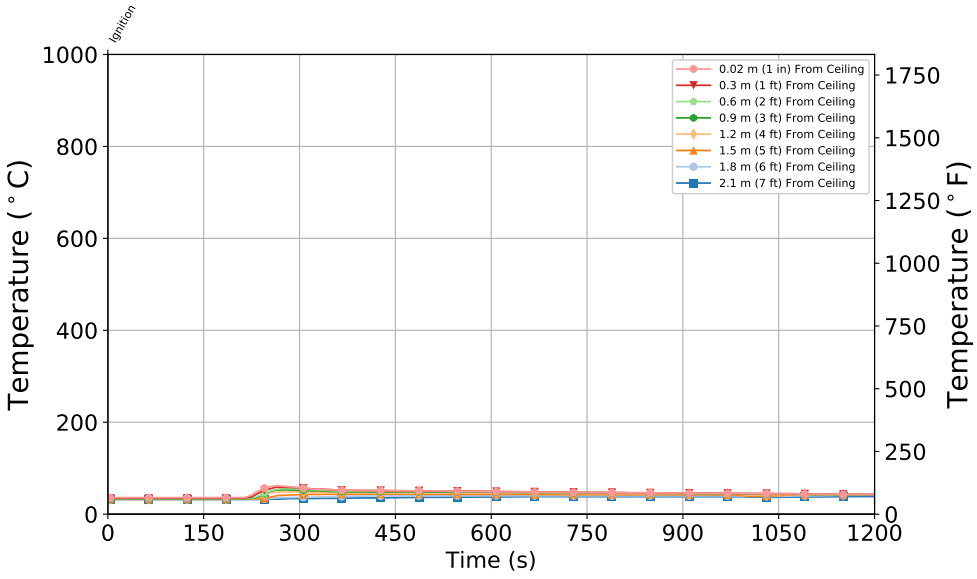

Figure B.48: Experiment 3 - Bedroom 2 (Open) Bedroom

B.4 Experiment 4

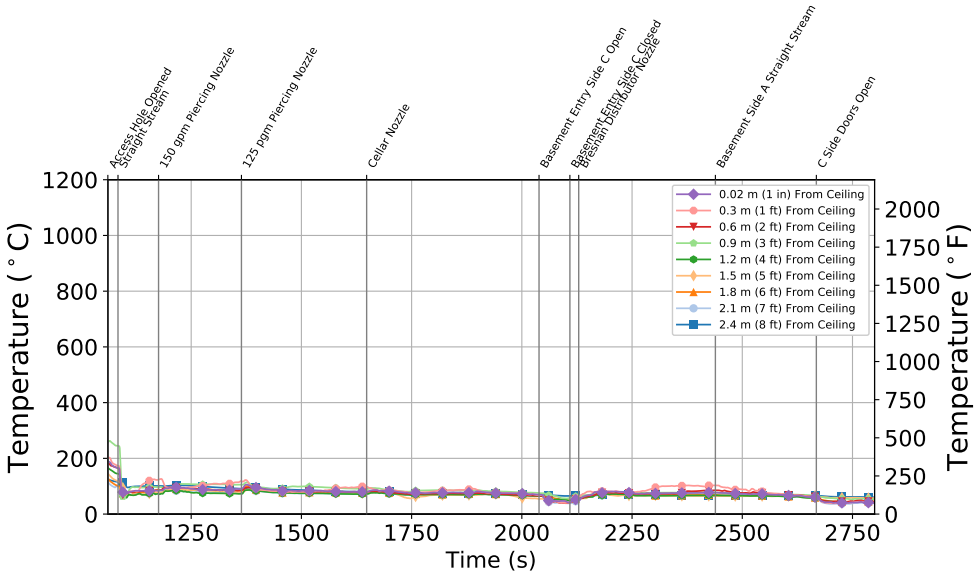

Figure B.49: Experiment 4 - Thermocouple temperature time histories from the Quadrant A thermocouple array in the basement.

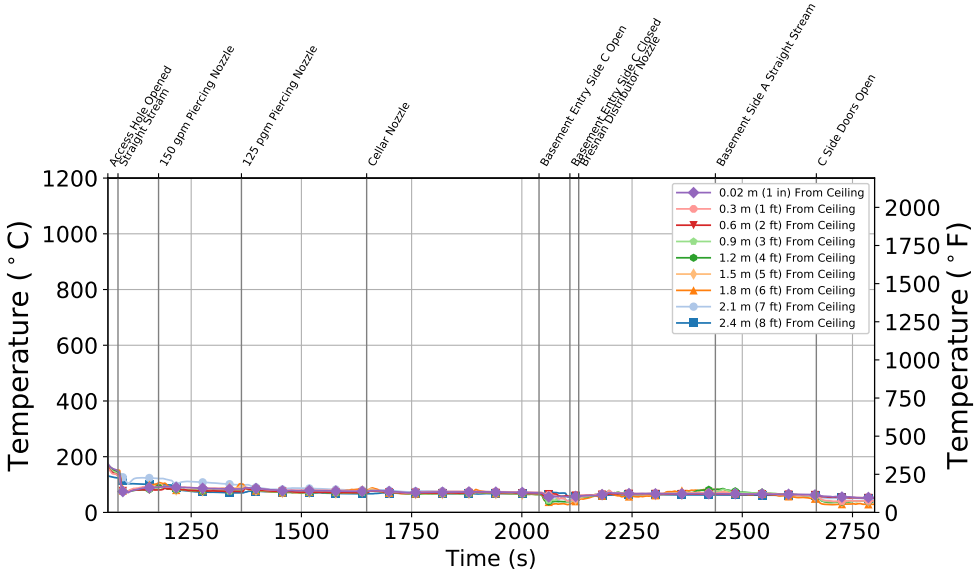

Figure B.50: Experiment 4 - Thermocouple temperature time histories from the Quadrant B thermocouple array in the basement.

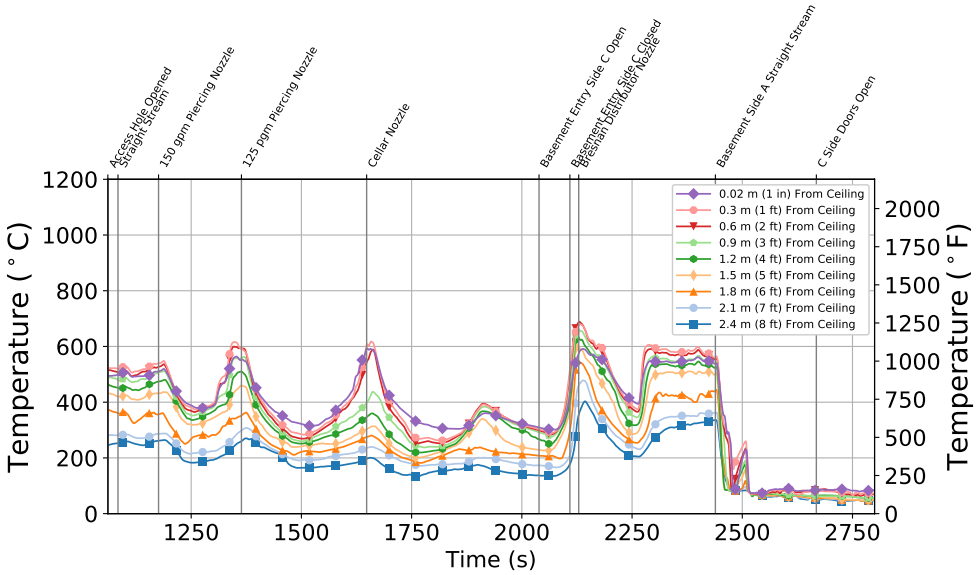

Figure B.51: Experiment 4 - Thermocouple temperature time histories from the Quadrant C thermocouple array in the basement.

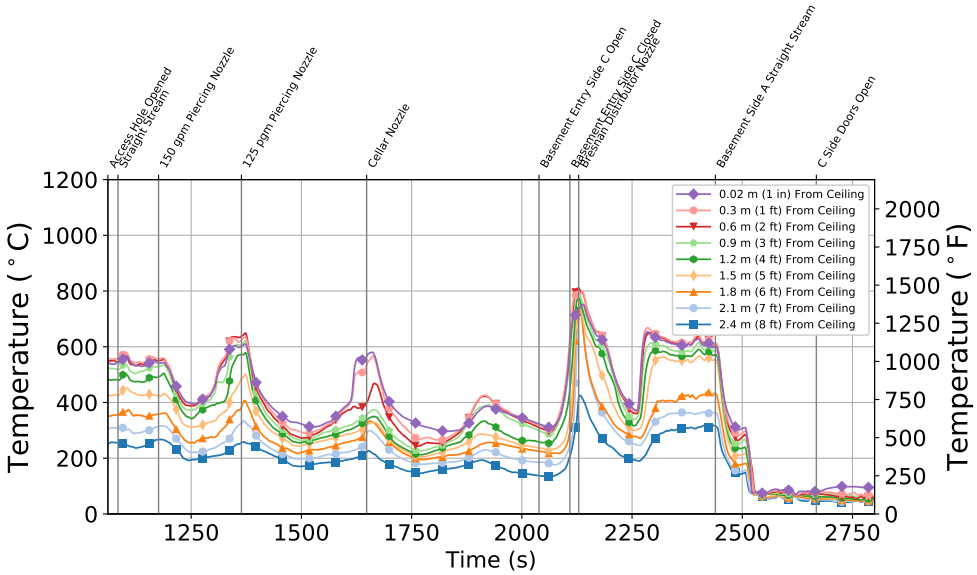

Figure B.52: Experiment 4 - Thermocouple temperature time histories from the Quadrant D thermocouple array in the basement.

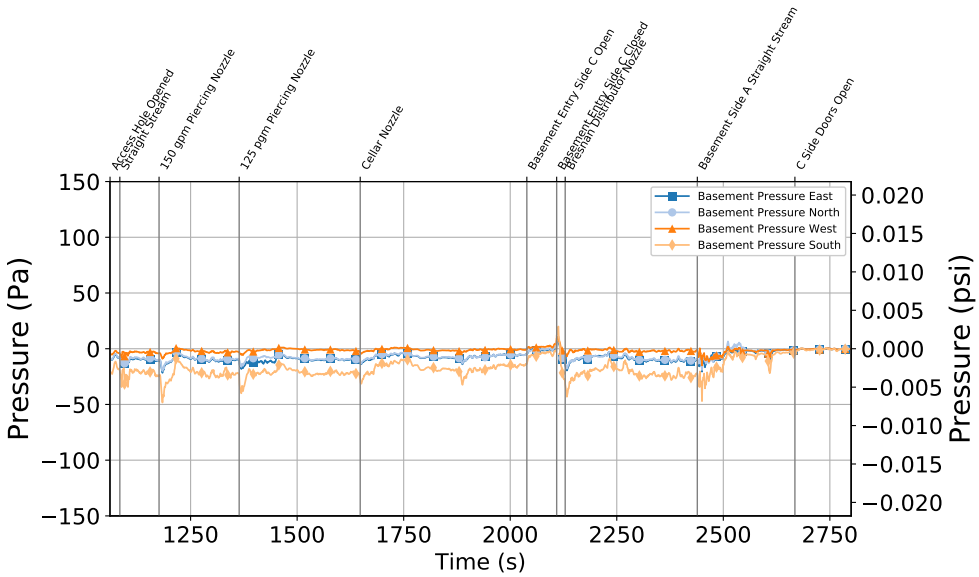

Figure B.53: Experiment 4 - Basement Pressure at 6 locations 1.2 m (4 ft) Above the Floor

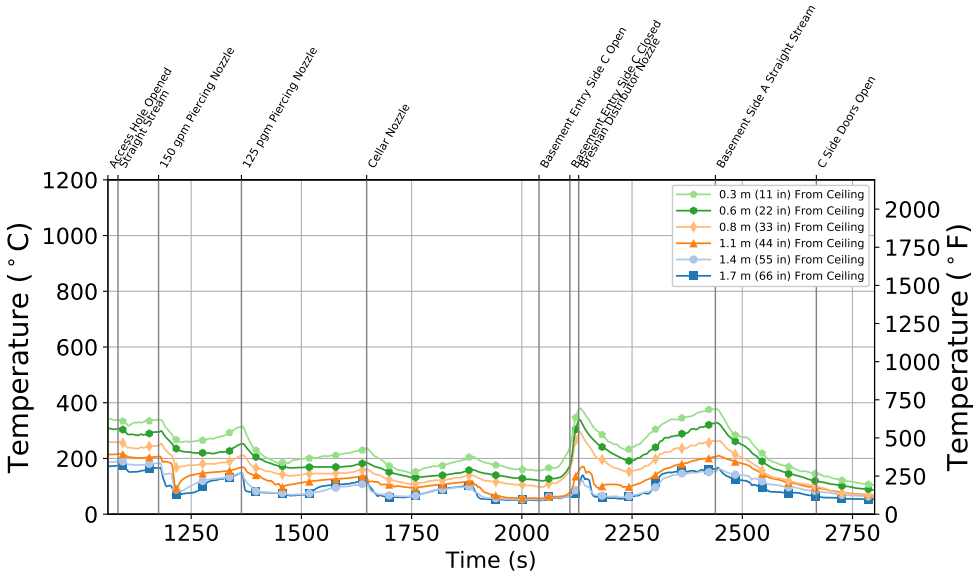

Figure B.54: Experiment 4 - Stair Thermocouple Temperature at Basement Level

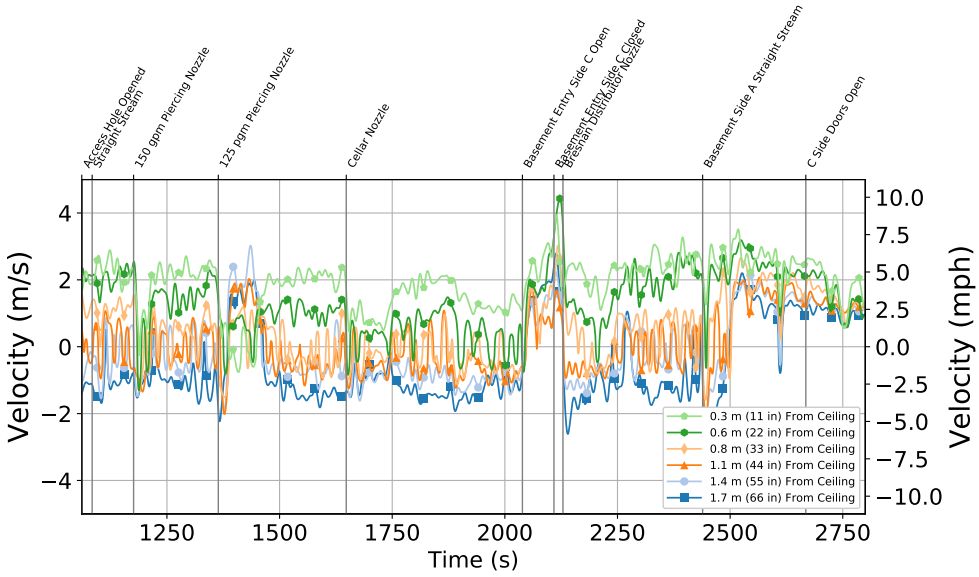

Figure B.55: Experiment 4 - Stair Velocity at Basement Level

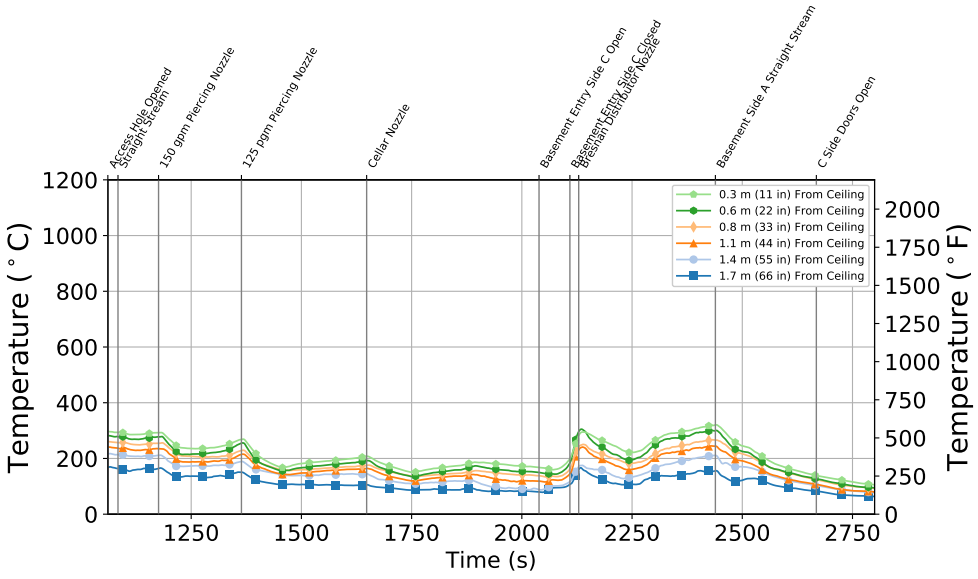

Figure B.56: Experiment 4 - Stair Thermocouple Temperature at First Floor

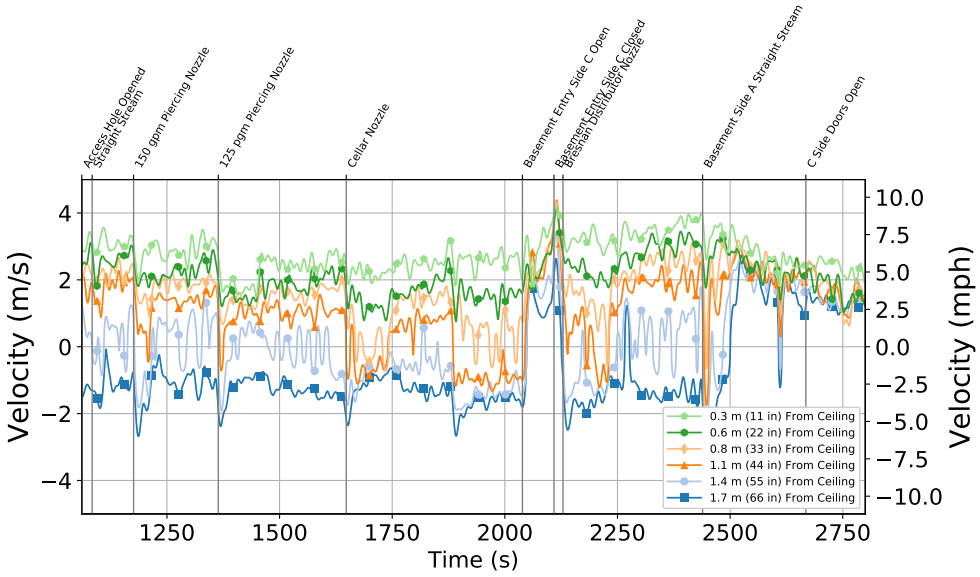

Figure B.57: Stair Velocity at First Floor

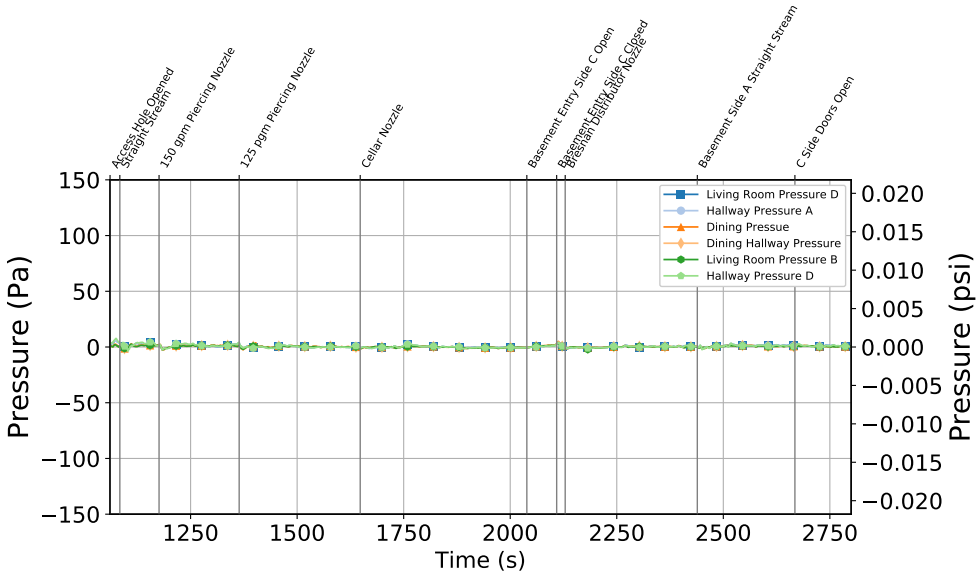

Figure B.58: Experiment 4 - First Floor Pressure at 6 locations 1.2 m (4 ft) Above the Floor

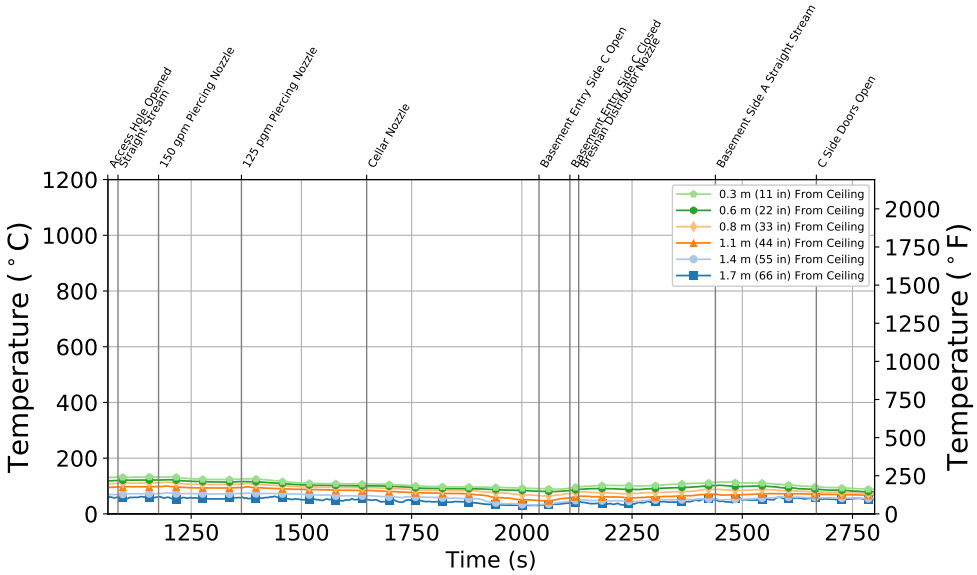

Figure B.59: Experiment 4 - Front Door Thermocouple Temperature at First Floor

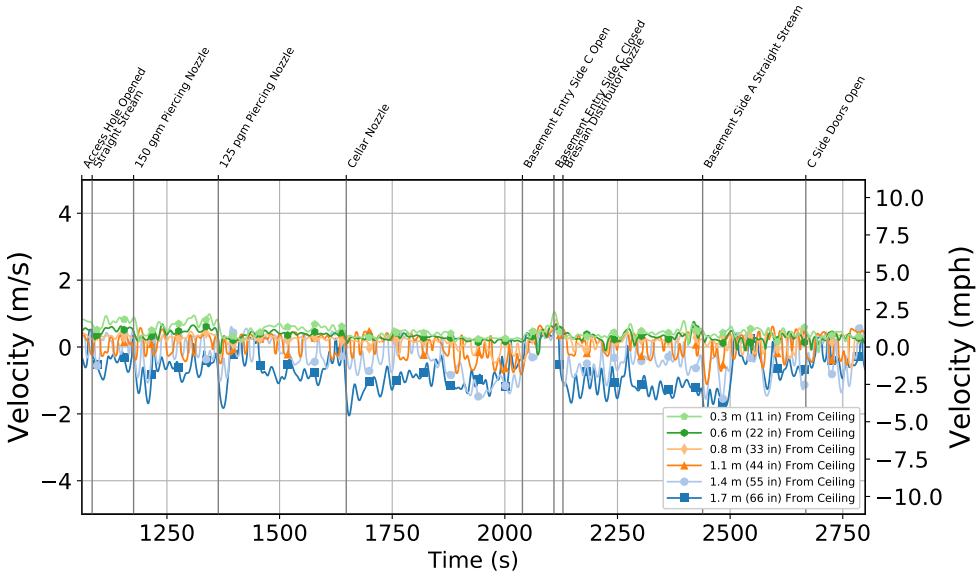

Figure B.60: Experiment 4 - Front Door Velocity at First Floor

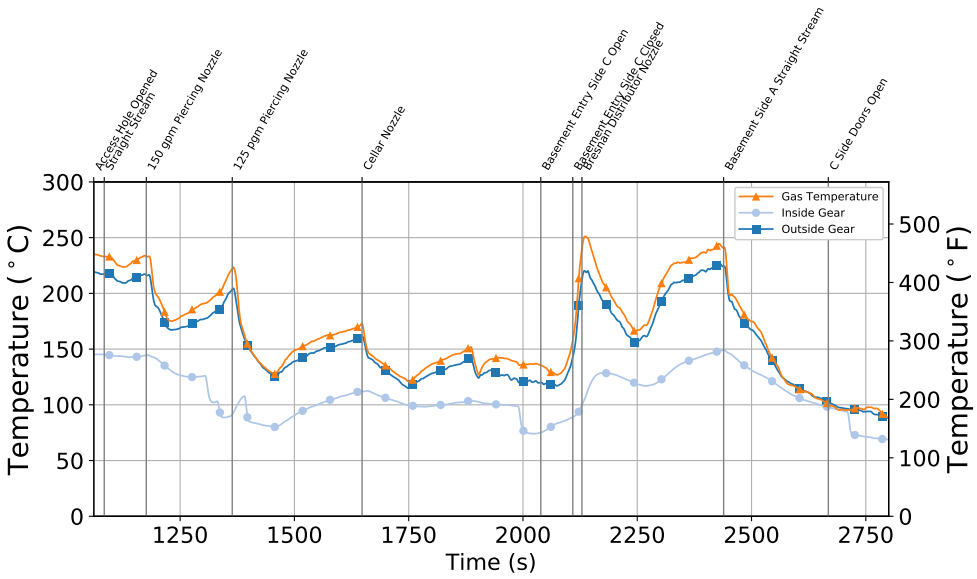

Figure B.61: Experiment 4 - Thermocouple Temperature on Inside and Outside of PPE Sample

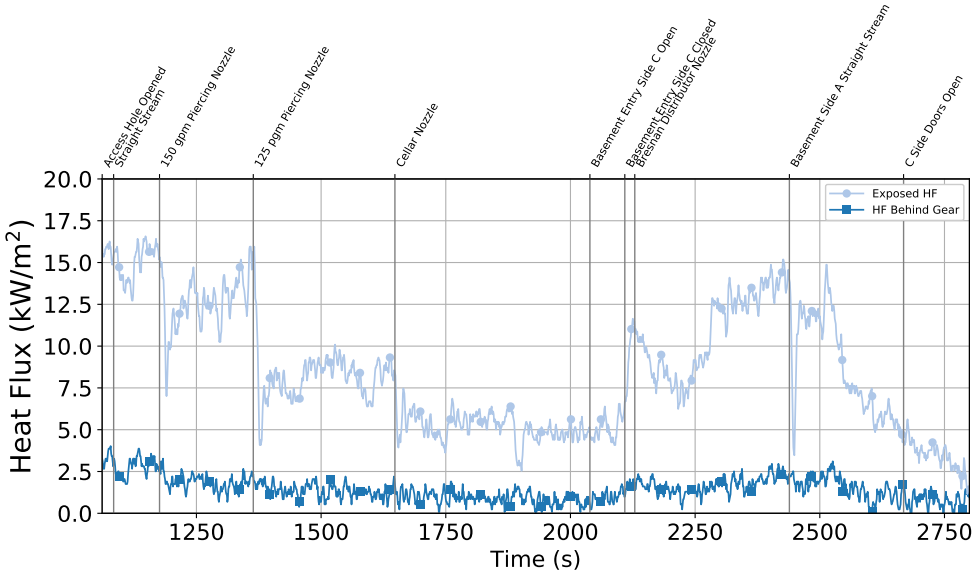

Figure B.62: Experiment 4 - Comparison of Heat Flux between Exposed Sensor and Protected Sensor

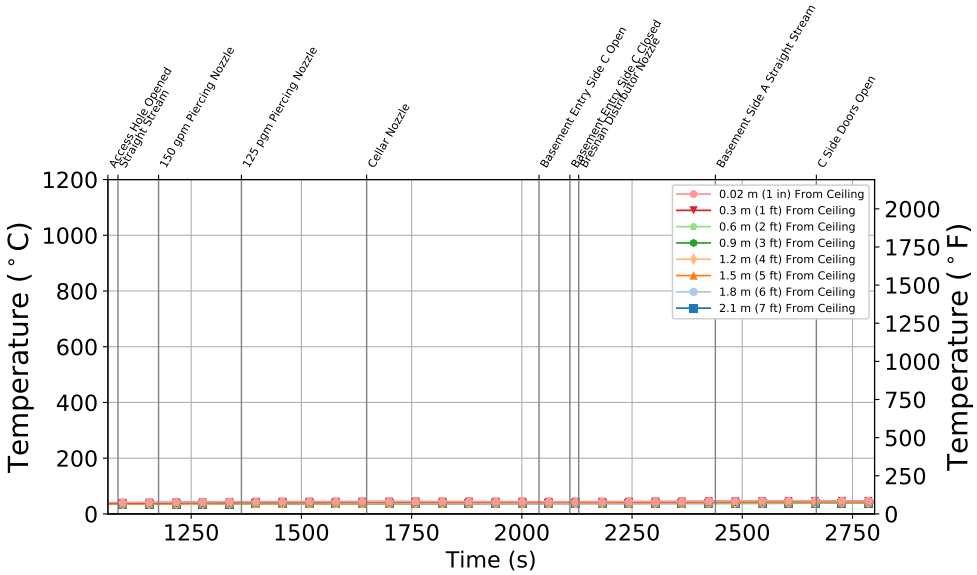

Figure B.63: Experiment 4 - Bedroom 3 (Closed) Bedroom

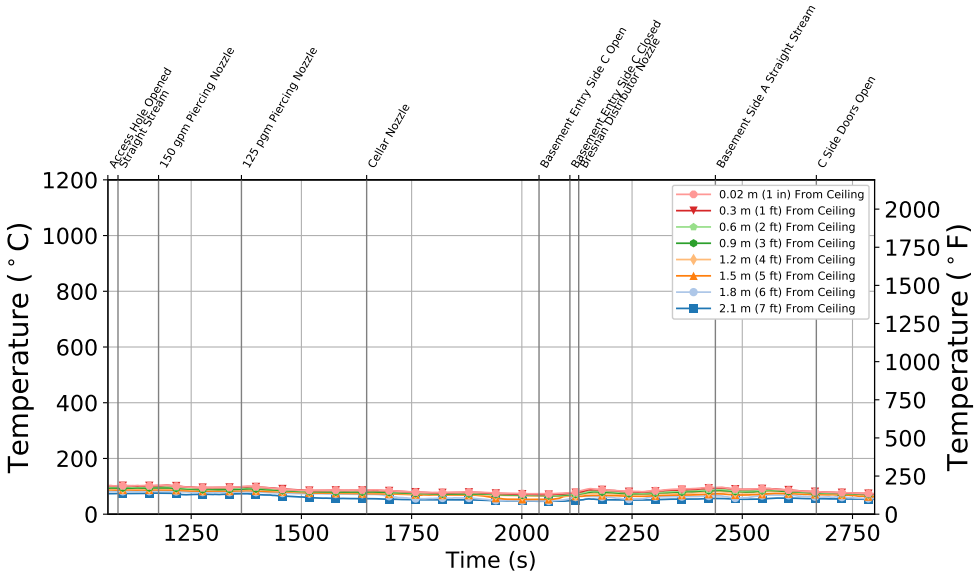

Figure B.64: Experiment 4 - Bedroom 2 (Open) Bedroom

B.5 Experiment 5

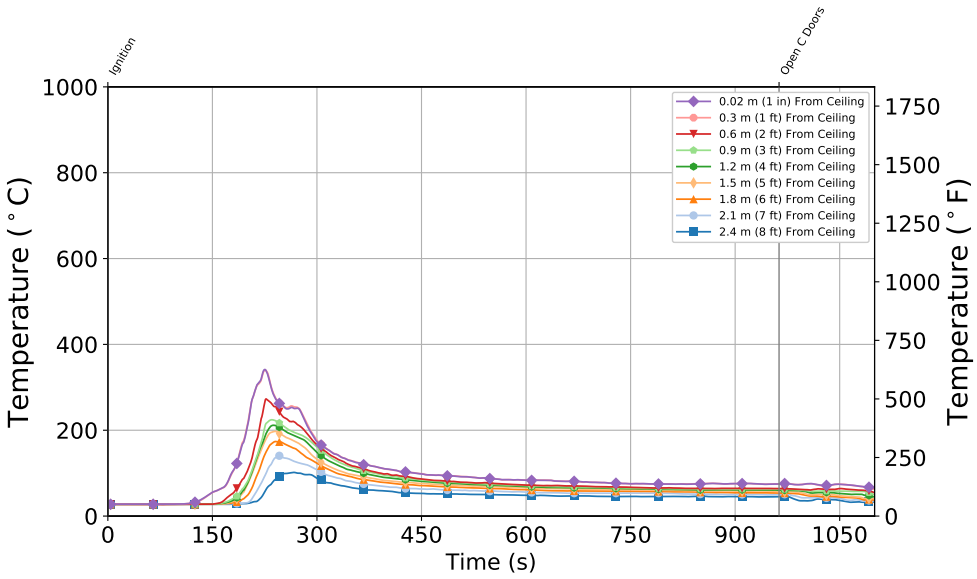

Figure B.65: Experiment 5 - Thermocouple temperature time histories from the Quadrant A thermocouple array in the basement.

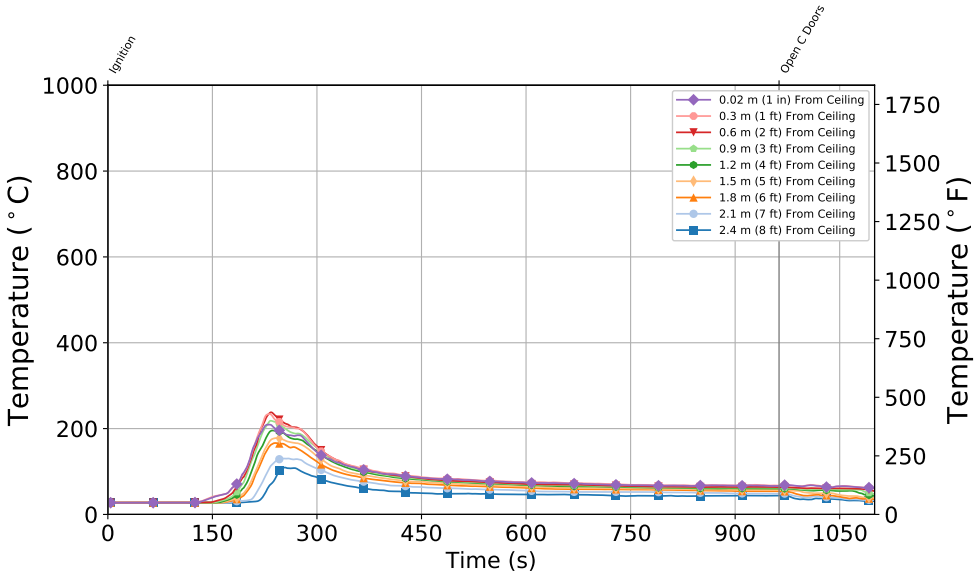

Figure B.66: Experiment 5 - Thermocouple temperature time histories from the Quadrant B thermocouple array in the basement.

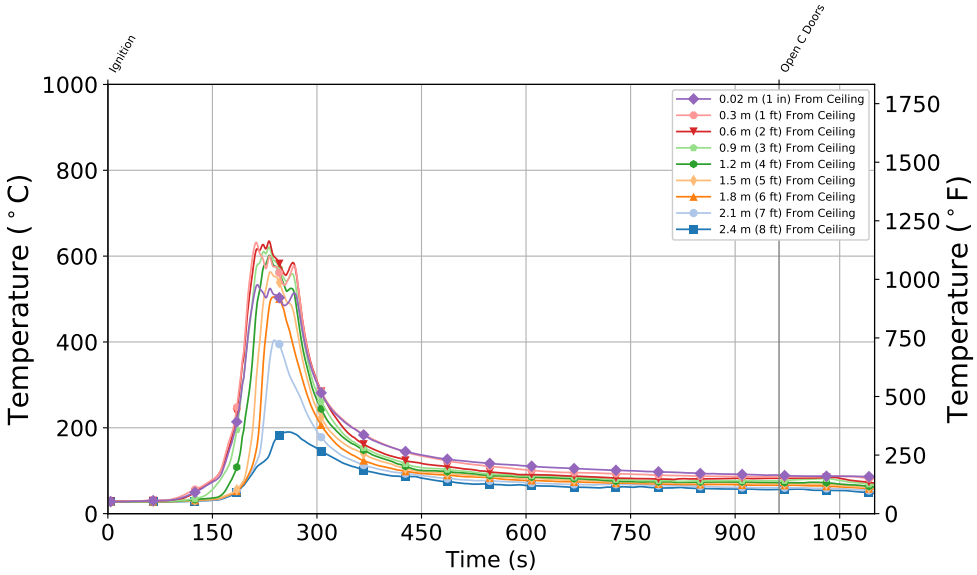

Figure B.67: Experiment 5 - Thermocouple temperature time histories from the Quadrant C thermocouple array in the basement.

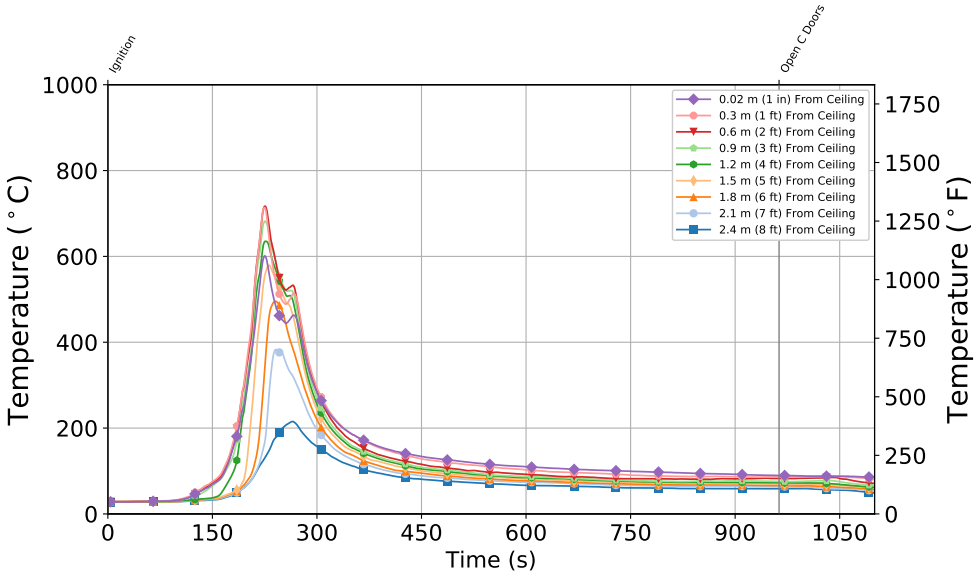

Figure B.68: Experiment 5 - Thermocouple temperature time histories from the Quadrant D thermocouple array in the basement.

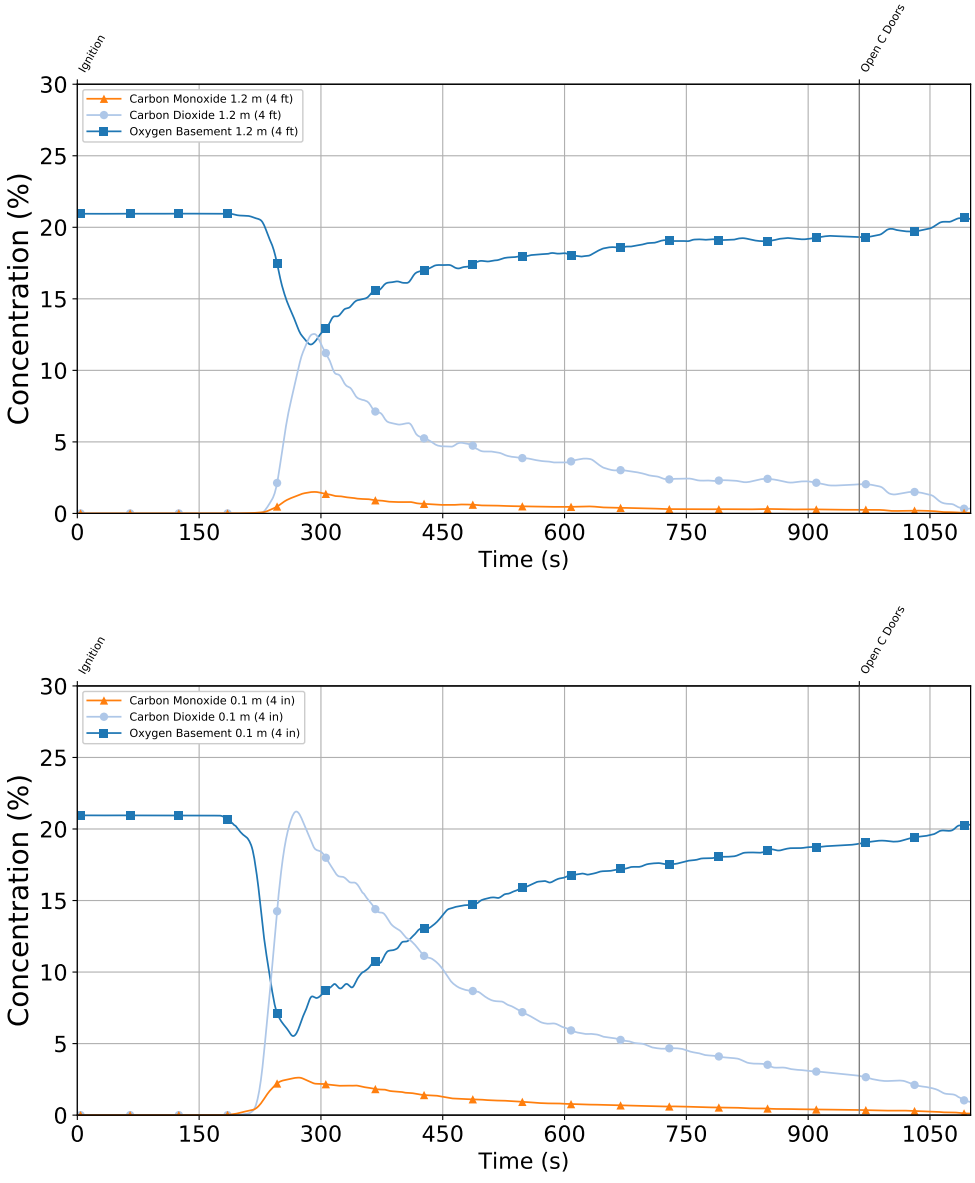

Figure B.69: Experiment 5 - Gas concentration time histories from the 1.2 m (4 ft) (top) and 0.1 m (4 in.) (bottom) elevations in the basement.

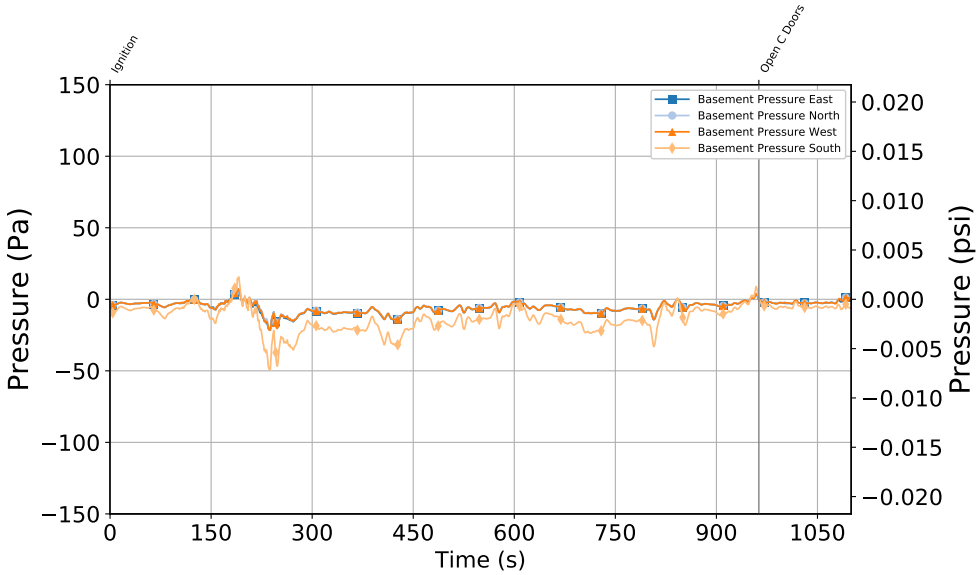

Figure B.70: Experiment 5 - Basement Pressure at 6 locations 1.2 m (4 ft) Above the Floor

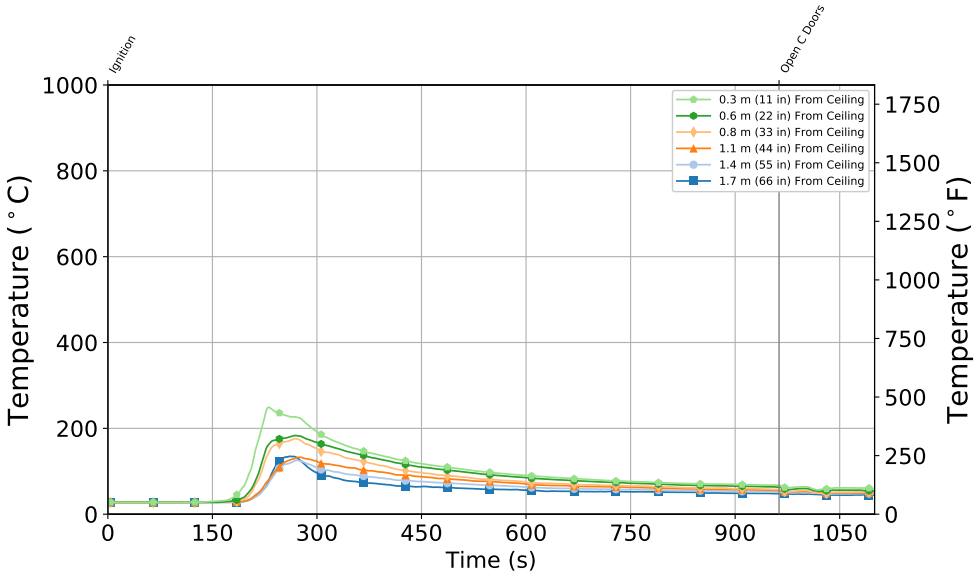

Figure B.71: Experiment 5 - Stair Thermocouple Temperature at Basement Level

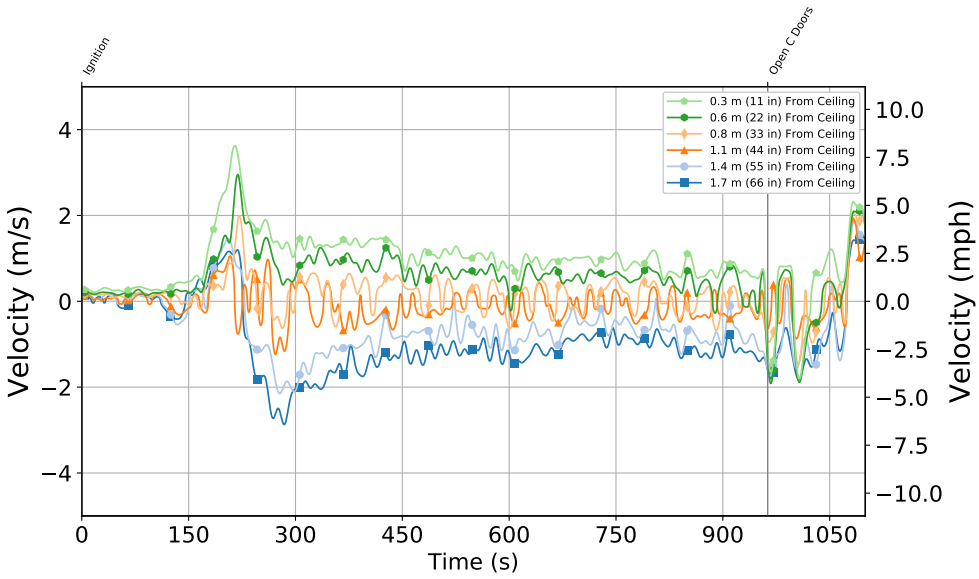

Figure B.72: Experiment 5 - Stair Velocity at Basement Level

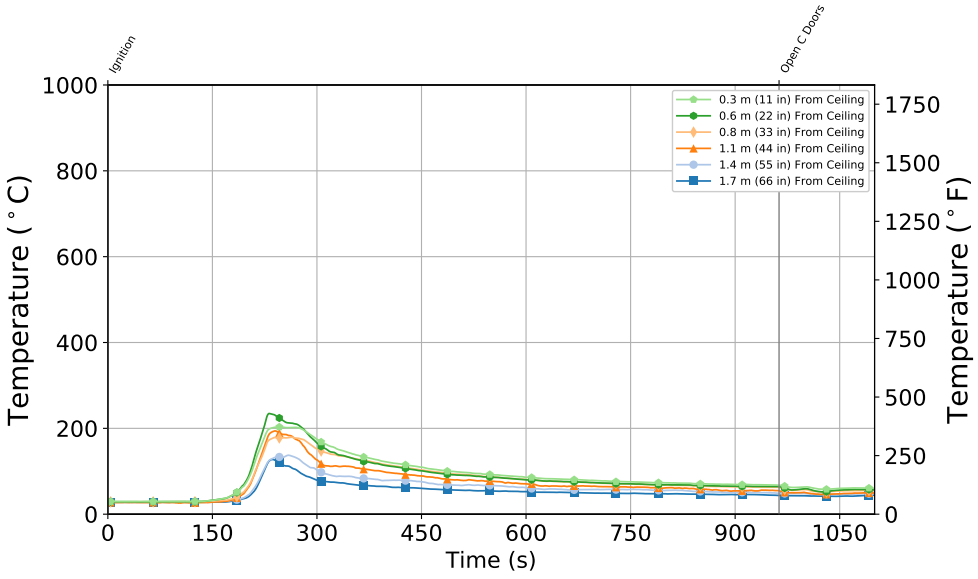

Figure B.73: Experiment 5 - Stair Thermocouple Temperature at First Floor

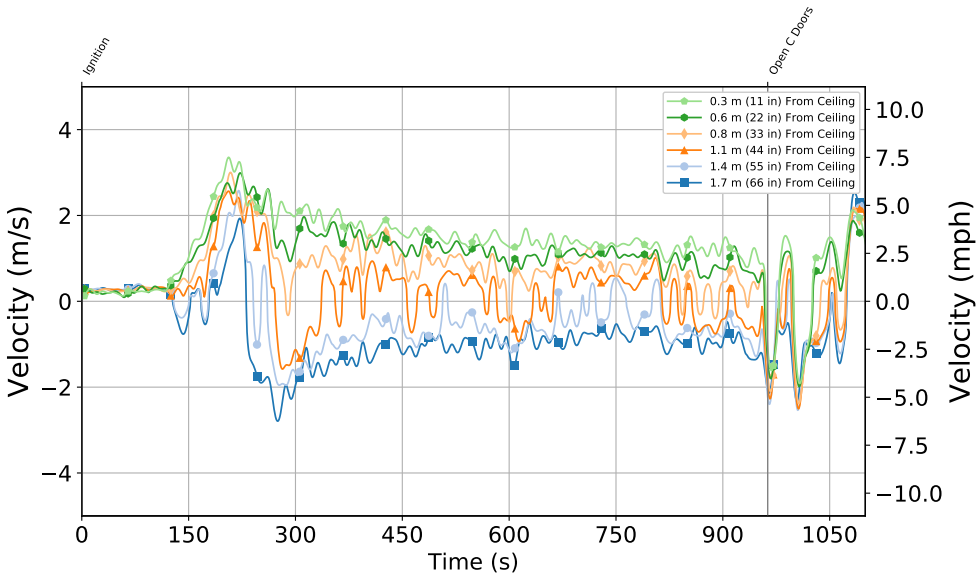

Figure B.74: Stair Velocity at First Floor

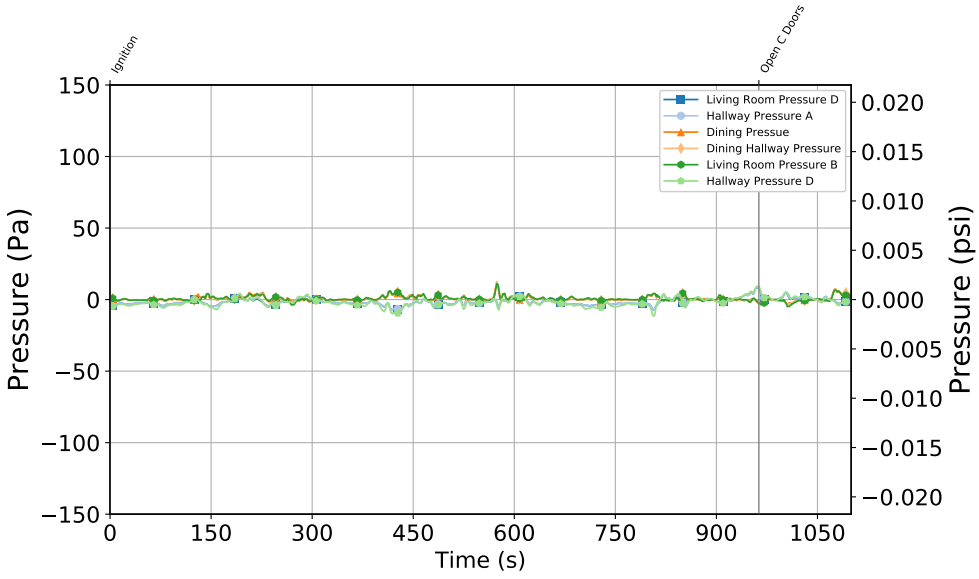

Figure B.75: Experiment 5 - First Floor Pressure at 6 locations 1.2 m (4 ft) Above the Floor

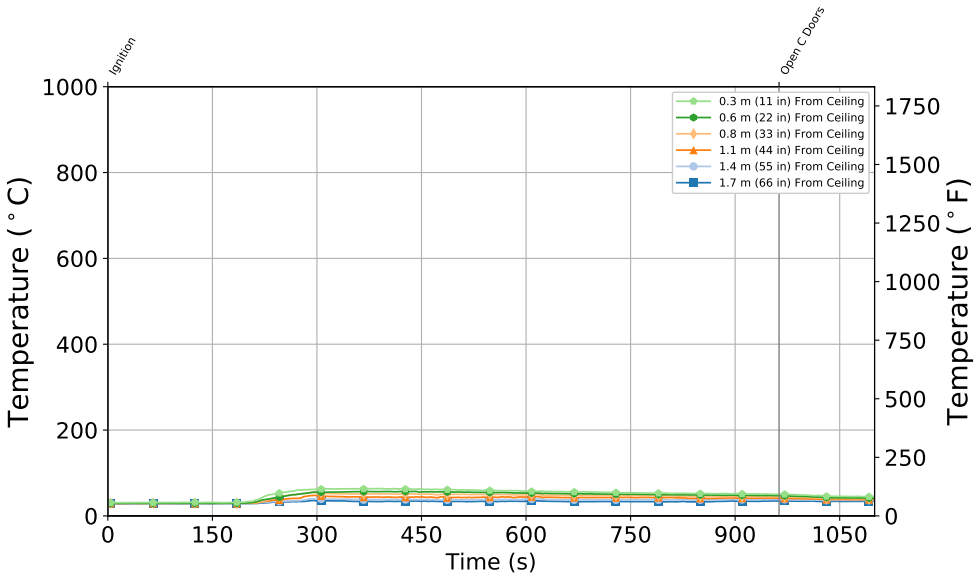

Figure B.76: Experiment 5 - Front Door Thermocouple Temperature at First Floor

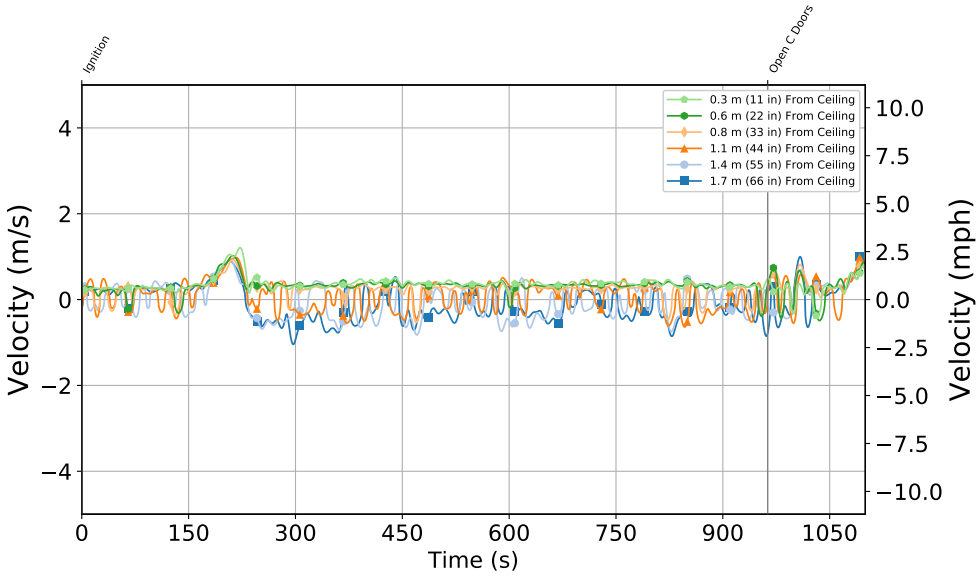

Figure B.77: Experiment 5 - Front Door Velocity at First Floor

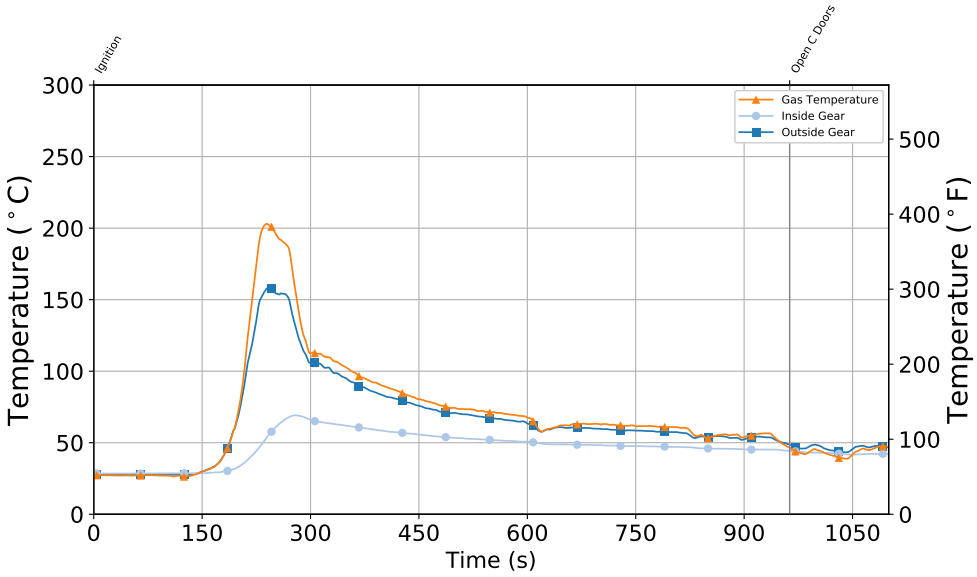

Figure B.78: Experiment 5 - Thermocouple Temperature on Inside and Outside of PPE Sample

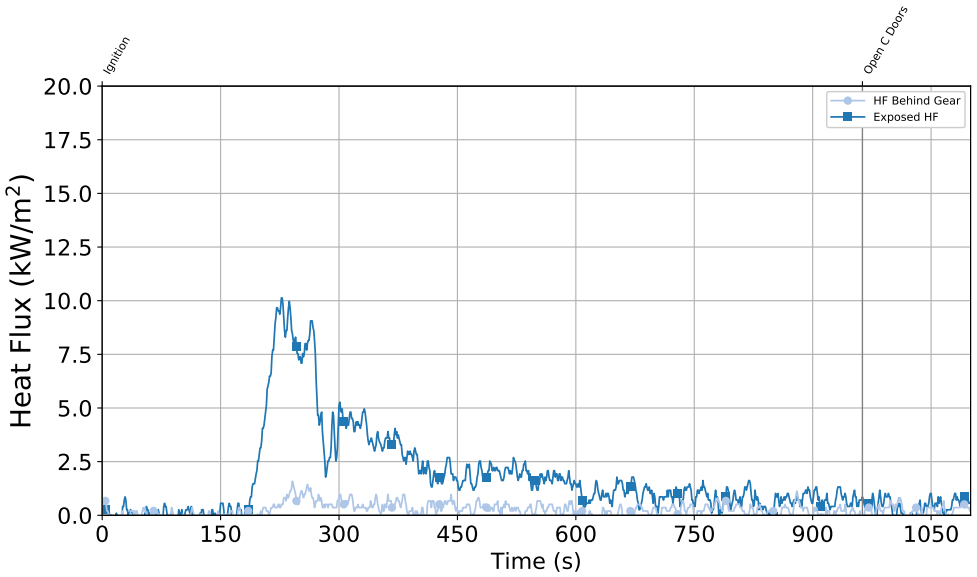

Figure B.79: Experiment 5 - Comparison of Heat Flux between Exposed Sensor and Protected Sensor

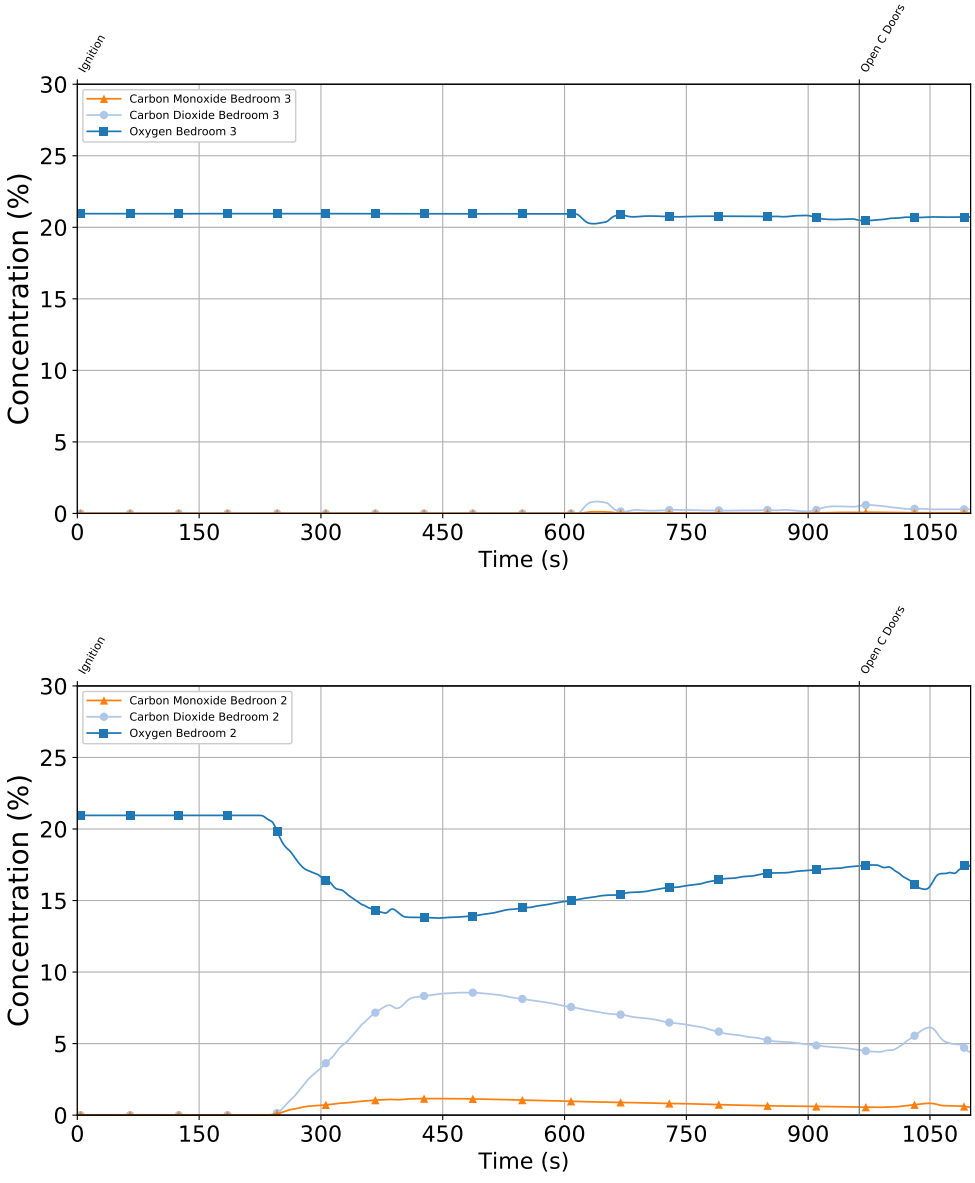

Figure B.80: Experiment 5 - Gas concentration time histories from the closed bedroom at 1.2 m (4 ft) (top) and from the open bedroom at 1.2 m (4 ft) (bottom).

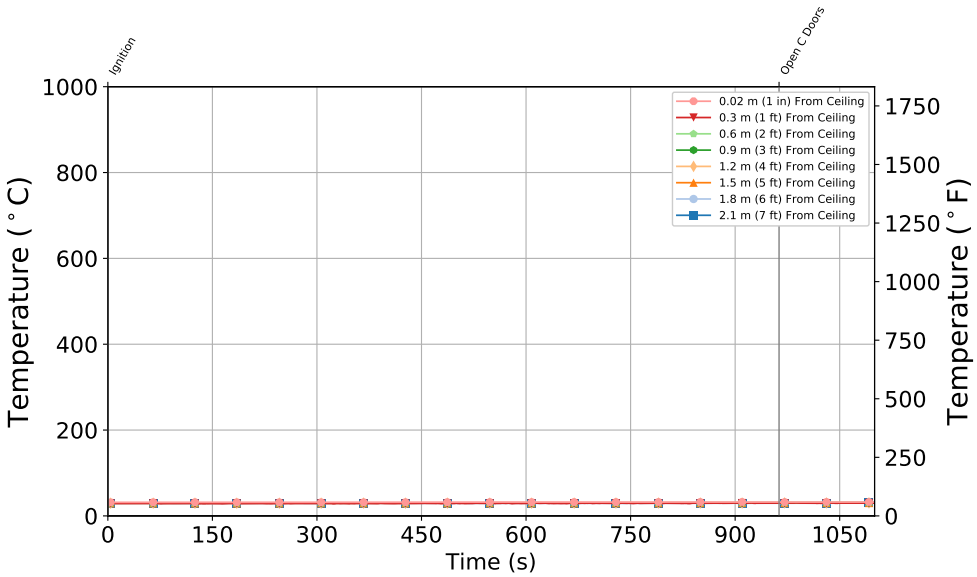

Figure B.81: Experiment 5 - Bedroom 3 (Closed) Bedroom

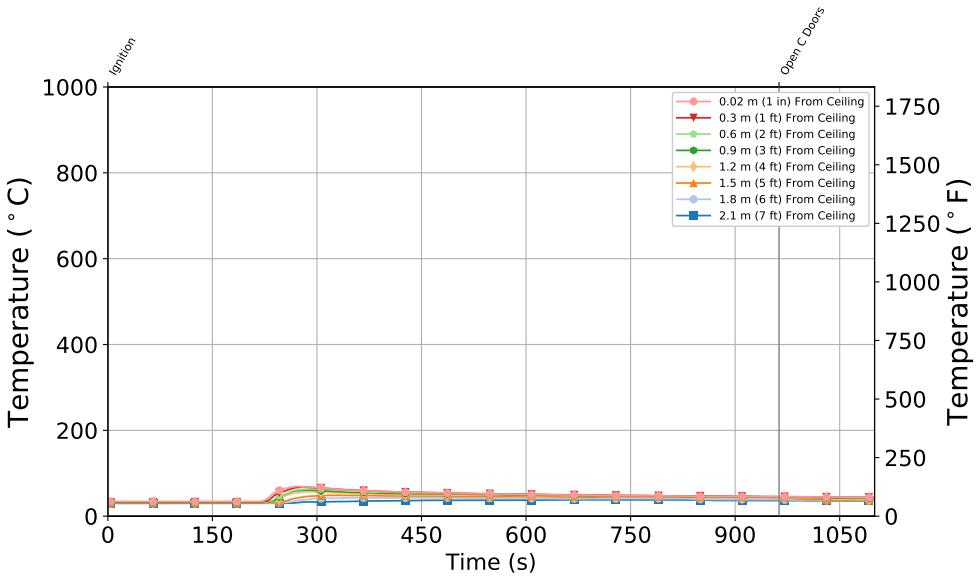

Figure B.82: Experiment 5 - Bedroom 2 (Open) Bedroom

B.6 Experiment 6

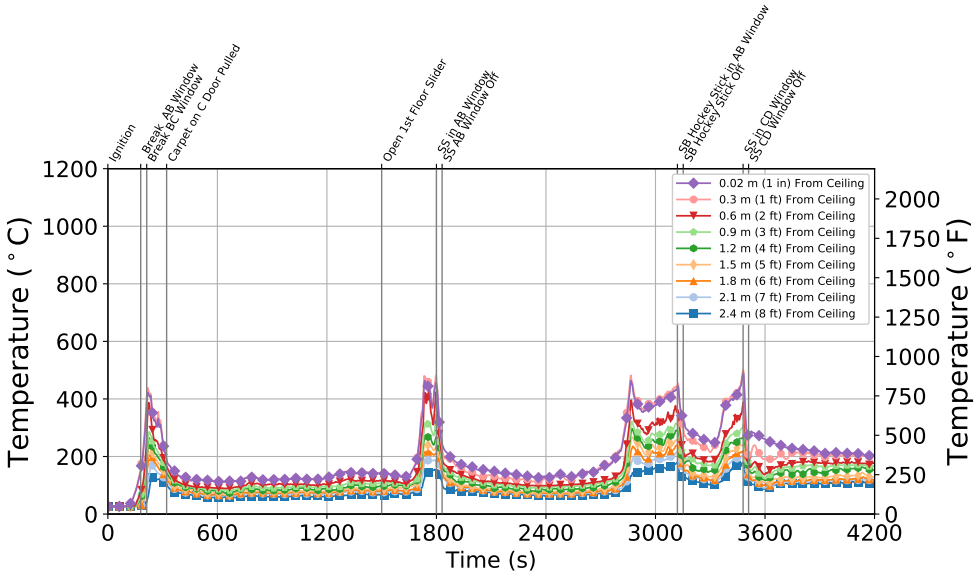

Figure B.83: Experiment 6 - Thermocouple temperature time histories from the Quadrant A thermocouple array in the basement.

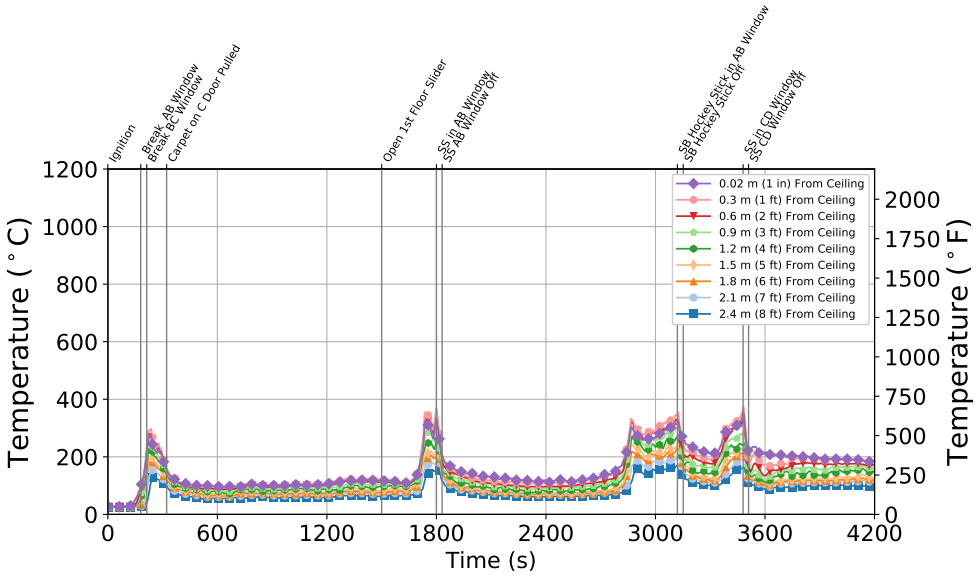

Figure B.84: Experiment 6 - Thermocouple temperature time histories from the Quadrant B thermocouple array in the basement.

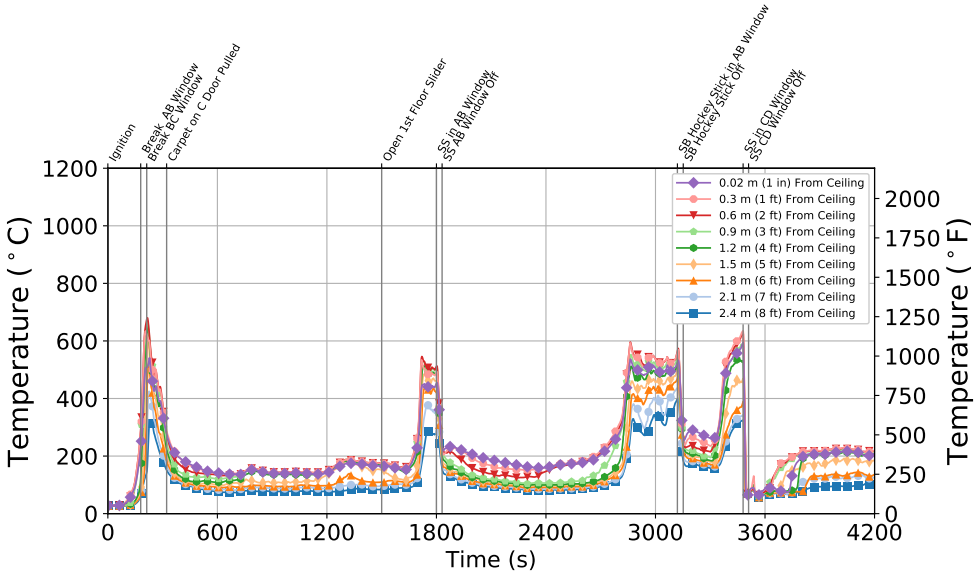

Figure B.85: Experiment 6 - Thermocouple temperature time histories from the Quadrant C thermocouple array in the basement.

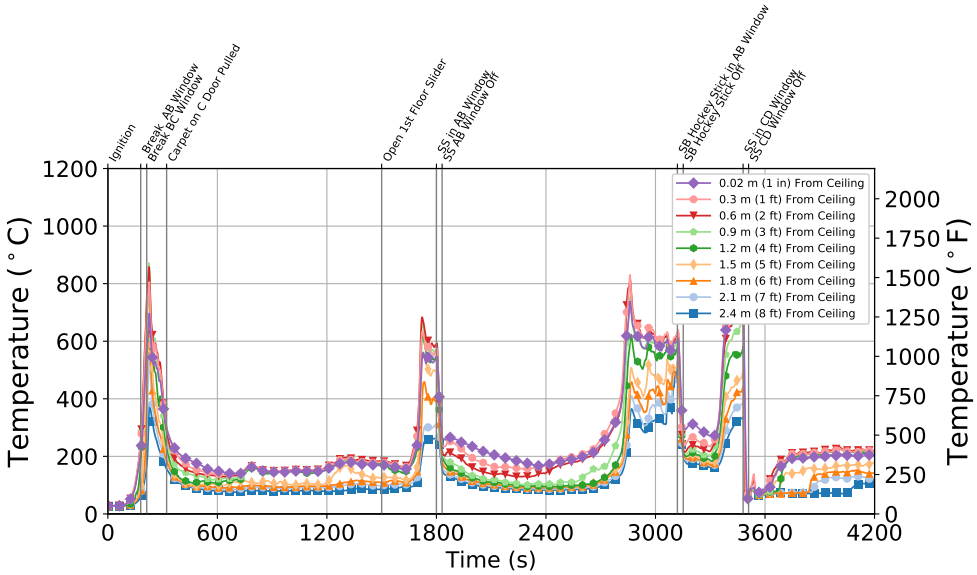

Figure B.86: Experiment 6 - Thermocouple temperature time histories from the Quadrant D thermocouple array in the basement.

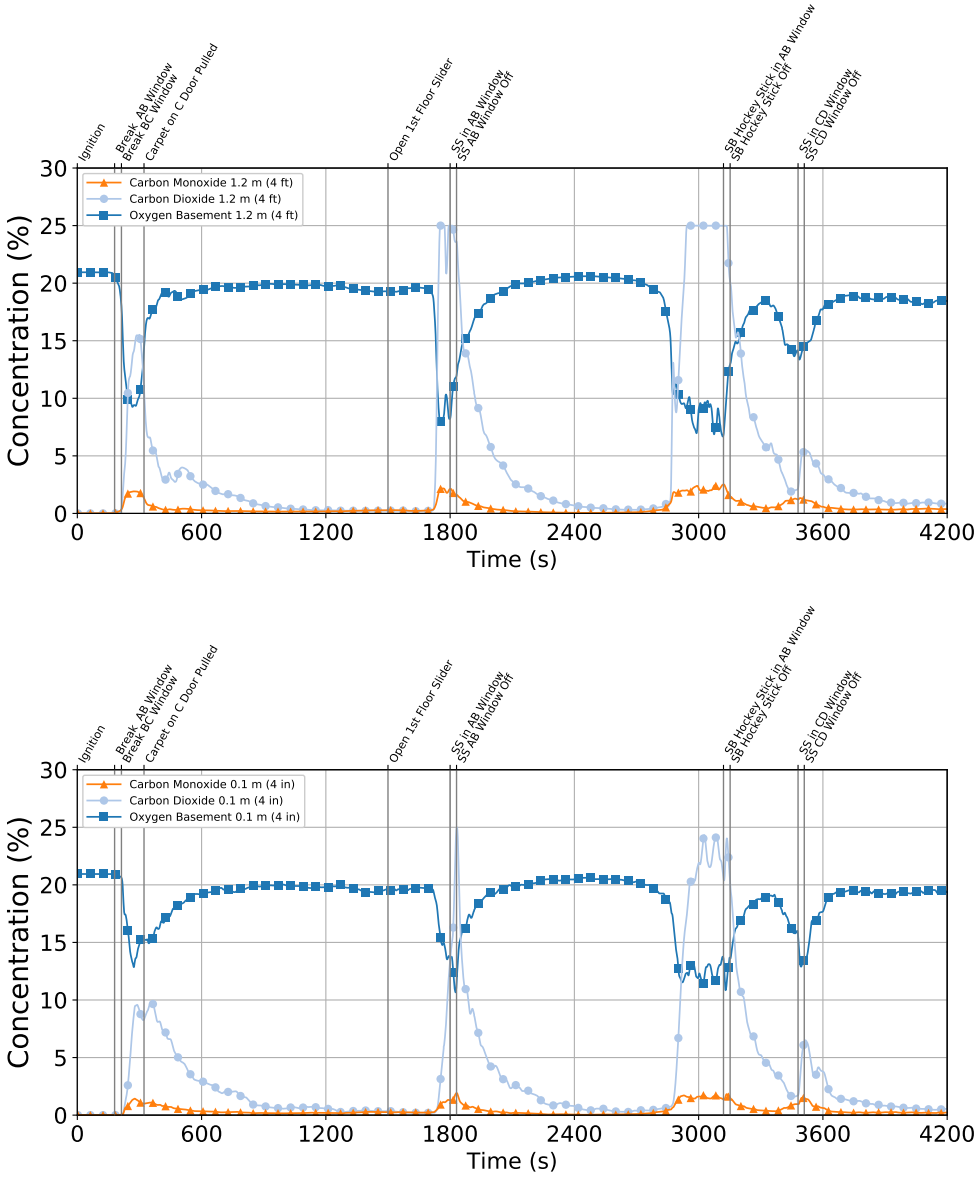

Figure B.87: Experiment 6 - Gas concentration time histories from the 1.2 m (4 ft) (top) and 0.1 m (4 in.) (bottom) elevations in the basement.

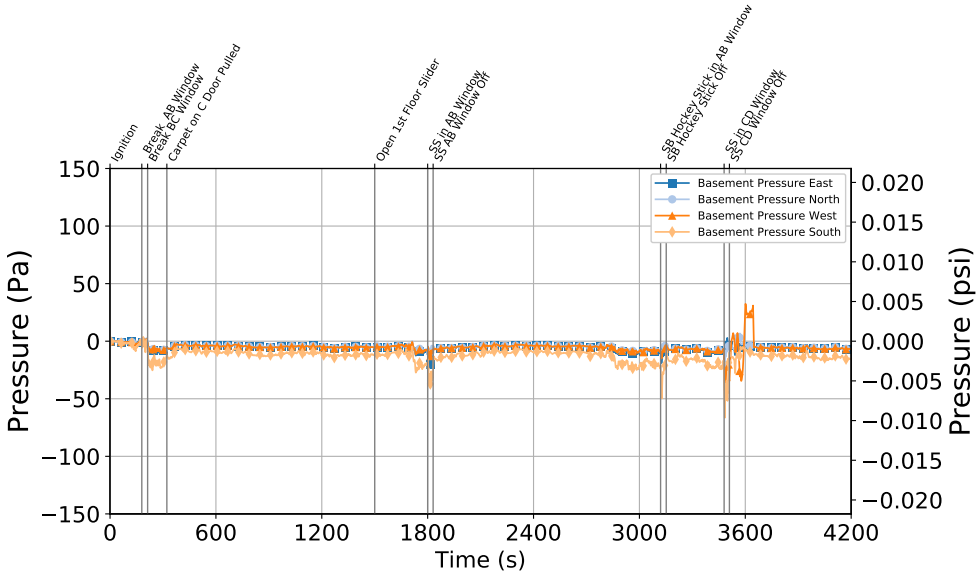

Figure B.88: Experiment 6 - Basement Pressure at 6 locations 1.2 m (4 ft) Above the Floor

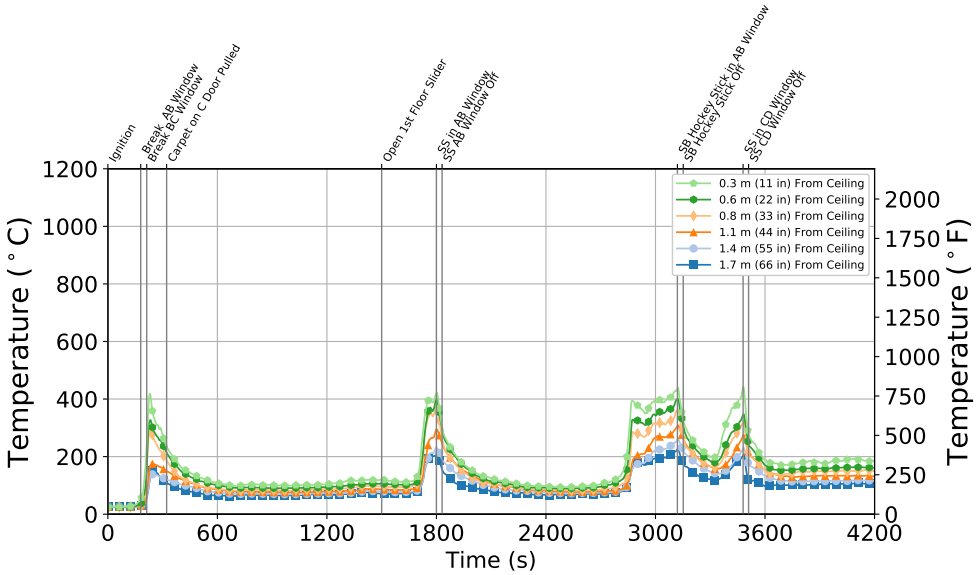

Figure B.89: Experiment 6 - Stair Thermocouple Temperature at Basement Level

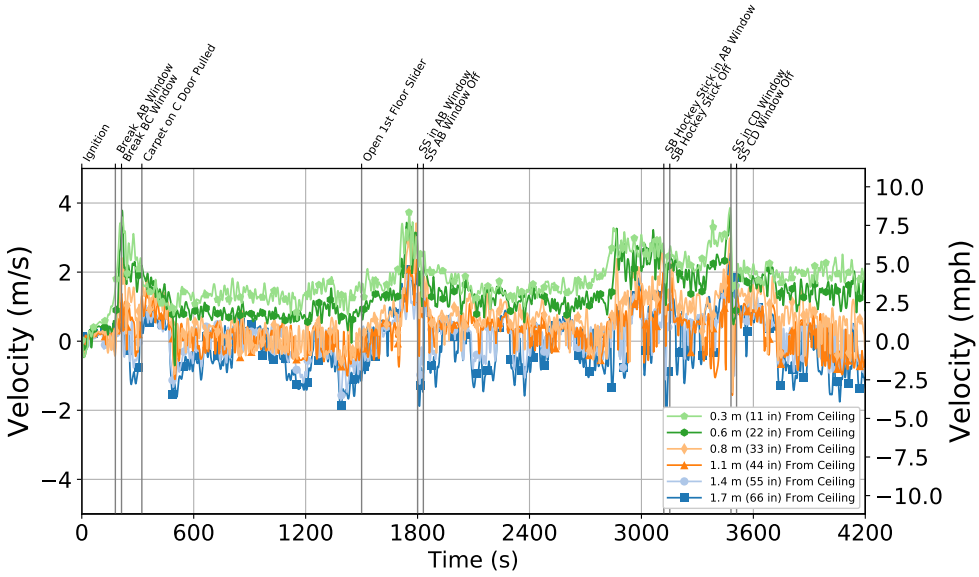

Figure B.90: Experiment 6 - Stair Velocity at Basement Level

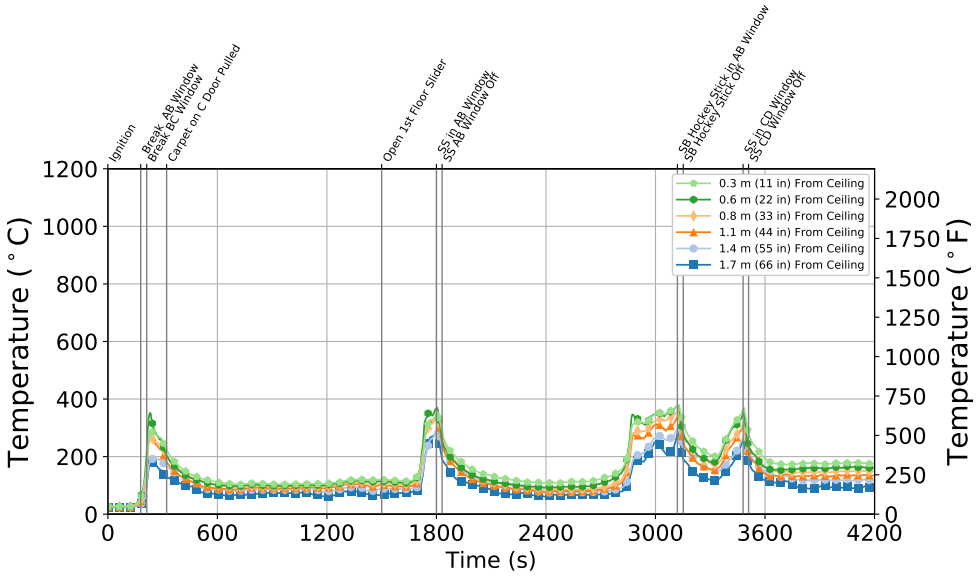

Figure B.91: Experiment 6 - Stair Thermocouple Temperature at First Floor

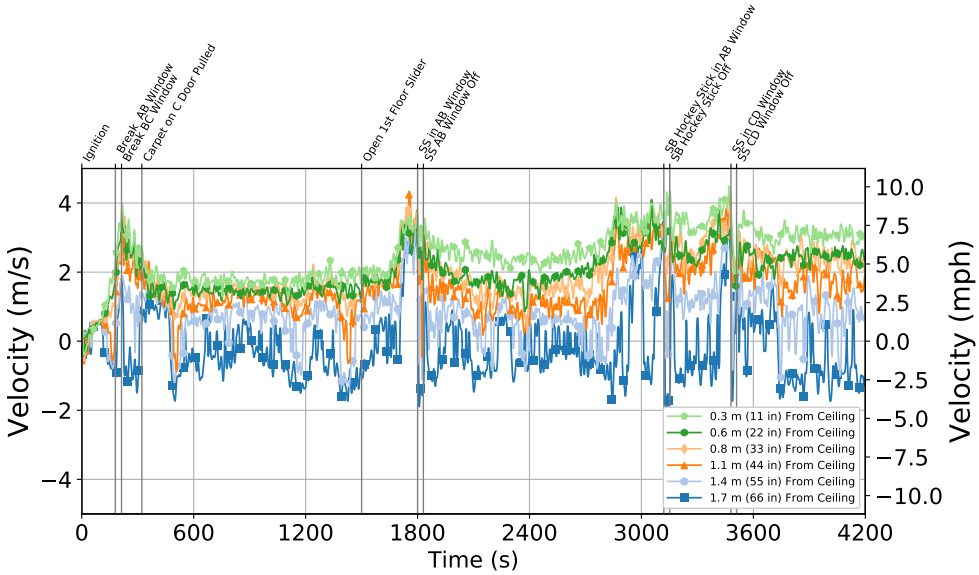

Figure B.92: Stair Velocity at First Floor

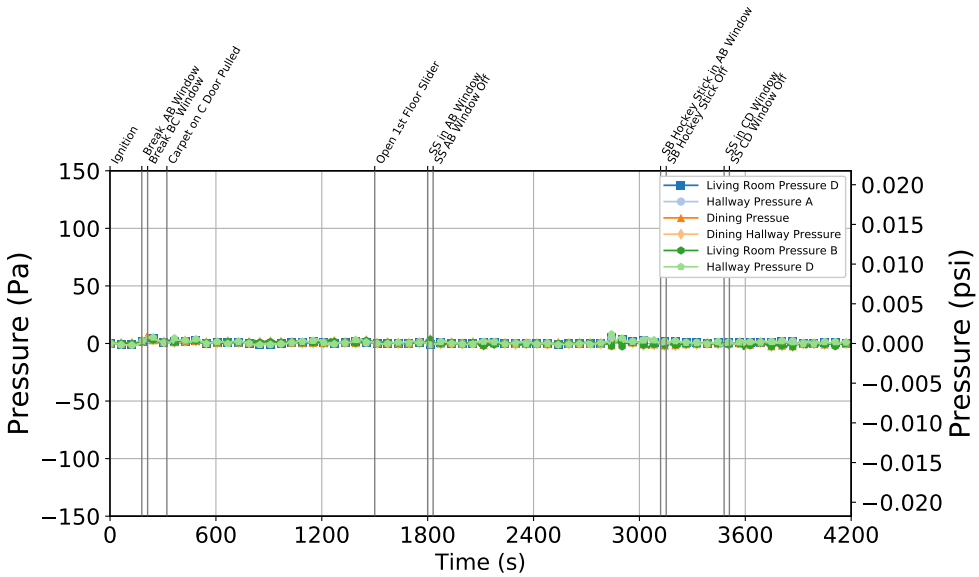

Figure B.93: Experiment 6 - First Floor Pressure at 6 locations 1.2 m (4 ft) Above the Floor

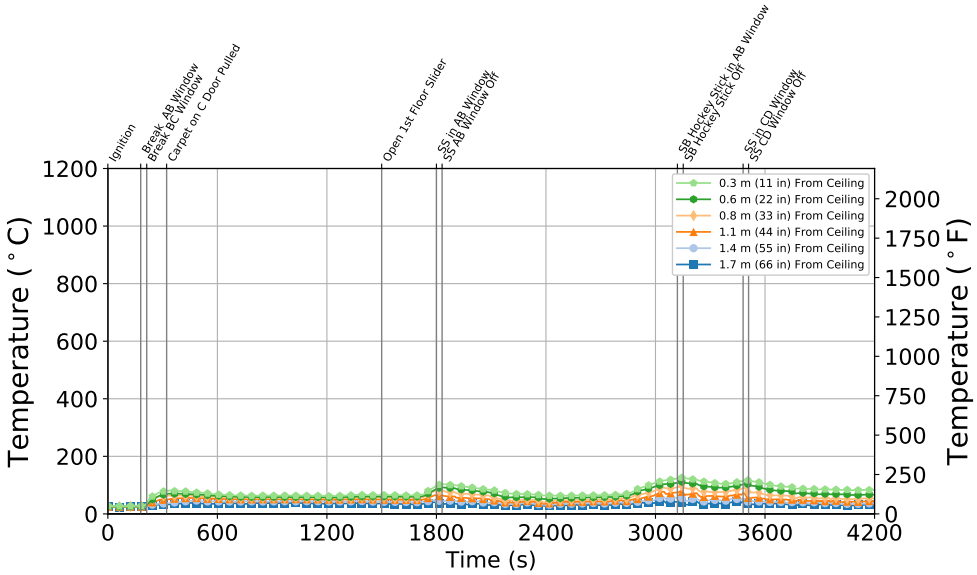

Figure B.94: Experiment 6 - Front Door Thermocouple Temperature at First Floor

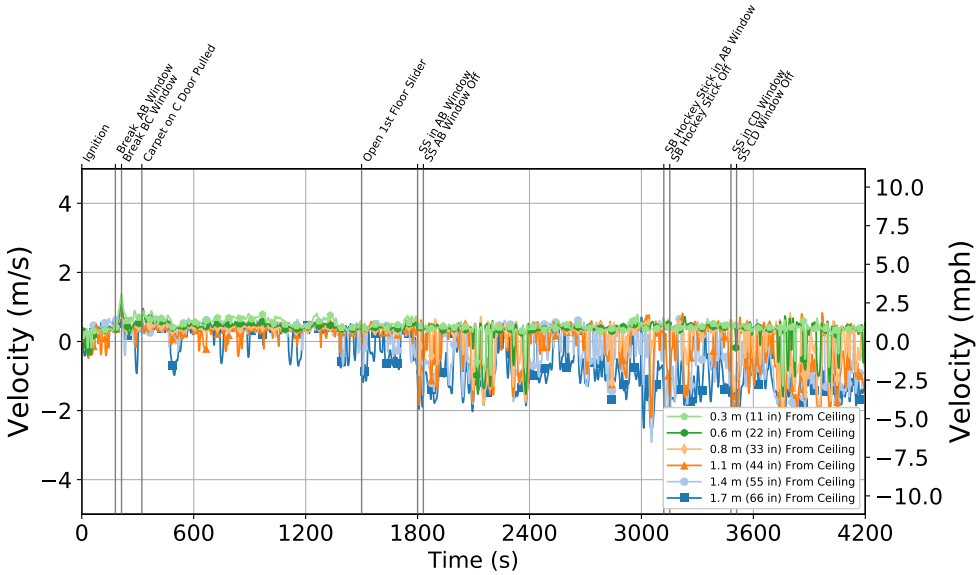

Figure B.95: Experiment 6 - Front Door Velocity at First Floor

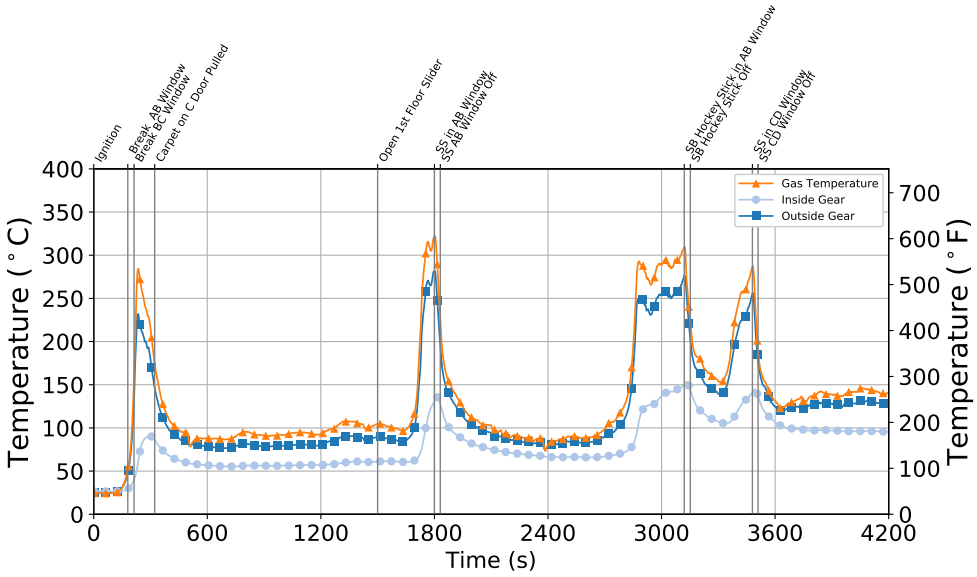

Figure B.96: Experiment 6 - Thermocouple Temperature on Inside and Outside of PPE Sample

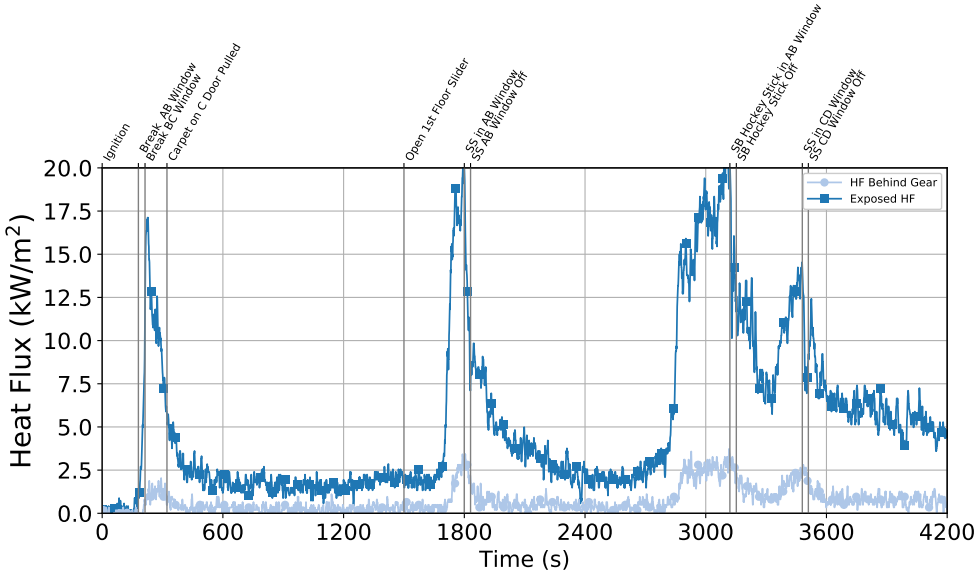

Figure B.97: Experiment 6 - Comparison of Heat Flux between Exposed Sensor and Protected Sensor

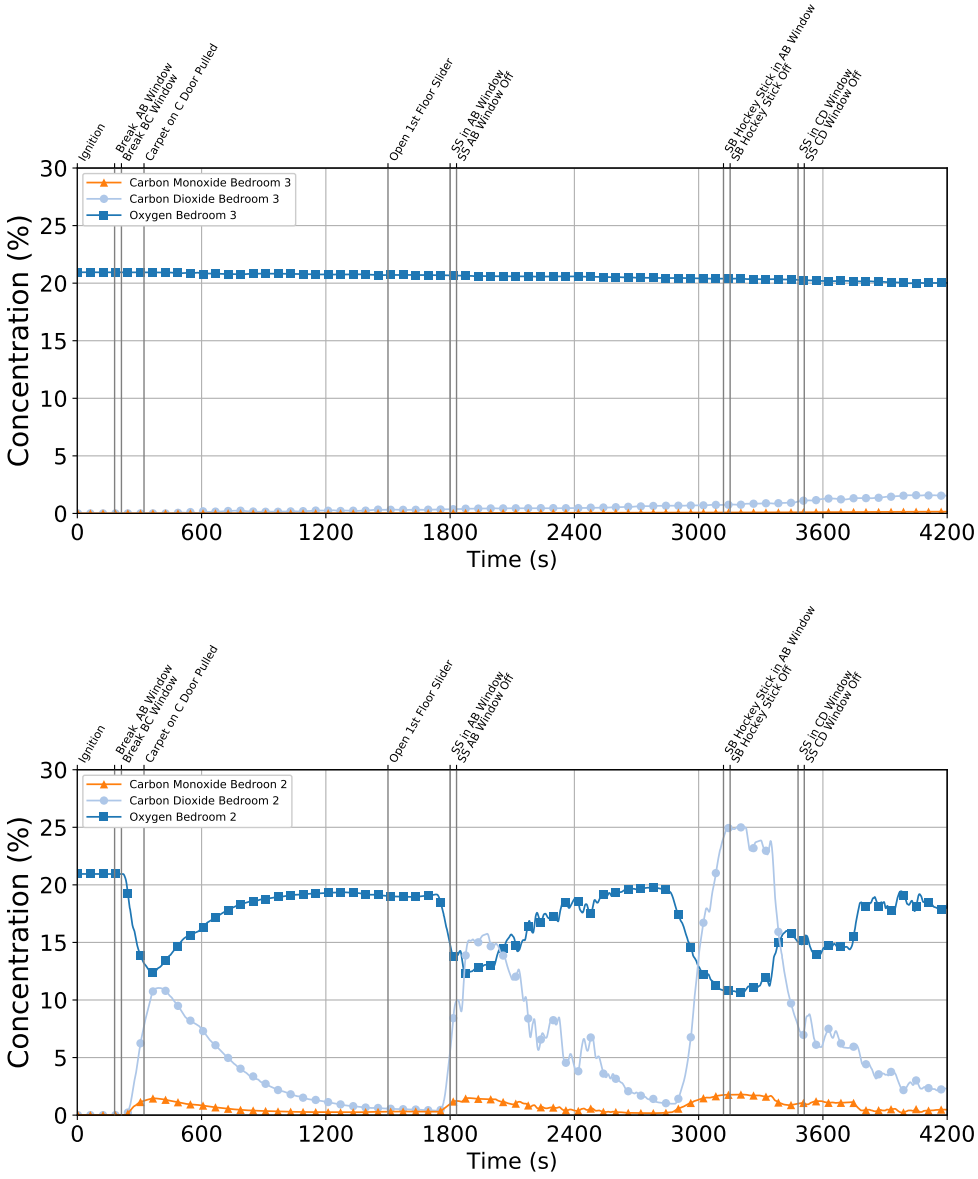

Figure B.98: Experiment 6 - Gas concentration time histories from the closed bedroom at 1.2 m (4 ft) (top) and from the open bedroom at 1.2 m (4 ft) (bottom).

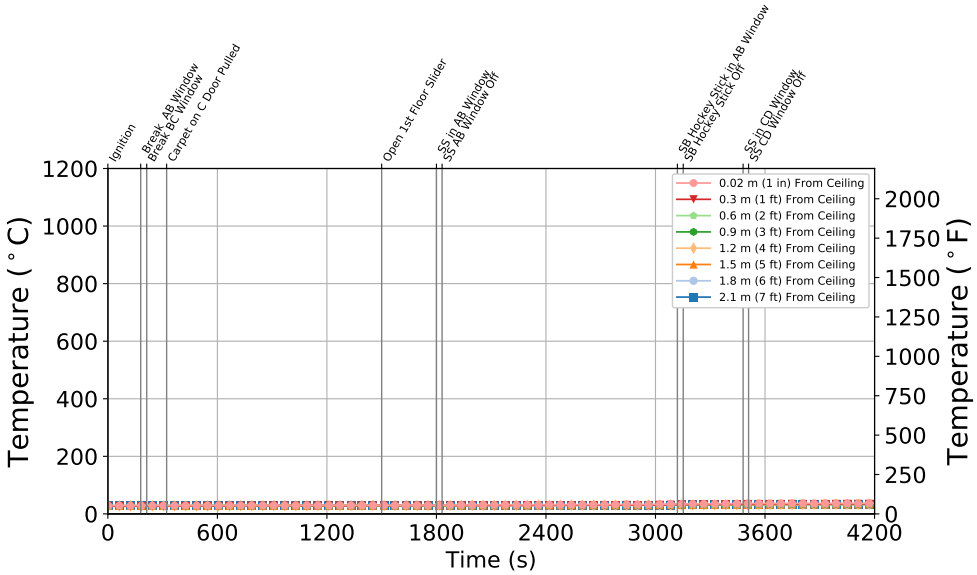

Figure B.99: Experiment 6 - Bedroom 3 (Closed) Bedroom

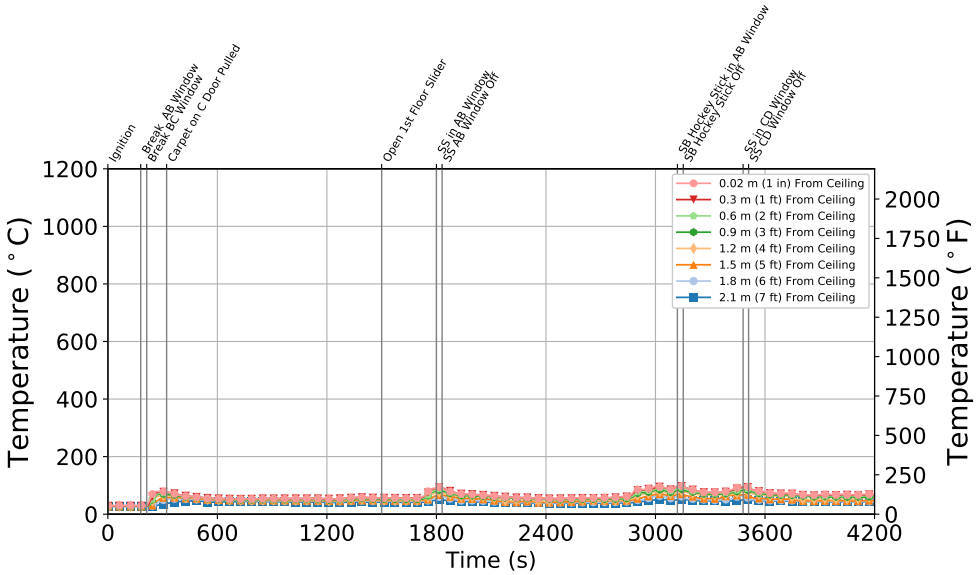

Figure B.100: Experiment 6 - Bedroom 2 (Open) Bedroom

B.7 Experiment 7

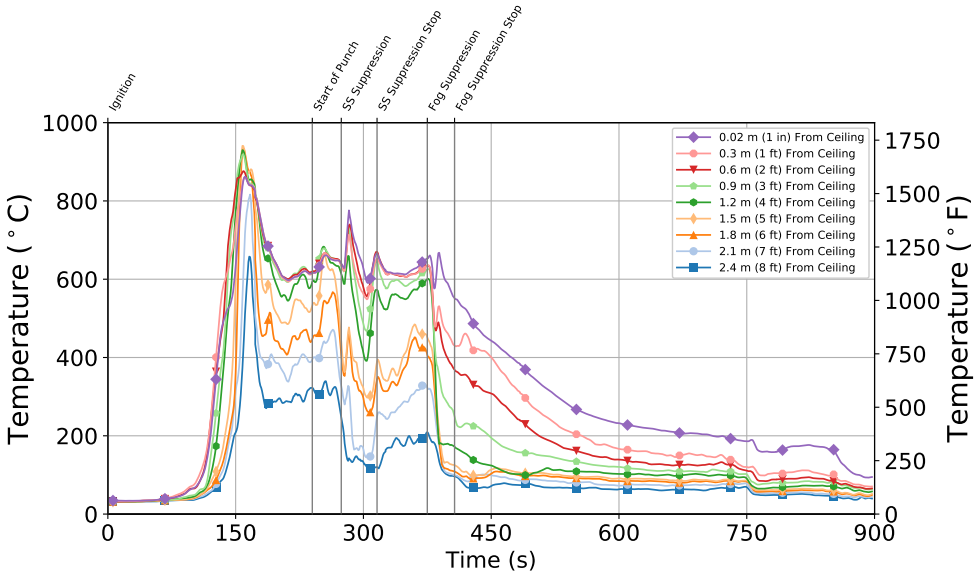

Figure B.101: Experiment 7 - Thermocouple temperature time histories from the Quadrant A thermocouple array in the basement.

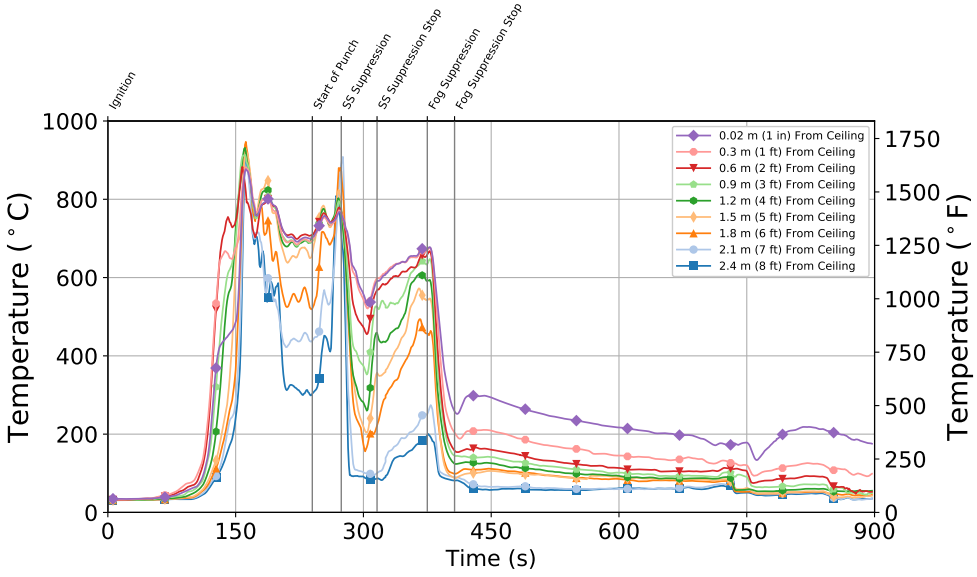

Figure B.102: Experiment 7 - Thermocouple temperature time histories from the Quadrant B thermocouple array in the basement.

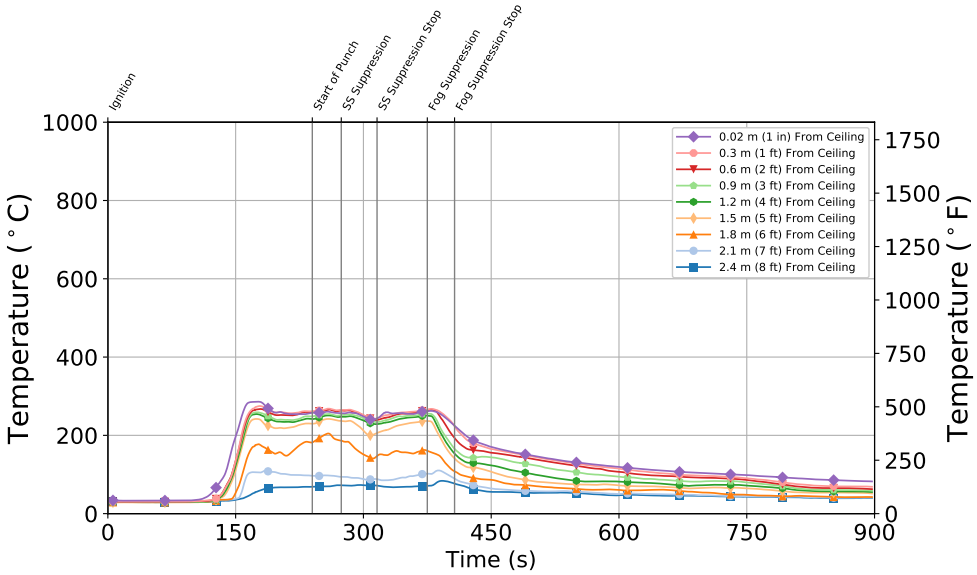

Figure B.103: Experiment 7 - Thermocouple temperature time histories from the Quadrant C thermocouple array in the basement.

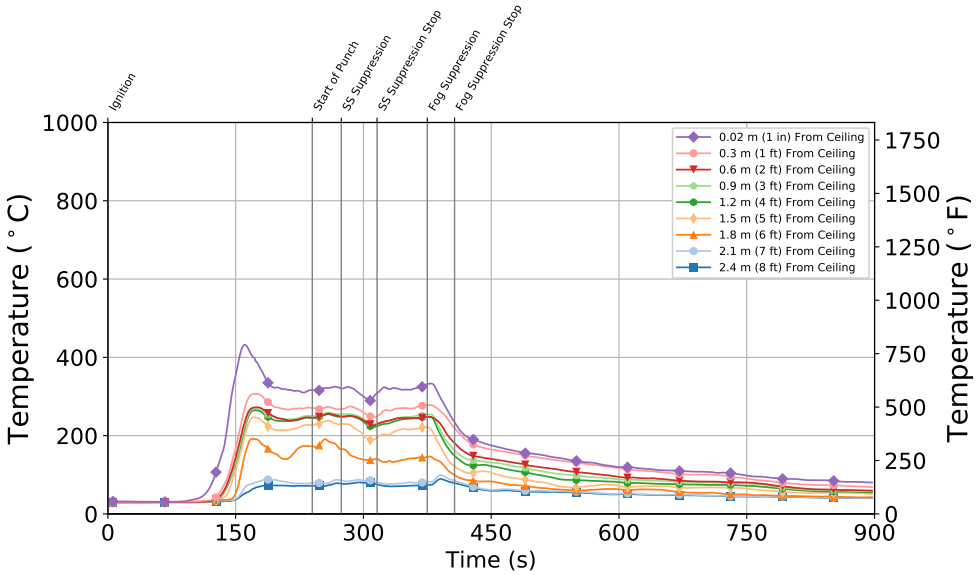

Figure B.104: Experiment 7 - Thermocouple temperature time histories from the Quadrant D thermocouple array in the basement.

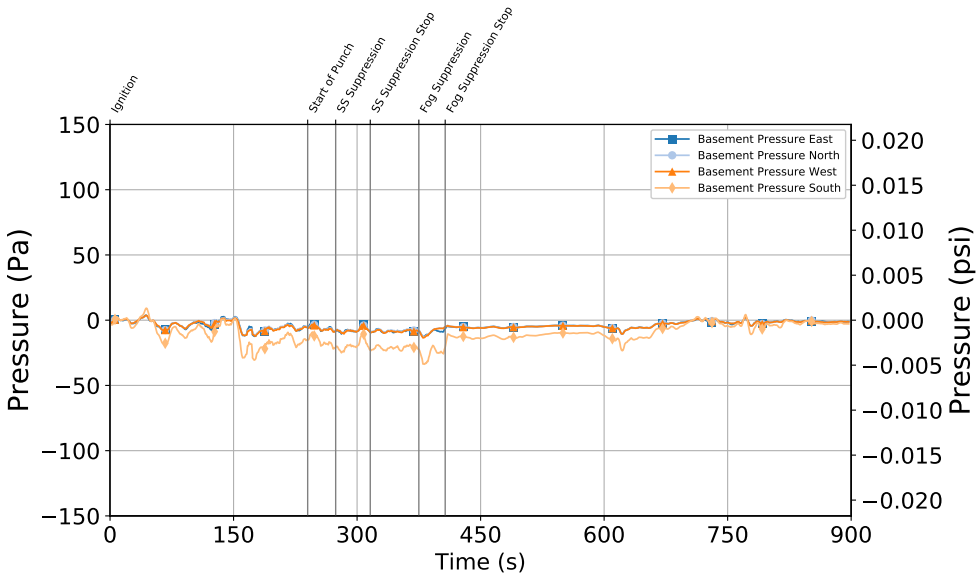

Figure B.105: Experiment 7 - Basement Pressure at 6 locations 1.2 m (4 ft) Above the Floor

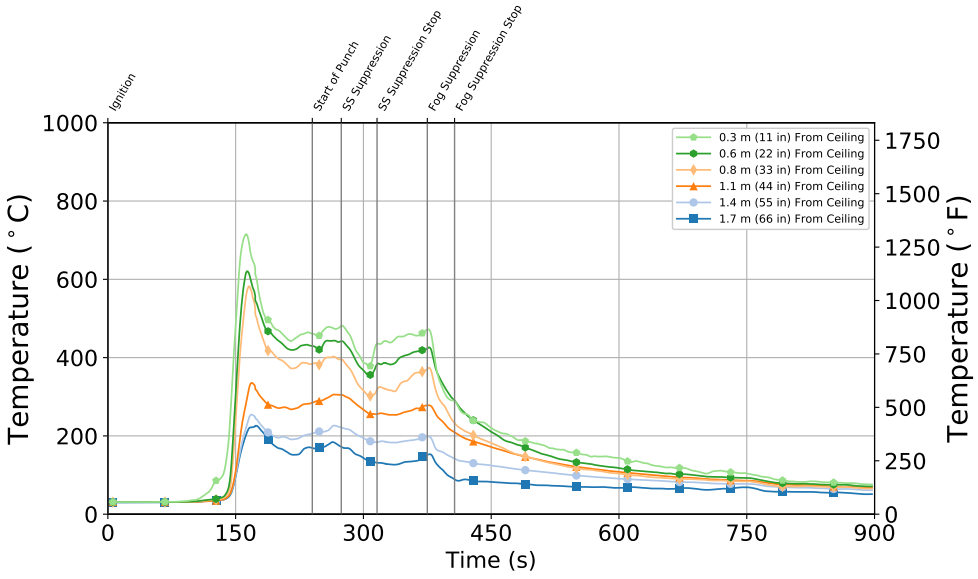

Figure B.106: Experiment 7 - Stair Thermocouple Temperature at Basement Level

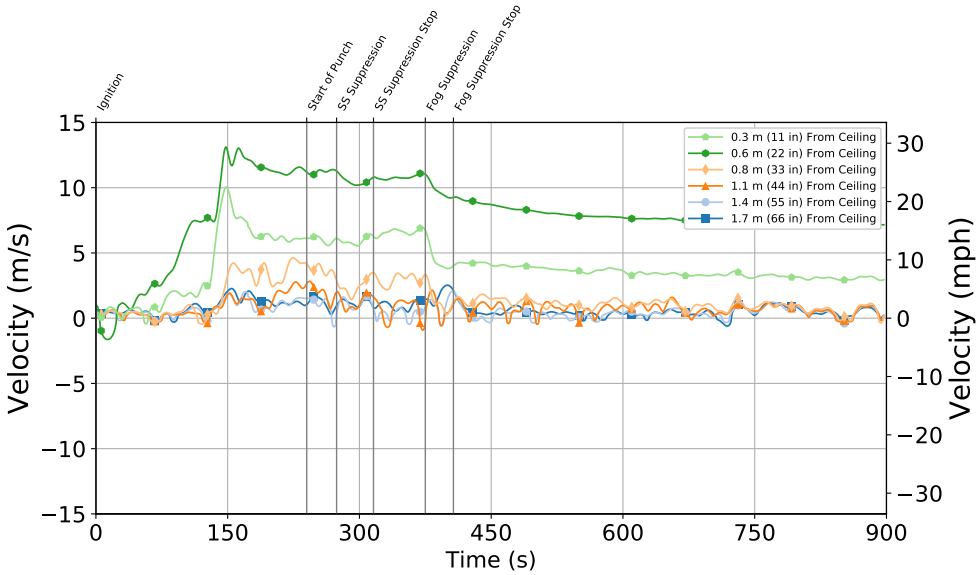

Figure B.107: Experiment 7 - Stair Velocity at Basement Level

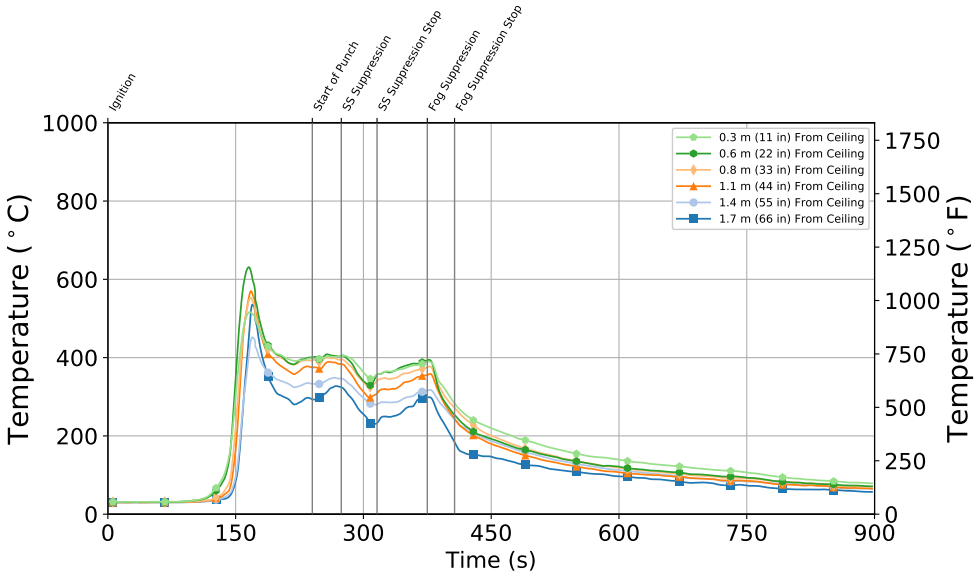

Figure B.108: Experiment 7 - Stair Thermocouple Temperature at First Floor

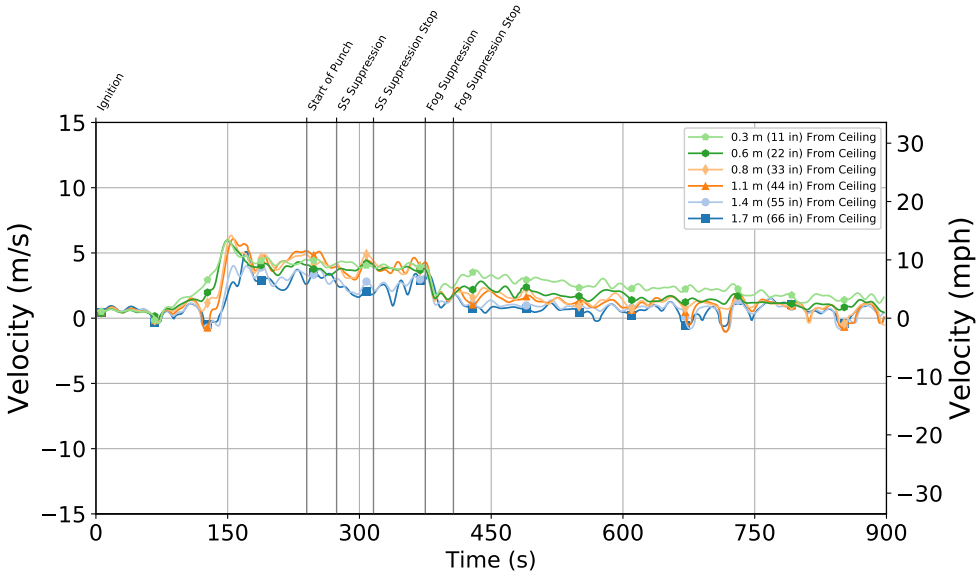

Figure B.109: Stair Velocity at First Floor

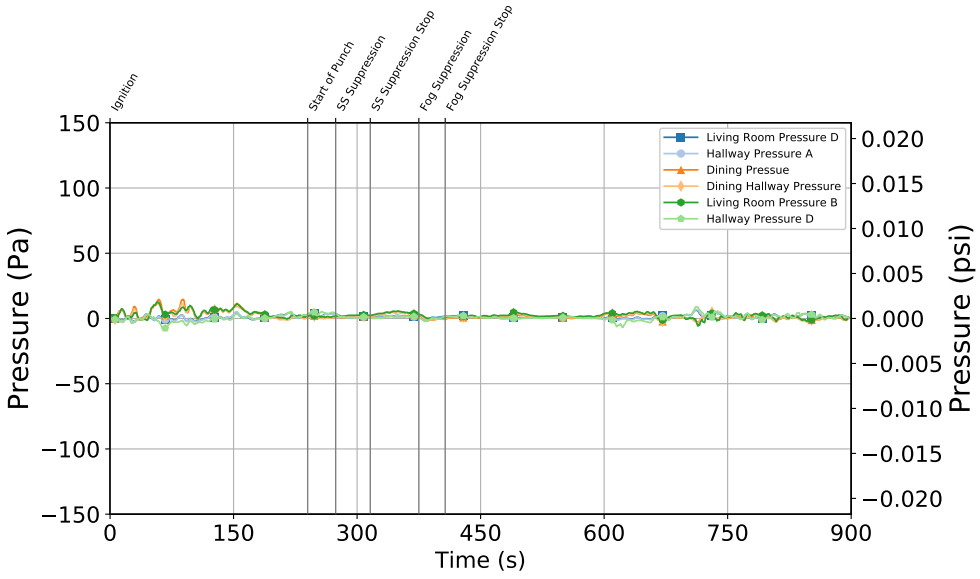

Figure B.110: Experiment 7 - First Floor Pressure at 6 locations 1.2 m (4 ft) Above the Floor

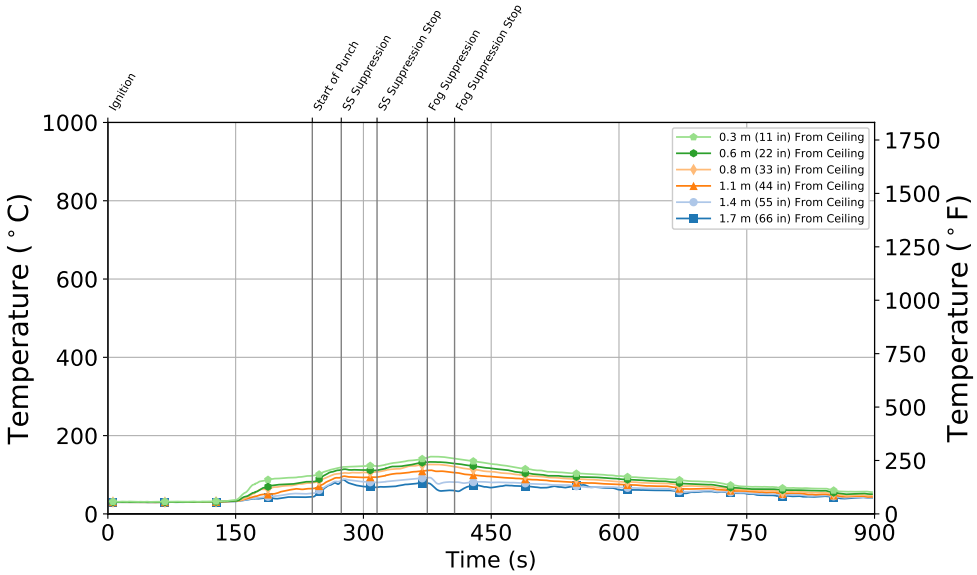

Figure B.111: Experiment 7 - Front Door Thermocouple Temperature at First Floor

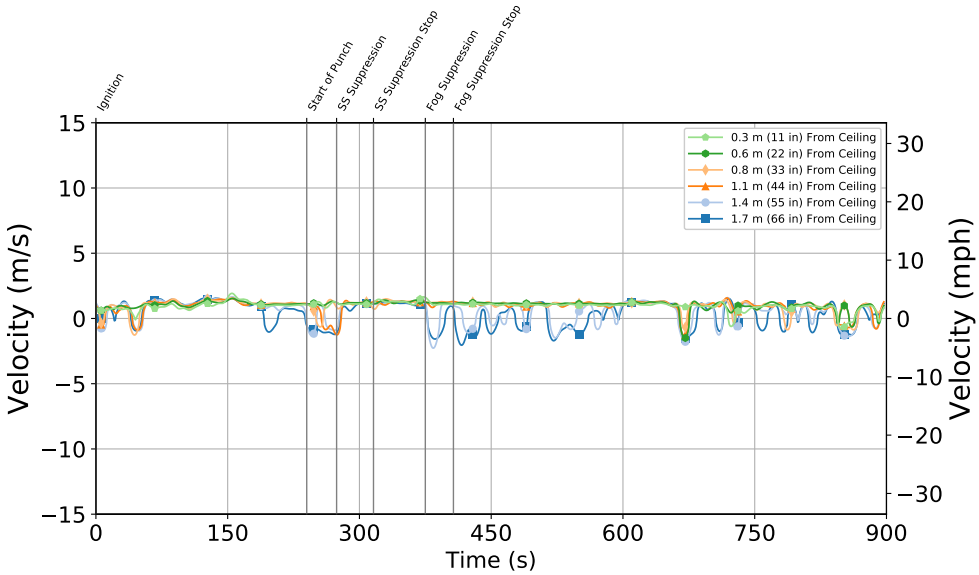

Figure B.112: Experiment 7 - Front Door Velocity at First Floor

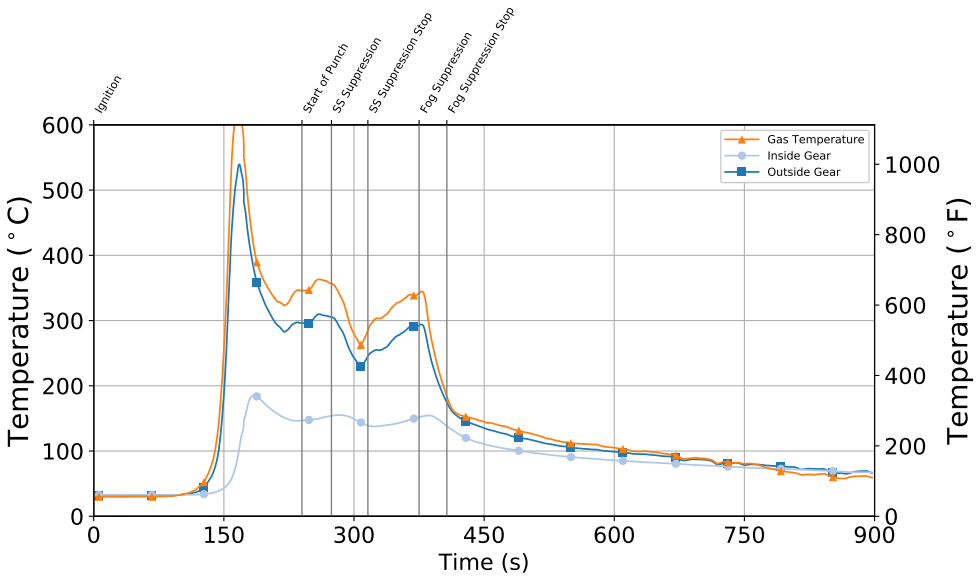

Figure B.113: Experiment 7 - Thermocouple Temperature on Inside and Outside of PPE Sample

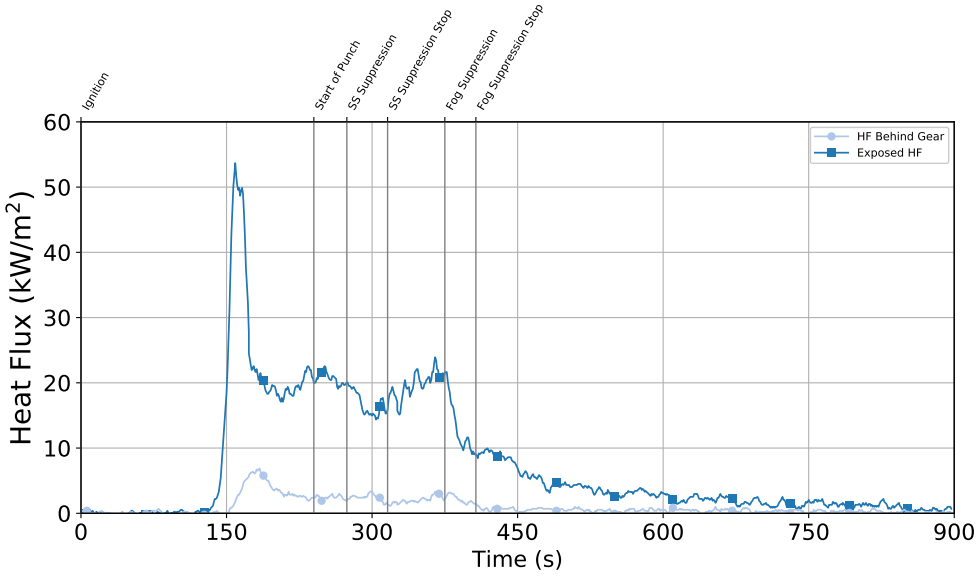

Figure B.114: Experiment 7 - Comparison of Heat Flux between Exposed Sensor and Protected Sensor

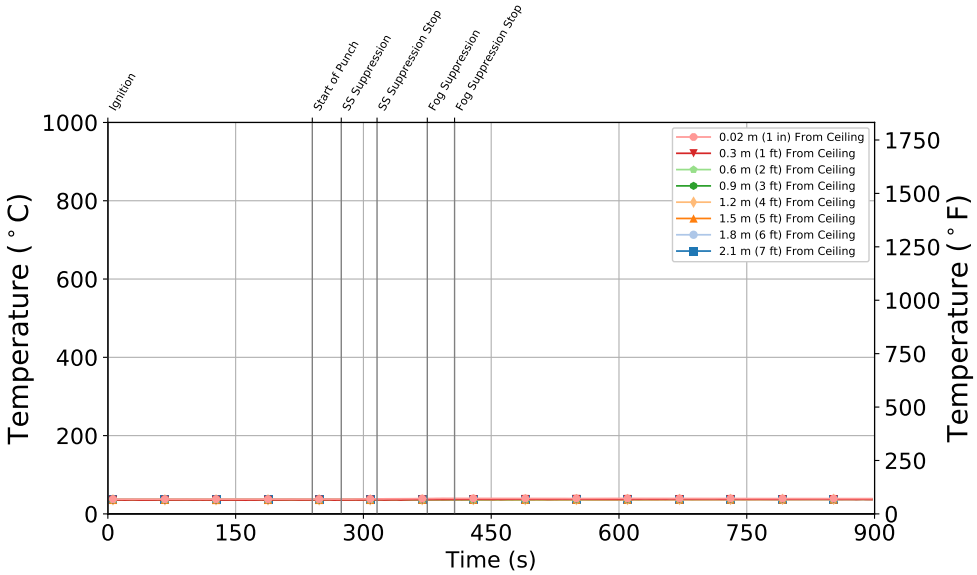

Figure B.115: Experiment 7 - Bedroom 3 (Closed) Bedroom

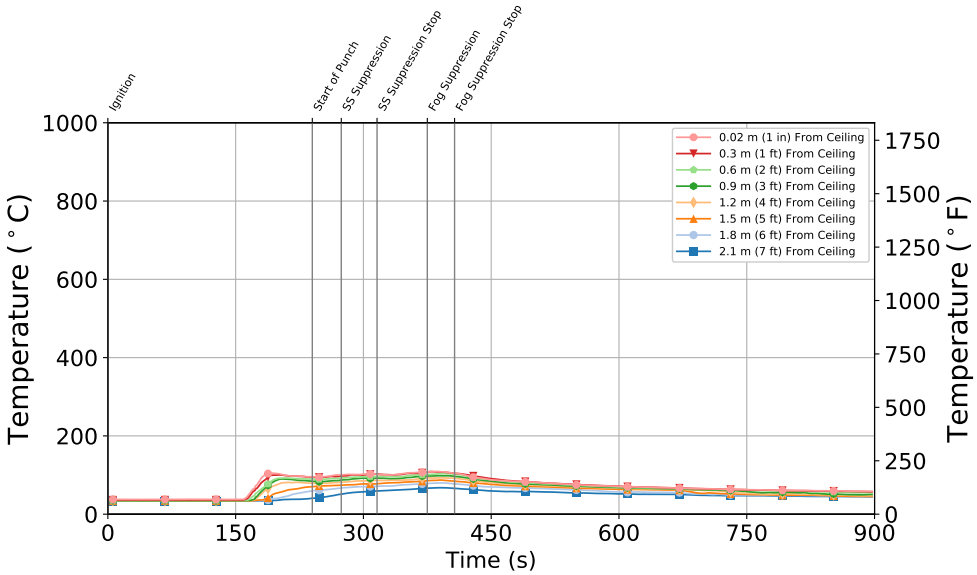

Figure B.116: Experiment 7 - Bedroom 2 (Open) Bedroom

B.8 Experiment 8

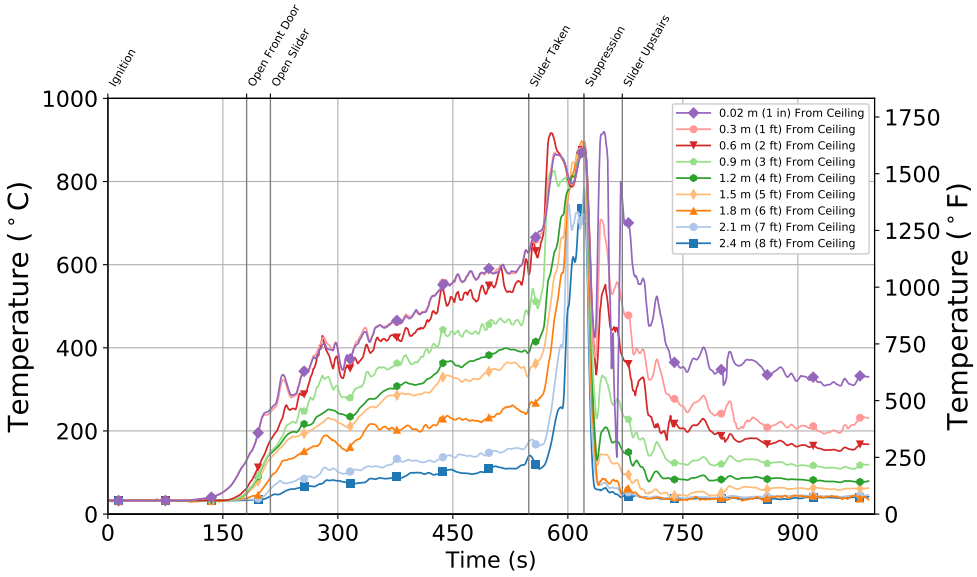

Figure B.117: Experiment 8 - Thermocouple temperature time histories from the Quadrant A thermocouple array in the basement.

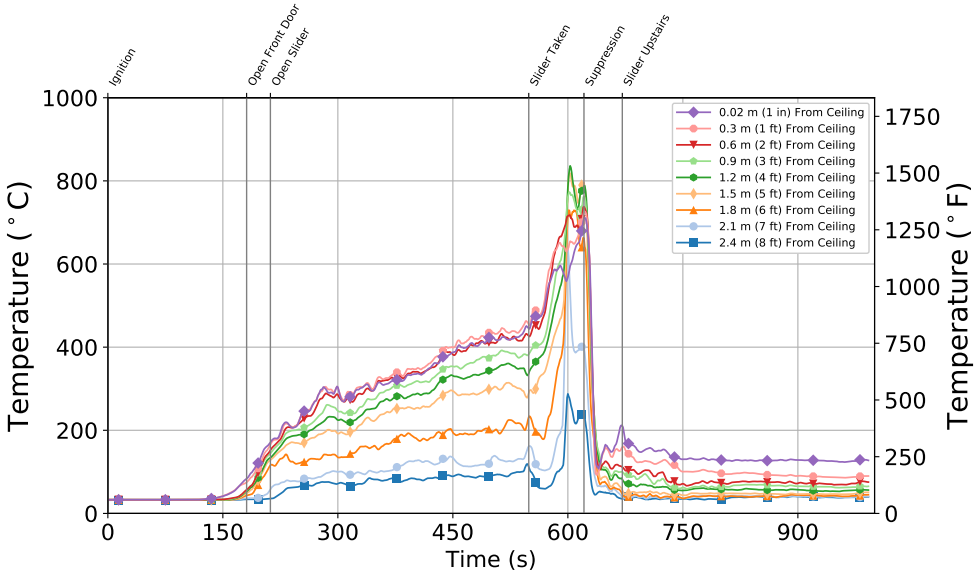

Figure B.118: Experiment 8 - Thermocouple temperature time histories from the Quadrant B thermocouple array in the basement.

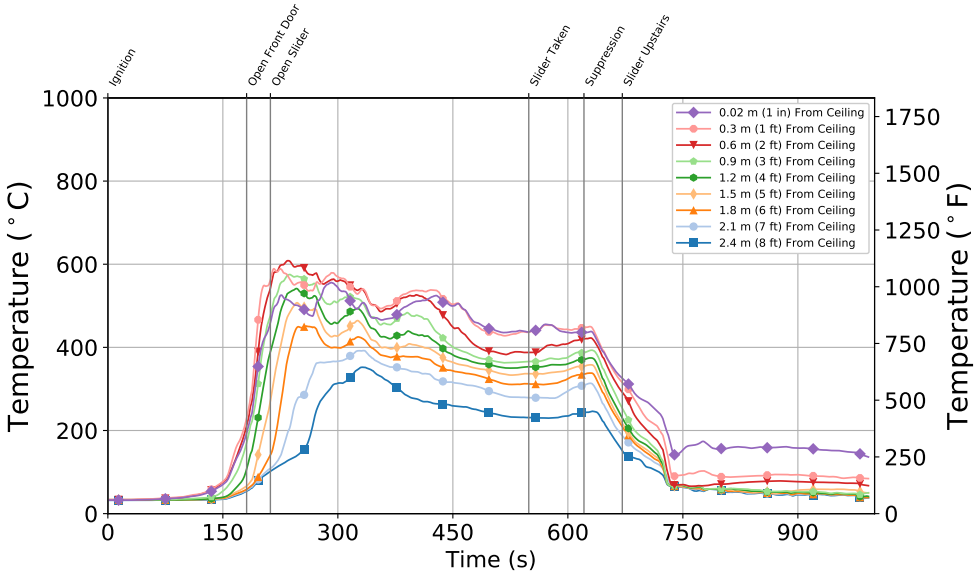

Figure B.119: Experiment 8 - Thermocouple temperature time histories from the Quadrant C thermocouple array in the basement.

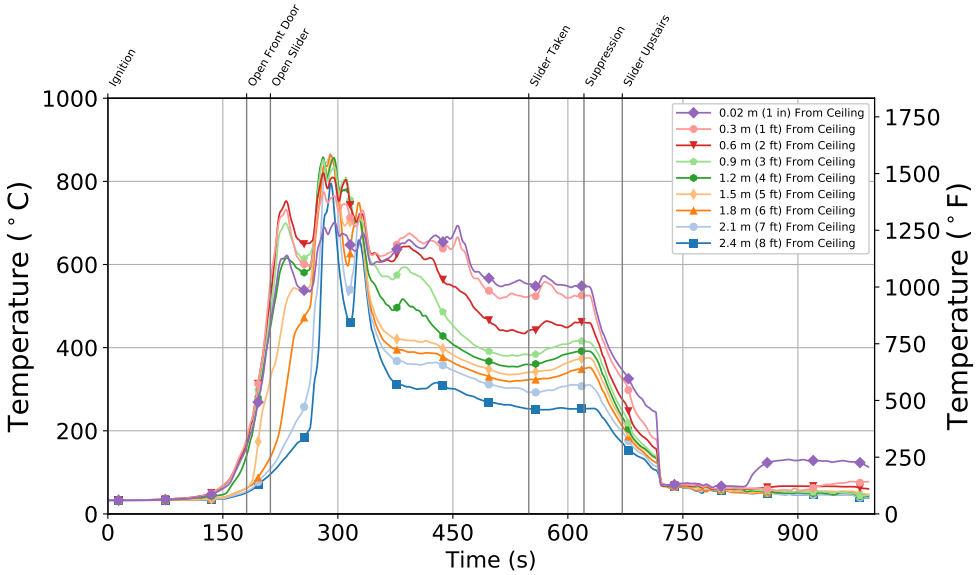

Figure B.120: Experiment 8 - Thermocouple temperature time histories from the Quadrant D thermocouple array in the basement.

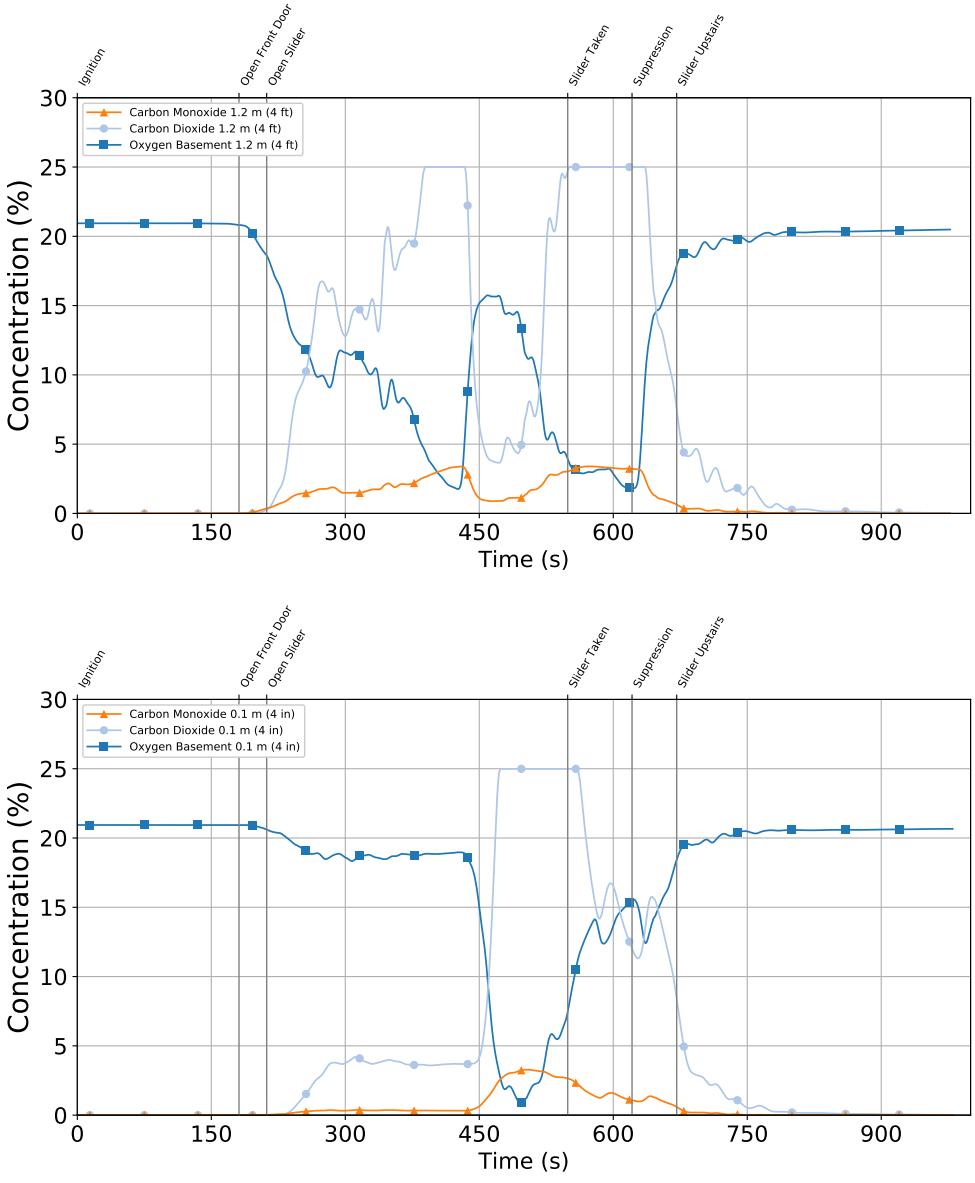

Figure B.121: Experiment 8 - Gas concentration time histories from the 1.2 m (4 ft) (top) and 0.1 m (4 in.) (bottom) elevations in the basement.

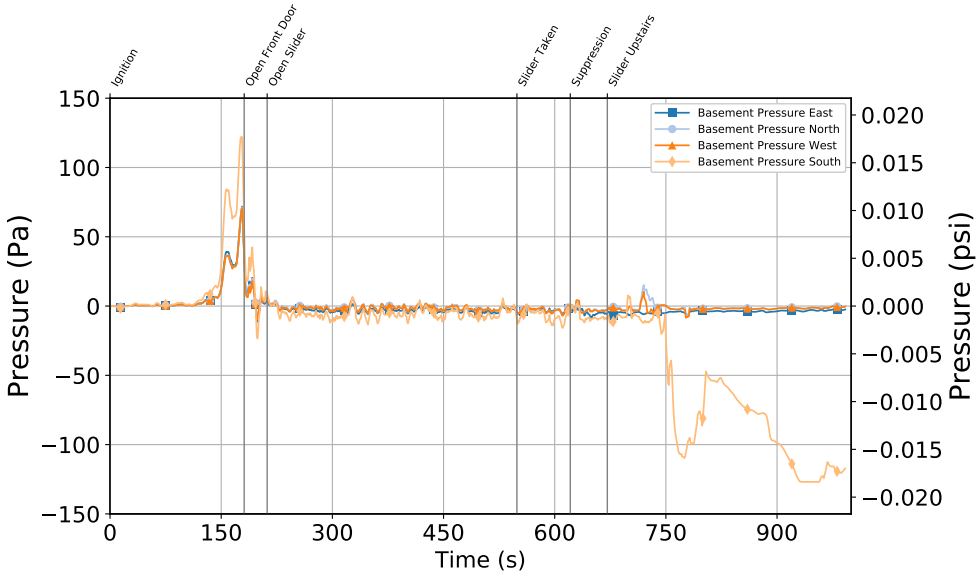

Figure B.122: Experiment 8 - Basement Pressure at 6 locations 1.2 m (4 ft) Above the Floor

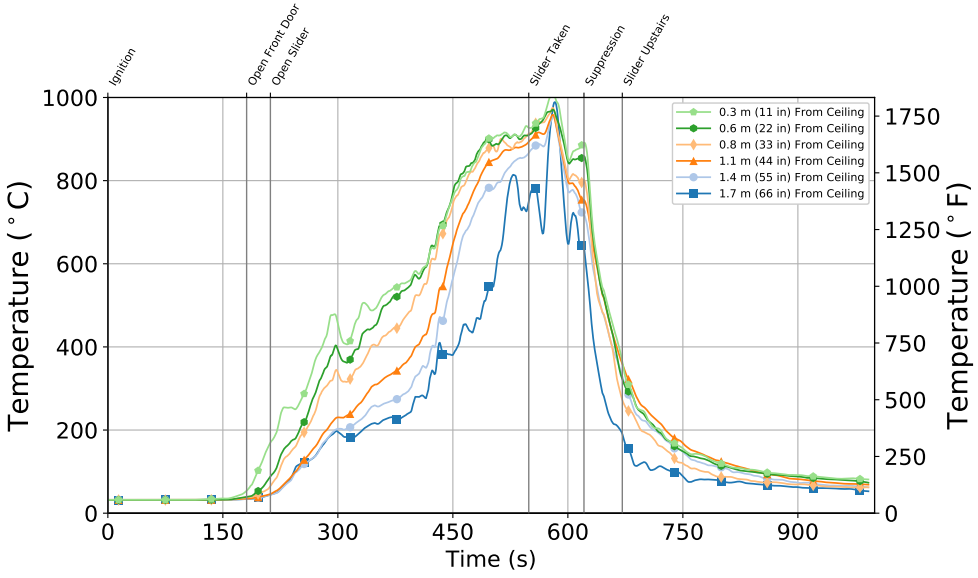

Figure B.123: Experiment 8 - Stair Thermocouple Temperature at Basement Level

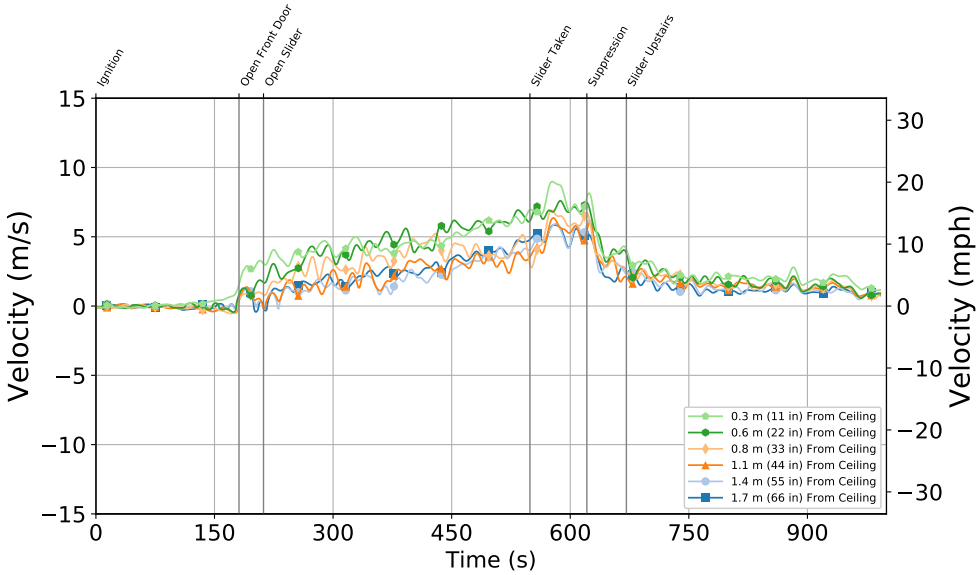

Figure B.124: Experiment 8 - Stair Velocity at Basement Level

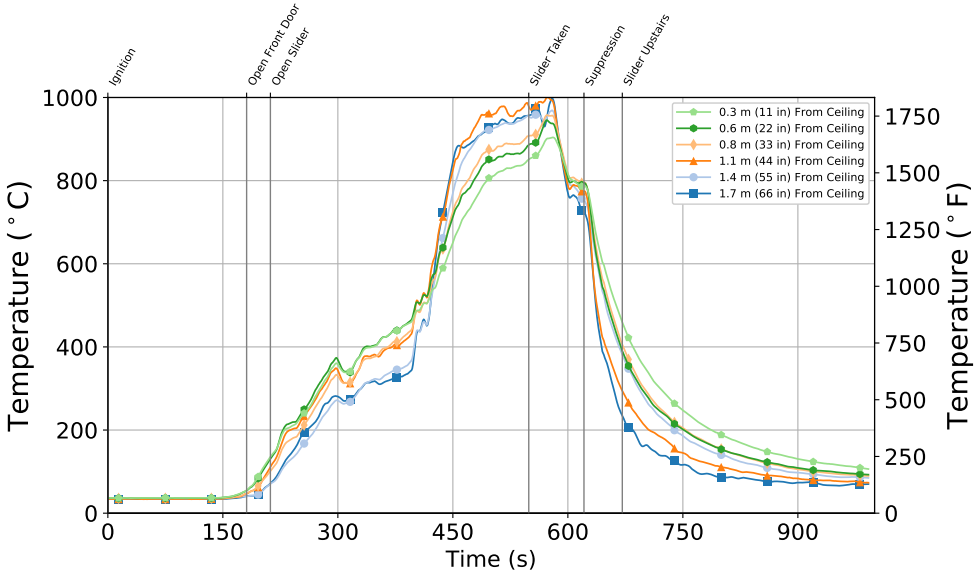

Figure B.125: Experiment 8 - Stair Thermocouple Temperature at First Floor

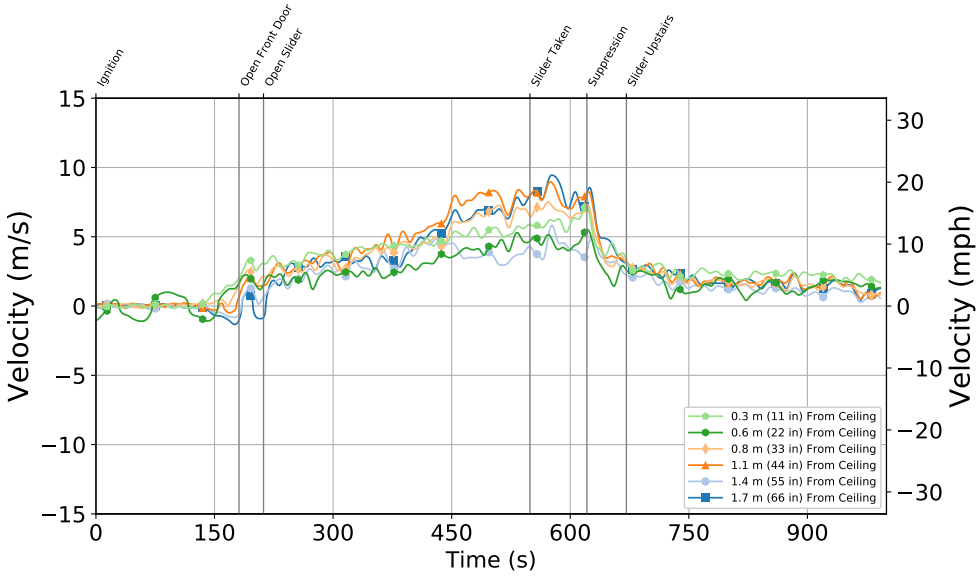

Figure B.126: Stair Velocity at First Floor

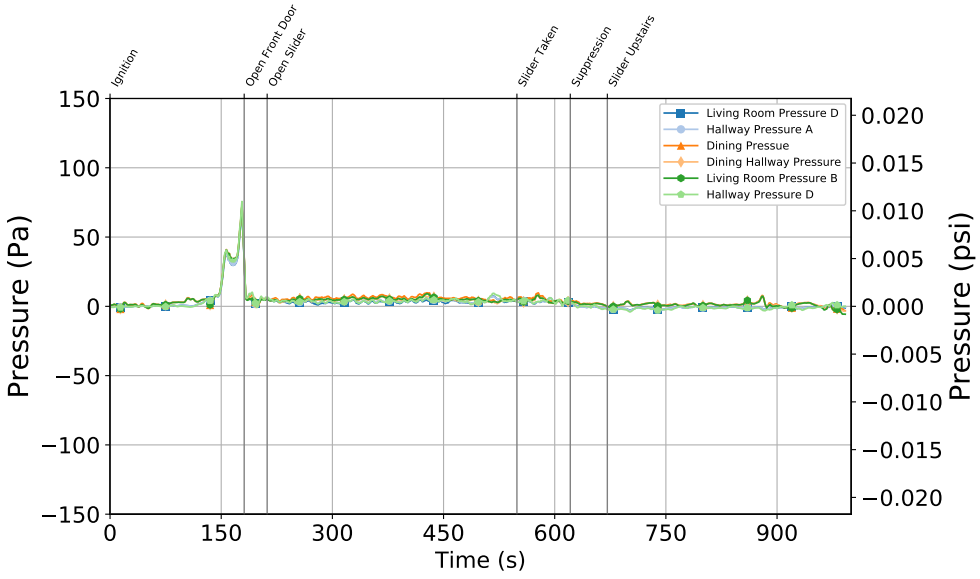

Figure B.127: Experiment 8 - First Floor Pressure at 6 locations 1.2 m (4 ft) Above the Floor

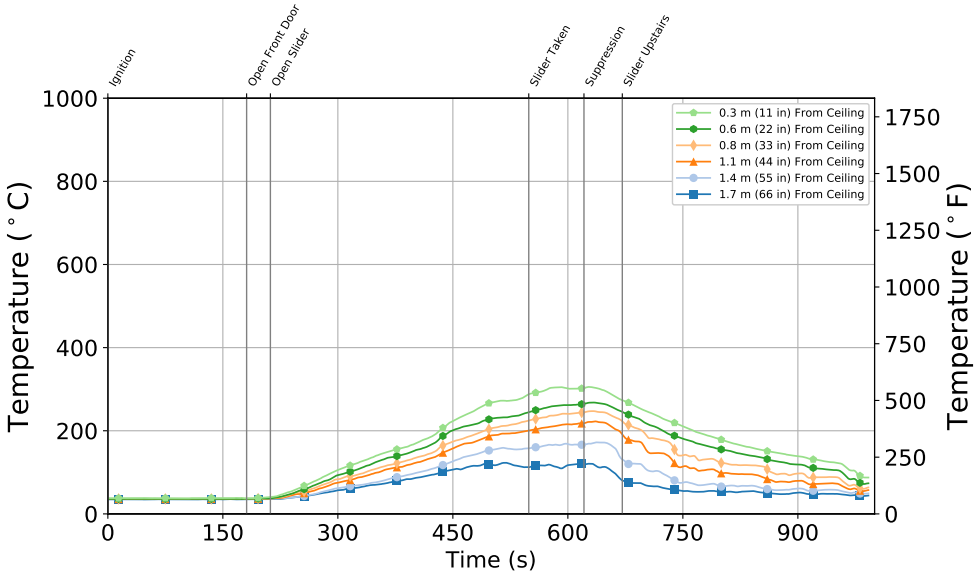

Figure B.128: Experiment 8 - Front Door Thermocouple Temperature at First Floor

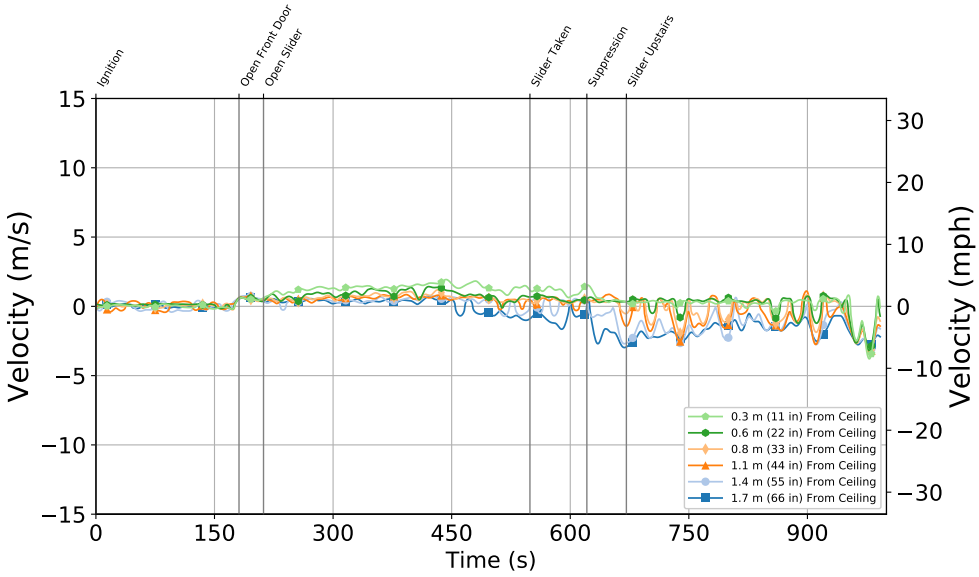

Figure B.129: Experiment 8 - Front Door Velocity at First Floor

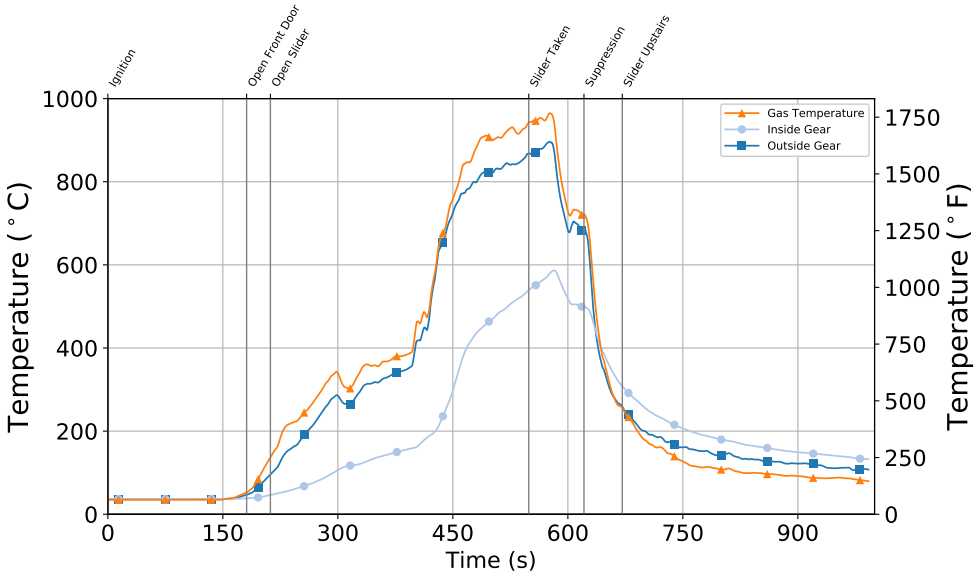

Figure B.130: Experiment 8 - Thermocouple Temperature on Inside and Outside of PPE Sample

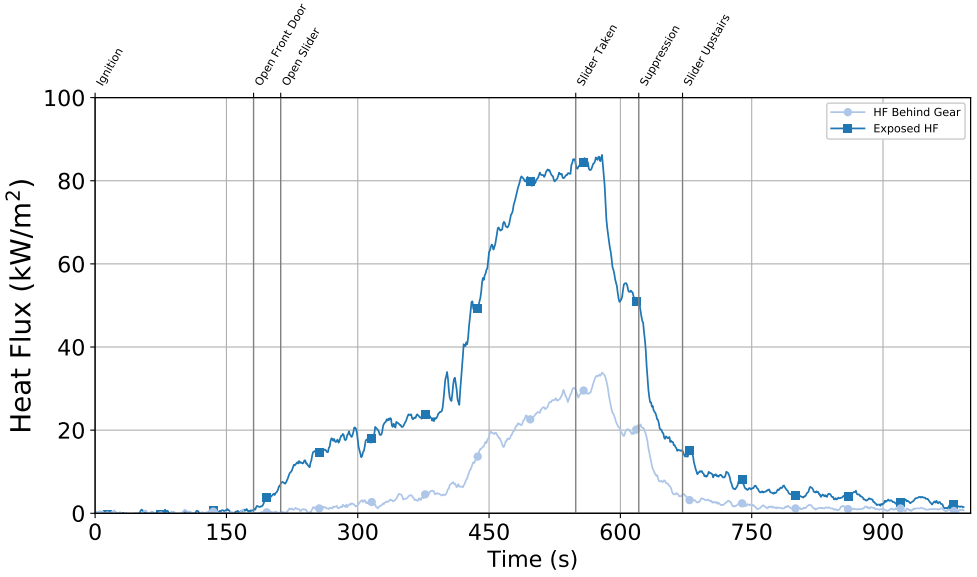

Figure B.131: Experiment 8 - Comparison of Heat Flux between Exposed Sensor and Protected Sensor

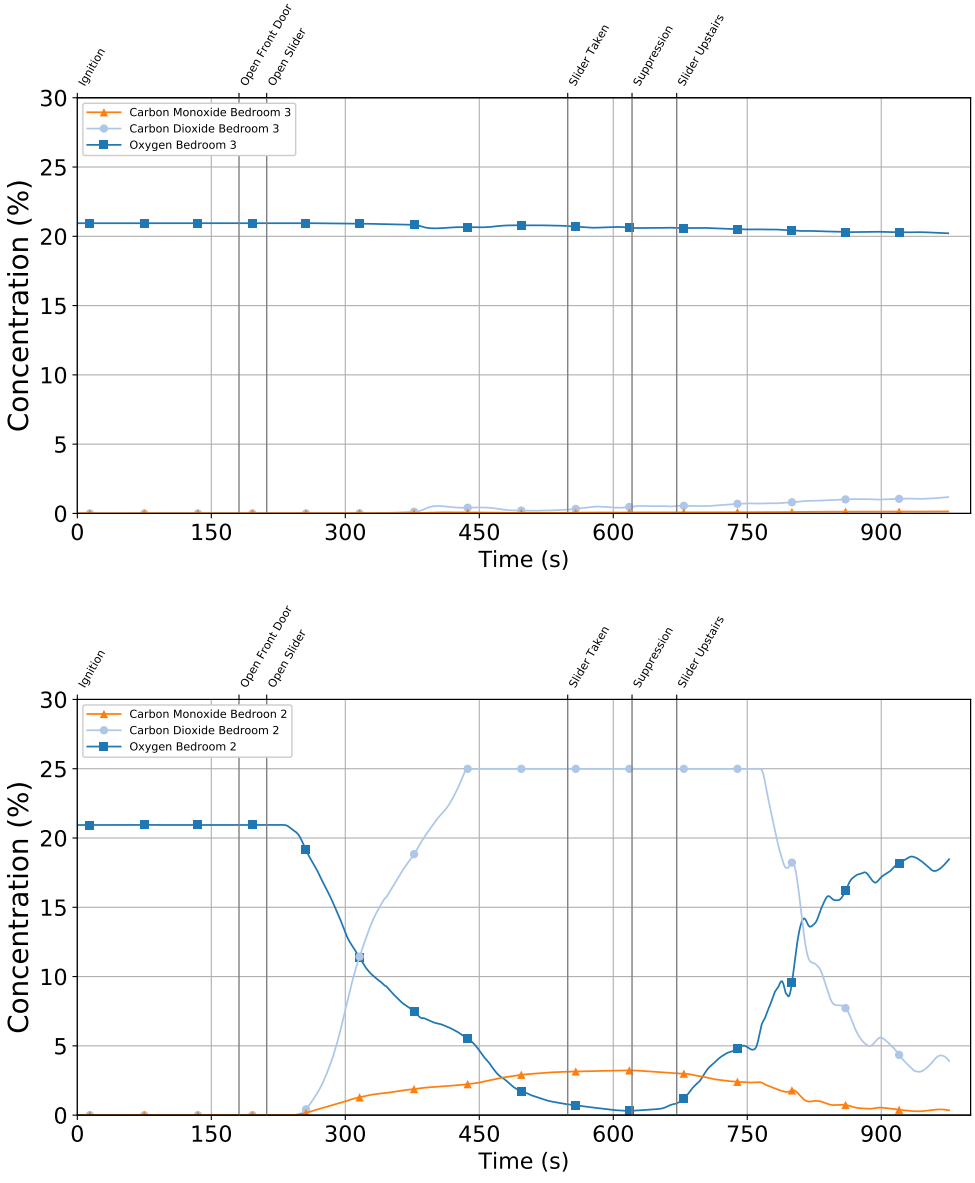

Figure B.132: Experiment 8 - Gas concentration time histories from the closed bedroom at 1.2 m (4 ft) (top) and from the open bedroom at 1.2 m (4 ft) (bottom).

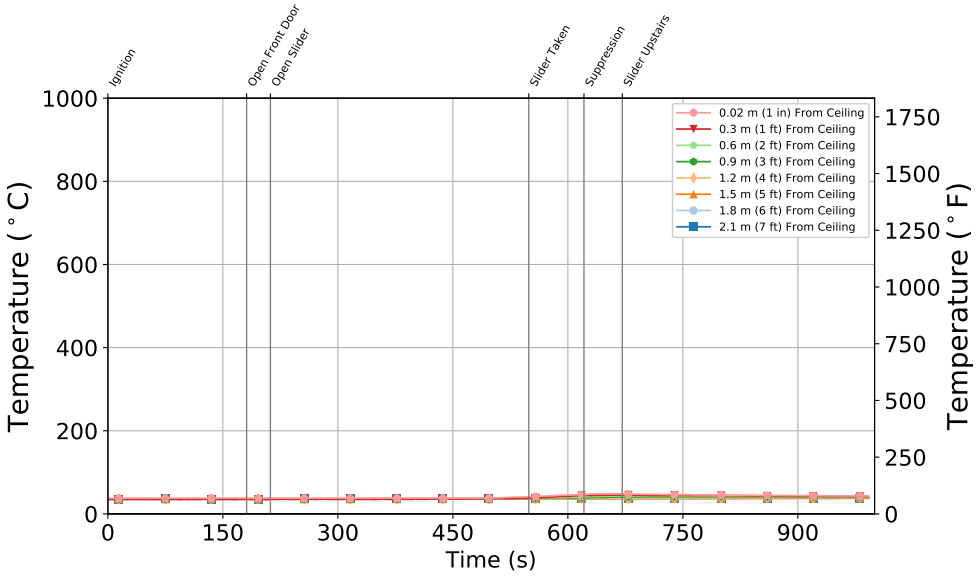

Figure B.133: Experiment 8 - Bedroom 3 (Closed) Bedroom

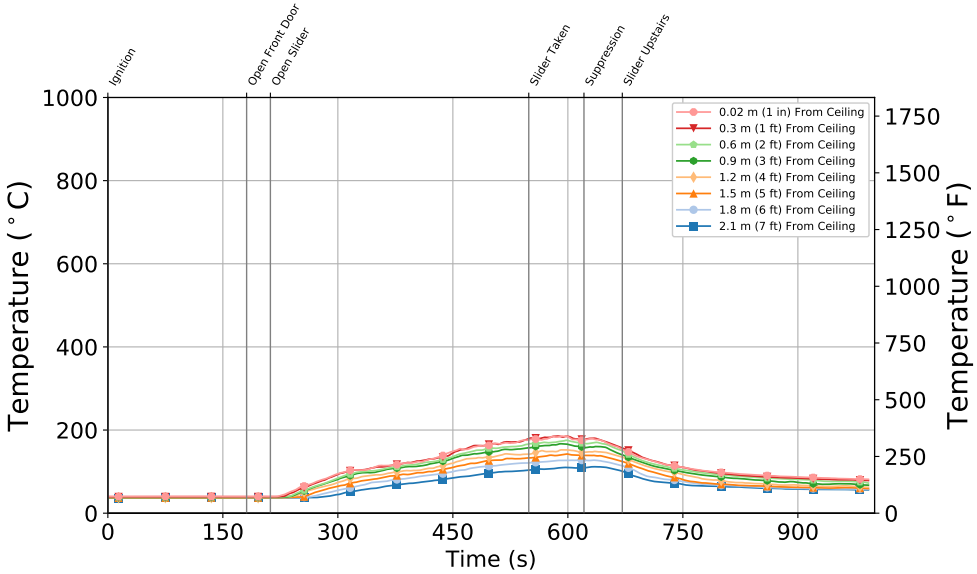

Figure B.134: Experiment 8 - Bedroom 2 (Open) Bedroom

B.9 Experiment 9

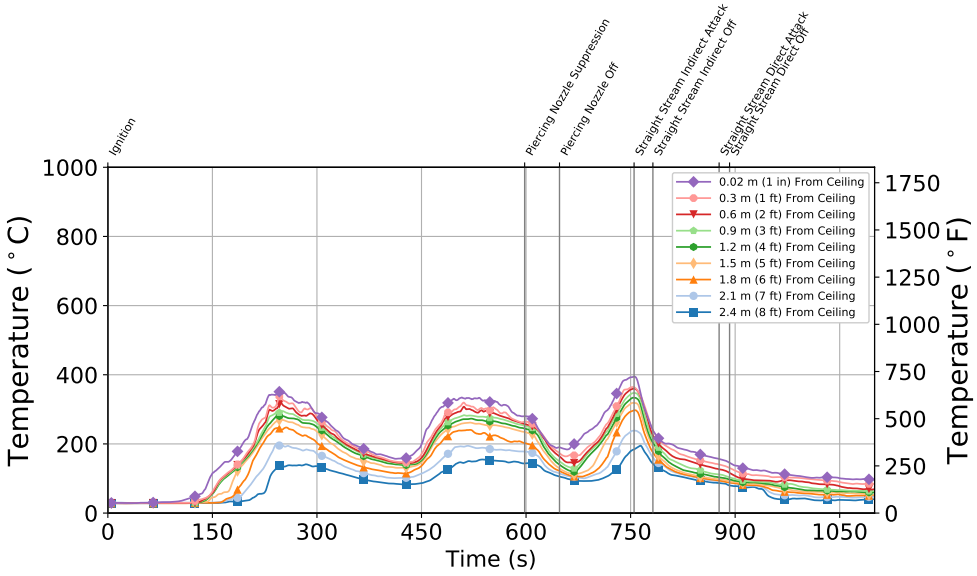

Figure B.135: Experiment 9 - Thermocouple temperature time histories from the Quadrant A thermocouple array in the basement.

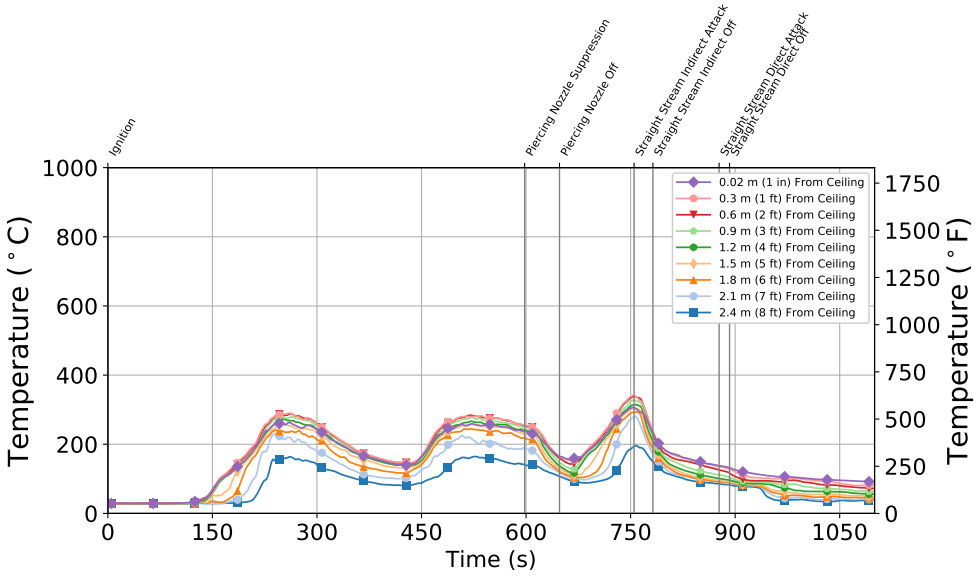

Figure B.136: Experiment 9 - Thermocouple temperature time histories from the Quadrant B thermocouple array in the basement.

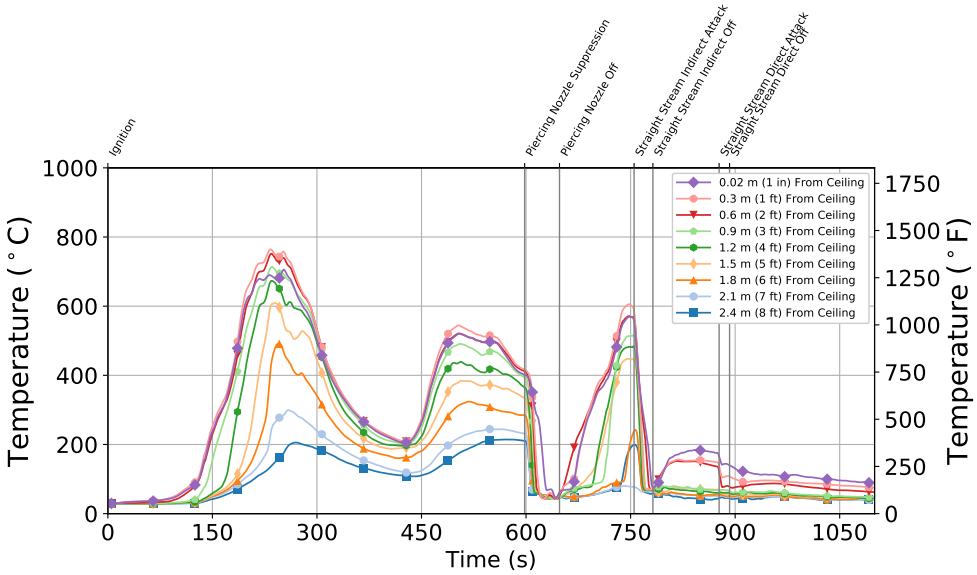

Figure B.137: Experiment 9 - Thermocouple temperature time histories from the Quadrant C thermocouple array in the basement.

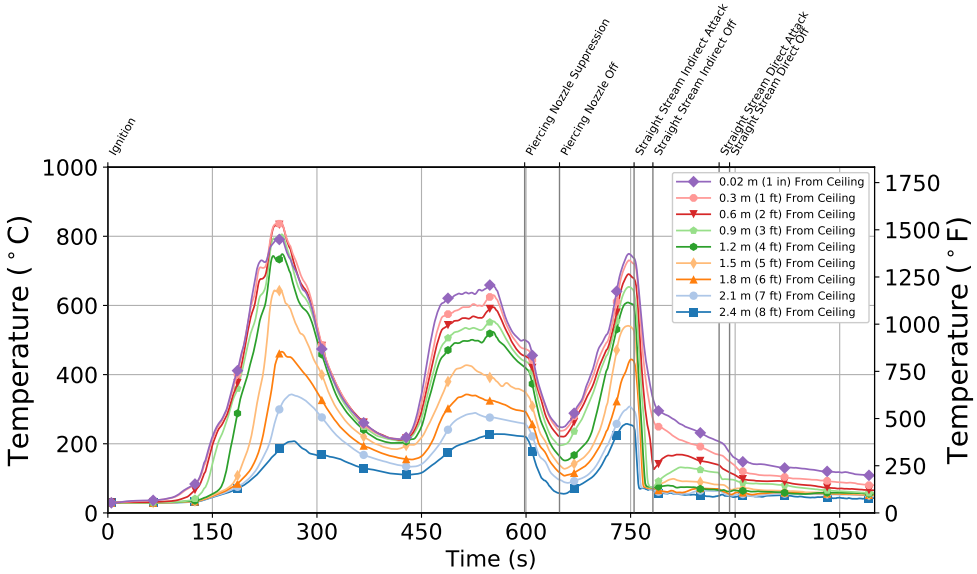

Figure B.138: Experiment 9 - Thermocouple temperature time histories from the Quadrant D thermocouple array in the basement.

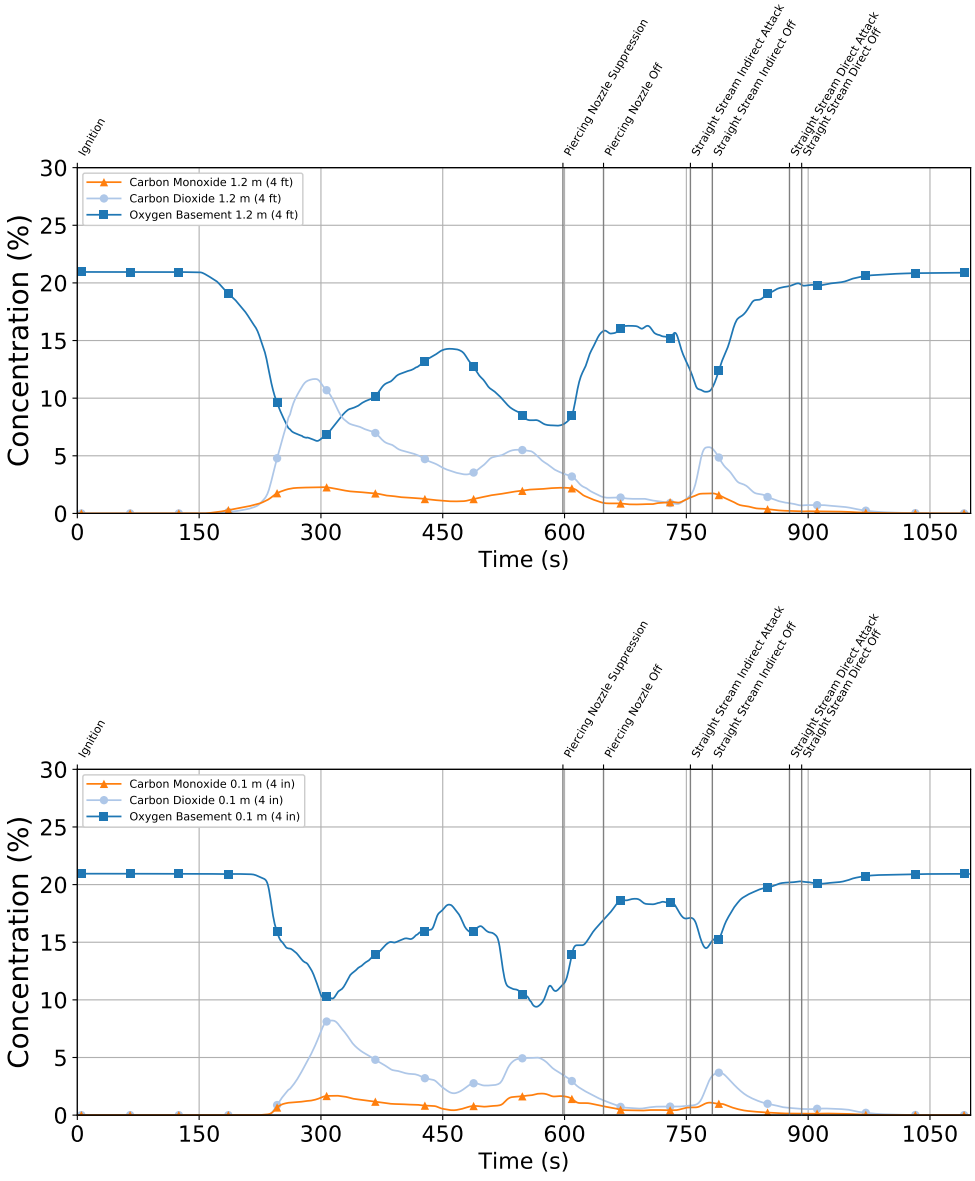

Figure B.139: Experiment 9 - Gas concentration time histories from the 1.2 m (4 ft) (top) and 0.1 m (4 in.) (bottom) elevations in the basement.

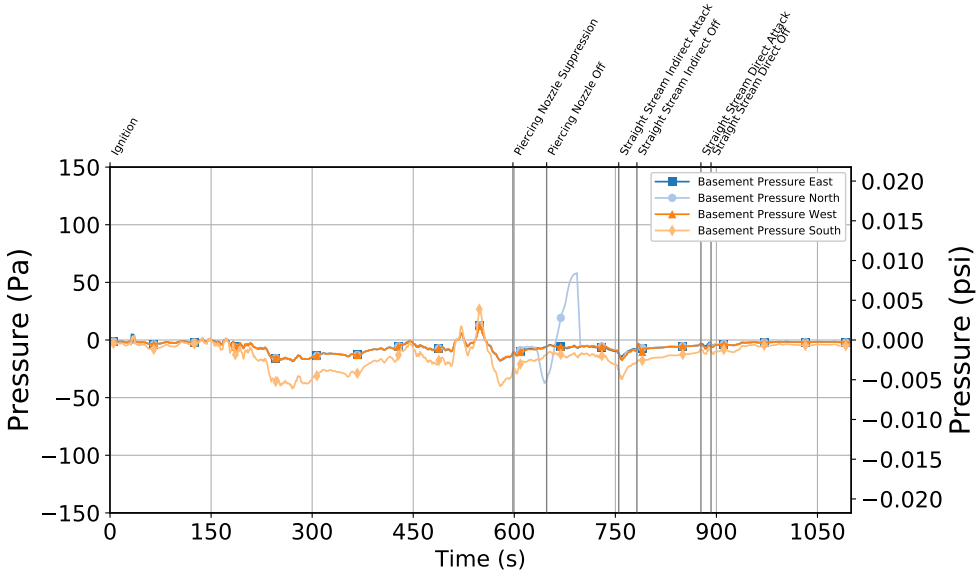

Figure B.140: Experiment 9 - Basement Pressure at 6 locations 1.2 m (4 ft) Above the Floor

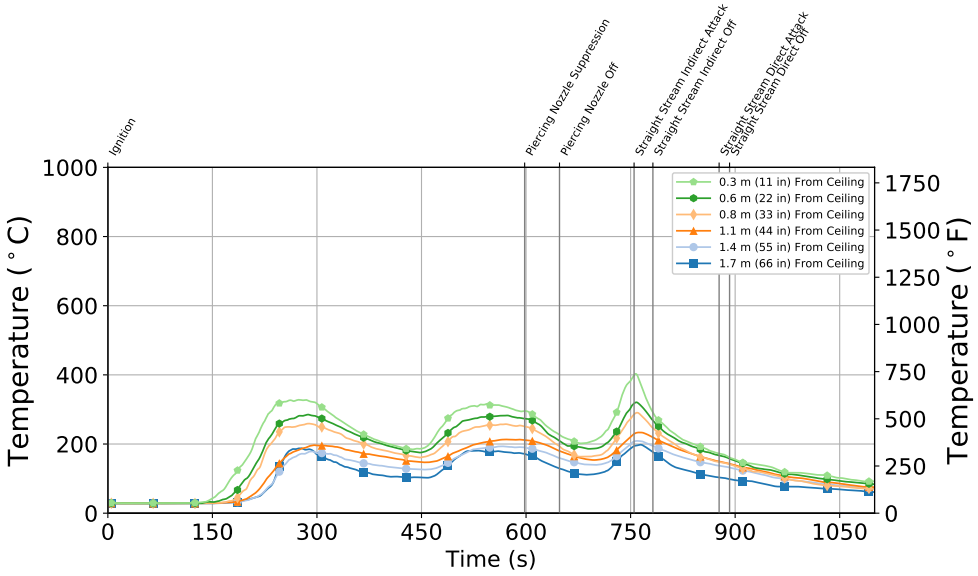

Figure B.141: Experiment 9 - Stair Thermocouple Temperature at Basement Level

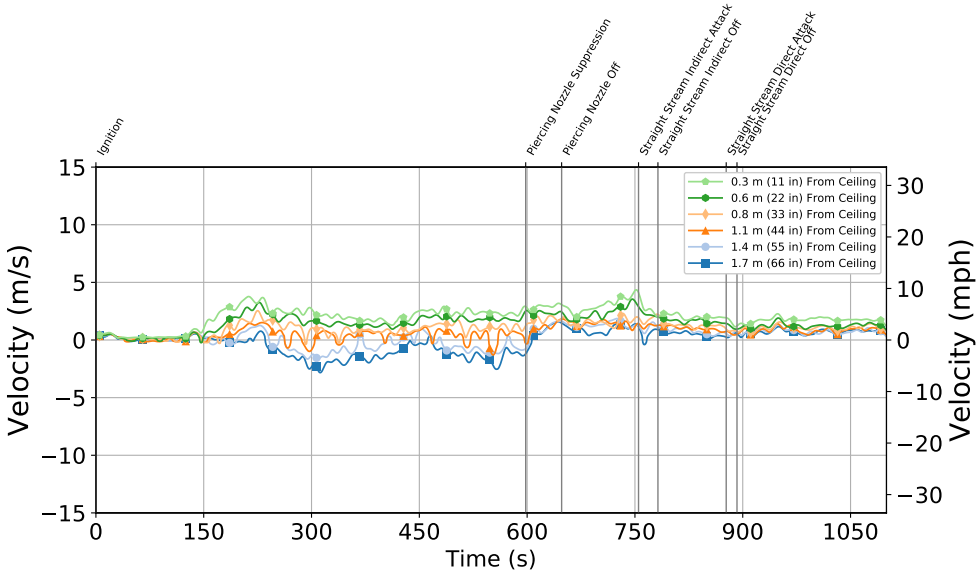

Figure B.142: Experiment 9 - Stair Velocity at Basement Level

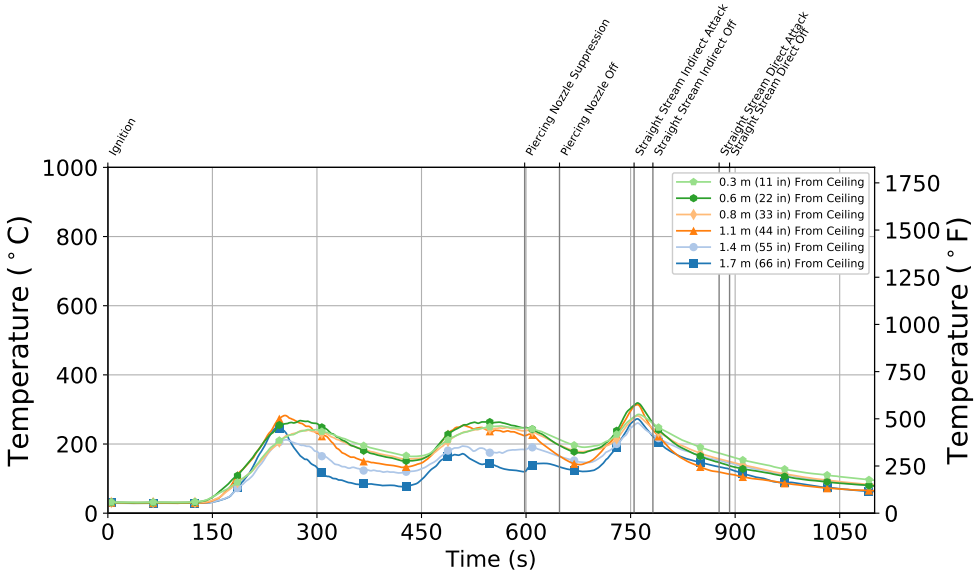

Figure B.143: Experiment 9 - Stair Thermocouple Temperature at First Floor

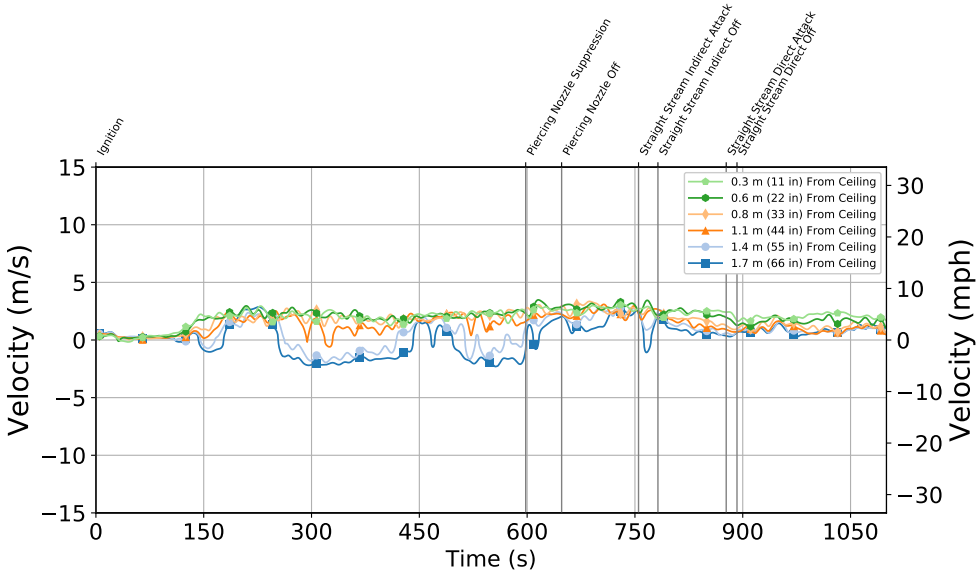

Figure B.144: Stair Velocity at First Floor

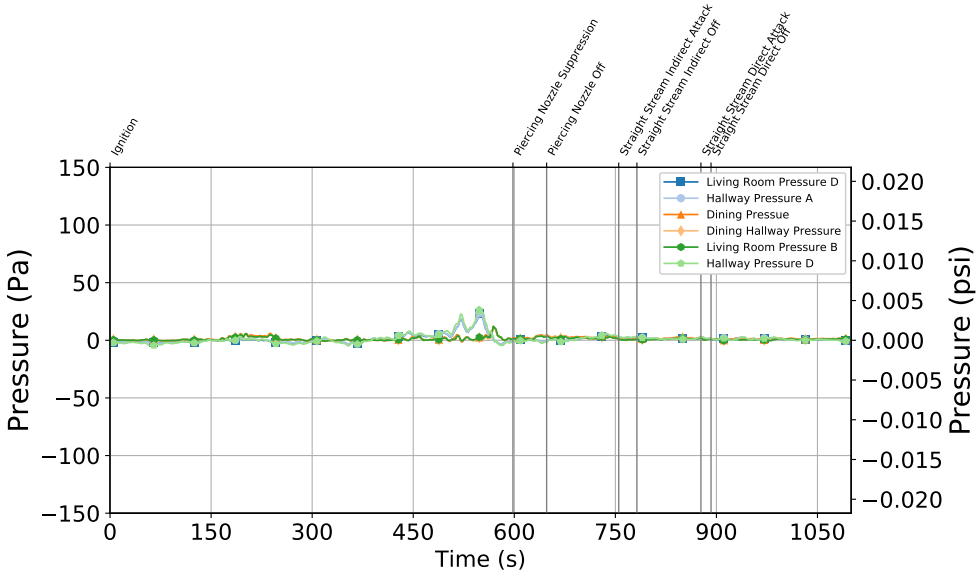

Figure B.145: Experiment 9 - First Floor Pressure at 6 locations 1.2 m (4 ft) Above the Floor

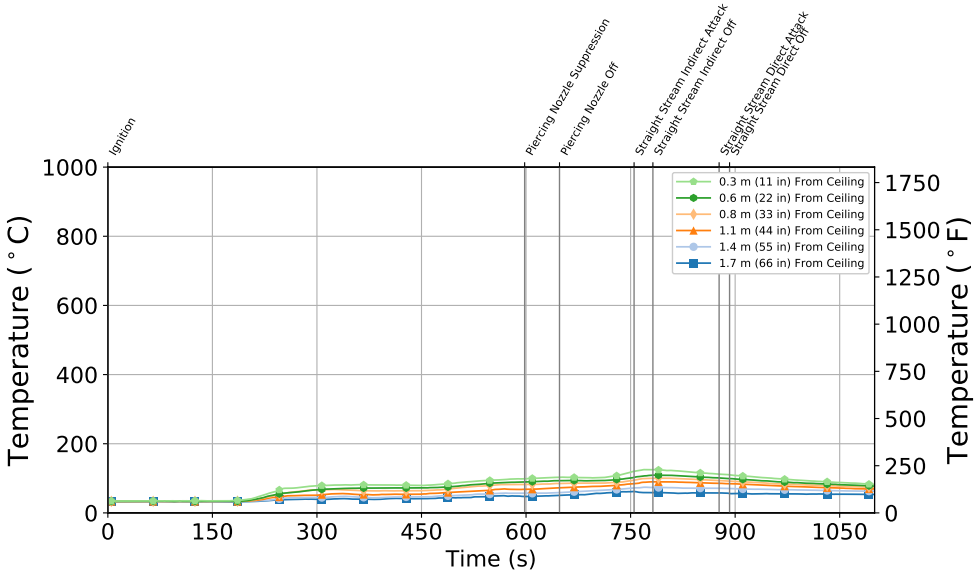

Figure B.146: Experiment 9 - Front Door Thermocouple Temperature at First Floor

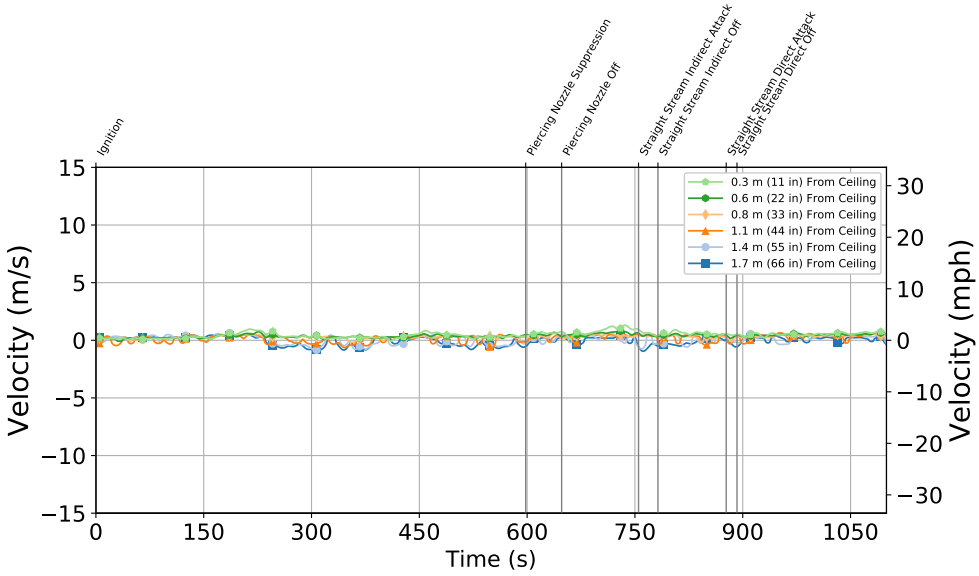

Figure B.147: Experiment 9 - Front Door Velocity at First Floor

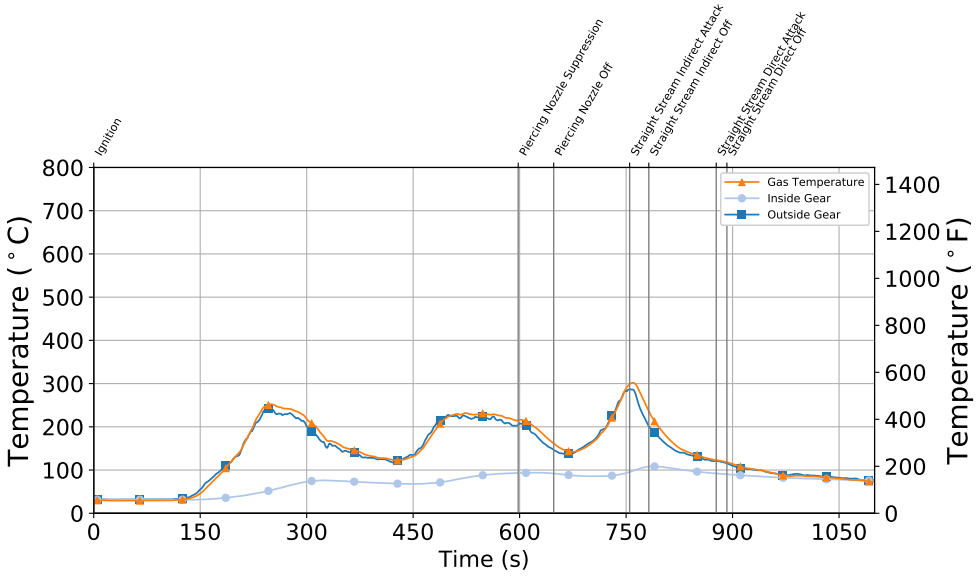

Figure B.148: Experiment 9 - Thermocouple Temperature on Inside and Outside of PPE Sample

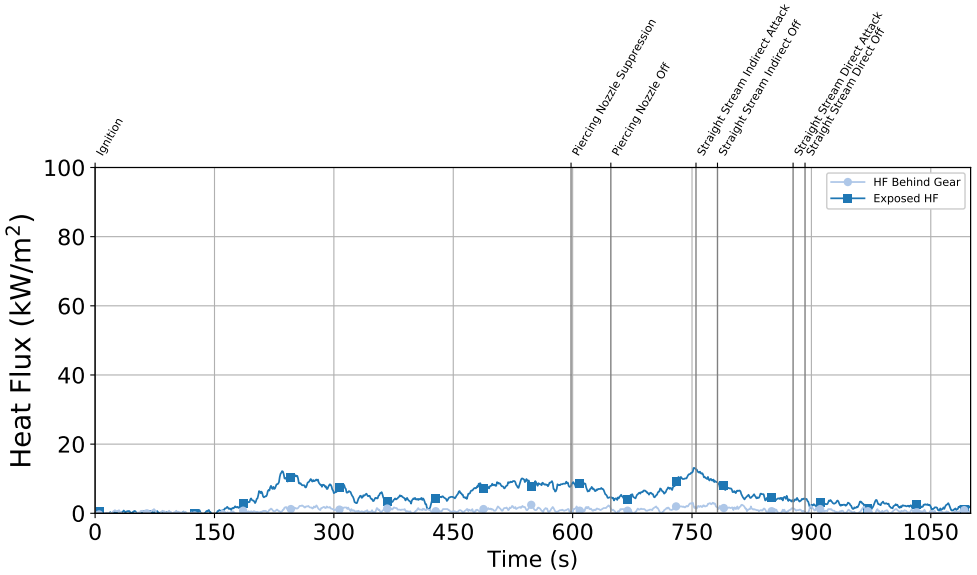

Figure B.149: Experiment 9 - Comparison of Heat Flux between Exposed Sensor and Protected Sensor

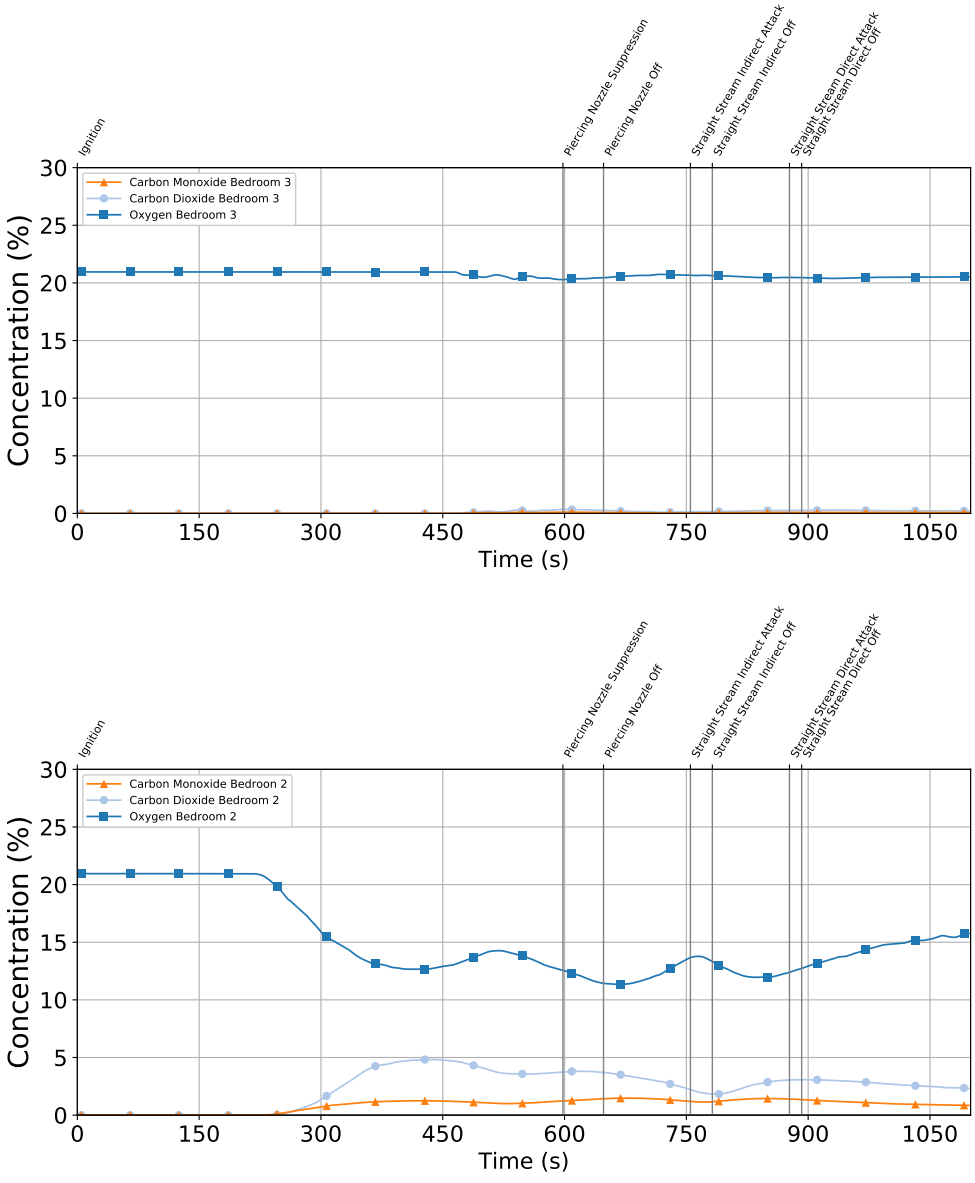

Figure B.150: Experiment 9 - Gas concentration time histories from the closed bedroom at 1.2 m (4 ft) (top) and from the open bedroom at 1.2 m (4 ft) (bottom).

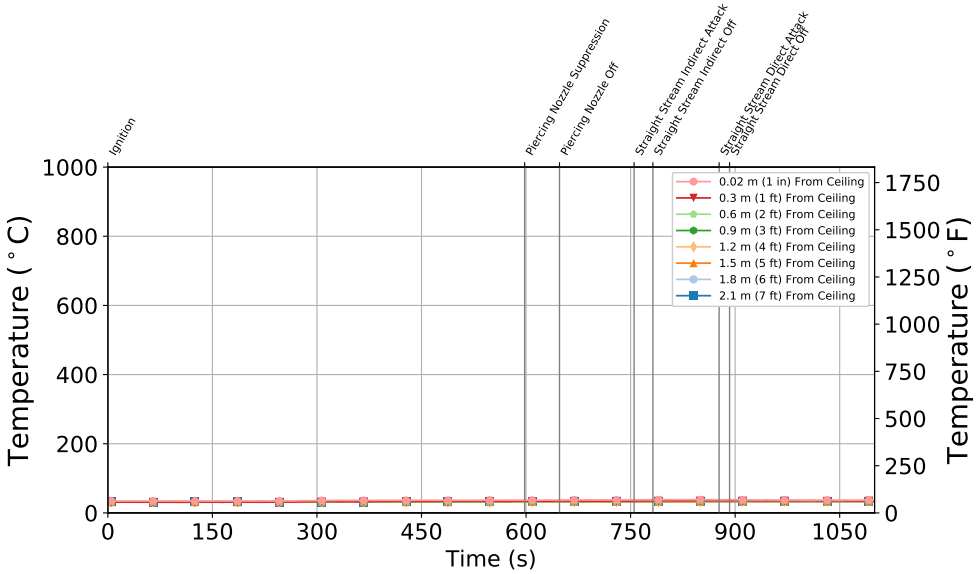

Figure B.151: Experiment 9 - Bedroom 3 (Closed) Bedroom

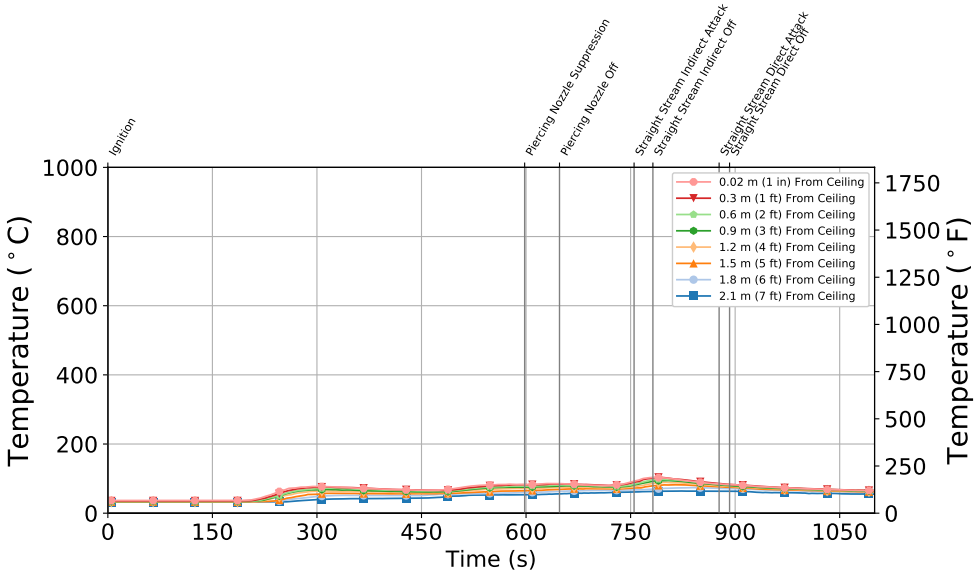

Figure B.152: Experiment 9 - Bedroom 2 (Open) Bedroom

B.10 Experiment 10

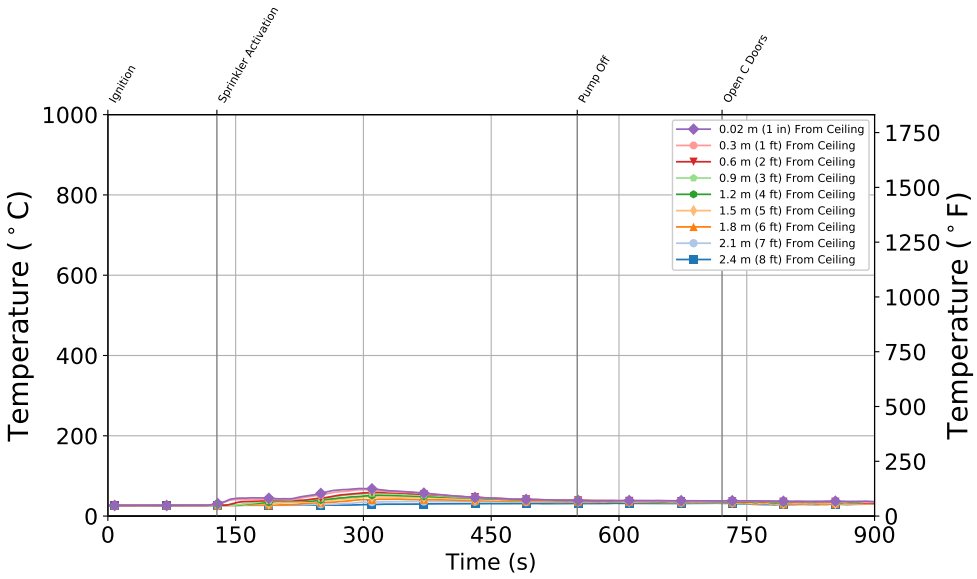

Figure B.153: Experiment 10 - Thermocouple temperature time histories from the Quadrant A thermocouple array in the basement.

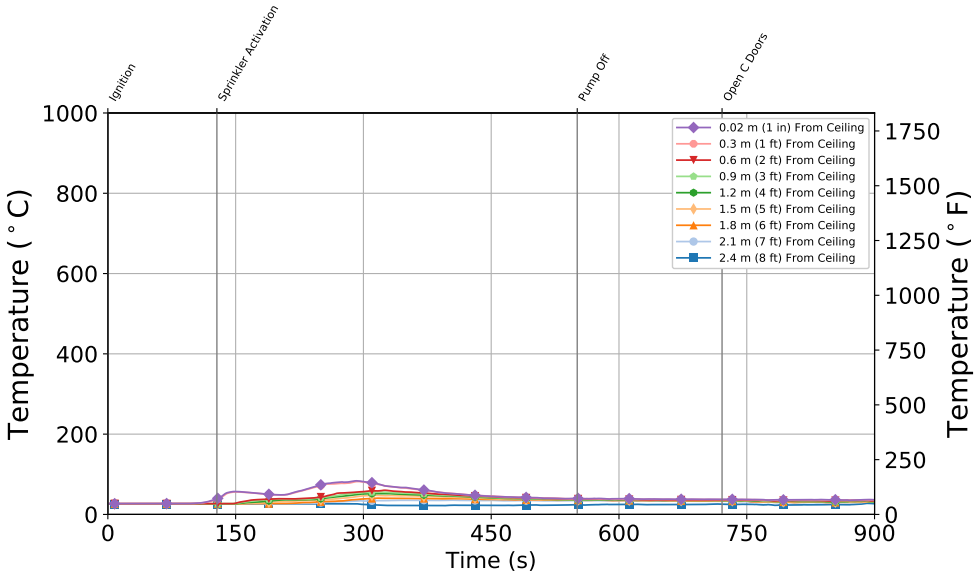

Figure B.154: Experiment 10 - Thermocouple temperature time histories from the Quadrant B thermocouple array in the basement.

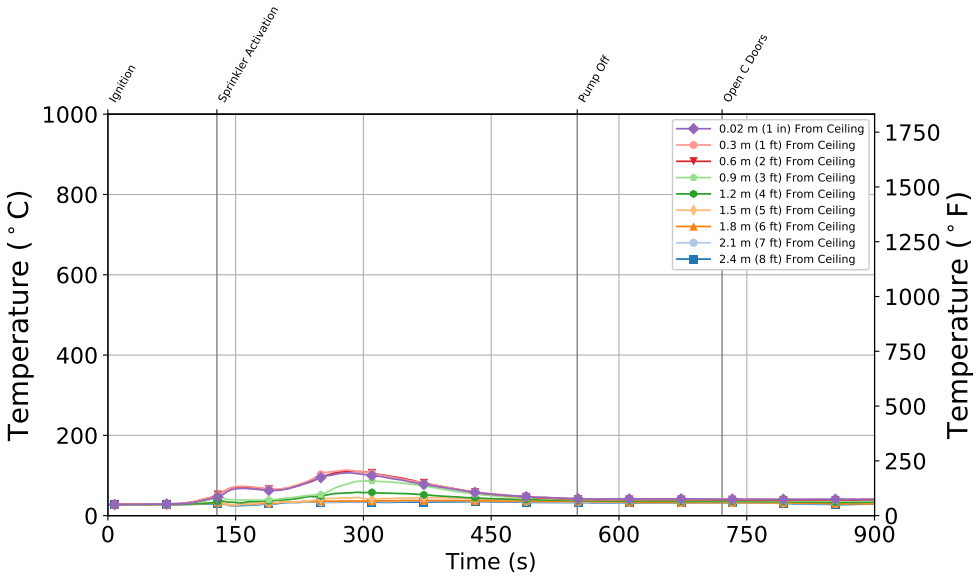

Figure B.155: Experiment 10 - Thermocouple temperature time histories from the Quadrant C thermocouple array in the basement.

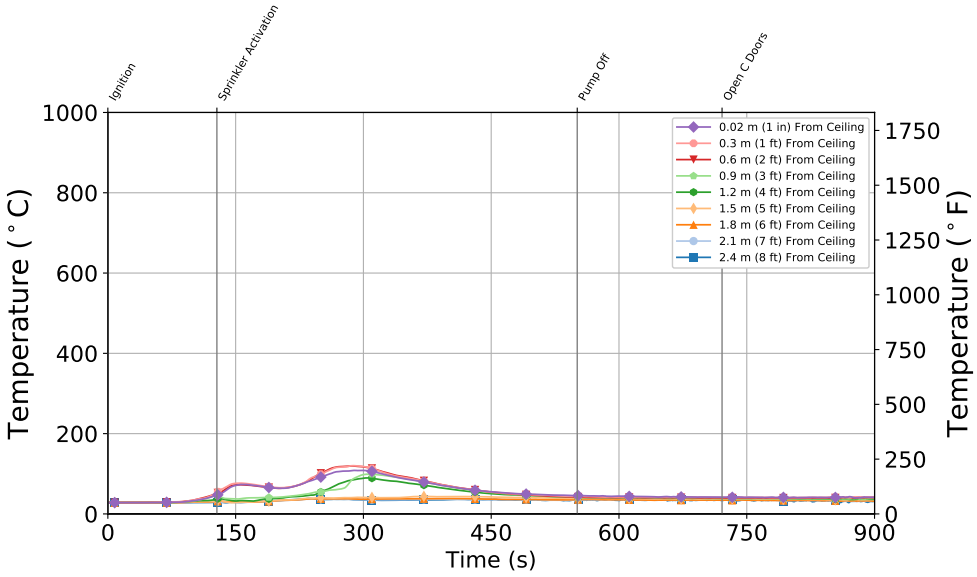

Figure B.156: Experiment 10 - Thermocouple temperature time histories from the Quadrant D thermocouple array in the basement.

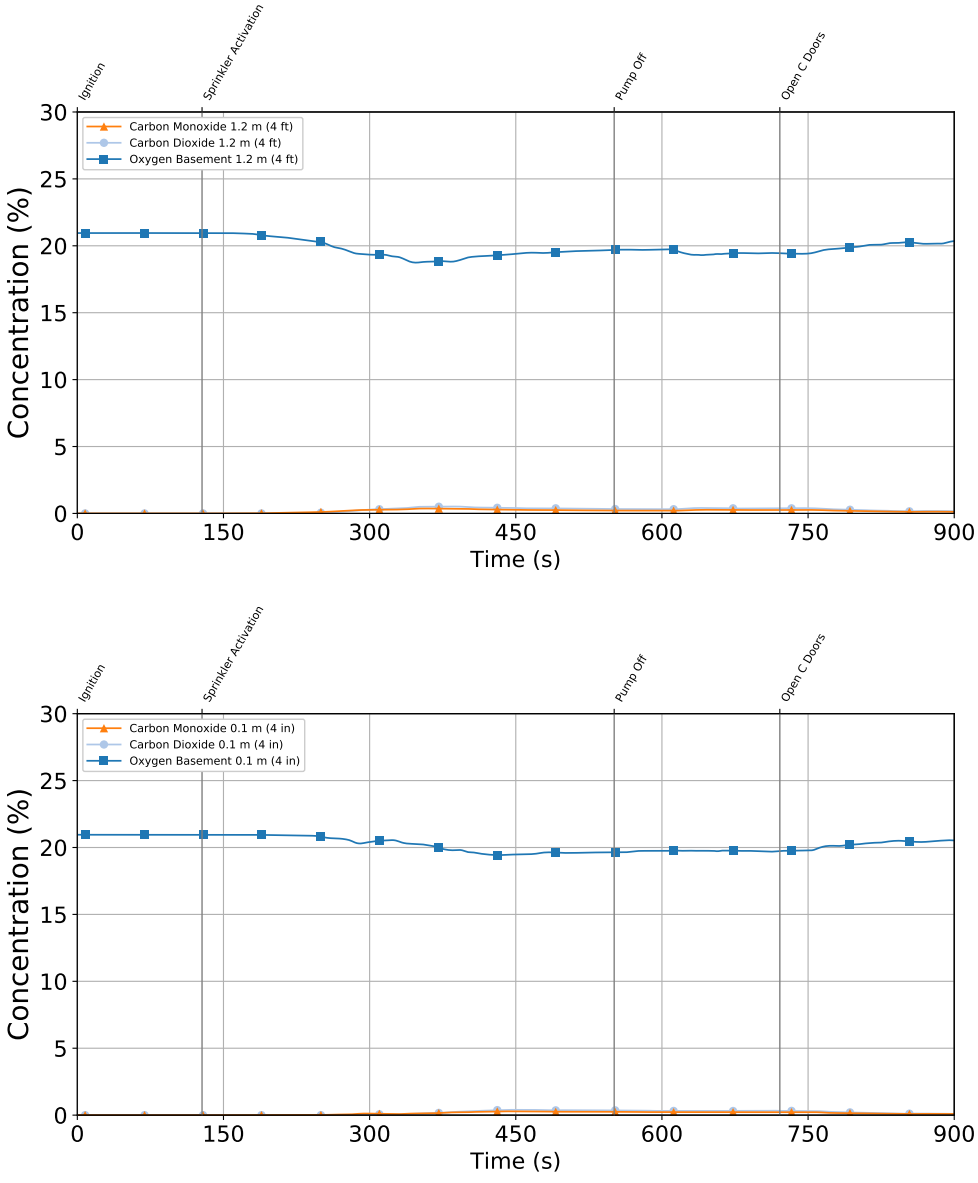

Figure B.157: Experiment 10 - Gas concentration time histories from the 1.2 m (4 ft) (top) and 0.1 m (4 in.) (bottom) elevations in the basement.

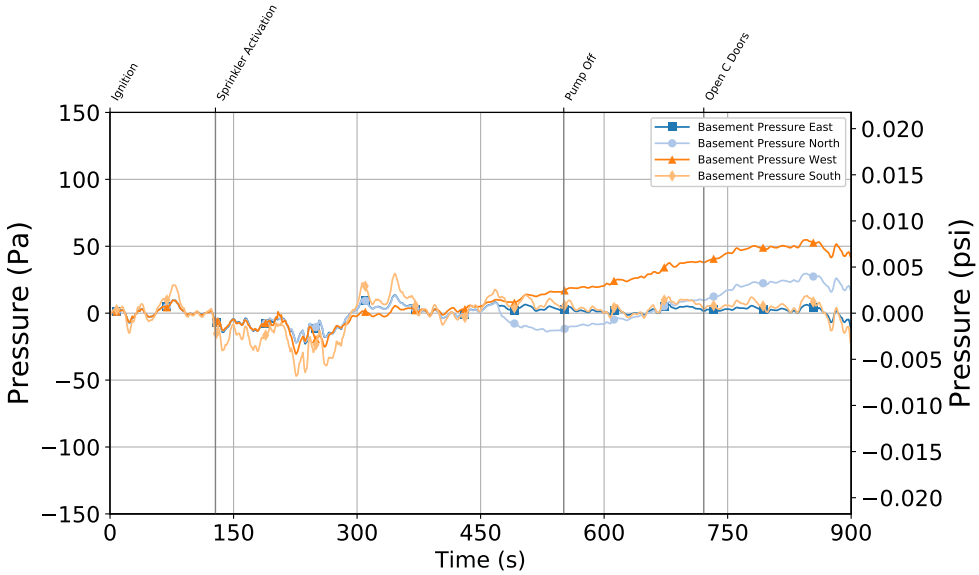

Figure B.158: Experiment 10 - Basement Pressure at 6 locations 1.2 m (4 ft) Above the Floor

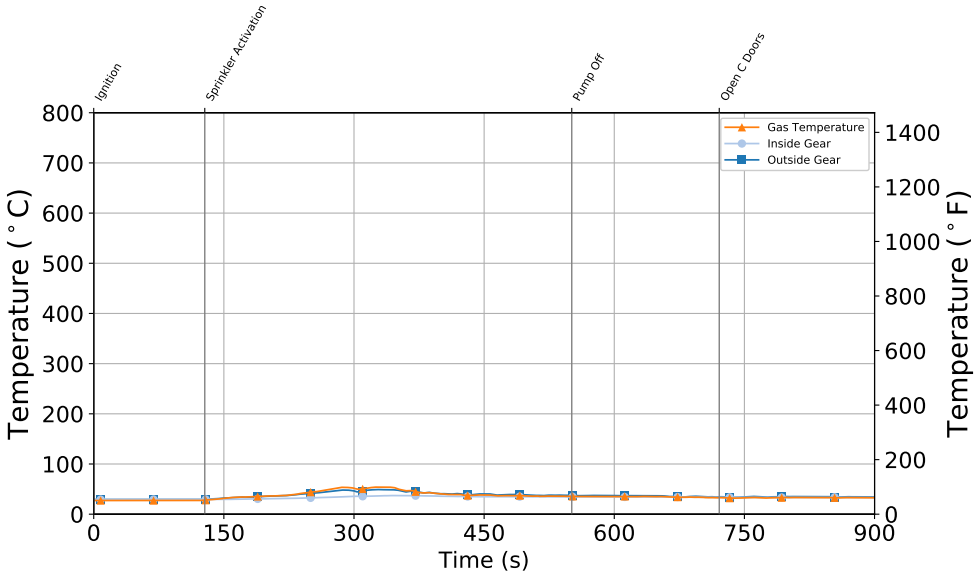

Figure B.159: Experiment 10 - Thermocouple Temperature on Inside and Outside of PPE Sample

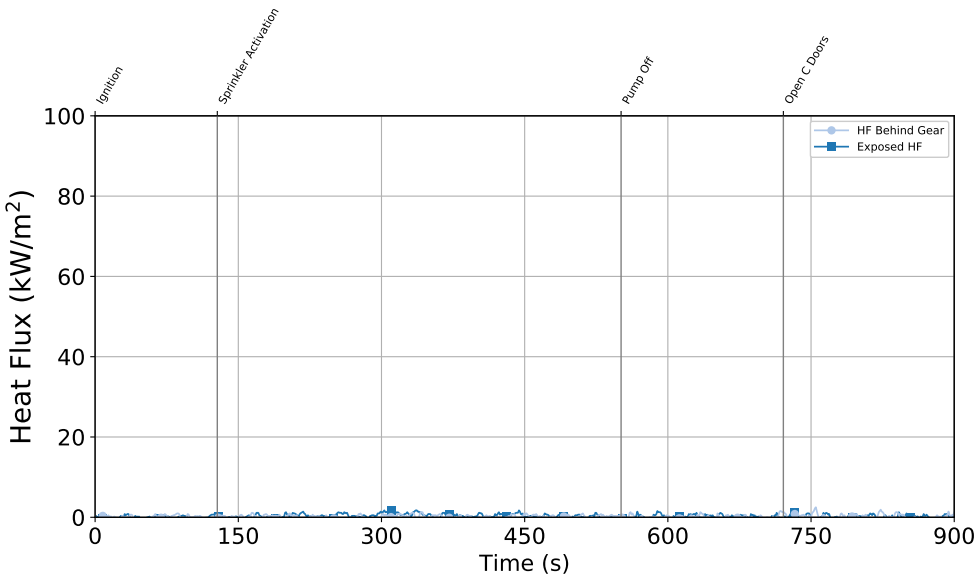

Figure B.160: Experiment 10 - Comparison of Heat Flux between Exposed Sensor and Protected Sensor

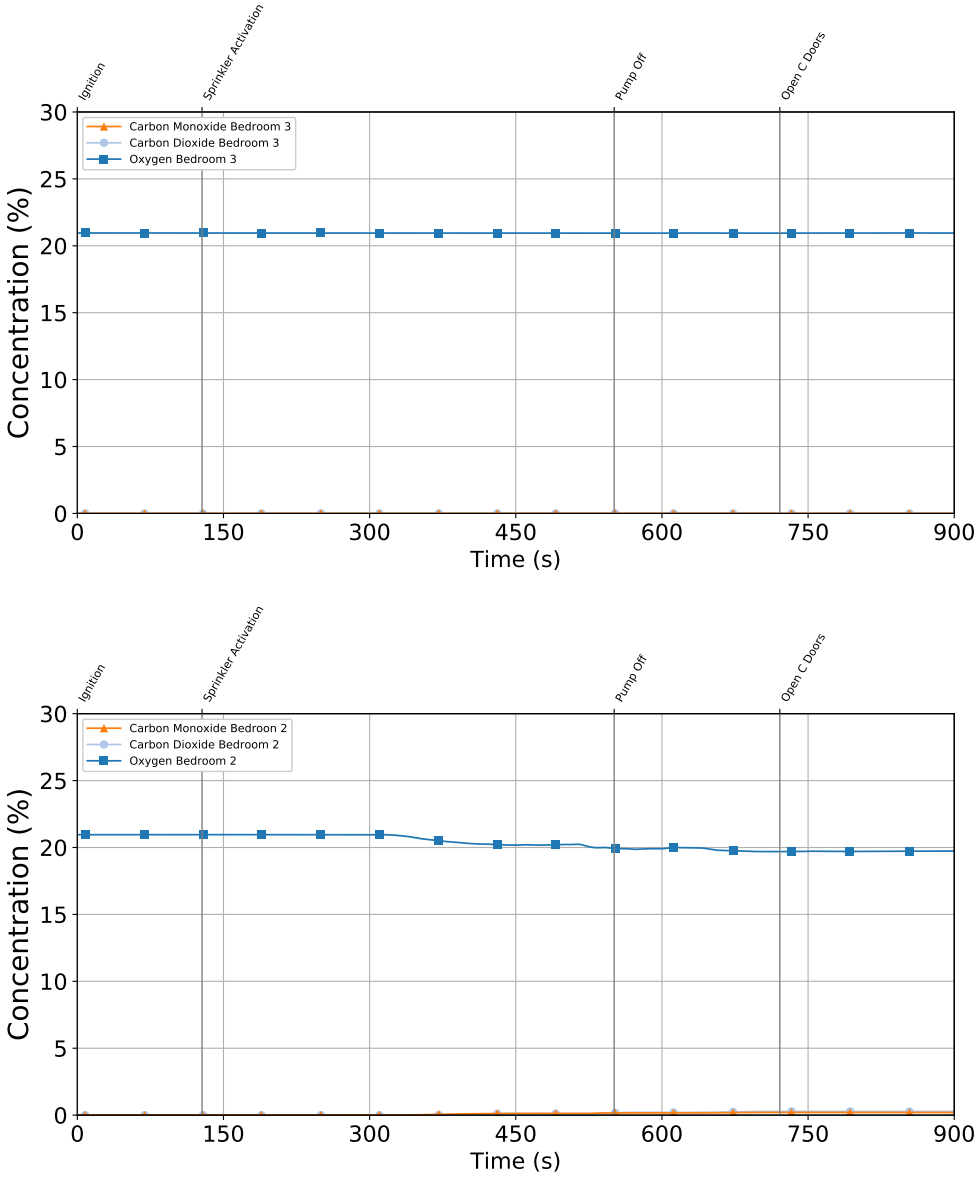

Figure B.161: Experiment 10 - Gas concentration time histories from the closed bedroom at 1.2 m (4 ft) (top) and from the open bedroom at 1.2 m (4 ft) (bottom).

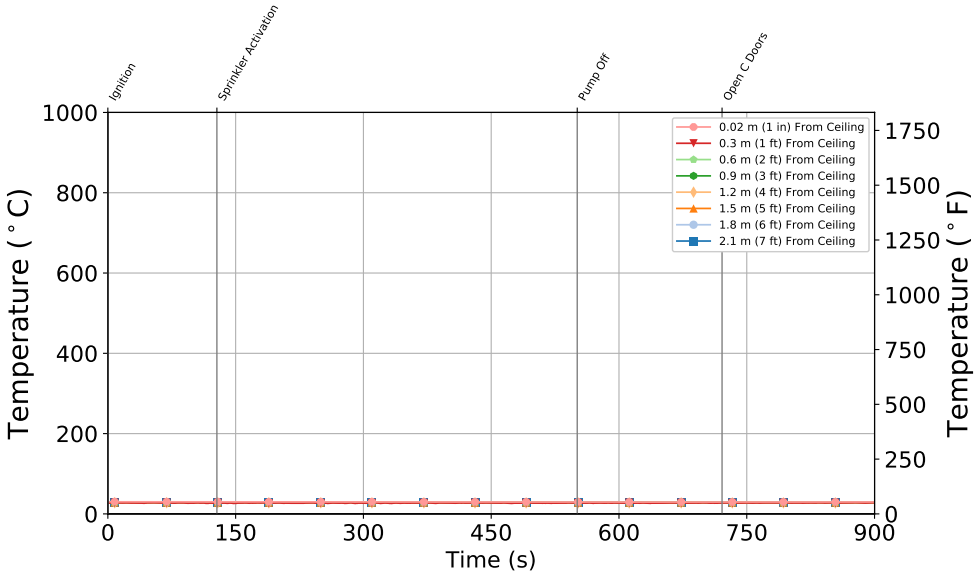

Figure B.162: Experiment 10 - Bedroom 3 (Closed) Bedroom

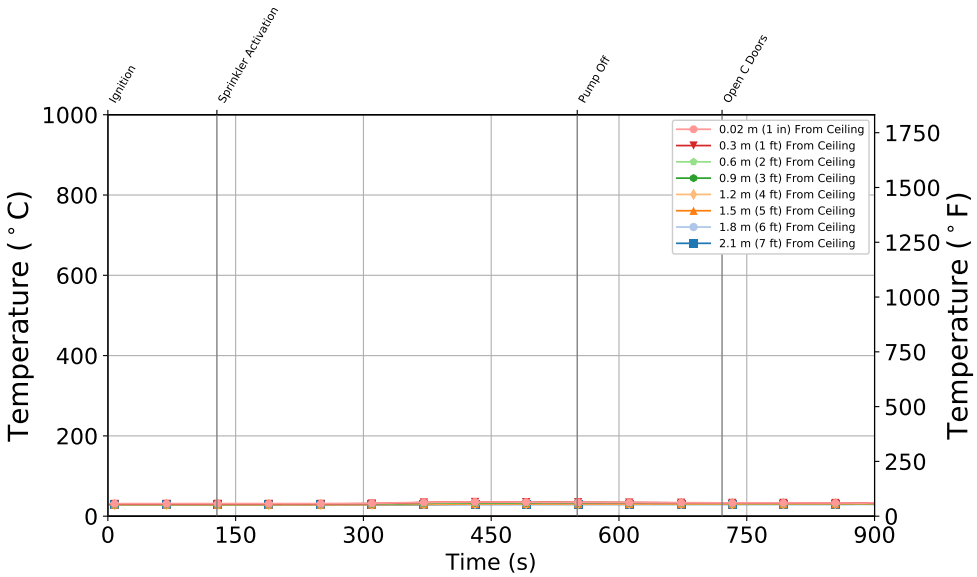

Figure B.163: Experiment 10 - Bedroom 2 (Open) Bedroom

B.11 Experiment 11

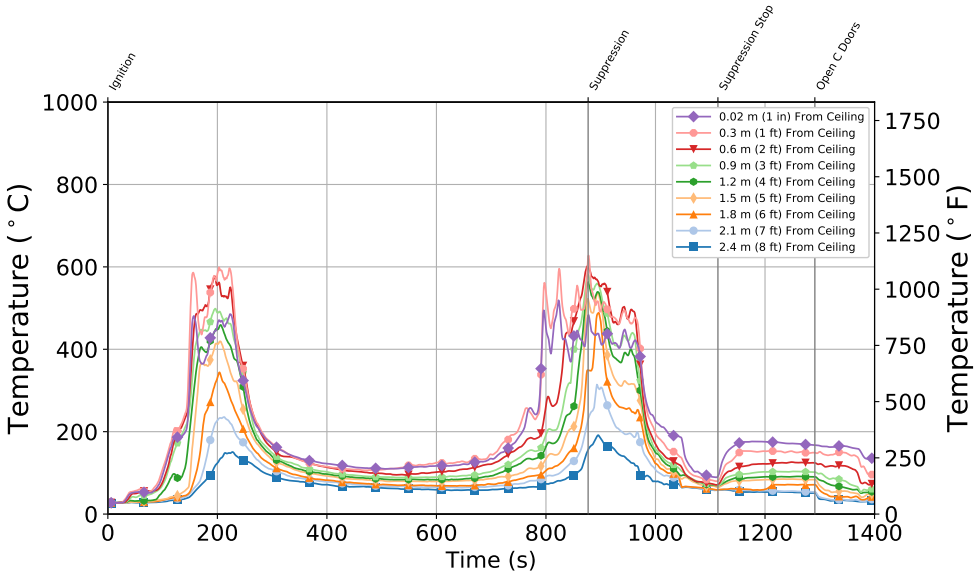

Figure B.164: Experiment 11 - Thermocouple temperature time histories from the Quadrant A thermocouple array in the basement.

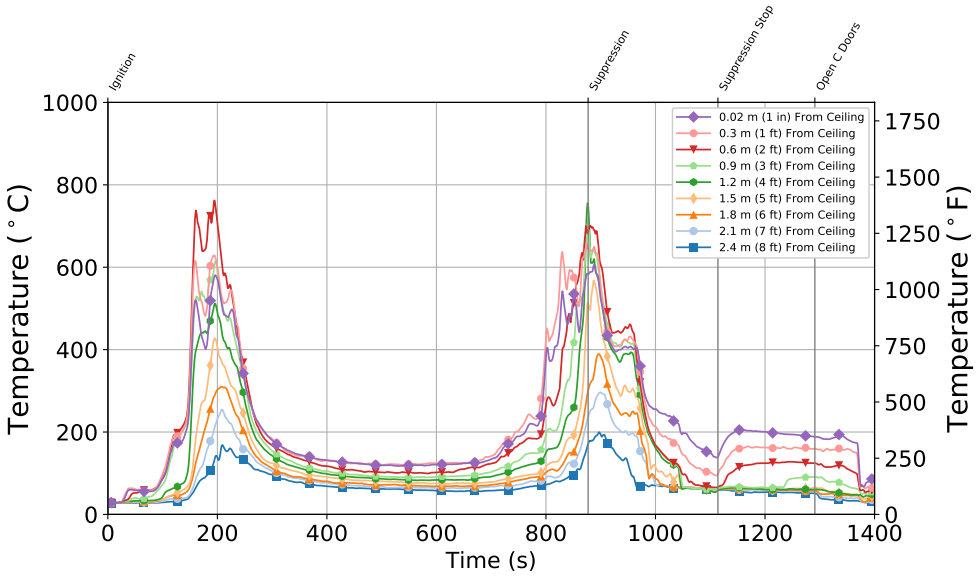

Figure B.165: Experiment 11 - Thermocouple temperature time histories from the Quadrant B thermocouple array in the basement.

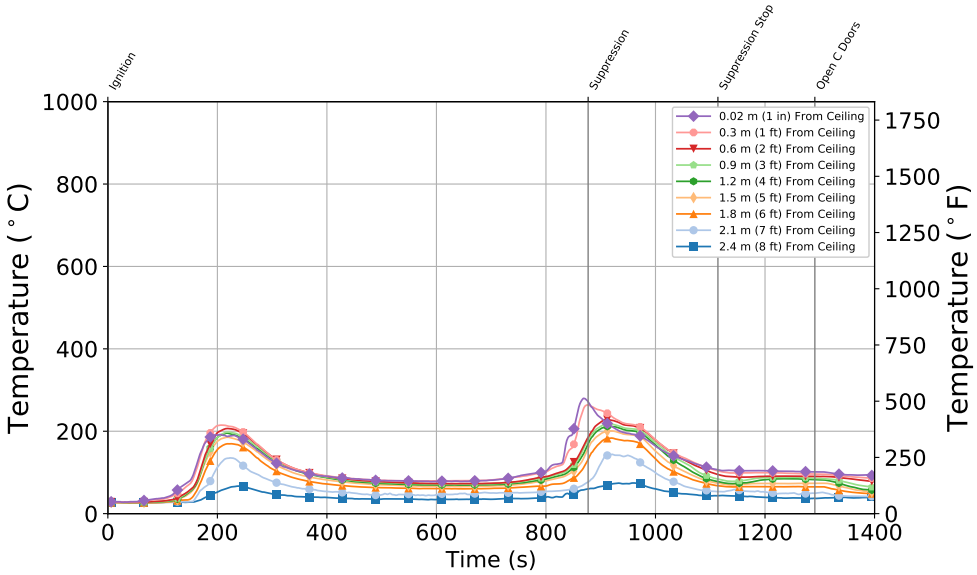

Figure B.166: Experiment 11 - Thermocouple temperature time histories from the Quadrant C thermocouple array in the basement.

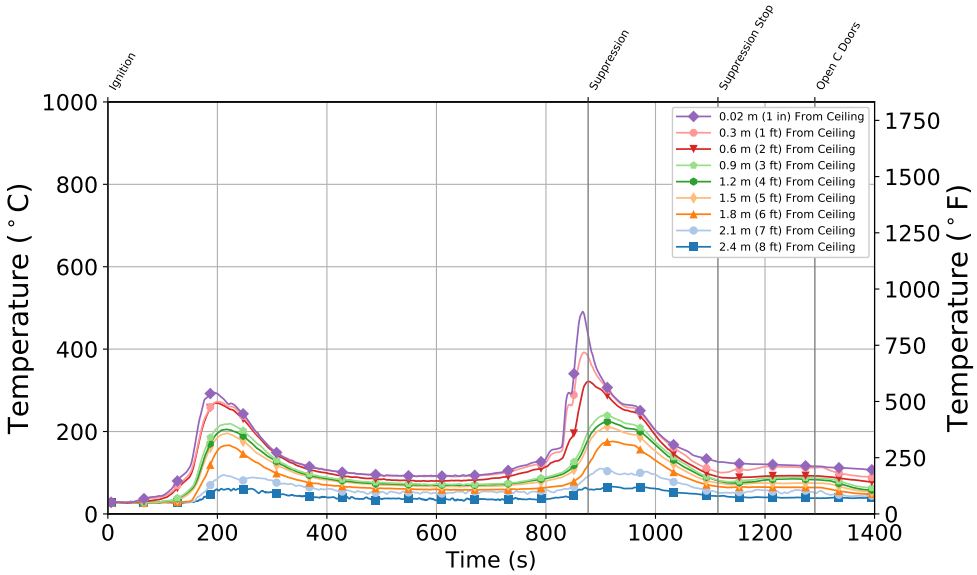

Figure B.167: Experiment 11 - Thermocouple temperature time histories from the Quadrant D thermocouple array in the basement.

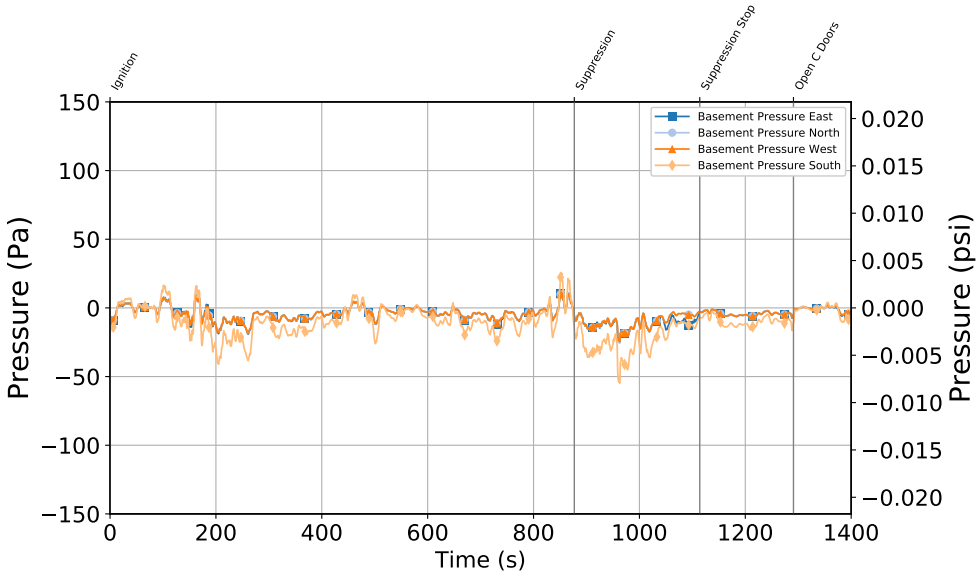

Figure B.168: Experiment 11 - Basement Pressure at 6 locations 1.2 m (4 ft) Above the Floor

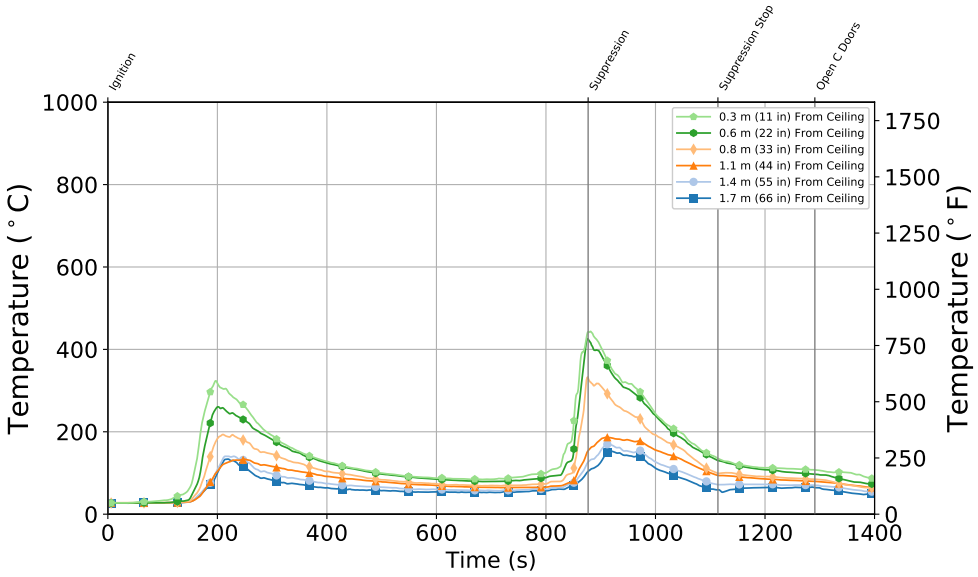

Figure B.169: Experiment 11 - Stair Thermocouple Temperature at Basement Level

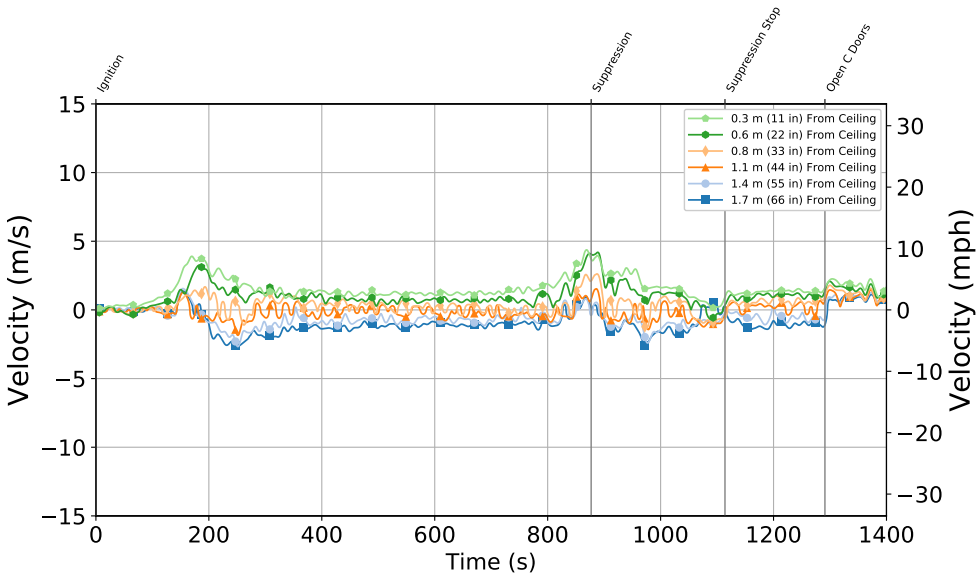

Figure B.170: Experiment 11 - Stair Velocity at Basement Level

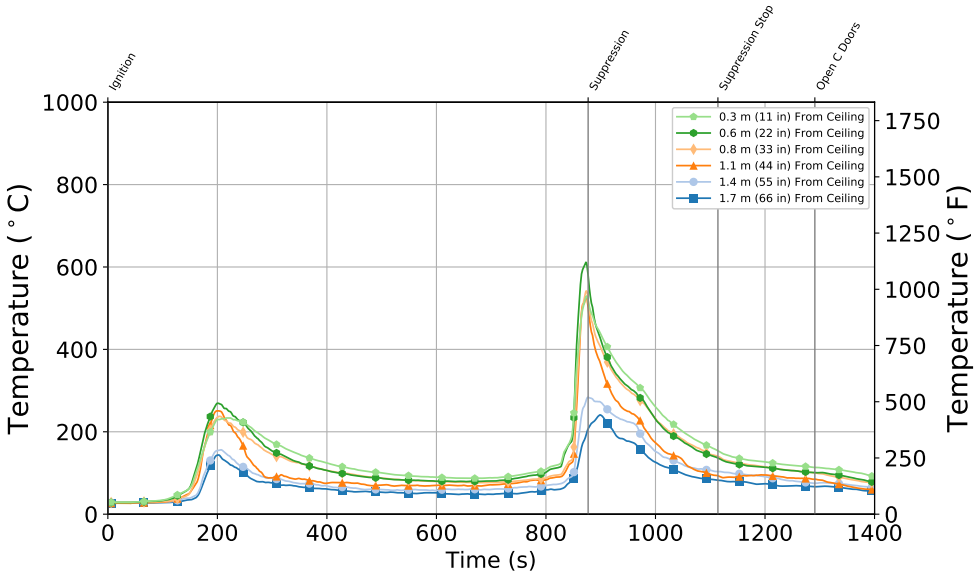

Figure B.171: Experiment 11 - Stair Thermocouple Temperature at First Floor

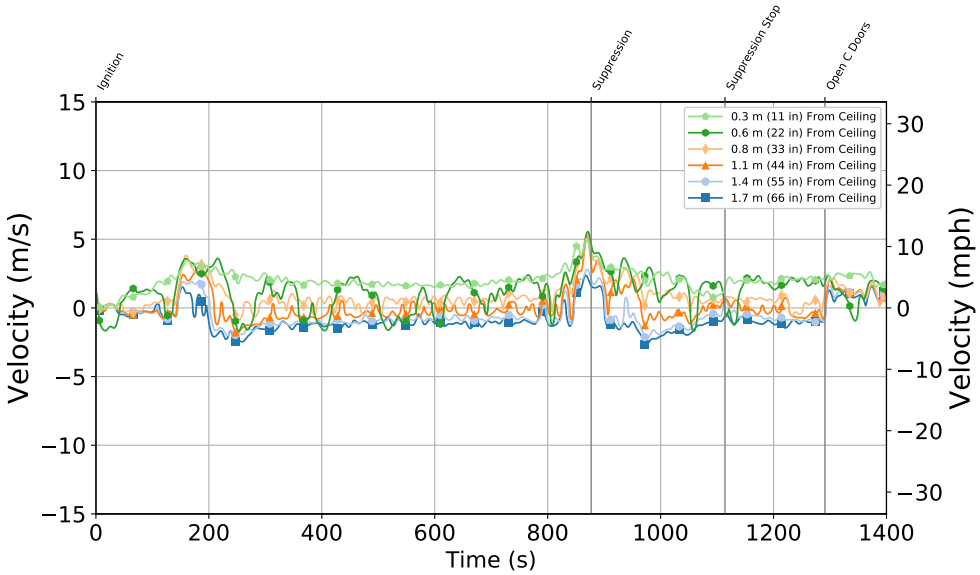

Figure B.172: Stair Velocity at First Floor

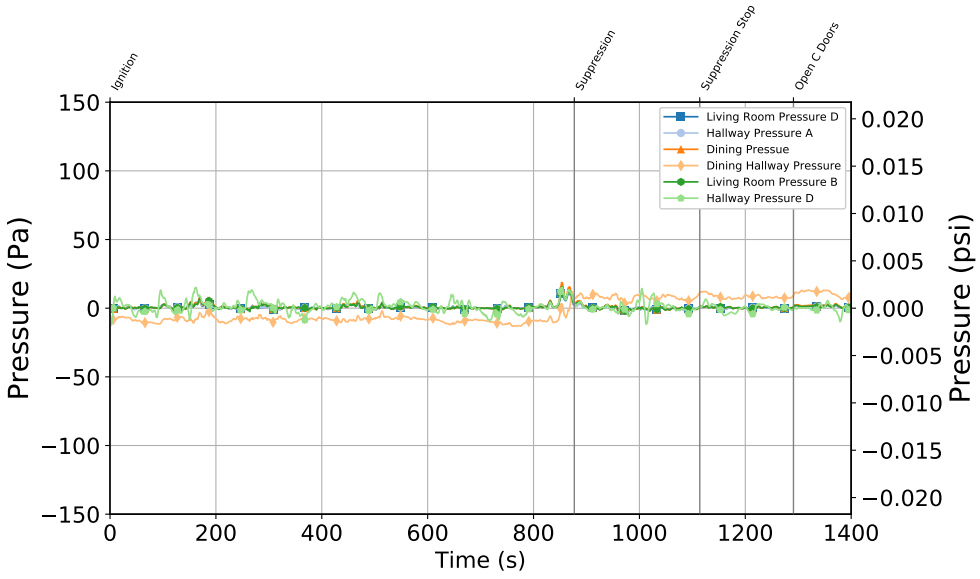

Figure B.173: Experiment 11 - First Floor Pressure at 6 locations 1.2 m (4 ft) Above the Floor

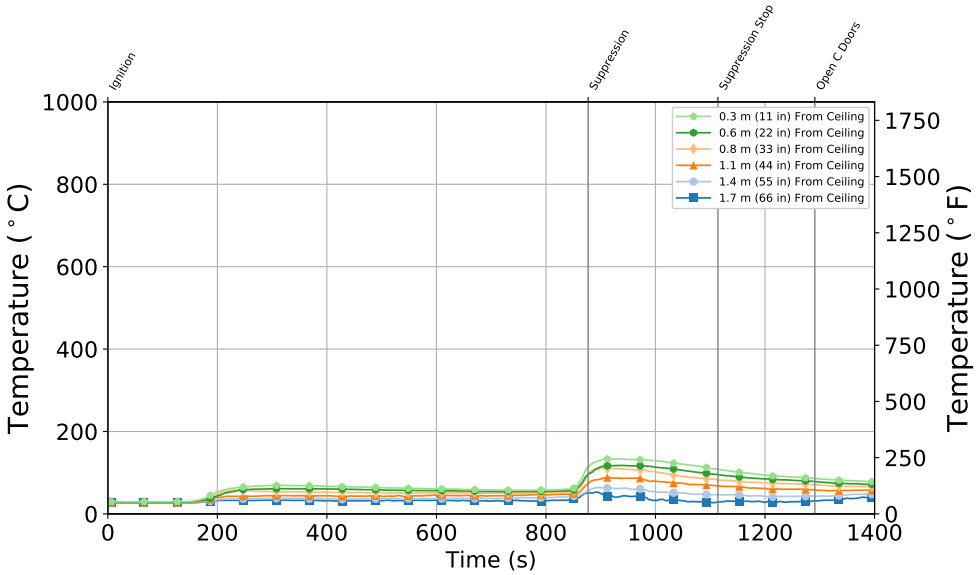

Figure B.174: Experiment 11 - Front Door Thermocouple Temperature at First Floor

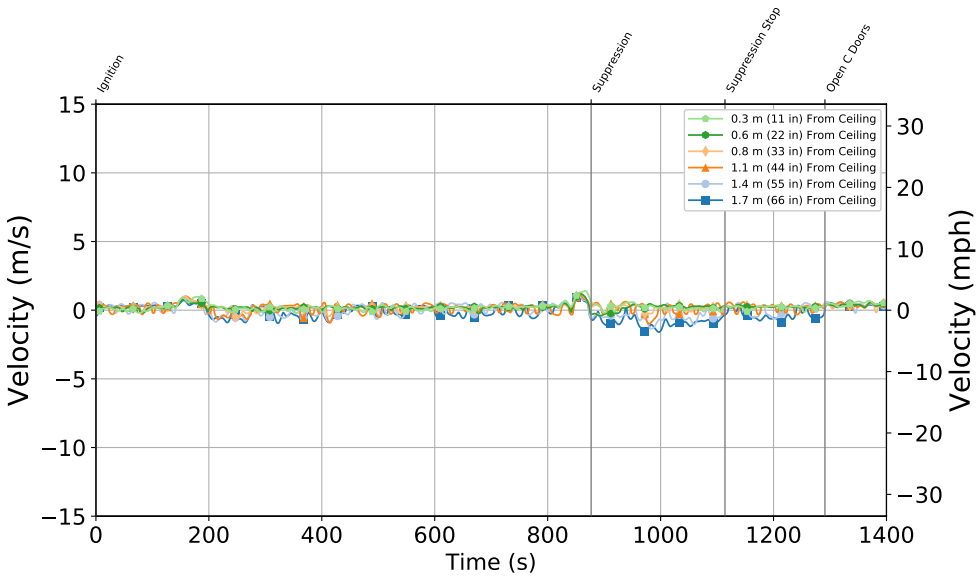

Figure B.175: Experiment 11 - Front Door Velocity at First Floor

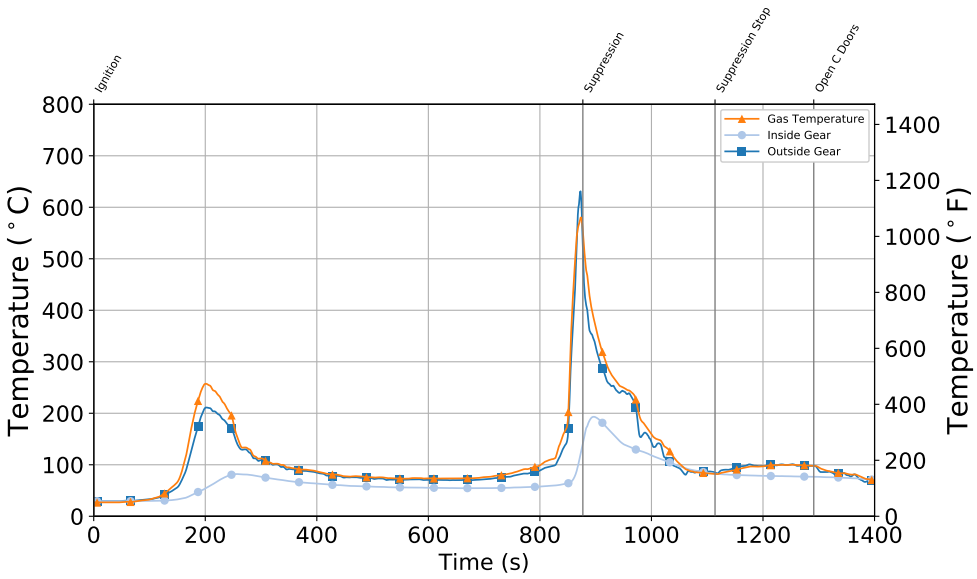

Figure B.176: Experiment 11 - Thermocouple Temperature on Inside and Outside of PPE Sample

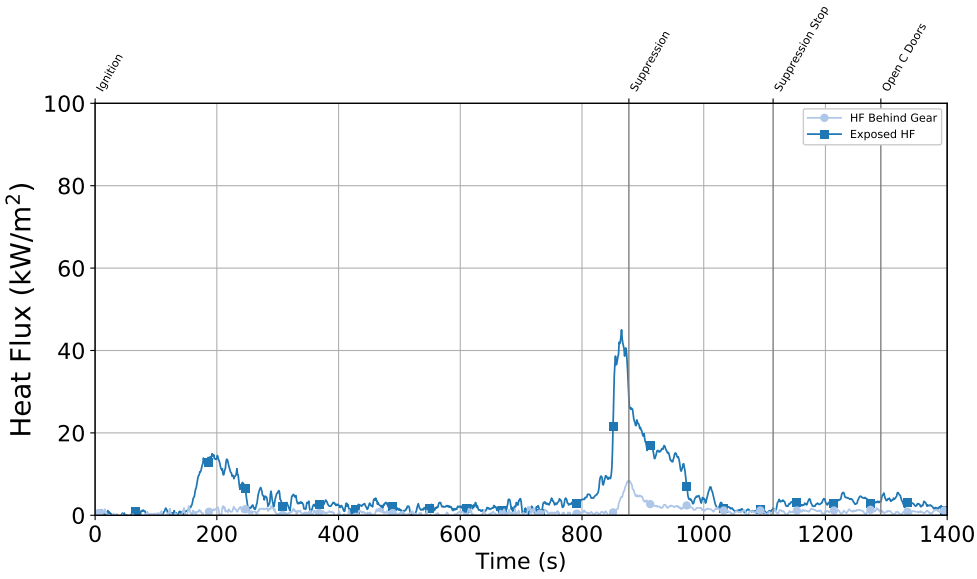

Figure B.177: Experiment 11 - Comparison of Heat Flux between Exposed Sensor and Protected Sensor

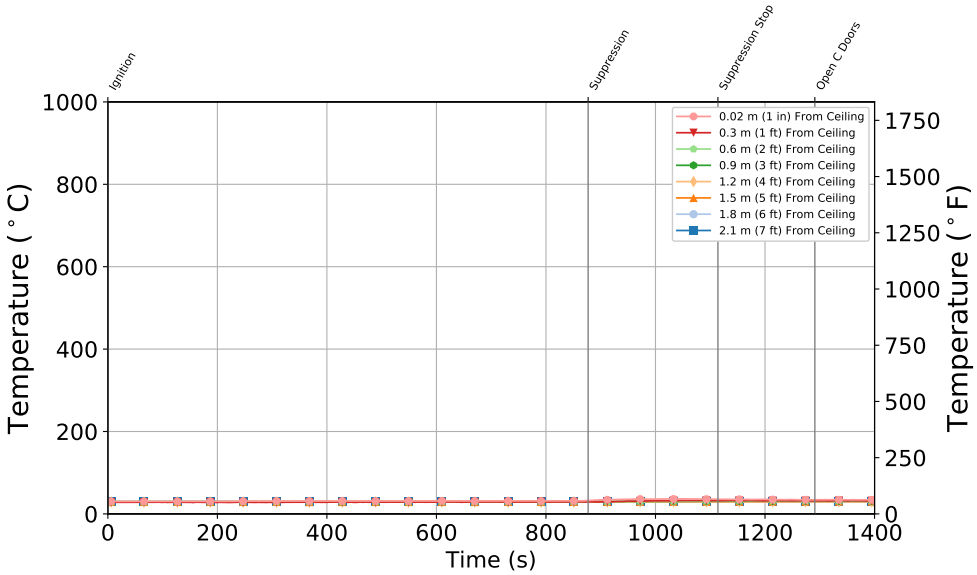

Figure B.178: Experiment 11 - Bedroom 3 (Closed) Bedroom

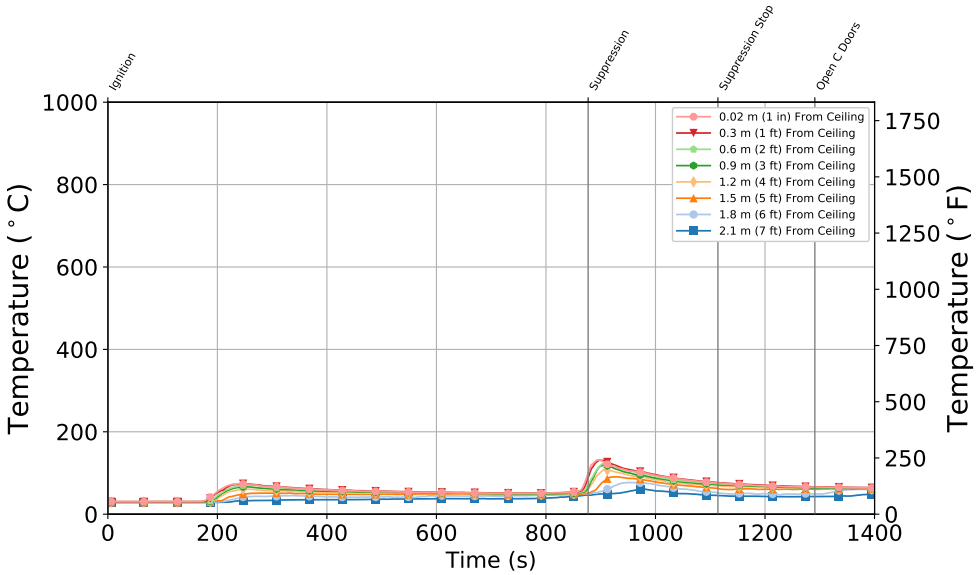

Figure B.179: Experiment 11 - Bedroom 2 (Open) Bedroom

B.12 Experiment 12

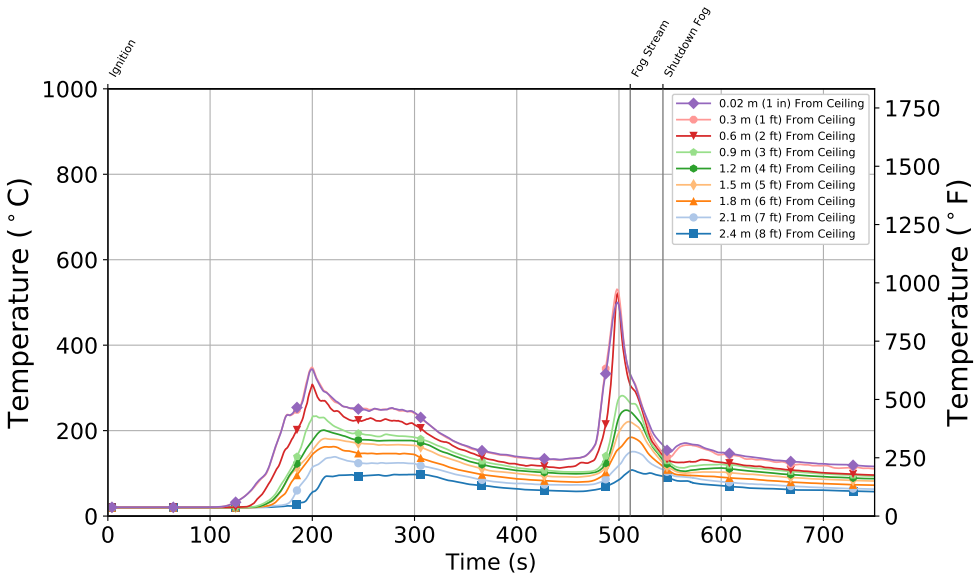

Figure B.180: Experiment 12 - Thermocouple temperature time histories from the Quadrant A thermocouple array in the basement.

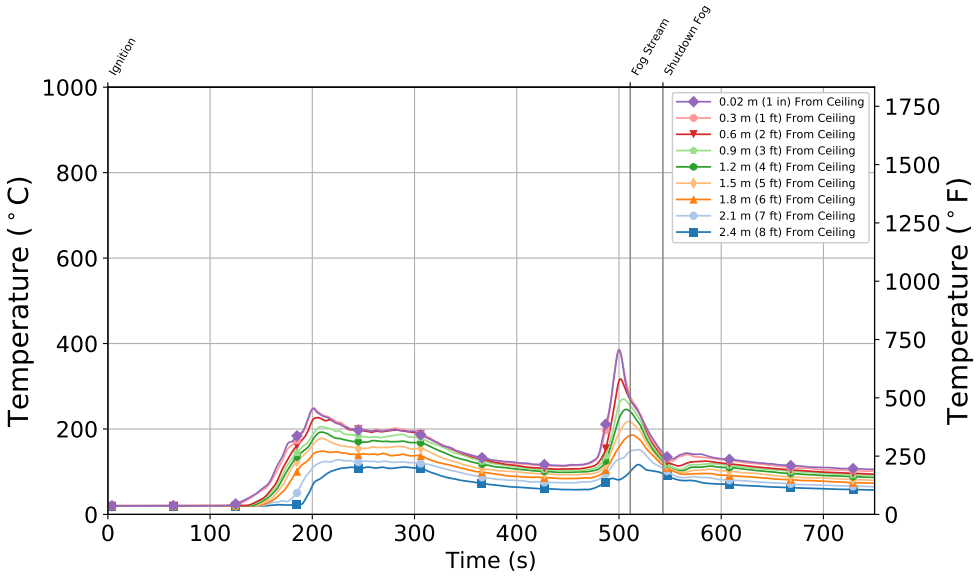

Figure B.181: Experiment 12 - Thermocouple temperature time histories from the Quadrant B thermocouple array in the basement.

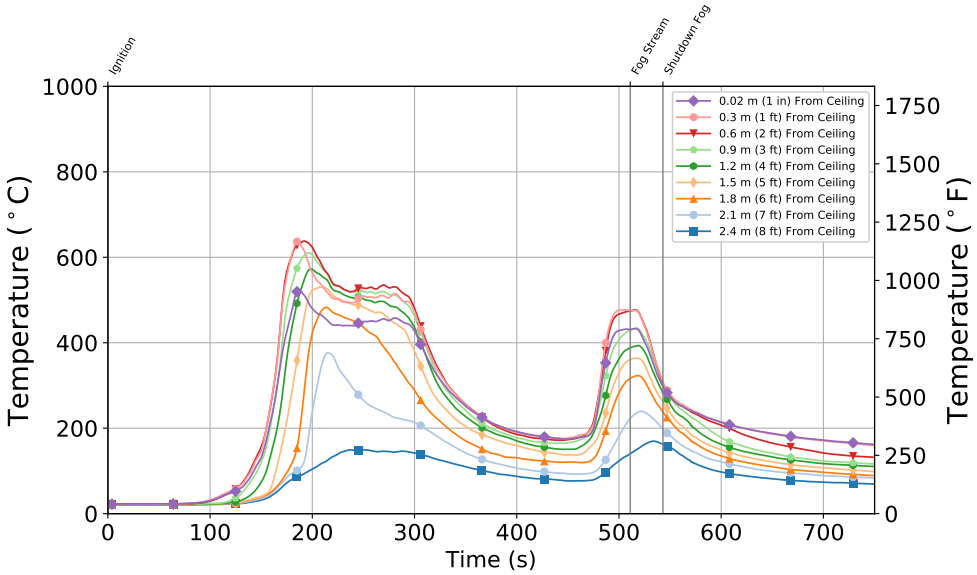

Figure B.182: Experiment 12 - Thermocouple temperature time histories from the Quadrant C thermocouple array in the basement.

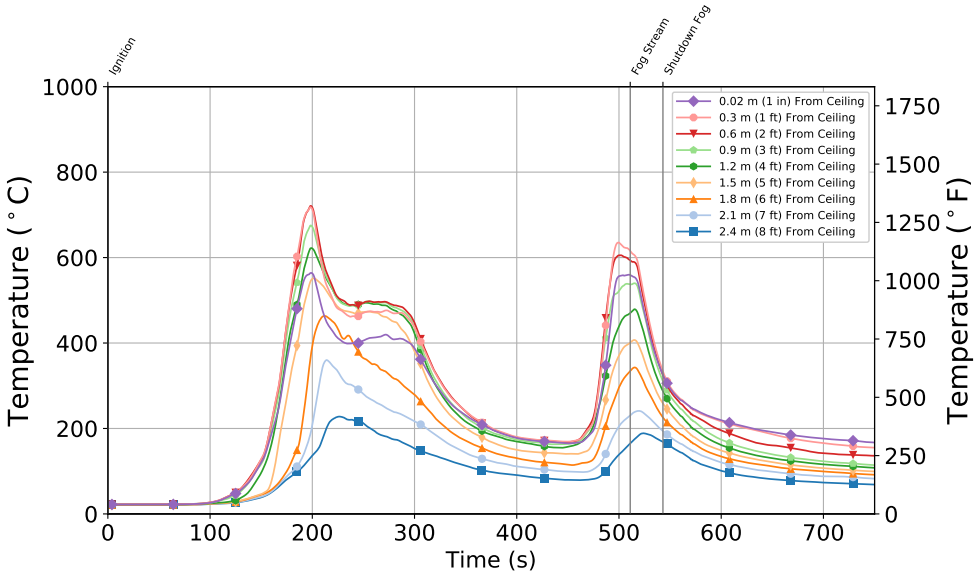

Figure B.183: Experiment 12 - Thermocouple temperature time histories from the Quadrant D thermocouple array in the basement.

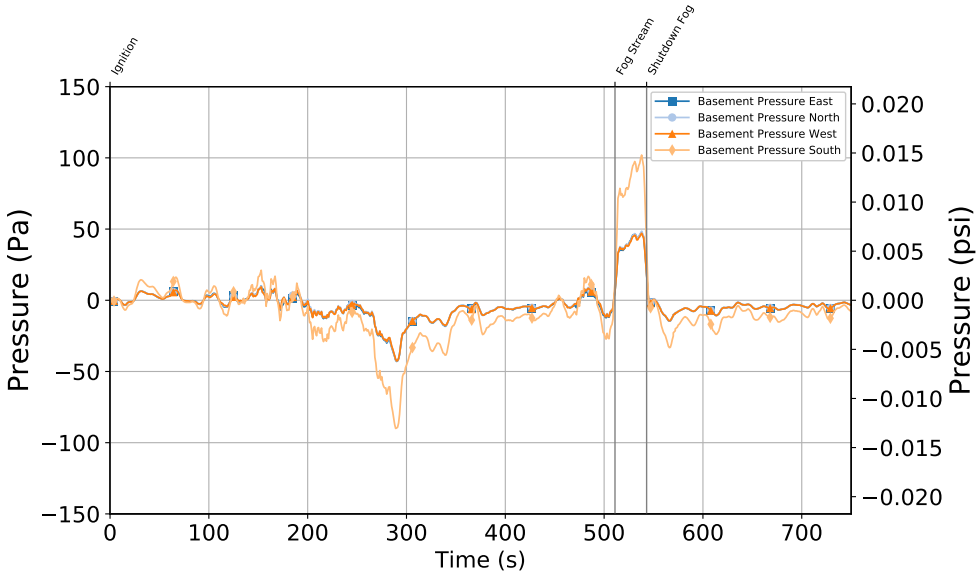

Figure B.184: Experiment 12 - Basement Pressure at 6 locations 1.2 m (4 ft) Above the Floor

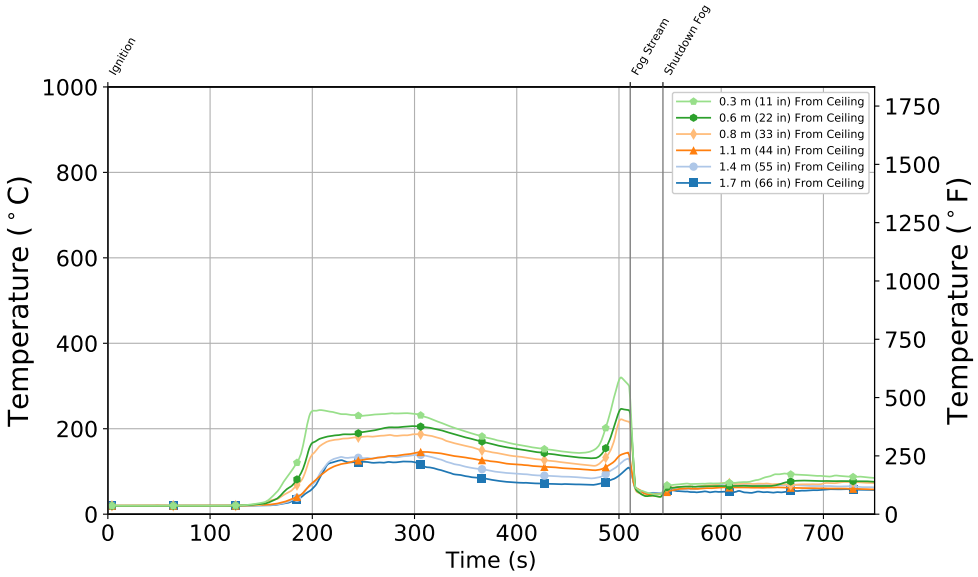

Figure B.185: Experiment 12 - Stair Thermocouple Temperature at Basement Level

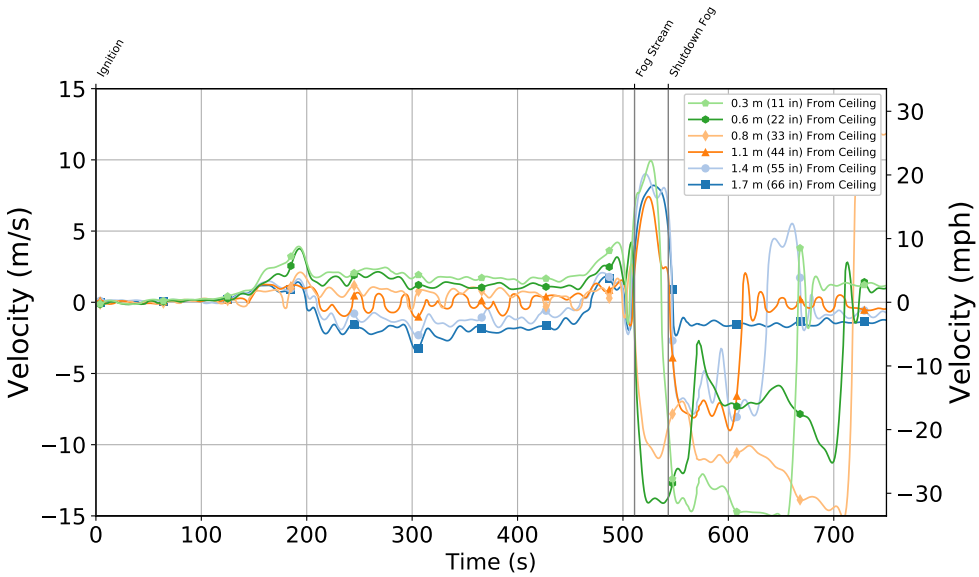

Figure B.186: Experiment 12 - Stair Velocity at Basement Level

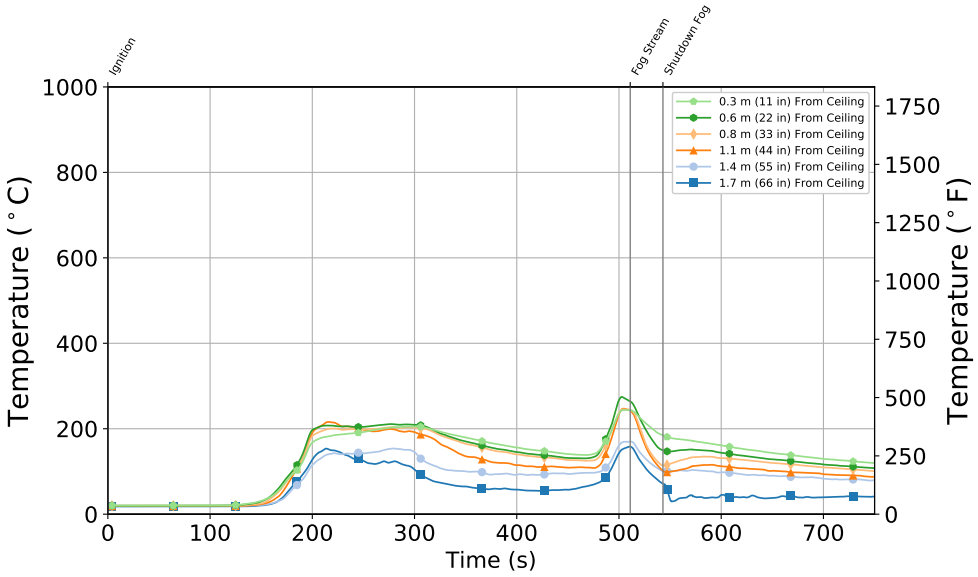

Figure B.187: Experiment 12 - Stair Thermocouple Temperature at First Floor

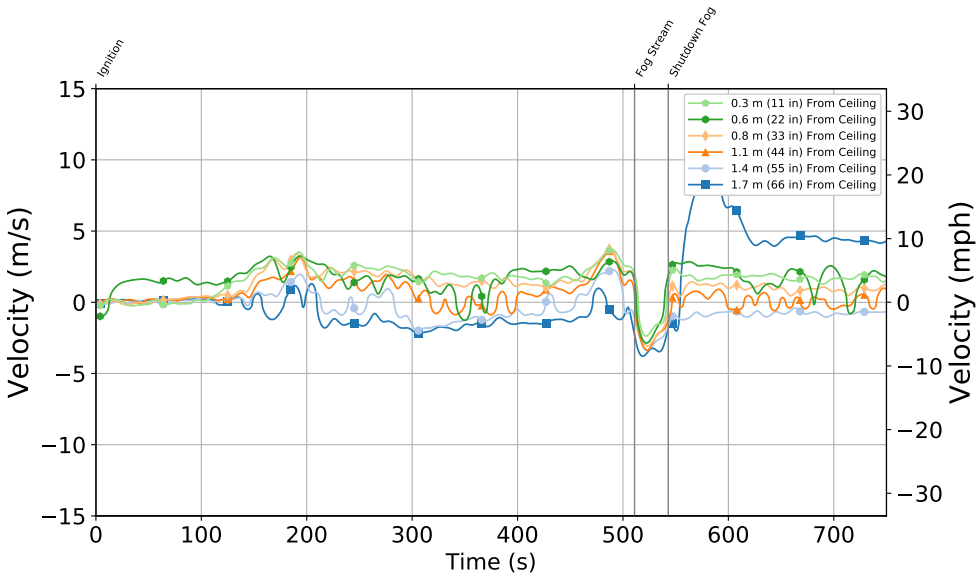

Figure B.188: Stair Velocity at First Floor

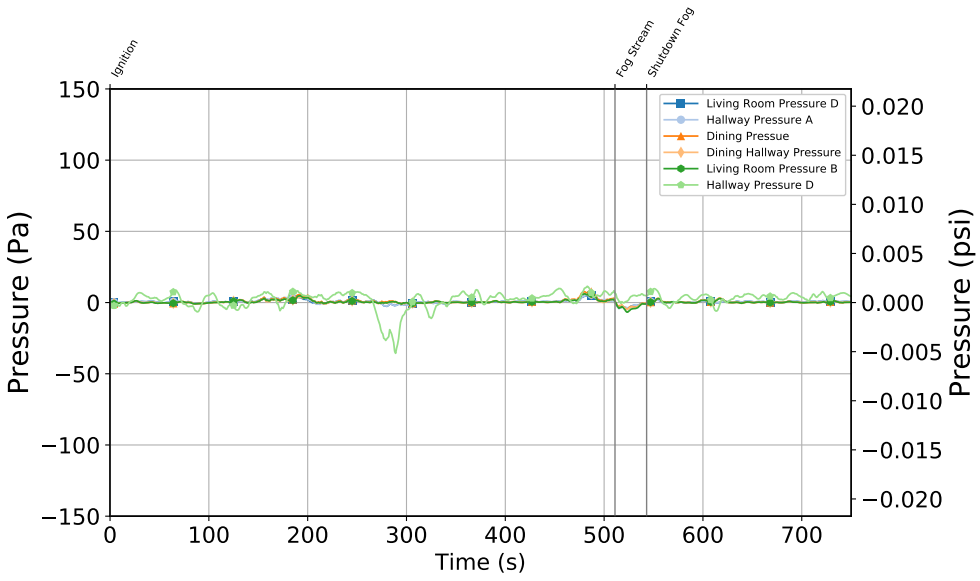

Figure B.189: Experiment 12 - First Floor Pressure at 6 locations 1.2 m (4 ft) Above the Floor

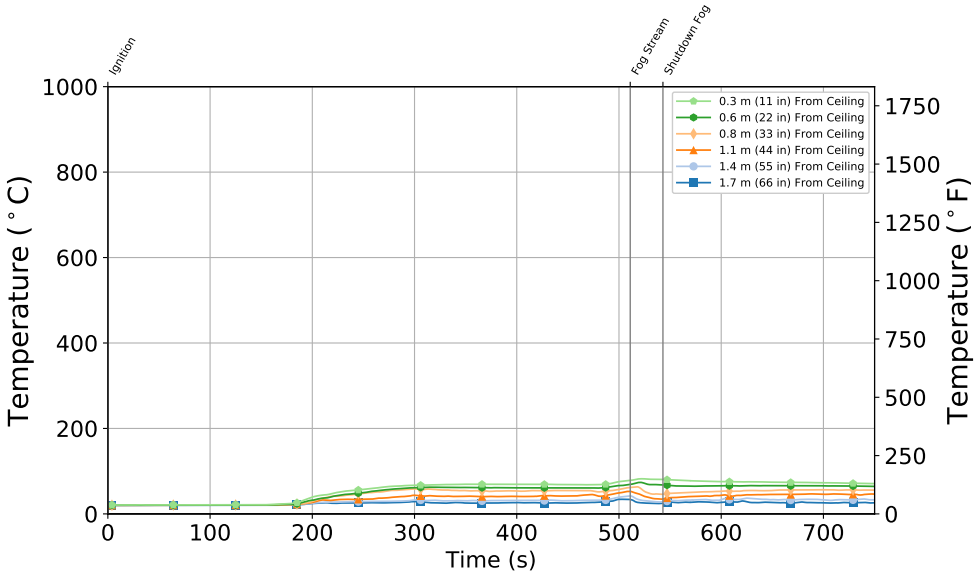

Figure B.190: Experiment 12 - Front Door Thermocouple Temperature at First Floor

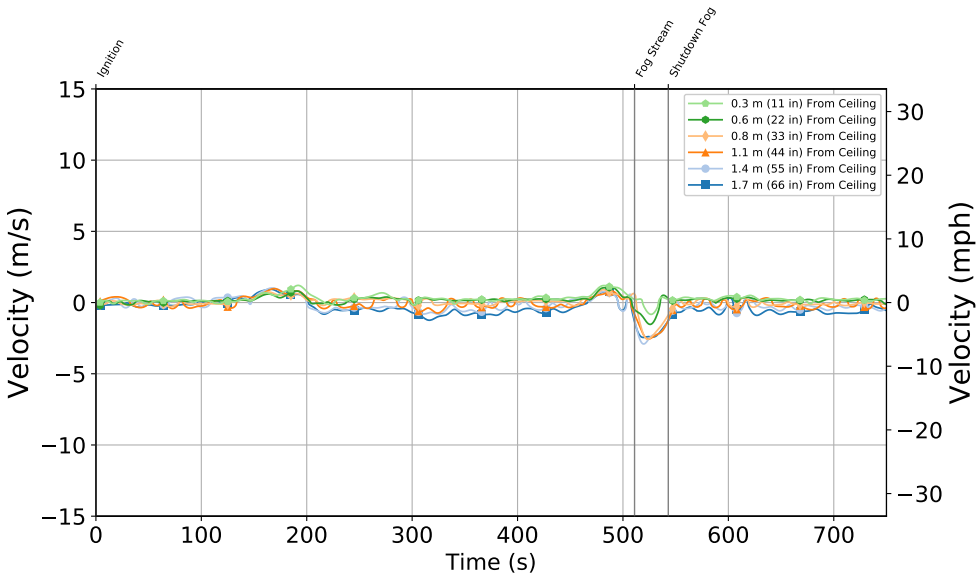

Figure B.191: Experiment 12 - Front Door Velocity at First Floor

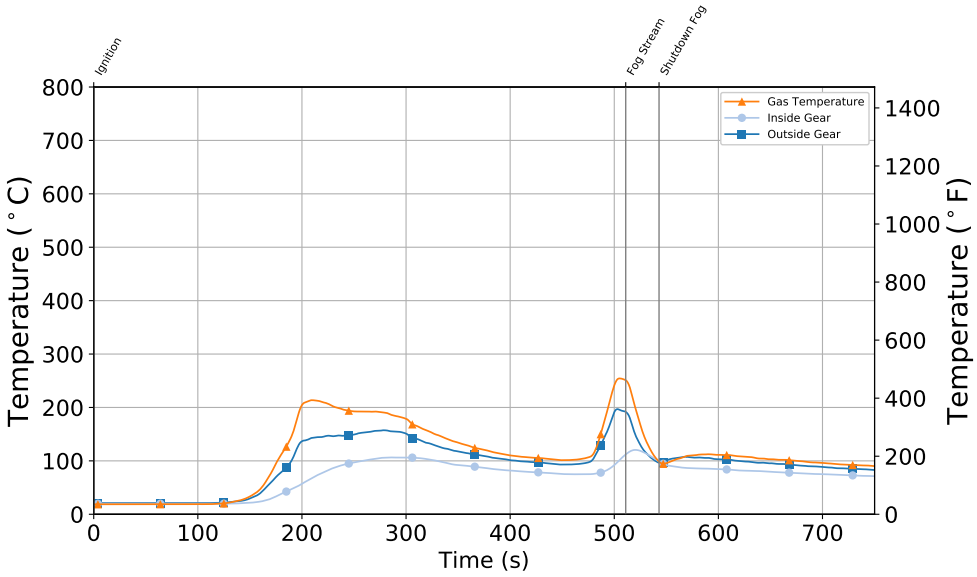

Figure B.192: Experiment 12 - Thermocouple Temperature on Inside and Outside of PPE Sample

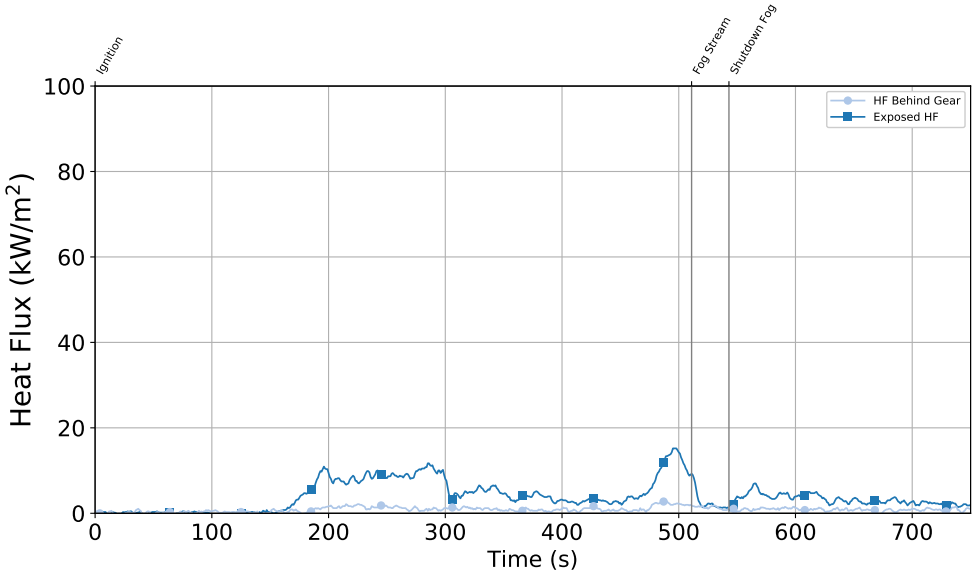

Figure B.193: Experiment 12 - Comparison of Heat Flux between Exposed Sensor and Protected Sensor

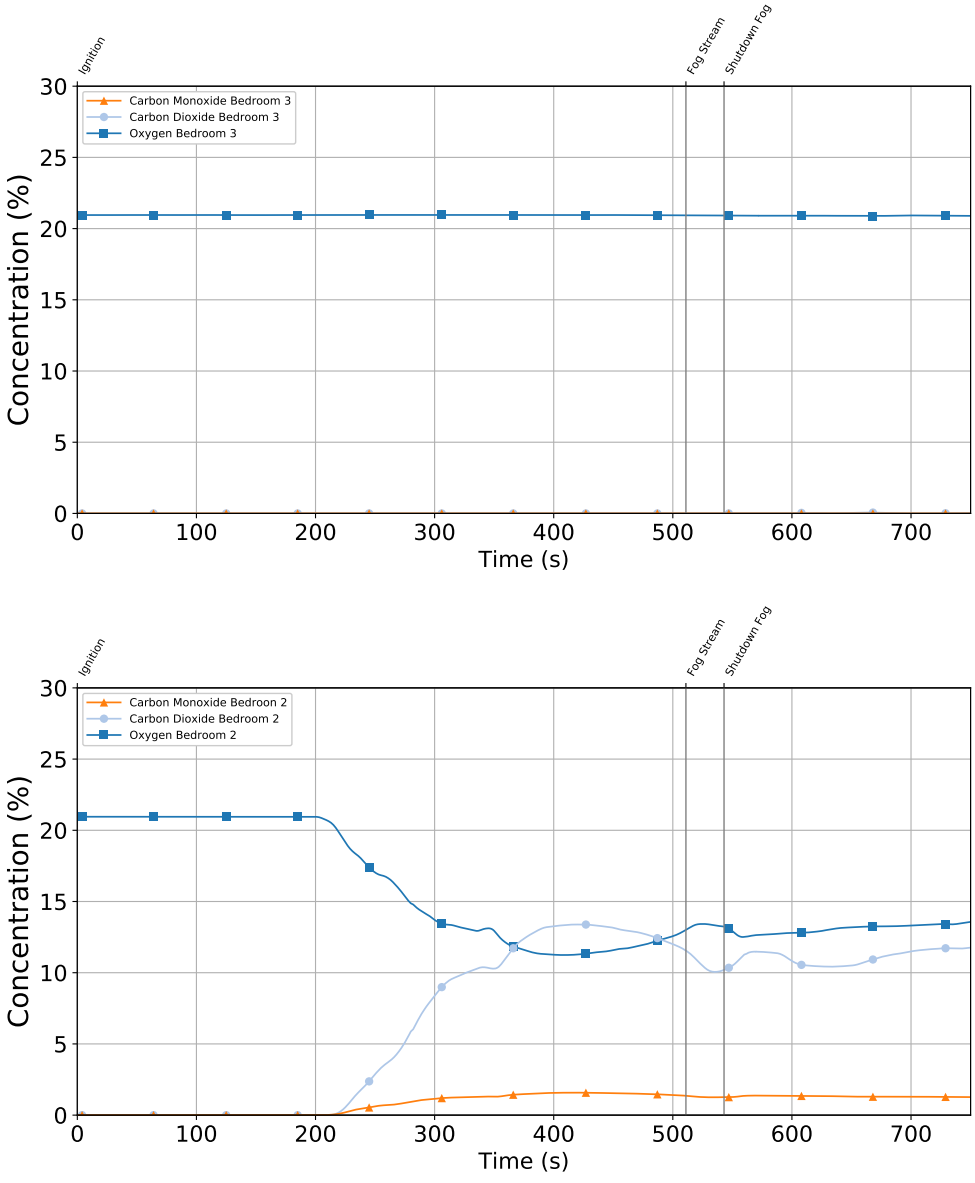

Figure B.194: Experiment 12 - Gas concentration time histories from the closed bedroom at 1.2 m (4 ft) (top) and from the open bedroom at 1.2 m (4 ft) (bottom).

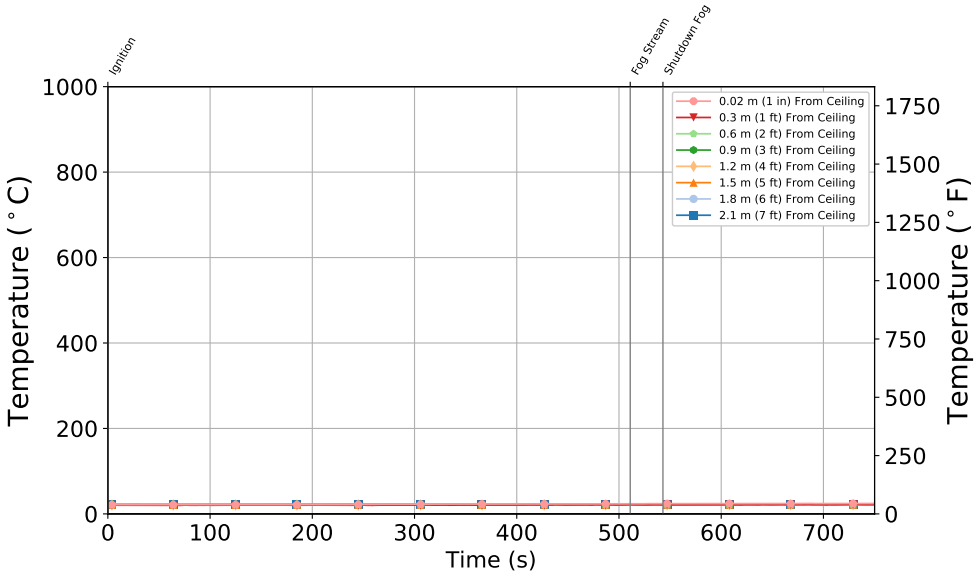

Figure B.195: Experiment 12 - Bedroom 3 (Closed) Bedroom

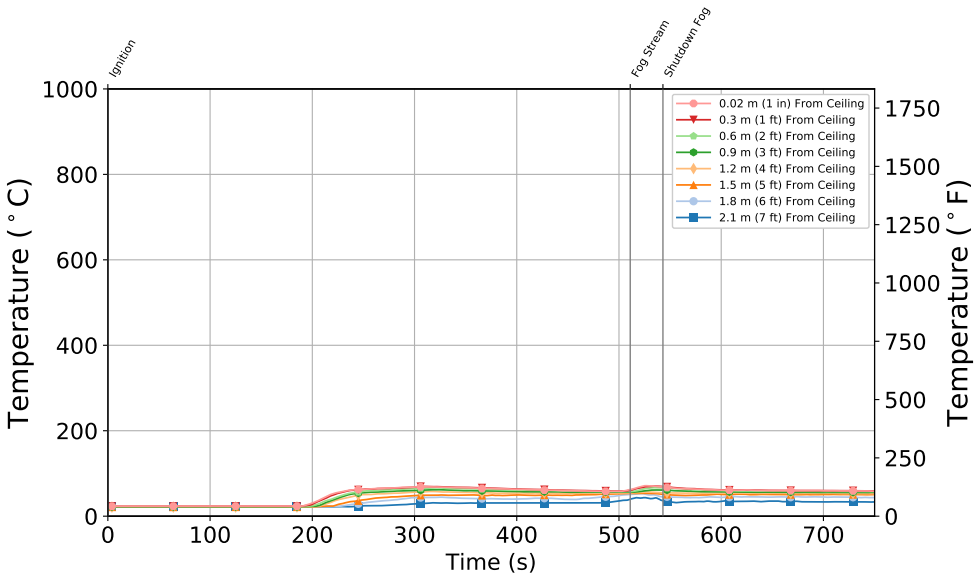

Figure B.196: Experiment 12 - Bedroom 2 (Open) Bedroom